2019

Innovative Approaches To Identify Regulators Of Liver Regeneration

Amber Weiching Wang
University of Pennsylvania

Innovative Approaches To Identify Regulators Of Liver Regeneration

Abstract

The mammalian liver possesses a remarkable ability to regenerate after injury to prevent immediate organ failure. However, amid a rising global burden of liver disease, the only curative treatment for patients with end-stage liver disease is transplantation. Elucidating the mechanisms underlying tissue repair and regrowth will enable identification of therapeutic targets to stimulate native liver regeneration, thereby circumventing the great paucity of available transplant organs. Here, utilizing the Fah-/- mouse model of liver repopulation, I applied transcriptomic and epigenomic techniques to investigate the changes occurring as hepatocytes restore organ mass following toxic injury. By labeling ribosomal or nuclear envelope proteins, I performed the first extensive characterization of gene expression and chromatin landscape changes specifically in repopulating hepatocytes in response to injury. Transcriptomic analysis showed that repopulating hepatocytes highly upregulate Slc7a11, a gene that encodes the cystine/glutamate antiporter. I demonstrated that ectopic Slc7a11 expression promotes liver regeneration and Slc7a11 mutation inhibits hepatocyte replication. Integrative bioinformatics analyses of chromatin accessibility revealed dynamic changes at promoters and liver-enriched enhancer regions that correlate with the activation of proliferation-associated genes and the repression of transcripts expressed in mature, quiescent hepatocytes. Furthermore, changes in chromatin accessibility and gene expression are associated with increased promoter binding of CCCTC-binding factor (CTCF) and decreased enhancer occupancy of hepatocyte nuclear factor 4α (HNF4α). In summary, my thesis work identifies Slc7a11 as a potential driver of liver regeneration, and provides insights into the complex crosstalk between chromatin accessibility and transcription factor occupancy to regulate gene expression in repopulating hepatocytes.

Degree Type

Dissertation

Degree Name

Doctor of Philosophy (PhD)

Graduate Group

Pharmacology

First Advisor

Klaus H. Kaestner

Keywords

ATAC-seq, Fah, hepatocytes, liver regeneration, multiomics analysis, TRAP-seq

Subject Categories

Bioinformatics | Genetics | Systems Biology

INNOVATIVE APPROACHES TO IDENTIFY REGULATORS OF LIVER REGENERATION

Amber Weiching Wang

A DISSERTATION

in

Pharmacology

Presented to the Faculties of the University of Pennsylvania

in

Partial Fulfillment of the Requirements for the

Degree of Doctor of Philosophy

2019

Supervisor of Dissertation

_____

Klaus H. Kaestner, Ph.D.

Thomas and Evelyn Suor Butterworth Professor in Genetics

Graduate Group Chairperson

_____

Julie A. Blendy, Ph.D.

Professor of Pharmacology

Dissertation Committee

Mitchell A. Lazar, M.D., Ph.D., Willard and Rhoda Ware Professor in Diabetes and Metabolic Diseases

Michael A. Pack, M.D., Professor of Medicine

Benjamin F. Voight, Ph.D., Associate Professor of Pharmacology

Kirk J. Wangensteen, M.D., Ph.D., Assistant Professor of Medicine

DEDICATION

Dedicated to my parents, Dr. Chuhsing Kate Hsiao and Dr. Chih-Hao Wang.

ACKNOWLEDGMENT

I would like to thank my advisor Dr. Klaus Kaestner for providing me with the mentorship and support to explore the field of bioinformatics while performing bench experiments. This thesis work would not be possible without his vision and belief in implementing novel technologies to advance biomedical research. I am also grateful for all the Kaestner lab members for their friendship and advice. Drs. Kirk Wangensteen, Julia Yue Wang, and Adam Zahm have been integral in helping me advance my thesis work as well as inspiring me to persevere throughout the Ph.D. process. Thank you to my thesis committee, Drs. Mitchell Lazar, Micheal Pack, Benjamin Voight, and Kirk Wangensteen, for their guidance and encouragement.

The tremendous help I received throughout training has enabled the progression of my thesis work. I would like to thank the Functional Genomics Core, Dr. Jonathan Schug, Shilpa Rao, Olga Smirnov, and Joseph Kutch, the Pharmacology Graduate Group, Dr. Julie Blendy, Sarah Squire, and my classmates, the Institute of Diabetes, Obesity, and Metabolism, especially Vesselina, for their assistance and company. I am blessed with the opportunity to meet the most intelligent and hardworking people at Penn, and I am particularly thankful to Drs. Kristy Ou, Julia Kieckhaefer, Yong Hoon Kim, Alexander Sakers, Ayano Kondo, Teguru Tembo, and Rebecca Myers for their invaluable friendship.

I am forever grateful to my family, my parents Kate and Peter, as well as my sister Leiya, for their unconditional love and endless support. My parents are my greatest inspiration to pursue a career in science and motivation to persist through any obstacles. I would also like to thank the Ho family, especially Yuging and Cojen, for making me feel closer to home. I am thankful to Wesley for all the love and laughter he brought into my life. Finally, thank you to our dog Mochi, for keeping me where the light is.

ABSTRACT

INNVOATIVE APPROACHES TO IDENTIFY REGULATORS OF LIVER REGENERATION

Amber W. Wang

Klaus H. Kaestner

The mammalian liver possesses a remarkable ability to regenerate after injury to prevent immediate organ failure. However, amid a rising global burden of liver disease, the only curative treatment for patients with end-stage liver disease is transplantation. Elucidating the mechanisms underlying tissue repair and regrowth will enable identification of therapeutic targets to stimulate native liver regeneration, thereby circumventing the great paucity of available transplant organs. Here, utilizing the *Fah*$^{-/-}$ mouse model of liver repopulation, I applied transcriptomic and epigenomic techniques to investigate the changes occurring as hepatocytes restore organ mass following toxic injury. By labeling ribosomal or nuclear envelope proteins, I performed the first extensive characterization of gene expression and chromatin landscape changes specifically in repopulating hepatocytes in response to injury. Transcriptomic analysis showed that repopulating hepatocytes highly upregulate *Slc7a11*, a gene that encodes the cystine/glutamate antiporter. I demonstrated that ectopic *Slc7a11* expression promotes liver regeneration and *Slc7a11* mutation inhibits hepatocyte replication. Integrative bioinformatics analyses of chromatin accessibility revealed dynamic changes at promoters and liver-enriched enhancer regions that correlate with the activation of proliferation-associated genes and the repression of transcripts expressed in mature, quiescent hepatocytes. Furthermore, changes in chromatin accessibility and gene expression are associated with increased promoter binding of CCCTC-binding factor (CTCF) and decreased enhancer occupancy of hepatocyte nuclear factor 4α (HNF4α). In summary, my thesis work identifies *Slc7a11* as a potential driver of liver regeneration, and provides insights into the complex crosstalk between chromatin accessibility and transcription factor occupancy to regulate gene expression in repopulating hepatocytes.

TABLE OF CONTENTS

LIST OF TABLES

LIST OF ILLUSTRATIONS

CHAPTER 1

INTRODUCTION

LIVER BIOLOGY

I. Function

As the hub of various biological processes, the liver performs a multitude of functions that can be categorized as the following.

(1) Regulation of carbohydrate, protein, and lipid homeostasis. The liver undergoes gluconeogenesis to release glycogen as glucose in response to fasting, packages excess lipids for storage in other tissues, and processes amino acids via deamination to convert the non-nitrogenous carbon skeleton to glucose or lipids [1,2].

(2) Metabolism of nutrients, wastes, and xenobiotics. The metabolic process consists of phases I and II. Phase I involves direct modification including oxidation, reduction, and hydrolysis often achieved by cytochrome P450 (CYP450) proteins. Phase II is carried out by enzymes to conjugate large molecules of phase I metabolites to decrease activity and increase solubility [3].

(3) Synthesis of bile, amino acids, coagulation factors, and serum proteins. The liver performs the conversion of ammonia to urea through the urea cycle [4] and carries out the conjugation of bilirubin for secretion into the bile that drains into the intestine for degradation [5]. The liver also synthesizes non-essential amino acids, bile acid from cholesterol, clotting factors for blood coagulation, and various serum proteins such as albumin (ALB) and transferrin [2,6].

II. Cell types

The liver consists of cell types of divergent embryological origin – with two main parenchymal cell types, hepatocytes and cholangiocytes, and nonparenchymal cells including Kupffer cells, stellate cells, and sinusoidal epithelial cells.

Hepatocytes are the main cell type that performs the majority of liver functions mentioned above. They occupy 60% of the liver by cell number and 80% by cell mass [7]. Cholangiocytes, also known as biliary epithelial cells (BEC), are cuboidal cells that line the bile duct to allow passage of bile acid from the liver to the intestine. They are less metabolic active compared to hepatocytes but still exhibit functions such as bicarbonate synthesis and electrolyte secretion [8].

Cholangiocytes also play an important role in regulating immune and inflammatory responses [8]. Small ducts embedded deep within the liver are called intrahepatic bile ducts whereas large ducts that exit the liver are extrahepatic bile ducts [7].

Kupffer cells are resident hepatic macrophages that recognize stimuli introduced through the portal circulation to perform phagocytosis and secret pro- or anti-inflammatory mediators to defend liver against bacterial and viral infections [9]. Stellate cells exist in two states – under quiescent conditions, they store vitamin A in lipid droplets whereas other functions remain unclear [2]; upon liver damage, they are activated to become proliferative myofibroblasts [10]. The myofibroblasts derived from stellate cells deposit collagen that contributes to the fibrosis or scarring of the liver tissue, which could progress to cirrhosis with chronic liver injury [10]. Sinusoidal endothelial cells are specific nonparenchymal cells that line the capillaries of the liver, also known as sinusoids, to form fenestrated sieve plates that permit access of macromolecules from the space of Disse, an interstitial area that surrounds hepatocytes. This structure allows hepatocytes to extract a variety of protein-bound substrates and xenobiotics from the circulation [11].

III. Structure

The liver is composed of building blocks termed ‘lobules’, which contains parenchymal and nonparenchymal cells, the bile duct, and vessels of the circulatory system including the hepatic artery, portal vein, and central vein (Figure 1.1). The portal vein, hepatic artery, and the bile duct are often referred to as the portal triad due to their spatial proximity. A typical lobule is considered to be a hexagonal unit with the central vein in the middle and the portal triad at the six corners [12]. The portal vein and the hepatic artery are the two main sources of blood supply for the liver, with the portal vein providing two-thirds of the blood from the small intestine and the hepatic artery contributing to the remaining one-third of the blood from the celiac artery. The blood from these two sources mixes as it passes through sinusoids, and enters the central vein to exit the liver [7]. Owing to the direction of the blood supply, which moves from the portal triad to the central vein, the portal area is considered ‘zone one’ and the central area as ‘zone three’.

Hepatocytes synthesize and transport bile acids via a specialized channel formed by two adjacent cells, also referred to as the canaliculus. Bile is produced in the canaliculi as a mixture of bile acids, metabolites, and bilirubin secreted from hepatocytes; it enters the bile ducts that ultimately drain into the duodenum. Bile acids assist in lipid and cholesterol emulsification in the intestines, and are reabsorbed from the terminal ileum and transported back to the liver through the portal vein, recycling in a route known as the enterohepatic circulation. Contrary to the blood flow, bile flows from zone three to zone one [6]. Hepatocytes in proximity to the portal triad are referred to as periportal or zone one hepatocytes, those adjacent to the central vein are pericentral or zone three hepatocytes, and cells between zone one and three are referred to as zone two hepatocytes.

Apart from the spatial distribution, hepatocytes from different zones express divergent sets of genes to carry out various metabolic functions, a property known as metabolic zonation, which is tightly controlled by the Wnt/β-catenin signaling pathway [13]. Periportal hepatocytes perform gluconeogenesis, fatty acid oxidation, urea production, and glutathione (GSH) detoxification, whereas pericentral hepatocytes conduct glycolysis, lipogenesis, ketogenesis, and xenobiotic metabolism [14]. Multiple cell types coupled with metabolic zonation allow the liver to carry out diverse metabolic and biosynthetic functions central to homeostasis.

IV. Development

In mice, the parenchymal cells of the liver develop from the definitive endoderm from the anterior primitive streak of the gastrulating embryo on embryonic day (E) 7.5 [15]. By E8.5, endoderm patterning is complete and can be categorized from the anterior to posterior as the foregut, midgut, and hindgut regions [16]. Hepatic specification subsequently begins on E9.0 when hepatic endoderm cells extend off the posterior foregut [17] and continue to thicken to establish the liver diverticulum [18]. Early signals important for the initiation of liver specification include fibroblast growth factor (FGF) family members emanating from the developing heart [19] and bone morphogenic proteins (BMP) from the septum transversum mesenchyme [20] of the mesoderm.

Simultaneously, transcription factors of the GATA binding proteins [21] and forkhead box A (FOXA) subfamily [22] activate transforming growth factor β (TGFβ), WNT, and NOTCH signaling within the endoderm. Additionally, FOXA1 and GATA4 function as 'pioneer factors' that bind to heterochromatic DNA to establish transcriptional competence of downstream gene programs required for further differentiation [2,23]. The liver bud gives rise to hepatoblasts, bipotential progenitor cells that express α-fetoprotein (AFP) and ALB [24,25]. Prior to differentiation, hepatoblasts continue to migrate and proliferate into the septum transversum assisted by a gradient TGFβ signal from the portal vein mesenchyme starting on E13.5 [26]. Cells in proximity to the portal vein receive a higher TGFβ concentration that promotes expression of hepatocyte nuclear factors 1β (HNF1β) and HNF6, leading to the expression of cholangiocyte marker genes such as cytokeratin 19 (CK19) [26]. Hepatoblasts located away from the portal vein receive lower levels of TGFβ, resulting in elevated expression of HNF1α and HNF4α, which induce hepatocyte-specific gene expression such as ALB and CYP450 [27]. Beginning on E18, the differentiated hepatocytes continue to mature and undergo a metabolic switch from a glucose-consuming tissue to a glucose-producing organ. Developing hepatocytes at distinct locations in the liver also experience metabolic zonation to establish differential gene expression and protein production [2]. This process is regulated by complex crosstalk of signaling networks including the hepatocyte growth factor (HGF), glucocorticoids, HNF, and the Wnt/β-catenin pathway [27].

V. Homeostasis

Tissue turnover typically occurs through two models: replication of existing cells and differentiation of progenitor cells. While the presence of stem cells in the adult liver has long been contested, it is currently accepted that mature resident hepatocytes proliferate for homeostatic maintenance. Since differentiated hepatocytes are long-lived cells with a turnover rate of up to several months *in vivo*, under normal physiological conditions, fewer than 0.1% of the hepatocytes undergo replication at any time in the uninjured adult liver [28]. It is, therefore, questionable whether

stem cells are required at all for normal liver maintenance considering the long life span and low replication rate of mature hepatocytes.

Lineage-tracing in rodents is widely used to identify the source of hepatocyte homeostasis. The most debated model, the 'streaming liver hypothesis', implemented DNA radiolabeling assays in the rat liver and observed that newly-formed hepatocytes occur near the portal vein and flow towards the central vein to replenish the liver parenchyma [29]. The streaming liver hypothesis implies the existence of a stem cell compartment proximal to zone one and posits that periportal hepatocytes display a higher replication capacity, hence the ability to derive new cells from the portal vein to the central vein. Over time, it is found that the entire liver lobule contains hepatocytes derived from zone one [29]. However, evidence both for and against the streaming liver hypothesis has been provided. Genetic tracking that utilizes the cholangiocyte marker 'sex-determining region Y (SRY)-box 9' (SOX9) to label all BECs via a tamoxifen-inducible system in the adult liver of *Sox9*^{CreERT2};*Rosa*$^{LSL\text{-}LacZ}$ mice observed LacZ spreading in a portal-to-central direction that eventually occupied the entire liver parenchyma within a year [30]. These studies suggest SOX9-positive cholangiocytes as a source of mature hepatocytes to maintain the homeostatic liver.

Nonetheless, studies using different lineage-tracing systems have not observed the same evidence [31,32]. Other radiolabeling assays failed to detect movement of marked periportal hepatocytes towards the pericentral area in the adult liver [32]. Another transgenic *Sox9*^{CreERT2};*Rosa*$^{LSL\text{-}YFP}$ line generated with a bacterial artificial chromosome (BAC) found that YFP-positive cholangiocytes are restricted within the bile ducts and do not migrate to the central vein [33]. Labeling of adult hepatocytes of the *Rosa*$^{LSL\text{-}YFP}$ mouse through injection of AAV8-TTR-Cre, a hepatotropic adeno-associated virus (AAV) serotype 8 that expresses the Cre recombinase under the hepatocyte-specific transthyretin (TTR) promoter, did not demonstrate any YFP-negative hepatocytes in the liver parenchyma or near the periportal region [34]. These results indicate that all newly-derived hepatocytes are from preexisting mature cells and exclude the possibility of progenitors contributing to adult liver homeostasis. More recently, a 'reverse-streaming hypothesis' in which WNT-enriched pericentral hepatocytes expand to the periportal region have been

proposed [35], albeit with much controversy. In summary, the current evidence does not support the notion of liver stem cells as a source of mature hepatocytes during normal homeostasis; instead, hepatocytes are likely maintained by replication of preexisting cells.

VI. Diseases

Liver disease accounts for roughly 2 million annual deaths worldwide, of which 15% of the mortality results from acute hepatitis, 35% from hepatocellular carcinoma (HCC), and 50% from complications related to cirrhosis [36]. Strikingly, the combination of cirrhosis and HCC constitutes 3.5% of global deaths [37]. Although accurate statistics are not available due to the scarcity of mortality data from developing countries [36] and the underestimation of liver diseases as a cause of death [38], there is a discernible increase in the global burden of both acute and chronic liver disease [36,37,39].

A. Types of liver disease

Alcoholic liver disease

Alcohol contributes to over 50% of cirrhosis-related mortality and heavy alcohol consumption is associated with the development of cirrhosis [40]. For heavy drinkers — daily ethanol consumption of over 30g — the incidence of cirrhosis ranges from 1-6%, depending on the dose [41]. Furthermore, alcohol use exacerbates preexisting liver injuries [37]. Approximately 20% of patients with alcoholism develop alcoholic hepatitis, a clinical representation of jaundice and liver failure after chronic alcohol abuse, with a daily mean ethanol consumption of 100g [42]. Coupled with the rising rate of obesity globally, the severity of alcoholic liver disease, especially alcoholic fatty liver disease, is expected to worsen [37].

The molecular mechanism of alcohol-induced liver injury involves the oxidative metabolism of ethanol that shifts the oxidative-reduction potential in the liver, preventing fatty acid oxidation and inhibiting the tricarboxylic acid cycle that normally promotes lipolysis [43]. Additionally, ethanol activates sterol regulatory element-binding protein 1 (SREBP-1) [44], prevents peroxisome

proliferator-activated receptor α (PPARα) binding to the DNA [45], and inhibits AMP-activated protein kinase (AMPK) activity [46], leading to activation of fatty acid synthesis and metabolic remodeling that contributes to the development of fatty liver [47].

Non-alcoholic fatty liver disease (NAFLD)

Fatty liver, also called steatosis, is defined as excess accumulation of triglycerides in over 5% of fat in hepatocytes [48]. NAFLD encompasses two distinct conditions, steatosis without liver injury and steatosis with hepatocyte necrosis, referred to as non-alcoholic steatohepatitis (NASH) [48]. The global prevalence of NAFLD is estimated to be 25.2% [49] and of NASH is between 2-7% [49–52]. Current epidemiological studies potentially underestimate due to the difficulty of detecting fatty liver unless through imaging or liver biopsies [49]. Moreover, the increasing rates of comorbid conditions associated with NASH such as obesity, type 2 diabetes mellitus, and hyperlipidemia contribute to the rapidly growing burden of NAFLD [49]. Particularly in the case of NASH, chronic liver injury followed by lobular and portal inflammation in the form of collagen deposition and scar tissue production often lead to progression to fibrosis, cirrhosis, and HCC [48].

The exact mechanisms of NAFLD and NASH development are not completely understood and likely involve extensive interactions between various pathways. Three leading sources have been identified to contribute to NAFLD. (1) Increased uptake of fatty acids via diet, activation of *de novo* lipogenesis, and increased adipose tissue lipolysis, resulting in the accumulation of hepatic fatty acids. (2) A combination of fatty acid-induced extrinsic cell death through upregulation of cell death receptors and their ligands [53], as well as intrinsic cell death via increased endoplasmic reticulum (ER) stress [54], leading to Jun N-terminal kinase (JNK) activation, reactive oxygen species (ROS) production, and mitochondrial uncoupling [55]. Fatty acid-induced cell death is followed by the release of damage-associated molecular patterns (DAMPs) into the extracellular space [56–58]. (3) Triggering of hepatic inflammation due to fatty acids, DAMPs released by dying hepatocytes, and endotoxin from the intestine [59], inducing the production of cytokines and chemokines with subsequent recruitment of immune cells [60] and activation of nonparenchymal

cells [61,62]. In particular, the transformation of stellate cells into collagen-producing myofibroblasts further exacerbates NASH and promotes progression to fibrosis [63,64].

Drug- or toxin-induced liver injury

The liver is the first organ to be perfused by blood through the portal vein from the intestine for first-pass metabolism and is thus the initial filter for molecules before they enter into the general circulation. Therefore, exposure to environmental toxins can be severely damaging to hepatocytes. Substances such as alcohol, acetaminophen, *Amanita phalloides* mushrooms, and idiosyncratically, common drugs including anabolic steroids and antibiotics can cause acute liver failure [65]. At a rate of 18%, drug-induced liver injury is the leading cause of post-market withdrawal during drug development [66]. Acetaminophen is the primary etiology for drug-induced liver injury in the US and the UK, whereas herbal and alternative medicine are the leading causes in the East [37]. The exact mechanisms of liver injury vary by the drug consumed or the toxin ingested, but generally involves oxidative stress accumulation, mitochondrial dysfunction, hepatocyte necrosis and apoptosis, immune response stimulation, and nonparenchymal cell activation [67].

Viral hepatitis

Viral hepatitis refers to liver inflammation induced by viral infections, routinely caused by five hepatotropic viruses, hepatitis viruses A, B, C, D, and E. While viral hepatitis affects individuals from all geographic locations, middle and low-income areas are disproportionately affected [37]. An estimated 1.34 million annual deaths are associated with hepatitis-related mortality [68]. Hepatitis A and E typically result in acute, self-contained illnesses, whereas hepatitis B and C lead to immune-mediated chronic liver disease. There is an increased risk of developing HCC and cholangiocarcinoma (CAA) among patients with hepatitis B and C, although the rate of cirrhosis progression and tumorigenesis display individual heterogeneity [69]. The pathogenesis of hepatitis

B and C virus includes complex crosstalk between the host and virus that involves immune activation of CD4+ helper T cells, CD8+ effector T cells, and natural killer cells [69,70].

B. Consequences of liver disease

Acute liver failure

Acute liver failure, also known as fulminant hepatic failure, is defined as the clinical presentation of severe liver injury and hepatic encephalopathy within 8 weeks of the first symptoms without preexisting liver disease [71]. Other than the liver and the brain, acute liver failure also affects organs including the heart, lungs, pancreas, and kidney [72]. Hepatitis A, B, and E infections are the predominant causes of acute liver failure worldwide [72]. In the US, drug-induced injury contributes to approximately 50% of acute liver failure cases [73].

Cirrhosis

Cirrhosis is the end-stage of all chronic liver disease that develops from an asymptomatic phase termed ‘compensated’ cirrhosis to a progressive ‘decompensated’ phase marked by complications of ascites, jaundice, encephalopathy, and variceal bleeding [74]. Features of cirrhosis include regenerative and nodular parenchyma, widespread deposition of fibrotic tissues, and hepatocyte necrosis [75]. Patients with cirrhosis have a 5-10-fold increased risk of mortality [76]; death occurs due to a variety of complications including infections, kidney failure, and gastrointestinal bleeding [77]. Common causes of cirrhosis include alcohol abuse (60-70%), chronic hepatitis B or C (10%), and NAFLD (10%) [78].

Liver cancer

Considering the late-stage at diagnosis in most cases, HCC exhibits a 5-year survival rate of 18.4% with an annual rise of mortality by 2.4% [79]. Currently, 40% of HCC results from hepatitis B, 40% from hepatitis C, 11% from alcohol use, and 9% from other causes [37]; however, the etiology varies significantly for different countries. Non-viral factors contribute to a larger pool of

HCC in regions with a low incidence of viral hepatitis. In the US, 25% of HCC patients present with alcoholic-liver disease and 20-30% could display metabolic syndrome or NAFLD [80]. In contrast, viral hepatitis contributes to approximately 90% of HCC cases in Vietnam [81]. The etiology is expected to change drastically due to the increasing prevalence of NAFLD and NASH [82].

LIVER REGENERATION

I. Historical overview

Regeneration, defined as cell regrowth or repair, is widely represented in metazoa [83]. In lower organisms, whole body or tissue regeneration is easily achieved. Invertebrates such as planarians are capable of whole-body regeneration from as little as 1/279th of the original body [84] and lower vertebrates including amphibians are capable of regenerating complete appendages. In mammals, the regenerative ability is restricted to select tissues including the skin, cartilage, digits, muscle, intestinal epithelium, and liver [85]. The evolutionary importance of the liver in maintaining a regenerative ability likely stems from it being the largest metabolic organ in the mammalian system, as nutrient and xenobiotic metabolism subject the liver to frequent, unpredictable environmental insults. It is presumed that the regenerative ability has been retained in animals in order to recover from massive liver injuries following exposure to food toxins [86]. Human's ability to regenerate the liver has long been known, even codified in Greek mythology by the story of Prometheus. After stealing fire and giving it to humanity, Prometheus is chained on Mount Atlas and punished to eternal torment by Zeus. An eagle would feed on his liver daily, only for it to grow back overnight just to be eaten again the next day [87].

Fewer than 0.1% of hepatocytes are in mitosis under physiological conditions [88] with the typical life span of 200-400 days [32]. The liver can regenerate upon loss of the parenchyma via toxin-induced liver injury or surgical tissue removal. Generally, mature hepatocytes replicate to repopulate the liver under normal conditions but hepatocyte progenitor cells (HPCs) can arise when hepatocyte DNA synthesis is severely impaired [89]. In fact, hepatocytes have an almost unlimited replicative capacity as serial partial hepatectomy (PHx) has demonstrated the rat liver to be able to regenerate after 18 surgeries [90], and serial transplantation of mouse hepatocytes showed their ability to replicate at least 69 times without loss of function [91]. Given a stimulus, hepatocytes can rapidly re-enter the cell cycle to restore liver mass and function. Furthermore, the process of cell proliferation is terminated as soon as the liver mass is restored to its original liver-to-body weight-ratio [88,92]. In the event when over 90% loss of the parenchyma occurs, the liver can fail to

regenerate [93]. With the increasing global burden of liver disease, understanding the regulation of liver regeneration promises to identify potential therapeutic targets to promote tissue repair and regrowth after liver injury.

II. Rodent models of liver regeneration

Various rodent models have been developed to study the regenerative response and can be categorized by the stimulus to induce hepatocyte proliferation into surgical-, chemical-, or genetically-induced liver injury paradigms.

A. Surgical-induced liver regeneration

Partial hepatectomy

PHx is the most widely-used technique to study liver regeneration in rodents, in which two-thirds of the liver is surgically removed to induce cell growth and proliferation of the remnant lobes to restore liver mass and function within 10-14 days [94]. Due to the clean removal of the liver lobes, the majority (~95%) of the remaining mature hepatocytes enter the cell cycle in a synchronous fashion that is also species-specific [95]. In both rats and mice, hepatocytes enter G1 4 h post-PHx [96]; DNA synthesis initiates at 12-18 h [97] and proliferation peaks at 24 h in rats [98], while a 20 h lag is observed in mice due to a longer G1 [96]. At 36 h after PHx, approximately 40% of hepatocytes are in S phase [99]. The well-defined time periods for various cell cycle entry points provide the opportunity to study the regulatory mechanisms of adult hepatocyte transitioning from G0 to G1, and from G1 to S *in vivo* [100]. While PHx reflects what is seen in living-donor liver transplantation, which occurs in less than 5% of transplant cases in the US annually [101], this model does not recapitulate what is seen in human liver diseases that involve inflammatory responses and necrotic cell death [102]. Nonetheless, the high accuracy and reproducibility of the PHx model have allowed understanding of the signaling pathways and transcriptional control that take place during hepatocyte replication. It is worth noting that even though injury responses are

not seen in PHx, the majority of signaling networks underlying the regenerative process are similar within most liver repopulation models [95].

Ischemia/reperfusion (I/R) injury

I/R injury occurs due to prolonged low oxygen tension in tissues followed by normalized oxygen perfusion, leading to significant inflammatory responses that cause organ damage and dysfunction, as often seen during liver transplantation or organ hemorrhage [103]. In rodents, I/R injury is modeled via an artery clamp in rats [104] and a lobular clamp in mice [105] to temporarily block the blood supply to the liver. Recovery from I/R injury varies depending on the duration of ischemia, which generally lasts for 30-90 min. A significant injury is frequently observed 12 h later, followed by a peak proliferative response at 48 h, with complete recovery by 96 h [106].

The process of I/R injury can be separated into two phases. In the initial phase, complement triggers Kupffer cell activation followed by the release of ROS that induces oxidative damage to hepatocytes [104]. The hepatic architecture is unchanged in the initial phase, but injured and dying hepatocytes release signals to exacerbate inflammation that feedforward to complement and Kupffer cell activation, leading to the production of tumor necrosis factor α (TNFα) [107] and cytokines such as interleukin 12 (IL12) [108]. In the late phase, the combination of adhesion molecule expression on sinusoidal endothelial cells and secretion of CXC chemokines from nonparenchymal cells result in the recruitment of neutrophils to the liver followed by the release of oxidants and proteases to induce widespread destruction of the parenchyma [109,110]. The late phase of I/R injury thus induces significant changes in the hepatic architecture mainly through necrotic cell death [103].

Bile duct ligation

In bile duct ligation, the common bile duct, which drains bile produced in the liver to the small intestine, is irreversibly ligated, resulting in inflammatory responses, obstructive cholestasis, and fibrosis within the first 2 weeks followed by cirrhosis at 4 weeks [111]. Contrary to PHx,

cholangiocytes are the main cell type to regenerate after bile duct ligation as an extensive proliferation of bile duct cells are observed; DNA synthesis begins at 24 h and peaks at 48 h after the surgery [112]. However, when the proliferative capacity of cholangiocytes is impaired, as in the case of treatment with the biliary toxin methylene diamiline, mature hepatocytes are able to transdifferentiate into cholangiocytes to rescue the biliary epithelium [113].

B. Chemical-induced liver regeneration

D-galactosamine (GalN)

Intraperitoneal injection of GalN contributes to hepatocyte death through three sources, (1) uridine 5'-diphospho (UDP)-galactosamine derivatives that inhibit RNA and protein synthesis [114], (2) endotoxin accumulation that leads to complement activation and necrotic cell death [115], and (3) mast cell degranulation that causes extensive inflammation [115]. Necrosis is scattered but more prevalent around the pericentral region [116]. Peak plasma alanine transferase (ALT) and aspartate aminotransferase (AST), as well as maximal necrosis, occur at 24 h followed by DNA synthesis that peaks at 48 h after GalN administration [117]. Hepatocyte proliferation, ensuing as early as 24 h post-GalN, is the main source of regeneration, but a contribution of oval cells 48-96 h after drug treatment is observed at higher GalN doses [116].

Carbon tetrachloride (CCl_4)

The main contributors of hepatotoxicity after CCl_4 administration are the zone 3 CYP450 enzymes [118]. CYP2B1, 2B2, and 2E1 [119,120] form reactive metabolites of CCl_4 including trichloromethyl (CCl_3*) and trichloromethyl peroxyl (CCl_3OO*) radicals that modify proteins, lipids, and DNA in hepatocytes, leading to necrotic cell death [121]. Parenchymal necrosis is most prominent in pericentral hepatocytes due to the high expression of CYP450 proteins [118]. The peak of cell death occurs at 24 h, followed by DNA synthesis highest at 36 h [122], and repopulation to replace lost liver mass that is completed within 7-10 days [106]. In addition, long-term CCl_4 exposure promotes fibrosis and even cirrhosis due to stellate cell activation that deposits collagen

and matrix proteins [123,124]. Thus, repeated CCl_4 treatment is often used as a model for chronic liver injury.

Thioacetamide (TA)

TA was initially introduced as a fungicide but quickly realized to be hepatotoxic and carcinogenic [125]. A single-dose administration leads to acute injury [126], subchronic exposure induces fibrosis [127], and chronic use results in liver cancer [125]. Similar to CCl_4, TA toxicity stems from bioactivation through CYP450 enzymes, especially CYP2E1 [128,129] that metabolizes TA to TA-sulfoxide and TA-sulfone, active intermediates that cause necrotic cell death [130]. In addition, toxic TA metabolites induce oxidative stress and lipoperoxidation, leading to the destruction of cell membranes [131,132]. However, the exact mechanisms of TA-sulfone-induced cell death and replication response are not clear, since TA has not been widely used as a hepatotoxin for liver regeneration studies. Hepatic necrosis peaks at 24 h [133] with maximal DNA synthesis at 36-48 h after TA administration [134].

Acetaminophen (APAP)

APAP is a common analgesic and antipyretic drug due to its safety and efficacy. In the US, APAP overdose is the most common cause of acute liver failure, accounting for 46% of cases [135]. APAP is normally eliminated by phase II conjugation reactions including glucuronidation and sulfation followed by excretion through the kidneys [136]. However, at toxic doses, the phase II enzymes are saturated and excess APAP is metabolized instead by CYP2E1 to the reactive metabolite N-acetyl-p-benzoquinone imine (NAPQI) [137] followed by depletion of GSH, the cell's primary defense against oxidative damage. Subsequently, excess NAPQI forms covalent bonds with proteins to induce reactive oxygen and nitrogen species such as peroxynitrite [138]. Translocation of JNK [139] and the cell death protein BCL2-associated X protein (BAX) [140] to the mitochondrial outer membrane further induces membrane permeabilization and the release of mitochondrial proteins, eventually leading to severe centrilobular hepatic necrosis [141,142].

Necrosis begins 12 h after APAP overdose, peaks at 36 h [143], and subsides gradually over 60 h [144], whereas hepatocyte proliferation begins at 12 h and peaks at 24-36 h post-APAP administration [144].

C. Genetically-induced liver regeneration

Fumarylacetoacetate hydrolase (FAH) deficiency

The *Fah*$^{-/-}$ mouse is a model of hereditary tyrosinemia type I (HTI), an autosomal recessive disease [145,146]. HTI patients are deficient in the enzyme FAH, the last enzyme in the tyrosine catabolic pathway [147], resulting in accumulation of the toxic metabolites succinylacetone (SA), succinylacetoacetate (SAA), fumarylacetoacetate (FAA), and maleylacetoacetate (MAA) that form DNA adducts [147]. In addition, FAA depletes intracellular GSH stores [148] and triggers cell cycle arrest in G2/M followed by induction of apoptosis [149]. FAA also activates cyclin-dependent kinase 1 (CDK1) and caspase-1 (CASP-1) to induce cell cycle arrest and subsequent expression of CASP-3, resulting in mitochondrial dysfunction as demonstrated by cytochrome c release [149]. FAH is primarily expressed in the liver and kidney [150], and at a lower level in endocrine glands and the gastrointestinal tract [151].

The incidence of tyrosinemia is around 1 in 100,000 to 1 in 120,000 worldwide and is considered a rare disease [152] except for Scandinavia and the province of Quebec, where the overall incidence is 1 in 16,000 [152]. In particular, the Saguenay-Lac-St-Jean area in Quebec has a prevalence of 1/1,846 [153,154] due to a founder effect [155]. To date, more than 35 mutations in FAH have been described [152], including missense mutations leading to 16 amino acid replacements, splice site mutations, and nonsense mutations [156]. Interestingly the pathophysiological phenotype differs between humans and mice, and disease severity also varies greatly between individuals [152].

While an oversimplification, liver phenotypes in HTI patients can be categorized into acute or chronic phases [157]. In the acute phase, morphological alterations can vary greatly and include an enlarged or shrunken liver, fibrosis with ductular proliferation in the surrounding region, and

different degrees of hepatocyte steatosis [158]. The most detrimental phenotype in the acute phase is liver crises, repeated episodes of liver insufficiencies due to liver decompensation, and generally manifests as hepatomegaly and coagulopathy [159]. Liver crises are typically present in early infancy before 2 years of age and historically speaking, around 80% of patients died before the age of 2 due to acute liver failure [159,160]. In the chronic phase, cirrhosis is often observed in HTI patients due to the prolonged hepatic injury [161]. There is also an increased risk of developing HCC in patients beyond 2 years of age, ranging from 15% [162] to 37% [163]. In addition, increased frequency of dysplasia, aneuploidy, and variable gene expression are observed in tyrosinemic livers [164]. The exact mechanism of elevated cancer risk is not completely understood but likely stems from the mutagenic environment in the liver due to the accumulation of reactive metabolites FAA, MAA, SA, and SAA, cultivating a milieu in which aberrant growth factors lead to altered gene and protein expression [164]. HTI patients also exhibit other organ dysfunctions including nephromegaly and renal failure [165], painful paresthesias and motor paralysis [166], and occasionally islet hypertrophy and hypoglycemia [167]. Orthotopic liver transplantation was considered the only curative treatment of HTI in the 1980s with an over 90% survival rate [168,169]. The development of 2-(2-nitro-4-trifluoromethylbenzoyl)-1,3-cyclohexanedione (NTBC) [170] gained widespread popularity as early treatment for HTI prevents HCC and circumvents the need for transplantation [171,172]. NTBC is a potent inhibitor of 4-hydroxyphenylpyruvate dioxygenase (HPPD) [173], the second enzyme in the tyrosine catabolic pathway, and thus prevents the production of the toxic intermediates SAA, SA, MAA, and FAA.

The mouse model of HTI was developed via targeted deletion of the FAH gene [145,146]. *Fah*$^{-/-}$ mice recapitulate the major biochemical and phenotypic alterations observed in HTI patients such as hypertyrosinemia, accumulation of SA, liver failure, renal tubular damage, and occasional tumorigenesis [174]. Interestingly, the *Fah*$^{-/-}$ mouse exhibits a much more severe liver phenotype than HTI patients as mice die within 12 h after birth from fulminant liver failure and hypoglycemia [145], likely attributed to higher levels of toxic metabolites, lower GSH concentrations, and increased sensitivity to FAA, MAA, and SAA in neonatal mice compared to humans [145,175]. *Fah*$^{-}$

$^{/-}$ mice require early treatment with NTBC to survive beyond birth and a portion of FAH-deficient livers still develop tumors despite long-term NTBC administration, possibly resulting from suboptimal NTBC doses or other metabolic pathways that produce FAA and MAA found only in mice [145].

Fah$^{-/-}$ mice undergo liver repopulation by viral- or nonviral-mediated gene therapy to restore FAH function, transplantation with FAH-positive hepatocytes, or genome editing to correct *Fah* mutations. Liver injury is induced upon NTBC withdrawal, and FAH-negative hepatocytes experience inflammation, necrosis, or apoptosis [145,174]. Only hepatocytes with FAH expression are selected *in vivo* to proliferate and repopulate the injured liver parenchyma [176]. Transplantation with wild type hepatocytes revealed the competitive growth advantage of FAH-positive cells to repopulate the mutant liver, as injection of as few as 1,000 hepatocytes successfully rescued the phenotype of FAH deletion, requiring on average an estimated 16 cell doublings to restore liver mass [176]. Liver repopulation can also be carried out through retroviral induction of FAH expression *ex vivo* in *Fah*$^{-/-}$ hepatocytes followed by transplantation of the transduced cells [177]. Gene transfer via retrovirus [176], adenovirus [178], and AAV2 or 8 [179] also results in significant colonization of FAH-expressing hepatocytes. However, 9 out of 13 mice treated with adenovirus developed HCC after 9 months of liver repopulation from untransduced cells that constitute less than 10% of the liver [178]. Additionally, DNA-mediated transposition with the *Sleeping Beauty* (SB) transposable element is able to achieve permanent transgene expression through genomic integration from the plasmid containing FAH complementary DNA (cDNA) following hydrodynamic tail-vein injection [180]. Less than 0.1% of hepatocytes display integration and repopulate the liver to reverse the lethal phenotype after NTBC removal [180]. More recently, the clustered regularly interspaced short palindromic repeats (CRISPR) system has been utilized in *Fah*$^{-/-}$ mice that harbor a point mutation [181]. Expression of single guide RNAs (sgRNA) and a repair template was successful in directing the CRISPR-associated protein 9 (CAS9) nuclease to produce a targeted, double-stranded DNA break followed by homologous recombination to repair the *Fah* gene defect [181].

Since only FAH-positive hepatocytes undergo clonal expansion to repopulate the injured liver, the *Fah*$^{-/-}$ mouse also provides a remarkable tool to lineage-trace regenerating hepatocytes by tracking FAH-expressing cells. Coexpression of markers such as luciferase [182] and GFP [183] can be utilized to specifically trace and isolate repopulating hepatocytes for phenotypic studies. Furthermore, gene-activating or -silencing molecules can be tethered to FAH expression to functionally identify the significance of multiple genes during liver regeneration, including the use of small hairpin RNA (shRNA) [184], cDNA [185], gRNA [186], and tough decoy (TuD) microRNA (miRNA) inhibitors [187]. *Fah*$^{-/-}$ immunodeficient mice are also used to grow billions of human hepatocytes (Azuma et al. 2007).

Urokinase plasminogen activator (uPA) overexpression

uPA is a fibrinolytic enzyme that transforms plasminogen into plasmin to remove fibrin clots [188]. Hepatocyte-specific uPA overexpression regulated under the albumin enhancer and promoter leads to increased plasma uPA levels, fibrinogen depletion, followed by neonatal death within 3 days postpartum due to bleeding of the abdominal cavity and intestinal tract [189]. Hepatocytes that silenced uPA expression, mediated mainly by intrachromosomal recombination, are able to achieve complete regeneration of uPA transgenic mice [190]. Similar to the case in the *Fah*$^{-/-}$ model, loss of transgene expression in individual hepatocytes confers a selective advantage so that clonal expansion of the uPA-normal cells reconstitute the liver parenchyma [190]. The uPA transgenic mice can also be corrected with transplantation of wild-type hepatocytes that undergo an estimation of 12-18 rounds of replication [191]. Furthermore, xenogenic cell transplantation from rat [192] or human [193] hepatocytes can be performed in immunodeficient mice carrying the uPA transgene to generate chimeric livers. The uPA transgenic model, therefore, serves as an excellent paradigm to study liver regeneration after cell transplantation [190,191], drug metabolism in the chimeric human livers [194], and liver diseases including HBV [195] and HCV [193].

D. Models to study HPCs

As introduced above, liver regeneration is carried out by the proliferation of preexisting mature hepatocytes under normal physiological conditions [97]. Only when the replicative ability of resident liver cells is severely hindered, in the case of drug treatment or chronic liver injury, will HPCs be called into action to regenerate the injured parenchyma [89]. One source of HPC is the 'oval cells', small cells with oval nuclei that emerge during chemical hepatocarcinogenesis [89] or hepatotoxin-induced injury in rodents [196]. Since oval cells display intermediary phenotypes and histology between hepatocytes and cholangiocytes, their activation is also referred to as 'ductular reaction' [197]. The origin and contribution of oval cells have long been contested due to the lack of genetic lineage-tracing evidence; thus, the progenitor/descendant relationship was mostly inferred from their spatial proximity to hepatocytes or cholangiocytes [198,199]. Mature hepatic cells are other sources of HPC as hepatocytes and cholangiocytes are able to assume the role of facultative stem cells for one another and transdifferentiate into the other parenchymal cell type.

2-acetylaminofluorene (2-AAF) + PHx

2-AAF is a carcinogen that causes DNA damage and prevents DNA synthesis in hepatocytes, leading to the development of liver cancer [200]. Treatment of dietary 2-AAF for 2 weeks followed by PHx has been used as a model to induce ductular reactions in rats, as hepatocytes are unable to undergo cell replication [201]. Activation of 2-AAF is mediated by N-sulfotransferase to generate the active N-OH 2-AAF radical that translocates into the nucleus to induce DNA damage [202]. However, N-sulfotransferase is not expressed in mice, thus limiting the use of 2-AAF as an inhibitor of DNA synthesis in this species [202]. Interestingly, isotope labeling to track DNA synthesis observed labeled ovals cells but few hepatocytes, indicating that oval cells do not become hepatocytes after AAF-induced liver injury [201]. Another later experiment, however, identified labeled ovals cells and subsequently hepatocytes, establishing a precursor-product relationship between the two cell types during liver regeneration [203]. 2-AAF is also used in

combination with CCl_4 or allyl alcohol in rats to cause centrilobular or periportal damages that induce oval cell activation [204].

3,5-dietoxycarbonyl-1,4-dihydro-collidine (DDC) diet

DDC prevents heme biosynthesis and causes the accumulation of protoporphyrin, leading to severe porphyria and liver injury [205]. Treatment with 0.01% DDC for 2-4 weeks activates a ductular reaction and prolonged treatment results in liver cancer in mice [206]. Currently, there is no consensus on HPC markers in the DDC model but induction of HPC markers including A6 [207], CK19 [208], epithelial cell adhesion molecule (EpCAM) [209], and FOXL1 [210,211] have been reported.

The choline-deficient, ethionine-supplemented (CDE) diet

Another model to induce a ductular reaction is the CDE diet, in which a choline-deficient diet supplemented with 0.05-0.15% (w/v) ethionine mixture in the drinking water is provided to rats [212] or mice [213] for up to 4 weeks. Choline is a lipotropic factor important for the secretion of very-low-density lipoprotein (VLDL) [214]; a deficiency in choline causes intracellular lipid accumulation and hepatocyte membrane rupture, ultimately leading to steatosis followed by cirrhosis [215,216]. When combined with the potent hepatocarcinogen ethionine, activation of oval cells can occur followed by induction of liver cancer [212].

III. Mechanisms of liver regeneration

The majority of mature hepatocytes reside in the reversible, nonreplicative G0 phase under homeostasis [28]. Upon injury, liver cells re-enter the cell cycle and progress through G1, S (DNA synthesis), G2, and M (mitosis) phases. The cell cycle is tightly-controlled by cyclin proteins, in which the levels rise and fall to activate downstream target CDKs that control progression through various cell cycle checkpoints (Figure 1.2) [217,218]. The cyclin D-CDK4/CDK6 complex is the first to be detected followed by cyclin E-CDK2 formation to promote G1/S transition [219–221]. Next,

cyclin A-CDK1/CDK2 is activated to regulate S phase along with cyclin B-CDK1 assembly to modulate G2/M entry [222,223]. Regenerating hepatocytes are highly synchronous in the PHx model [224], whereas in other paradigms, hepatocytes traverse the cell cycle in a non-synchronous order [95]. While most studies regarding the mechanisms underlying liver regeneration are conducted in the PHx model due to its popularity, numerous signaling pathways have been shown to be important for other models as well. Regardless of the source of injury, liver regeneration is composed of three distinct phases, the initial 'priming' phase where hepatocytes acquire an enhanced ability to replicate [225], the second 'progression' phase that allows hepatocytes to proceed through the cell cycle to recreate an adequate cell number and mass [226–228], and the final 'termination' phase where liver cell proliferation is stopped once liver mass has returned to normal [86,228,229].

A. Priming

The priming phase is the initiating event in which terminally-differentiated hepatocytes acquire enhanced replicative ability that allows for the transition from a quiescent state (G0) to a competent state (G1) [225,226]. Cytokines released from non-parenchymal cells in the liver act as paracrine factors to promote signaling pathways in hepatocytes [228]; TNFα [230,231] and IL6 [232] are essential cytokines secreted by Kupffer cells in the early signaling phase. Pretreatment with TNFα increases the proliferative response to growth factors in rats [233], while administration of TNFα antibodies [231] as well as deletion of type I TNFα receptor (TNFR1) [234] inhibits DNA replication and impairs liver regeneration. TNFα activates nuclear factor kappa B (NF-κB) both in Kupffer cells to increase IL6 transcription [234] and in hepatocytes to activate cell proliferation [235].

IL6 is a proinflammatory cytokine that mediates the acute-phase response [236]. During the initial phase of liver injury and repopulation, IL6 is secreted from Kupffer cells due to stimulation by TNFα [231,234]. IL6 binds to its receptor glycoprotein 130 (gp130) [237] to activate transcription factors, usually within the first hour of PHx, including NF-κB, activator protein 1 (AP-1), signal transducers and activators of transcription 3 (STAT3), and CCAAT enhancer-binding protein β

(C/EBPβ), ultimately leading to the expression of immediate-early genes such as *Jun*, *Fos*, and *Myc* [238,239]. Later studies identified induction of as many as 73 immediate-early genes during the priming phase [240] and another study reported that almost 40% of immediate-early genes are induced via IL6 [241]. Deletion of IL6 leads to a decrease of immediate-early gene expression followed by a 70% reduction of DNA synthesis [232].

The importance of TNFα and IL6 as priming factors can be replicated in other regeneration paradigms including I/R injury [242], CCl_4 [243,244], and APAP hepatotoxicity [245,246], in which downstream activation of pathways including NF-κB and STAT3 induces expression of immediate-early genes to promote cell cycle entry. Nonetheless, controversies regarding the role of cytokines during the priming phase arise when conflicting results were found. TNFα-deficient mice do not exhibit reduced DNA synthesis or delayed regeneration after PHx [247,248]. Similarly, studies utilizing IL6- or gp130-deleted mice have demonstrated that IL6 does not mediate cell cycle entry but activates adaptive responses and apoptosis to fine-tune the regenerative process [237,249,250].

B. Progression

Hepatocytes acquire proliferative competence after priming and transition from G1 to S phase [226–228]. Commitment to progress through the cell cycle is mediated through early G1 exposure to growth factors including epidermal growth factor (EGF) [251], TGFα [252,253], and HGF [254]. These factors are also known as ‘direct mitogens’ due to their ability to independently induce cell growth in cultured hepatocytes. Furthermore, infusion or overexpression of EGF [255], HGF [256], or TGFα [257] triggers hepatocyte proliferation and liver enlargement in normal rats. Both HGF and EGF stimulate liver regeneration as paracrine factors [258,259], while TGFα promotes hepatocyte replication in an autocrine fashion [253].

HGF is produced primarily by stellate cells [260], activated by urokinase [261], and released from the extracellular matrix during liver regeneration [259]. Plasma levels of HGF are increased by 20-fold as early as 1 h after PHx in rats [262]. HGF binds to the receptor tyrosine

kinase HGF receptor (MET) [263] to induce TGFα synthesis in hepatocytes [264], as well as to stimulate proliferation and survival pathways such as mitogen-activated protein kinase (MAPK) and phosphoinositide 3-kinase (PI3K) signaling directly, leading to the activation of transcription factors ETS domain-containing protein (ELK1), MYC, and C/EBPβ [265,266]. Inhibition of HGF activation, including deletion of urokinase [267], administration of an anti-HGF antibody [268], and conditional disruption of *Met* [269,270] causes an impaired regenerative response after PHx and hepatotoxin-induced liver injury.

EGF is produced by the Brunner's gland in the duodenum [271] and continuously supplied to the liver through the portal circulation [258]. Interestingly, no significant change in plasma EGF concentration was detected after PHx [258], with another study suggesting activation of the sympathetic system could increase EGF production via norepinephrine [272]. Alternatively, the removal of two-thirds of the liver mass has been suggested to increase the load of EGF per hepatocyte by 3-fold [86,229].

TGFα is released from the hepatocyte plasma membrane by the TNFα-converting enzyme (TACE) that is activated through secreted TNFα during the priming phase [273]. The transcript level of TGFα increases after 2-3 h, peaks at 12-24 h, and persists for 48 h post-PHx [253]. Both EGF and TGFα activate the receptor tyrosine kinase EGF receptor (EGFR) [274] to induce proliferation and prevent apoptosis via activation of MAPK, PI3K, and STAT pathways [265,266,275]. Treatment with antisense oligonucleotides and antibodies against TGFα reduces the number of replicating hepatocytes [264,276]. However, the redundancy of EGFR ligands has made it difficult to definitively demonstrate the requirement of EGF and TGFα for regeneration. *Tgfa*$^{-/-}$ mice do not show a significant decrease in DNA synthesis or a delay in regeneration after PHx [277], possibly due to EGF compensation. However, mice with targeted EGFR deletion display a delayed G1 to S phase transition and a decreased expression of cyclin D1 after PHx [278], documenting the importance of EGFR signaling during the progression phase.

C. Termination

After cell growth and proliferation to restore the loss parenchyma are complete, liver regeneration stops through the activation of termination signals. Most research has focused on the mechanisms that induce hepatocyte replication and less is understood about the termination process. Additionally, the connections between the termination of liver regeneration and the pathogenesis of liver cancer have equally attracted attention.

TGFβ is the most well-known factor to repress hepatocyte proliferation. Produced by stellate cells [279], TGFβ is normally sequestered in the extracellular matrix [280]. Many mechanisms are implicated to release TGFβ during liver regeneration, but no direct evidence has been provided [281], suggesting multiple factors could be at play to exert the tight regulation of TGFβ localization. TGFβ mRNA is increased within 3-4 h and peaks at 48-72 h after PHx in rats [282]. Contrarily, all three TGFβ receptor subtypes are downregulated at the transcript and protein levels following PHx and only recover at 120 h [283], causing a decreased TGFβ sensitivity in regenerating hepatocytes isolated after 24-72 h post-PHx [284]. Resistance towards TGFβ via norepinephrine modulation could explain the observation that hepatocytes are able to continue DNA synthesis until 72 h post-PHx despite increased TGFβ levels [285]. Cascades of the 'small mothers against decapentaplegic' (SMAD) proteins are activated upon TGFβ receptor phosphorylation [286,287] to increase expression of CDK inhibitor p15 [288] and prevent assembly of cyclins and CDK complexes, including cyclin E-CDK2 [289,290] and cyclin D-CDK4 [290], leading to reversible cell cycle arrest at G1 [289]. TGFβ is a potent inhibitor of EGF-induced DNA synthesis in cultured rat hepatocytes [291], and infusion of TGFβ reversibly prevents hepatocyte replication by over 60% at 24 h that returns to normal by 72 h after PHx in rats [292]. Conflicting studies, however, have questioned the significance of TGFβ as a termination factor. Overexpression of TGFβ1 under control by the albumin promoter causes hepatic fibrosis due to collagen deposition but does not affect liver regeneration [293]. Similarly, conditional removal of the TGFβ type II receptor increases cyclin D and E expression, allowing accelerated S phase entry to enhance hepatocyte proliferation, but no effect on the termination of regeneration was observed

[294]. Activin, another member of the TGFβ family, is also implicated in the termination phase as an autocrine agent that inhibits DNA replication, as its pharmacological inhibition with follistatin promotes DNA synthesis and leads to hepatomegaly following PHx in rats [295,296].

C/EBPα is a hepatocyte-enriched transcription factor that regulates the expression of multiple liver-specific genes [297,298]. C/EBPα is transcriptionally regulated during liver regeneration with a decrease in gene expression by 60-80% 1-3 h [299] and remains repressed until 24 h after PHx [300]. The drop of *Cebpa* transcripts during hepatocyte replication echoes previous observations of its antiproliferative quality in terminally-differentiated adipocytes [301]. C/EBPα induces cell-cycle arrest through various pathways including stabilization of the CDK inhibitor p21 to disrupt formation of cyclin-CDK complexes [302,303], modulation of growth-inhibiting E2F-RB complexes [304,305], direct inhibition of CDK2 and CDK4 [306], induction of proteasome-dependent degradation of CDK4 [307], and others [308]. *Cebpa*$^{-/-}$ hepatocytes exhibit increased DNA synthesis in culture and rapidly form proliferative nodules when inoculated into mice [309]. Similarly, *Cebpa*$^{-/-}$ mice display elevated transcript levels of *Jun* and *Myc*, as well as an increased hepatocyte proliferation [310].

Another important regulator of liver mass is the Hippo pathway, named after the *Drosophila hippo* gene, which encodes a kinase that regulates organ growth, cell proliferation, and developmental apoptosis [311,312]. The mammalian orthologs ‘mammalian sterile 20-like 1’ (MST1) and 2 kinases [311] activate the large tumor suppressor 1 (LATS1) and 2 proteins to phosphorylate and inhibit the activity of the transcriptional coactivator yes-associated protein (YAP), leading to its nuclear export and protein degradation [313,314]. The Hippo signaling pathway is altered after PHx, with increased nuclear localization of YAP by 4 h [315] and decreased kinase activity of MST1 and MST2 1-3 days post-PHx [316]. Upon activation, YAP increases the expression of genes involved in hepatocyte proliferation such as *Ki67*, *Myc*, and *H19* [313]. Conditional YAP activation induces liver overgrowth by over 50% after 1 week, and persistent YAP elevation causes tumorigenesis [313,317]. Similarly, deletion of MST1 and MST2 in mouse livers leads to loss of YAP phosphorylation and nuclear retention, followed by hepatomegaly and HCC

[318]. The mechanism of YAP inactivation at the end of liver regeneration is not fully understood but is hypothesized to include regulation by components of the extracellular matrix such as integrin-linked kinase (ILK) [319,320] and glypican-3 [321,322] to prevent nuclear localization of YAP in both PHx and toxin-induced liver injury.

D. Other factors to consider

Liver regeneration depends on a complex regulatory network that includes multiple additional soluble mediators, signaling pathways, and transcription factors not discussed above. (1) Growth factors including vascular endothelial growth factor (VEGF) [323,324], platelet-derived growth factor (PDGF) [325,326], FGF [327,328], and heparin-binding EGF-like growth factor (HB-EGF) [329]. (2) Extracellular signals such as bile acids [330], serotonin [331], insulin [332,333], norepinephrine [334,335], complement [336], and CXC chemokines [337,338]. (3) Pathways such as Wnt/β-catenin [339,340] and Notch/Jagged [341] signaling. (4) Growth-promoting nuclear receptors including [342] retinoid X receptor (RXR) [343], PPARα [344,345], farnesoid X receptor (FXR) [330], and pregnane X receptor (PXR) [346]. (5) Growth-inhibiting nuclear receptors [342] such as PPARγ [347,348] and HNF4α [349]. (6) Other factors such as microRNAs [350].

These signaling pathways have been implicated in multiple liver regeneration models and manipulation of the pathways generally shows consistent outcomes across various paradigms with some exceptions. For instance, CXC chemokines promote regeneration after PHx [337] but inhibit hepatocyte proliferation during I/R [351]. This could be due to the difference in CXC concentration — 10 times higher following I/R — suggesting that a moderate increase of CXC chemokines promotes but higher expression inhibits hepatocyte proliferation [352]. Another example is TNFα signaling, in which TNFR1 deletion prevents DNA synthesis and delays liver regeneration after PHx [353], but an overexpression cDNA screen identified TNFR1 to be a potent repressor of liver repopulation in the *Fah*$^{-/-}$ mouse [185]. The difference in TNFR1 expression levels, TNFα signaling activation, injury duration, or the inflammatory context could explain the divergent findings [185]. Finally, it is also worth noting that no single gene deletion results in complete abrogation of the

regenerative process, but at most causes a reduction of replicating hepatocytes and a delay of cell cycle progression, suggesting substantial redundancy of the diverse signaling pathways modulating liver regrowth [354].

IV. Source of regenerating hepatocytes

Regenerating hepatocytes can arise from three main sources in a context-dependent manner: expansion of preexisting hepatocytes, differentiation of oval cells, or transdifferentiation from cholangiocytes. As discussed above, resident hepatocytes are the first responders to replenish the hepatocyte pool but oval cells and cholangiocytes have been suggested more than sixty years ago as contributors of liver regeneration when DNA synthesis is severely impaired in hepatocytes. During the past decade, several lineage-tracing studies in mice have attempted to qualify the contribution of various proposed progenitor cells to hepatocyte regeneration. Using the *Sox9*^{CreERT2} system to trace all cholangiocytes, 1-2% of regenerating hepatocytes were lineage-labeled after CCl_4, APAP, and DDC administration, indicating that only a small percentage of BECs contribute to liver regeneration under these settings [30,34]. A similar conclusion was drawn when oval cells are labeled with osteopontin (OPN) after CDE diet but not with CCl_4 or DDC treatment [355]. Other studies have suggested that FOXL1-expressing HPCs give rise to hepatocytes after a DDC-supplemented diet [211], or that LGR5-positive organoids can repopulate *Fah*$^{-/-}$ mouse livers after transplantation [356]. Interestingly, using a *Krt19*^{CreERT2} system in conjunction with DDC or CDE treatment, no label-bearing hepatocytes arise after regeneration, suggesting that all new hepatocytes come from preexisting liver cells [357]. This was likely due to limited injury which did not completely block hepatocyte proliferation, thus deviating the need for replacement from cholangiocytes acting as facultative progenitors. However, when hepatocyte regeneration is completely abrogated by severe liver injury, inhibition of hepatocyte replication, or induction of hepatocyte senescence, a large contribution of cholangiocyte-derived hepatocytes to the regenerating liver has been documented [358–360]. As it turns out, mouse hepatocytes are more resilient than those from rats in terms of retaining proliferative potential in the face of liver injury,

possibly explaining some of the discrepancies in the literature regarding the importance of cholangiocytes and oval cells as facultative hepatocyte.

V. Clinical implications

To date, the only curative treatment for end-stage liver disease is liver transplant. While it is the second most common solid organ transplantation after kidney transplant, less than 10% of global liver transplantation needs are met at current rates [37]. Multiple strategies under active research for the treatment of liver disease [361,362] include (1) transplantation of primary hepatocytes or induced pluripotent stem cells (iPSCs), (2) induction of endogenous hepatocyte replication via pharmacological agents, cytokines, or growth factors, (3) bioartificial livers that incorporate hepatocytes into a dialysis-based artificial system to carry out the main metabolic functions of the liver, and (4) organ bioengineering that utilizes a xenogenic scaffold infused with mature hepatocytes to produce a functional liver graft. With the rising healthcare burden of chronic liver disease, a deeper understanding of the mechanisms underlying liver repair and regrowth will enable a broader utilization of regenerative medicine.

LIVER TRANSCRIPTIONAL CONTROL

I. Overview

Gene regulation is fundamental for all organisms; in particular, the complexity of eukaryotic transcriptional control allows intricate regulation of expression patterns to adapt to environmental queues. Transcriptional regulation occurs on several levels. (1) *Cis*-regulatory modules provide essential information for transcription factor binding and serve as a platform for the assembly of regulatory complexes. (2) Chromatin architecture including nucleosome patterning, histone modification, and DNA methylation impacts the accessibility of the transcriptional machinery. (3) Intra- and interchromosomal interactions establish topological hotspots for long-range regulation of gene expression [363].

A. Transcription factors

Transcription factors are *trans*-acting proteins that bind to *cis*-regulatory modules at the promoter or enhancer to activate or repress transcription [364]. Regulation of gene expression is achieved through various mechanisms including stabilization or blockade of RNA polymerase II [365], direct or indirect modification of chromatin structure [366], and recruitment of coactivator or corepressor proteins to the protein-DNA complex [367]. Recruitment of transcription factors to target sites is established mainly through the structure and sequence of the DNA-binding domains [363]. Evolutionarily-related transcription factors often share similar DNA recognition motifs and demonstrate binding redundancy. The specificity of transcription factors is determined by (1) cooperative or competitive binding with other regulatory proteins [368,369], (2) flexibility of the DNA-binding domain to recognize noncanonical motifs with mechanisms not yet clear [370], and (3) posttranslational modifications to affect subcellular localization, protein-protein interactions, and DNA binding activity of the transcription factors [371]. These mechanisms allow spatiotemporal binding of transcription factors to fine-tune eukaryotic gene transcription and establish distinct gene expression patterns.

B. Chromatin architecture

DNA is compacted into chromatin in the eukaryotic genome. The basic unit of chromatin is the nucleosome, which consists of 147 base pairs (bp) of DNA tightly wrapped around a histone octamer with two copies of core histones H2A, H2B, H3, and H4 each [372]. Chromatin is historically categorized into one of two states based on its accessibility to the transcriptional machinery. Heterochromatin is highly condensed, transcriptionally inactive, and associates with repressive histone modifications, whereas euchromatin is relatively accessible to transcriptional complexes, marked with active histone modifications, and contains actively-transcribed genes [373,374]. Diverse mechanisms contribute to the modification of chromatin structure and subsequent changes to DNA accessibility, including nucleosome positioning and occupancy via ATP-dependent chromatin remodelers [375,376], DNA methylation through DNA methyltransferases (DNMT) and demethylation via ten-eleven translocation (TET) proteins [377], and epigenetic modifications of the core histones such as methylation, acetylation, phosphorylation, and ubiquitination [378].

C. Three-dimensional structure

The three-dimensional structure of chromatin provides an additional layer of transcriptional control through the regulation of nuclear organization and chromosomal interactions.

(1) Nuclear organization. The nucleus is divided into functional domains in which chromosomes occupancy at different regions is associated with divergent transcriptional activity [379]. The non-uniform compartment of the nuclear interior enables highly-organized structures to establish chromatin territories based on gene activity and density; gene-rich regions are typically located in the nuclear center and gene-poor chromatin in the periphery [380].

(2) Chromosomal interactions. The identification of *cis*-regulatory modules located far from the promoters they regulate has led to the discovery of looping as the predominant mechanism for enhancer-promoter interactions [381]. Long-range chromatin communication includes interactions between regulatory sequences of a single locus [382], among elements within a gene complex

[383], and between chromosomes [384]. Technological advances utilizing proximity-ligation followed by deep-sequencing [385] and high-resolution microscopy [386] methods will further allow the elucidation of inter- and intrachromosomal interactions to establish cell type-specific transcriptional regulation.

II. Discovery of liver transcriptional control

A. Liver-specific gene expression

Studies on transcriptional control were pioneered by the laboratory of James Darnell starting in the early 1980s [387]. Rat liver nuclei became one of the first mammalian systems used to investigate gene expression regulation due to the large number of available cells and the relatively pure cell types, where hepatocytes constitute approximately 80% of the liver mass [388] and 60% of liver cell number [389]. Liver-specific gene sequences were isolated via the extraction of polyadenylated (poly(A)) RNA, reverse transcription into cDNA, and recombination with antibiotic-resistant *E. coli* plasmids [390]. DNA from individual colonies was used as a template to hybridize with nascent, radiolabeled mRNA isolated from rat liver nuclei [390]. The hybridization signals from liver nuclear RNA is at least 10 times stronger than those from non-liver cells, suggesting a differential abundance of tissue-specific mRNA [390]. Further analysis to compare the transcription rate of liver-enriched mRNA in liver and brain nuclei revealed that transcriptional regulation plays a primary role in establishing differential gene expression in various terminally-differentiated cell types [390].

B. Liver-specific regulatory regions

Analysis of liver-enriched genes in human and rodent ensued, unveiling tissue-specific regulatory regions including proximal promoters and distal enhancers that control the expression of cell type-specific genes. For instance, the 5' flanking sequences of rat *Alb* drives efficient expression of a reporter gene, chloramphenicol acetyltransferase, preferentially in ALB-expressing hepatoma cells [391]. The promoter-proximal region of human *SERPINA1* that encodes the α1-

antitrypsin (AAT) enzyme is sufficient for the transcription in Hep3B, a human hepatoma cell line, but not in HeLa cells [392]. Similarly, expression of distal enhancers of the mouse *Ttr*, encoding transthyretin (TTR), activates β-globulin transcription specifically in human hepatoma cells HepG2 but not in HeLa cells [393]. These observations suggest a combination of *cis*-regulatory sequences and *trans*-acting factors in particular cell types establishes tissue-specific expression regulation.

In addition, two hypotheses concerning cell type-specific transcriptional control through *trans*-acting proteins emerged [392,394]. It was proposed that activating factors expressed only in particular tissues govern gene expression. However, some liver-enriched genes are also expressed in other cell types, such as *Serpina1* in macrophages [395], certain apolipoproteins in the gut [396]*, and Ttr* in the choroid plexus [397]. This implicates that the activating mechanism in addition to the distribution of the activating factors exhibits liver specificity [394]. Furthermore, it was later shown that most, if not all, so-called 'liver-specific' transcription factors are also expressed in other cell types [398–401]. Another line of hypothesis suggested the presence of inhibiting factors to prevent gene expression in specific tissues [392,394]. This implies that a repressor is required for each gene to be not expressed in a certain cell type, suggesting a requirement for a large number of negative factors to restrict transcription in non-expressing tissues. Thus, a more plausible explanation of tissue-specific transcriptional control is that a unique combination of several liver-enriched positive and negative *trans*-acting factors modulate expression in a cell type-specific manner [402]. Various liver-enriched, but not necessarily liver-specific, activators induce expression [402,403] and repressors inhibit transcription to establish a liver-specific gene expression profile [404].

C. Liver-specific transcription factors

From the late 1980s to 1990s, the use of DNA sequence affinity chromatography with rat liver nuclear extracts enabled identification of several transcription factors highly expressed in the liver, collectively referred to as hepatocyte nuclear factors [398,403,405,406]. DNA sequences of liver-enriched genes suspected to encompass transcription factor binding sites were used as bait

to isolate protein-DNA complexes followed by high-performance liquid chromatography (HPLC) to purify the protein of interest. The partial amino acid sequences of the protein peptides were determined and used to design primers for PCR amplification from hepatoma cell lines. The amplified products were then used to screen rat cDNA libraries to obtain clones that encode the gene sequence of each liver-enriched transcription factor.

III. Hepatocyte nuclear factors

A. HNF1

HNF1 was identified as a nuclear protein that binds to the promoters of fibrinogen α and β chains, as well as AAT in hepatocytes [405]. The HNF1 subfamily contains two isoforms, HNF1α and HNF1β. Analysis of the ALB promoter established the requirement of the albumin proximal factor (APF), later found to be HNF1α, for *Alb* transcription [407]. HNF1α was initially only detected in differentiated rat hepatoma cells whereas HNF1β, originally identified as modified APF (vAPF), was observed in two dedifferentiated rat hepatoma cell lines [407]. Later studies confirmed expression of HNF1α and HNF1β in the liver, pancreas, intestine, and kidney [399,408], with HNF1α detected at much higher levels and HNF1β lower except for in the kidney [409,410]. HNF1β could exhibit broader physiological implications as it is also observed in the lung, testis, and ovary [401,411].

HNF1 is a member of the POU homeobox gene family [412]. The N-terminal contains the dimerization domain that allows the homeoproteins to dimerize [409], the DNA-binding domain consists of a bipartite POU homeodomain [412], and the C-terminal includes different transactivation domains less conserved within the subfamily, in which HNF1α demonstrates a higher transactivation potency than that of HNF1β [413]. Analysis of the promoters of various liver-enriched genes from rat, mouse, and human predicted the HNF1 consensus binding sequence as GTTAATNATTAAC [414]; both isoforms share the same DNA-binding motif with different transcriptional activity [415]. The homeoproteins form homo- and heterodimers within the subfamily [409,410], where HNF1α is able to dimerize without binding to the DNA recognition sequence.

Additionally, a dimerization cofactor of HNF1α, DCoH, selectively stabilizes the homodimers and assembles a tetrameric complex to enhance the *trans*-activating ability of HNF1α [416].

Sequence homology analysis determined additional HNF1α target genes including *Alb* [407], *Ttr* [414], *Afp* [414,417], *Apoa2* that produces apolipoprotein A-II (ApoA-II) [418], and *Apob*, encoding the protein ApoB-100 [419]. Genome-wide analysis of HNF1α footprinting with chromatin immunoprecipitation (ChIP) followed by high-throughput sequencing (ChIP-seq) further identified HNF1α targets crucial for liver synthetic functions, such as carbohydrates, cholesterol, apolipoproteins, CYP450, and serum proteins [420]. Similar to HNF1α, HNF1β occupies the *Alb* proximal promoter to activate transcription [409]. Additional HNF1β targets determined through loss of HNF1β include *Slco1a1* that encodes the member 1a1 of the solute carrier organic anion transporter family (OATP-1) for bile acid reabsorption, and *Acadvl*, the very long-chain-acyl-Coenzyme A dehydrogenase (VCLAD) required for fatty acid oxidation [421].

During development, HNF1β is first detected on E4.5 in the endoderm of the foregut, while HNF1α expression is activated later on E8.5 in the yolk sac [422]. HNF1α and HNF1β are also present on E10.5 after the initiation of hepatocyte lineage in the liver primordia and continue to be expressed throughout embryonic development [423]. These observations suggest that HNF1β participates in the initial transcriptional activation of genes in the visceral endoderm, and the later activation of HNF1α could be required to maintain target gene expression for liver function [422]. *Hnf1a* transcript levels gradually decrease at the late period of embryonic liver development while *Hnf1b* increases [424].

Hnf1a$^{-/-}$ mice die around weaning due to hepatic dysfunction, phenylketonuria, and renal Fanconi syndrome [425]. HNF1α-deficient livers are enlarged with decreased *Alb* expression but a compensatory increase of HNF1β partially rescues the expression of ALB, AAT, and fibrinogen [425]. Since HNF1α deletion is not embryonically lethal, it is likely not required for specification of the hepatocyte cell lineage but important for the expression of differentiated liver function genes.

HNF1β-deficient mice die by E7.5 due to the lack of extraembryonic endoderm development [426]. *Hnf1b*$^{-/-}$ tetraploid complementation established that HNF1β activity is required

for visceral endoderm differentiation to direct the expression of HNF4 and other endoderm marker genes [408]. Further tetraploid embryo complement analysis showed that *Hnf1b*$^{-/-}$ mice do not form the hepatic bud and lack expression of liver-enriched genes [427]. Conditional HNF1β ablation using the *Hnf1b*$^{F/F}$;*Alfp*^{Cre} mouse causes abnormal gallbladder and intrahepatic bile duct formation, resulting in severe growth retardation and jaundice; liver metabolism was also affected, with downregulation of genes involved in bile acid sensing and fatty acid oxidation [421]. These studies implicate that HNF1β is required for endoderm commitment, hepatic specification, and bile duct morphogenesis during liver organogenesis.

Altogether, HNF1 proteins are important in establishing mature hepatic functions and appropriate bile duct differentiation. Interestingly, heterozygous human HNF1 mutations do not cause abnormalities in the liver but rather dysfunctions of the pancreatic islets; HNF1α mutations lead to autosomal dominant maturity-onset diabetes of the young type 3 (MODY3) [428] and HNF1β mutations result in MODY5 [429].

B. HNF3/FOXA3

HNF3 proteins were described due to their ability to occupy TTR and AAT promoters at sites distinct from HNF1 and C/EBP [403]. *Ttr* contains two recognition sequences for HNF3 within 150 bp upstream of the transcriptional start site. Mutation of the most 3' HNF3 binding site results in decreased *Ttr* expression, despite all other enhancer and promoter sequences being intact, indicating the importance of HNF3 for *Ttr* transcriptional activation [403]. The HNF3 family consists of three members identified from the purification of distinct protein-DNA complexes that bind to the mouse *Ttr* promoter, HNF3α, 3β, and 3γ [430–432]. The DNA-binding domains of all three members are highly conserved and share 90% amino acid similarity that matches the sequences of the *Drosophila* Fox nuclear protein [433]. Therefore, HNF3 proteins were renamed according to the nomenclature of all forkhead transcription factors to 'FOXA' [434]. The FOXA proteins are functionally redundant in the liver [435], of which FOXA3 exhibits the highest expression in adult hepatocytes [436].

FOXA proteins are members of the FOX family [430] and belong to the FOXA subfamily [434]. The forkhead box DNA binding domain is comprised of three α-helices flanked by two winged-like loops, thus the DNA recognition sequence is also referred to as the winged-helix domain [437]. All FOXA proteins share up to 95% sequence similarity in the DNA binding domain flanked by the nuclear localization sequence [438]. Outside of the FOX domain, the N and C termini also demonstrate high sequence conservation, and functional analysis of FOXA2 revealed their activity as transcriptional activators [432,438]. Within these domains, regions II, III, and IV contribute to transactivation, where the activity of region IV is dependent on the other two [432]. Analysis of FOXA binding sites in *Ttr* and *Serpina1* regulatory regions indicated the consensus sequence as TATTAGAYTTWG, where Y is C/T and W is A/T [403]. FOXA proteins bind to DNA as monomers [439].

Other hepatocyte-specific genes regulated by FOXA proteins include the *Alb* enhancer [404] and promoter [440], the *Afp* distal enhancer [441], the *Apob* promoter [442], and the *Pfkfb1* proximal promoter that controls the expression of 6-phosphofructo-2-kinase/fructose-2,6-bisphosphatase 1 (PFK/FBPase 1) [443]. Furthermore, the structure of the winged-helix domain is similar to that of linker histones H1 and H5, proteins that induce DNA compaction with the nucleosome core to repress gene expression [437]. FOXA proteins are able to bind DNA on the nucleosome core to displace linker histones and increase chromatin accessibility, leading to transcriptional activation [444]; hence, FOXA proteins are also known as ‘pioneer factors’.

FOXA2 is expressed on E6.5 in the node at the anterior primitive streak and is the first member of the FOXA subfamily to be expressed [445]. Its expression persists throughout the development of endoderm-derived tissues such as the liver, pancreas, and the intestine, and continues into adulthood [445]. FOXA1 displays a similar expression pattern as that of FOXA2 but is detected later on E7.0 in the primitive endoderm, whereas FOXA3 is expressed starting on E8.5 during hindgut differentiation [445].

Foxa1$^{-/-}$ embryos develop to term but have severe postnatal growth retardation and die between postnatal day 2 (P2) to P12 [446]. FOXA1-deficient mice experience hypoglycemia and

changes in islet glucagon gene expression, but no liver phenotype is observed prior to death [446], suggesting that FOXA1 is not required for early mouse development but is central to the regulation of glucose homeostasis.

FOXA2 deletion is embryonically lethal by E11 due to the lack of node and notochord formation, causing death prior to the formation of liver bud [447,448]. Conditional FOXA2 ablation with the *Foxa2*$^{F/F}$;*Alb*^{Cre} mouse does not induce any significant disruption of the liver phenotype or cause apparent changes in gene expression, indicating that FOXA2 is dispensable in maintaining hepatocytes at a differentiated state [435]. However, *Foxa2*$^{F/F}$;*Alfp*^{Cre} livers fail to integrate transcriptional response during prolonged fasting since expression of gluconeogenic enzymes typically activated during fasting is not induced, as seen in the cases of *Pck1* that encodes the cytosolic phosphoenolpyruvate carboxykinase (PEPCK-C), *Tat* that produces tyrosine aminotransferase (TAT), and *Igfbp1*, encoding insulin-like growth factor-binding protein 1 (IGFBP-1) [449]. Whole-body FOXA1 deletion and endoderm-specific ablation of FOXA2 with the *Foxa1*$^{-/-}$;*Foxa2*$^{F/F}$;*Foxa3*^{Cre} mouse showed a lack of liver bud formation and loss of hepatoblast marker *Afp*, indicating that FOXA1 and 2 are required for hepatognesis during embryonic development [22]. Furthermore, combinatorial deletion of FOXA1 and 2 in the liver through *Foxa1*$^{F/F}$;*Foxa2*$^{F/F}$;*Alfp*^{Cre} mice causes bile duct expansion and proliferation, leading to biliary tree hyperplasia while liver differentiation is unaffected [450]. In short, these studies indicate that FOXA2 is required for early embryonic development prior to liver differentiation as well as bile duct maintenance, and FOXA1 and 2 are essential for liver bud specification.

FOXA3 ablation results in a 50-70% decrease in the expression of several hepatocyte-specific genes, including *Pck1*, *Tat*, and *Tf* (*Trf*) that encodes transferrin along with a compensatory increase of FOXA1 and 2 [451]. Additionally, *Foxa3*$^{-/-}$ mice exhibit hypoglycemia after prolonged fasting that associates with a decreased liver expression of *Slc2a2* (*Glut2*), encoding the type 2 glucose transporter (GLUT-2) [452]. While FOXA3 deletion is not sufficient to cause severe liver function defects, it is required for mediating fasting glucose homeostasis.

During the acute phase after PHx, *Foxa1* expression is dramatically decreased followed by the downregulation of its target gene *Ttr*, whereas *Foxa3* level fluctuates minimally, suggesting that FOXA1, but not 3, is regulated by proliferative signals during liver regeneration [453]. On the other hand, both *Foxa2* and *Foxa3* expression are significantly reduced in CCl_4-induced liver injury [454,455]. Furthermore, injection of AAV8-TBG-Cre into *Foxa2*$^{F/F}$ mice exacerbates CCl_4-induced liver fibrosis while FOXA2 overexpression alleviates collagen deposition and reduces ER stress, indicating the hepatoprotective potential of FOXA2 during liver injury [455].

C. HNF4

HNF4 was identified as a nuclear protein with distinct recognition properties from C/EBP, HNF1, and FOXA in its binding to the promoters of TTR and AAT [403]. HNF4 proteins include three isoforms, HNF4α, 4β, and 4γ, but HNF4β is not detected in human or mouse [456]. HNF4α is expressed in the liver, kidney, pancreas, small intestine, colon, and testis [400], while HNF4γ is observed in all tissues mentioned above except for the liver [400]. HNF4α is transcriptionally regulated through two developmentally-controlled promoters P1 and P2 that are separated by more than 45 kilobases (kb) [457]. Differential promoter usage combined with alternative splicing produces six P1 isoforms, HNF4α1 to α6, and three P2 isoforms, HNFα7 to α12 [400,457,458]. However, the impact of HNF4α isoforms on the transcriptional control of downstream targets remains largely unknown.

HNF4 belongs to the nuclear hormone receptor superfamily that includes receptors for steroids, retinoids, thyroid hormones, and vitamin D [459,460]. Originally classified as an orphan member of the superfamily due to the lack of defined ligands, it was later observed that fatty acyl-CoA thioesters modulate HNF4 activity [461] and linoleic acid acts as the endogenous HNF4α ligand [462]. HNF4α displays the conventional modular structure of nuclear receptors that encompasses six functional regions A-F [460]. The N terminal contains the less conserved A/B region with the activation function 1 (AF-1) domain that acts as a constitutive autonomous transactivator [463]. Region C encodes the highly-conserved DNA-binding domain with two zinc

fingers [459] and is responsible for dimerization on the DNA [464]. Region D refers to a hinge that connects regions C and E [460], in which region E represents a conserved ligand-binding domain that contributes to protein dimerization in the absence of DNA binding [464]. The ligand-binding domain also prevents heterodimerization with RXRα and potentially other nuclear receptors that share similar DNA recognition sequences [465]. Additionally, region E consists of a second activation domain AF-2 with ligand-dependent transcriptional activity, providing an additional layer of HNF4α regulation [463]. Region F is located at the C-terminus and contains a unique repressive feature of the nuclear receptor superfamily to inhibit AF-2 [463]. Together, AF-1 and AF-2 activate transcription in a cell type-independent manner [463]. All HNF4α isoforms share the same DNA-binding domain and 90% of protein structure homology. The main difference between P1 and P2 classes is the lack of AF-1 at the N-terminus in P2 isoforms [466]. Finally, the zinc finger motifs bind to the hormone response elements located in promoters exclusively as homodimers to modulate transcription of HNF4α target genes [464,467].

Initial analysis of the HNF4 binding sites at regulatory regions of *Ttr*, *Serpina1*, and *Apoc3*, which encodes Apoc-III, suggested the consensus sequence as KGCWARGKYCAY, where K is G/T, W is A/T, R is A/G, and Y is C/T [459]. Later analyses demonstrated that HNF4 recognizes repeats of half-site motifs AGGTCA separated by one or two nucleotides [465], as well as a sequence of NNNNCAAAGTCCA [468]. HNF4α regulates gene expression involved in glucose, cholesterol, and fatty acid metabolism through binding to promoters of apolipoproteins *Apoa1* [469], *Apob [470]*, and *Apoc3* [470,471], as well as *Hnf1a* [459], *Tf* [472], and *F7* that produces the human coagulation factor VII [473].

HNF4α mRNA is detected as early as E4.5 in the primitive endoderm of the blastocyte [474]; expression persists throughout liver development until adulthood to maintain hepatocytes at a differentiated state [466]. HNF4α ablation is embryonically lethal due to the lack of extraembryonic tissue development past E5.0 [475]. Tetraploid rescue of *Hnf4a*$^{-/-}$ embryos displays liver specification without full differentiation that lacks expression of a number of liver marker genes such as *Alb*, *Afp*, *Tf*, apolipoproteins *Apoa1*, *Apoa4*, *Apob*, *Apoc2*, and *Apoc3*, *Nr1i2* (*Pxr*), *Pah* that

produces phenylalanine-4-hydroxylase (PAH), and liver-type fatty acid-binding protein (L-FABP) encoded by *Fabp1* [476]. *Hnf4a*$^{F/F}$;*Alfp*^{Cre} mice fail to undergo fetal liver epithelial transformation due to the lack of expression involved in cell adhesion and cell junction assembly [477]. On E18.5, HNF4α-deficient embryonic hepatocytes also demonstrate decreased gene expression related to glucose homeostasis including *Pck1*, *Gys2* that encodes the liver glycogen synthase, and *G6pc* that produces glucose-6-phosphatase (G6Pase) [478]. Conditional HNF4α deletion with *Hnf4a*$^{F/F}$;*Alb*^{Cre} results in lipid accumulation with reduced serum cholesterol and triglyceride, while serum bile acid level is increased, coinciding with the reduction of *Apob*, *Fabp1*, *Slco1a1*, and *Slc10a1* (*Ntcp*) that encodes the sodium/bile acid cotransporter [479]. Furthermore, *Hnf4a*$^{F/F}$;*Alb*^{CreERT2} mice treated with tamoxifen to remove HNF4α from mature hepatocytes exhibit elevated hepatocyte proliferation with increased expression of cell cycle genes [349]. Together, these studies utilizing transgenic mice suggest the requirement of HNF4α from early liver development for the establishment of epithelial morphology to maintenance of the mature hepatocyte phenotype including lipid, bile acid, cholesterol, and glucose homeostasis through gluconeogenesis and glycogen synthesis. Similar to that observed for HNF1, heterozygous HNF4α mutation affects the pancreas and causes autosomal dominant MODY1 in humans, with no obvious phenotypic deficiencies observed in the liver [480].

HNF4α activity is modulated through post-translational modifications. Phosphorylation of tyrosine residues is necessary for proper nuclear compartment localization, as well as the maintenance of DNA-binding activity and transactivation ability [481]. Additionally, cyclic AMP (cAMP) response element-binding protein (CBP) acetylation of lysine residues within the nuclear localization sequence is required for nuclear retention, DNA sequence binding, and target gene activation [482].

D. HNF6

HNF6 was identified via the protein-DNA complex formed with *Pfkfb1* [483], which encodes a bifunctional enzyme that synthesizes and degrades the key regulator of glycolysis, fructose 2,6-

bisphosphate [484]. Analysis of the *Pfkfb1* promoter identified two *cis*-acting sequences that account for approximately 50% of the transcriptional activity [406]. DNA-affinity labeling from rat liver nuclear proteins with the sequence from site IV of the *Pfkfb1* promoter was utilized to extract and purify a liver-specific factor originally identified as LP4 and later renamed HNF6 [483]. The HNF6 subfamily includes two isoforms HNF6α and HNF6β that differ by the linker sequence between the cut domain and the homeodomain [483]. Both isoforms display transactivating abilities, but the DNA-binding affinity depends on the target gene sequence [485].

HNF6 belongs to the ONECUT homeodomain family that includes HNF6 (OC1), OC2, and OC3 [483]. CUT homeodomain proteins were initially described in the *Drosophila cut* gene [486] and the mammalian homologs *mclox* gene [487], both consisting of three CUT domains. Interestingly, HNF6 only exhibits a single CUT domain, hence the nomenclature as 'ONECUT' homeodomain [485]. The N terminus contains the STP box, a serine/threonine/proline-enriched region, that functions as a transcriptional activator [483]; the C terminus encompasses the bipartite DNA-binding domain formed by the CUT domain (CD) and the homeodomain (HD) [485]. Both HNF6 isoforms bind DNA as monomers and do not form heterodimers [485].

Comparison of HNF6 binding sites of liver-enriched genes including *Afp*, *Hnf3b*, *Pck1*, and *Ttr* determined the consensus sequence as DWRTCMATND, where D is not C, W is A/T, R is A/G, M is A/C [485]. In addition to controlling *Foxa2* [488] and *Hnf4a* [489] expression, HNF6 activates the promoters of various liver function genes including *Ttr* [490], *Afp* [485], and *Gck* that encodes glucokinase (GCK) [491].

HNF6 is expressed at early developmental stages in the liver, pancreas, and neurons, suggesting its importance in regulating various differentiation programs [489]. HNF6 is detected on E9 prior to liver differentiation and continues to be expressed in the liver and the extrahepatic biliary system throughout development [489]. *Hnf6*$^{-/-}$ embryos lack the gallbladder primordium, resulting in abnormal morphology of extrahepatic bile ducts and perturbed development of intrahepatic bile ducts [492]. HNF6-deficient mice exhibit abnormal bile duct morphogenesis with increased mortality between P1-10 likely due to increased cholestasis that results in liver necrosis [492]. *Hnf6*$^{-}$

$^{/-}$ mice also display reduced HNF1β expression in the biliary epithelial cells during development [492]. *Hnf6*$^{F/F}$;*Alb*^{Cre} mice demonstrate normal intrahepatic bile duct morphology with no indication of liver injury as measured by serum AST, ALT, and total bilirubin levels [493]. Nonetheless, a later study examining conditional *Hnf6* ablation in the adult mouse liver through AAV8-TBG-Cre injection into *Hnf6*$^{F/F}$ mice showed severe hepatosteatosis with the induction of genes involved in oxidation-reduction and lipid metabolism [494]. Furthermore, ectopic HNF6 overexpression via adenovirus prior to PHx leads to an increased number of replicating hepatocytes entering S phase as well as upregulation of the mitogen TGFα, cell cycle regulator cyclin D1, and the transcription factor FOXM1 [495]. These observations implicate a crucial role of HNF6 during liver development and cholangiocyte differentiation, as well as its importance in transcriptional repression of lipid metabolic genes and the stimulation of hepatocyte proliferation during liver regeneration.

HNF6 expression can be elevated by growth hormone [496] through increased STAT5 and HNF4α occupancy [497] in conjunction with the displacement of C/EBPα at the HNF6 promoter [498].

E. C/EBP

C/EBP was discovered as a heat-stable nuclear protein to selectively bind to the CCAAT motif of several viral promoters [499] and viral enhancer core elements [500] in the rat liver nuclei [501]. The C/EBP subfamily consists of several isoforms including C/EBPα, C/EBPβ, C/EBPγ, C/EBPδ, C/EBPε, and C/EBPζ, but only the first three are enriched in the liver [502], with C/EBPα the most predominant isoform expressed in adult hepatocytes [503].

C/EBPα, originally named C/EBP, was identified through analysis of *Alb*, *Ttr*, and *Serpina1* promoters and the simian virus 40 (SV40) core C enhancer element [297,298]. C/EBPβ was described as a nuclear factor to activate IL6 transcription after IL1 induction, hence its original nomenclature, NF-IL6 [504]. C/EBPβ also binds to regulatory regions of several acute-phase genes including TNF and IL8, indicating its importance to regulate acute inflammatory responses [504]. C/EBPγ was purified as a protein to bind the B cell-specific enhancer and promoter regions of the

immunoglobulin heavy chain (IgH) [505]. Subsequent structural analysis of C/EBPγ demonstrated the lack of transactivating domain observed in C/EBPα and β, suggesting the unlikelihood of C/EBPγ as a direct transcriptional activator or repressor [506]. Rather, C/EBPγ functions as a transdominant negative inhibitor and heterodimerizes with C/EBPα or β to repress their transcriptional activity [506].

C/EBP proteins belong to a larger structural category of the basic leucine zipper (bZIP) family of transcription factors [507], one of the most conserved groups of eukaryotic transcription factors that include JUN, FOS, and cAMP-responsive element-binding (CREB) proteins [502]. The C/EBP subfamily exhibits modular structures that contain an N-terminal transactivating region [508], a basic DNA-binding domain, and a C-terminal leucine zipper [508]; all C/EBP isoforms share over 90% of sequence homology at the bZIP domain [501,507,509]. C/EBP binds to the DNA as homo- or heterodimers and forms intrafamilial heterodimers to recognize the same consensus sequence, with the exception of C/EBPζ [505,507,510].

The consensus motif for C/EBP proteins is RTTGCGYAAY, where R is A/G and Y is C/T [511]. Other than *Alb* and *Ttr*, C/EBPα also regulates the expression of liver-specific or -enriched genes including *Pck1* [512]*, Tf* [472], *Slc2a2* [513], *Igf1* that produces the insulin-like growth factor I (IGF-1) [514], *F9* that encodes the coagulation factor IX [515], and several CYP450 genes [442]. C/EBPβ controls metabolic gene production such as *Cyp2d5* [516], *Pck1* [517], *Aldh1a1* that encodes the cytosolic aldehyde dehydrogenase (RALDH 1) [518], *Ca3* (*Car3*) that produces carbonic anhydrase 3 (CA-III) [518], and several other genes encoding acute-phase proteins during inflammation such as serum amyloid A (SAA) [519] and C-reactive protein (CRP) [520].

C/EBP transcription factors are pivotal for a variety of functions including cell proliferation, differentiation, metabolism, inflammation, tumorigenesis, and apoptosis, particularly in hepatocytes, adipocytes, and hematopoietic cells [521]. C/EBPα expression is detected on E9.5 in the mouse endoderm in the liver primordium, while C/EBPβ expression is detected between E13.5 and E14.5 in the liver [522]. *Cebpa*$^{-/-}$ mice fail to store hepatic glycogen and die within 8 hours after birth due to hypoglycemia associated with reduced or delayed gene expression of *Gys2* and two

gluconeogenic enzymes, PEPCK and G6Pase [523]. Injection of AAV-Cre into *Cebpa*$^{F/F}$ mice to remove up to 90% of C/EBPα expression in the adult liver demonstrated decreased expression of bilirubin UDP-glucuronosyltransferase (UGT), an enzyme required for bilirubin conjugation and detoxification [524], leading to adult-onset jaundice [525]. Expression of *Pck1*, *Gys2*, and *F9* was also decreased in the adult mouse liver with conditional C/EBPα ablation [525]. These experiments demonstrate the importance of C/EBPα as a central role for gluconeogenesis, glycogen synthesis, and bilirubin homeostasis in the liver.

The role of C/EBPβ in metabolic regulation is complex. Half of *Cebpb*$^{-/-}$ mice exhibit steadystate glucose homeostasis but demonstrate fasting hypoglycemia and impaired hepatic glucose production. The other half die at birth due to hypoglycemia attributed to the absence of PEPCK expression followed by the inability to mobilize glycogen stores [517]. In mice injected with concanavalin A to induce immune-mediated liver injury, C/EBPβ nuclear expression is increased as early as 1 h and mRNA levels increased 4 h after liver injury, but returns to normal before entering S phase [526]. C/EBPβ-deficient mice display decreased DNA synthesis and suppression of immediate-early growth response genes, *Mkp1* and *Egr1*, 1 h post-PHx [239]. Furthermore, *Cebpb*$^{-/-}$ livers also show sustained hypoglycemia in conjunction with dysregulation of genes important for hepatic gluconeogenesis after PHx [239], suggesting the significance of C/EBPβ for glucose homeostasis after profound metabolic stress such as PHx.

IV. Regulatory circuits of liver-enriched transcription factors

The liver-enriched transcription factors form a cooperative network to establish transcriptional control and to synergistically interact with one another to maintain a hepatocyte-specific gene expression profile [527,528]. Of all transcription factors highly-expressed in hepatocytes, HNF1α and HNF4α deficiency correlate with the lack of liver-specific gene expression in dedifferentiated hepatomas and hepatocyte-fibroblast hybrids [527]. Furthermore, HNF1α and HNF4α reexpression correspond to the transcription of hepatocyte-specific genes in hybrid cells

[529]. These observations led to the hypothesis that HNF1α and HNF4α are the primary transcriptional regulators to maintain the differentiated hepatic phenotype.

In particular, several independent observations suggest that HNF4α could function as the master regulator that sits atop the transcriptional cascade during hepatocyte differentiation [459,474]. (1) HNF4α mRNA is detected as early as E4.5 in the primitive endoderm of the blastocyte [474], preceding the expression of HNF1α on E8.5 [422]. (2) HNF4α is able to overcome the repression in dedifferentiated hepatoma cells to induce expression of epithelial marker genes [530,531]. (3) HNF4α transcriptionally activates HNF1α [459]. (4) *Hnfa*$^{-/-}$ mice are embryonically lethal due to the lack of extraembryonic tissue development [475] while *Hnf1a*$^{-/-}$ mice are viable at birth and die around weaning due to hepatic dysfunction [425]. (5) HNF4α occupies around 12% of the hepatocyte genome as determined with human DNA microarray, while HNF1α targets 1.6% and HNF6 1.4%, implying that HNF4α contributes to the regulation of a large portion of liver gene expression [420].

Later studies revealed the complex regulation between liver-enriched transcription factors and proposed that the interplay of hepatocyte nuclear factors presumably resembles a regulatory circuitry, rather than a linear hierarchy [527], in a context-dependent manner [420] summarized in **Figure 1.3**.

SPECIFIC AIMS

In summary, liver regeneration encompasses crosstalk from different cell types, interactions of various signaling pathways, and modulation of the chromatin architecture to initiate complex networks of transcriptional regulation. While the regenerative response is well described in PHx, it is less evident in injury models. Hence, the goal of this thesis is to utilize unbiased transcriptome- and epigenome-wide techniques to identify regulators of liver regeneration following acute injury. I hypothesize that investigating the modifications of gene expression and chromatin accessibility via cell type-specific analyses of regenerating hepatocytes in the *Fah*$^{-/-}$ model will enable the identification of essential factors of liver repopulation.

In Specific Aim 1, I propose to perform transcriptomic profiling of regenerating hepatocytes to identify drivers of liver proliferation. With the combination of the translating ribosome affinity purification (TRAP) system [532] and the *Fah*$^{-/-}$ model, regenerating hepatocytes will be explicitly isolated followed by high-throughput RNA-sequencing (TRAP-seq) to interrogate gene expression alterations during liver repopulation. Overexpression and inhibition studies will be carried out to investigate the functional significance of genes of interest as promoters of hepatocyte replication following acute liver injury.

In Specific Aim 2, I will assess the assotiation of chromatin accessibility modification and gene expression regulation during the repopulation process. With the implementation of the ' isolation of nuclei tagged in specific cell types' (INTACT) method [533] in the *Fah*$^{-/-}$ mouse, regenerating hepatocyte nuclei will be labeled and sorted followed by the 'assay for transposase accessible chromatin with high-throughput sequencing' (ATAC-seq) [534] to elucidate changes in the chromatin landscape. I propose to integrate multiomic datasets to identify crucial transcription factors and regulatory networks that underlie the regenerative process.

This thesis combines a mouse model reflective of human diseases, systematic *in vivo* analyses, and functional validation of genes and transcription factors during liver regeneration. By addressing these aims, I expect to identify novel therapeutic targets and critical regulators to enhance liver regeneration following acute injury.

FIGURES

Figure 0.1. Schematic representation of a liver lobule.

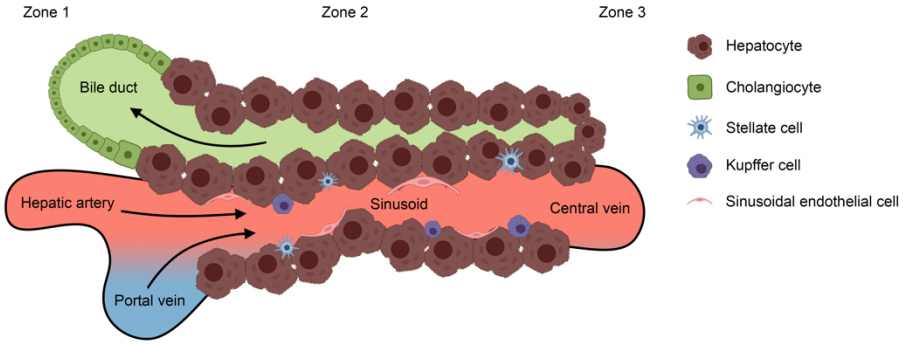

The liver consists of various cell types including hepatocytes, cholangiocytes, stellate cells, Kupffer cells, and sinusoidal endothelial cells. The portal triad is located in zone one and contains the bile duct, hepatic artery, and portal vein, whereas the central vein resides in zone three. Together, the portal vein and the hepatic artery move through the sinusoid toward the central vein to provide blood supply to the liver. On the contrary, bile acids move from zone three to zone one in the bile duct.

Figure 0.2. Regulation of the cell cycle by cyclin proteins and cyclin-dependent kinases (CDK).

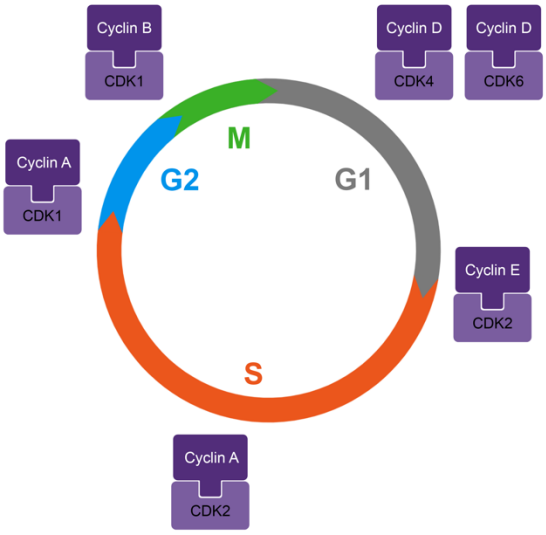

The cell cycle is tightly controlled by the rise and fall of cyclin proteins that lead to the activation of CDKs to promote progression through cell cycle checkpoints.

Figure 0.3. Liver-enriched transcription factors form a complex regulatory network.

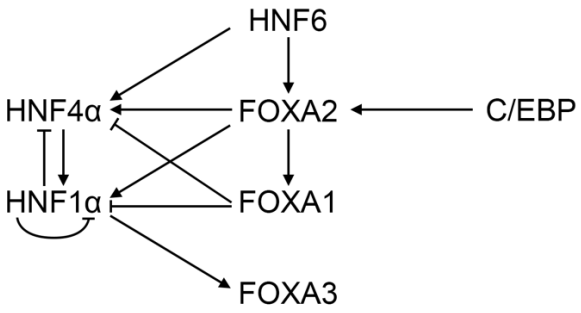

HNF4α activates HNF1α expression [459,535]. HNF1α negatively autoregulates its own expression [536] and inhibits HNF4α via suppression of the AF2- domain [537]. HNF1α also binds to a 3' enhancer site to activate FOXA3 transcription [538]. HNF6 activates FOXA2 [488] and HNF4α [489], while FOXA2 is required for FOXA1 expression [539]. Additionally, FOXA1 and 2 compete for FOXA motifs on HNF1α and HNF4α, in which FOXA1 represses while FOXA2 induces HNF1α and HNF4α transcription [539]. Finally, C/EBPα binds to the FOXA2 promoter for transcriptional activation [540].

REFERENCES

1. Jungermann K, Kietzmann T. Zonation of parenchymal and nonparenchymal metabolism in liver. Annu Rev Nutr. 1996;16: 179–203.
2. Trefts E, Gannon M, Wasserman DH. The liver. Curr Biol. 2017;27: R1147–R1151.
3. Williams RT. Comparative patterns of drug metabolism. Fed Proc. 1967;26: 1029–1039.
4. Dimski DS. Ammonia metabolism and the urea cycle: function and clinical implications. J Vet Intern Med. 1994;8: 73–78.
5. Lester R, Schmid R. BILIRUBIN METABOLISM. N Engl J Med. 1964;270: 779–786.
6. Vlahcevic ZR, Heuman DM, Hylemon PB. Regulation of bile acid synthesis. Hepatology. 1991;13: 590–600.
7. Stanger BZ. Cellular Homeostasis and Repair in the Mammalian Liver. Annu Rev Physiol. 2015;77: 179–200.
8. Strazzabosco M. New insights into cholangiocyte physiology. J Hepatol. 1997;27: 945–952.
9. Wardle EN. Kupffer cells and their function. Liver. 1987;7: 63–75.
10. Kawada N. The hepatic perisinusoidal stellate cell. Histol Histopathol. 1997;12: 1069–1080.
11. Reichen J. The Role of the Sinusoidal Endothelium in Liver Function. News Physiol Sci. 1999;14: 117–121.
12. Kiernan F. The Anatomy and Physiology of the Liver [Internet]. Proceedings of the Royal Society of London. 1830. pp. 211–212. doi:10.1098/rspl.1830.0129
13. Gebhardt R, Hovhannisyan A. Organ patterning in the adult stage: the role of Wnt/beta-catenin signaling in liver zonation and beyond. Dev Dyn. 2010;239: 45–55.
14. Jungermann K, Katz N. Functional specialization of different hepatocyte populations. Physiol Rev. 1989;69: 708–764.
15. Tam PP, Behringer RR. Mouse gastrulation: the formation of a mammalian body plan. Mech Dev. 1997;68: 3–25.
16. Zorn AM, Wells JM. Vertebrate endoderm development and organ formation. Annu Rev Cell Dev Biol. 2009;25: 221–251.
17. Tremblay KD, Zaret KS. Distinct populations of endoderm cells converge to generate the embryonic liver bud and ventral foregut tissues. Dev Biol. 2005;280: 87–99.
18. Bort R, Signore M, Tremblay K, Martinez Barbera JP, Zaret KS. Hex homeobox gene controls the transition of the endoderm to a pseudostratified, cell emergent epithelium for liver bud development. Dev Biol. 2006;290: 44–56.
19. Jung J, Zheng M, Goldfarb M, Zaret KS. Initiation of mammalian liver development from endoderm by fibroblast growth factors. Science. 1999;284: 1998–2003.
20. Rossi JM, Dunn NR, Hogan BL, Zaret KS. Distinct mesodermal signals, including BMPs from the septum transversum mesenchyme, are required in combination for hepatogenesis from the endoderm. Genes Dev. 2001;15: 1998–2009.
21. Bossard P, Zaret KS. GATA transcription factors as potentiators of gut endoderm differentiation. Development. 1998;125: 4909–4917.
22. Lee CS, Friedman JR, Fulmer JT, Kaestner KH. The initiation of liver development is dependent on Foxa transcription factors. Nature. 2005;435: 944–947.
23. Si-Tayeb K, Lemaigre FP, Duncan SA. Organogenesis and development of the liver. Dev Cell. 2010;18: 175–189.
24. Shiojiri N. Enzymo- and immunocytochemical analyses of the differentiation of liver cells in the prenatal mouse. J Embryol Exp Morphol. 1981;62: 139–152.
25. Cascio S, Zaret KS. Hepatocyte differentiation initiates during endodermal-mesenchymal interactions prior to liver formation. Development. 1991;113: 217–225.
26. Clotman F, Jacquemin P, Plumb-Rudewiez N, Pierreux CE, Van der Smissen P, Dietz HC, et al. Control of liver cell fate decision by a gradient of TGF beta signaling modulated by Onecut transcription factors. Genes Dev. 2005;19: 1849–1854.
27. Gordillo M, Evans T, Gouon-Evans V. Orchestrating liver development. Development. 2015;142: 2094–2108.

28. Macdonald RA. “Lifespan” of liver cells. Autoradio-graphic study using tritiated thymidine in normal, cirrhotic, and partially hepatectomized rats. Arch Intern Med. 1961;107: 335–343.
29. Zajicek G, Oren R, Weinreb M. The streaming liver. Liver. 1985;5: 293–300.
30. Furuyama K, Kawaguchi Y, Akiyama H, Horiguchi M, Kodama S, Kuhara T, et al. Continuous cell supply from a Sox9-expressing progenitor zone in adult liver, exocrine pancreas and intestine. Nat Genet. 2011;43: 34–41.
31. Bralet MP, Branchereau S, Brechot C, Ferry N. Cell lineage study in the liver using retroviral mediated gene transfer. Evidence against the streaming of hepatocytes in normal liver. Am J Pathol. 1994;144: 896–905.
32. Magami Y, Azuma T, Inokuchi H, Kokuno S, Moriyasu F, Kawai K, et al. Cell proliferation and renewal of normal hepatocytes and bile duct cells in adult mouse liver. Liver. 2002;22: 419–425.
33. Carpentier R, Suñer RE, van Hul N, Kopp JL, Beaudry J-B, Cordi S, et al. Embryonic ductal plate cells give rise to cholangiocytes, periportal hepatocytes, and adult liver progenitor cells. Gastroenterology. 2011;141: 1432–8, 1438.e1–4.
34. Malato Y, Naqvi S, Schürmann N, Ng R, Wang B, Zape J, et al. Fate tracing of mature hepatocytes in mouse liver homeostasis and regeneration. J Clin Invest. 2011;121: 4850–4860.
35. Wang B, Zhao L, Fish M, Logan CY, Nusse R. Self-renewing diploid Axin2(+) cells fuel homeostatic renewal of the liver. Nature. 2015;524: 180–185.
36. Mokdad AA, Lopez AD, Shahraz S, Lozano R, Mokdad AH, Stanaway J, et al. Liver cirrhosis mortality in 187 countries between 1980 and 2010: a systematic analysis. BMC Med. 2014;12: 145.
37. Asrani SK, Devarbhavi H, Eaton J, Kamath PS. Burden of liver diseases in the world. J Hepatol. 2019;70: 151–171.
38. Asrani SK, Larson JJ, Yawn B, Therneau TM, Kim WR. Underestimation of liver-related mortality in the United States. Gastroenterology. 2013;145: 375–82.e1–2.
39. Mokdad AH, Forouzanfar MH, Daoud F, Mokdad AA, El Bcheraoui C, Moradi-Lakeh M, et al. Global burden of diseases, injuries, and risk factors for young people’s health during 1990-2013: a systematic analysis for the Global Burden of Disease Study 2013. Lancet. 2016;387: 2383–2401.
40. Stein E, Cruz-Lemini M, Altamirano J, Ndugga N, Couper D, Abraldes JG, et al. Heavy daily alcohol intake at the population level predicts the weight of alcohol in cirrhosis burden worldwide. J Hepatol. 2016;65: 998–1005.
41. Bellentani S, Saccoccio G, Costa G, Tiribelli C, Manenti F, Sodde M, et al. Drinking habits as cofactors of risk for alcohol induced liver damage. The Dionysos Study Group. Gut. 1997;41: 845–850.
42. Naveau S, Giraud V, Borotto E, Aubert A, Capron F, Chaput JC. Excess weight risk factor for alcoholic liver disease. Hepatology. 1997;25: 108–111.
43. You M, Crabb DW. Recent advances in alcoholic liver disease II. Minireview: molecular mechanisms of alcoholic fatty liver. Am J Physiol Gastrointest Liver Physiol. 2004;287: G1–6.
44. You M, Fischer M, Deeg MA, Crabb DW. Ethanol induces fatty acid synthesis pathways by activation of sterol regulatory element-binding protein (SREBP). J Biol Chem. 2002;277: 29342–29347.
45. Fischer M, You M, Matsumoto M, Crabb DW. Peroxisome proliferator-activated receptor alpha (PPARalpha) agonist treatment reverses PPARalpha dysfunction and abnormalities in hepatic lipid metabolism in ethanol-fed mice. J Biol Chem. 2003;278: 27997–28004.
46. You M, Matsumoto M, Pacold CM, Cho WK, Crabb DW. The role of AMP-activated protein kinase in the action of ethanol in the liver. Gastroenterology. 2004;127: 1798–1808.
47. Lucey MR, Mathurin P, Morgan TR. Alcoholic hepatitis. N Engl J Med. 2009;360: 2758–2769.
48. Brunt EM, Wong VW-S, Nobili V, Day CP, Sookoian S, Maher JJ, et al. Nonalcoholic fatty liver disease. Nat Rev Dis Primers. 2015;1: 15080.

49. Younossi ZM, Koenig AB, Abdelatif D, Fazel Y, Henry L, Wymer M. Global epidemiology of nonalcoholic fatty liver disease-Meta-analytic assessment of prevalence, incidence, and outcomes. Hepatology. 2016;64: 73–84.
50. Younossi ZM, Loomba R, Anstee QM, Rinella ME, Bugianesi E, Marchesini G, et al. Diagnostic modalities for nonalcoholic fatty liver disease, nonalcoholic steatohepatitis, and associated fibrosis. Hepatology. 2018;68: 349–360.
51. Younossi ZM, Loomba R, Rinella ME, Bugianesi E, Marchesini G, Neuschwander-Tetri BA, et al. Current and future therapeutic regimens for nonalcoholic fatty liver disease and nonalcoholic steatohepatitis. Hepatology. 2018;68: 361–371.
52. Younossi ZM. The epidemiology of nonalcoholic steatohepatitis. Clin Liver Dis. 2018;11: 92–94.
53. Feldstein AE, Canbay A, Angulo P, Taniai M, Burgart LJ, Lindor KD, et al. Hepatocyte apoptosis and fas expression are prominent features of human nonalcoholic steatohepatitis. Gastroenterology. 2003;125: 437–443.
54. Upton J-P, Austgen K, Nishino M, Coakley KM, Hagen A, Han D, et al. Caspase-2 cleavage of BID is a critical apoptotic signal downstream of endoplasmic reticulum stress. Mol Cell Biol. 2008;28: 3943–3951.
55. Koliaki C, Szendroedi J, Kaul K, Jelenik T, Nowotny P, Jankowiak F, et al. Adaptation of hepatic mitochondrial function in humans with non-alcoholic fatty liver is lost in steatohepatitis. Cell Metab. 2015;21: 739–746.
56. Tsung A, Sahai R, Tanaka H, Nakao A, Fink MP, Lotze MT, et al. The nuclear factor HMGB1 mediates hepatic injury after murine liver ischemia-reperfusion. J Exp Med. 2005;201: 1135–1143.
57. Imaeda AB, Watanabe A, Sohail MA, Mahmood S, Mohamadnejad M, Sutterwala FS, et al. Acetaminophen-induced hepatotoxicity in mice is dependent on Tlr9 and the Nalp3 inflammasome. J Clin Invest. 2009;119: 305–314.
58. Luedde T, Kaplowitz N, Schwabe RF. Cell death and cell death responses in liver disease: mechanisms and clinical relevance. Gastroenterology. 2014;147: 765–783.e4.
59. Farhadi A, Gundlapalli S, Shaikh M, Frantzides C, Harrell L, Kwasny MM, et al. Susceptibility to gut leakiness: a possible mechanism for endotoxaemia in non-alcoholic steatohepatitis. Liver Int. 2008;28: 1026–1033.
60. Wehr A, Baeck C, Ulmer F, Gassler N, Hittatiya K, Luedde T, et al. Pharmacological inhibition of the chemokine CXCL16 diminishes liver macrophage infiltration and steatohepatitis in chronic hepatic injury. PLoS One. 2014;9: e112327.
61. Tosello-Trampont A-C, Landes SG, Nguyen V, Novobrantseva TI, Hahn YS. Kuppfer cells trigger nonalcoholic steatohepatitis development in diet-induced mouse model through tumor necrosis factor-α production. J Biol Chem. 2012;287: 40161–40172.
62. Leroux A, Ferrere G, Godie V, Cailleux F, Renoud M-L, Gaudin F, et al. Toxic lipids stored by Kupffer cells correlates with their pro-inflammatory phenotype at an early stage of steatohepatitis. J Hepatol. 2012;57: 141–149.
63. Teratani T, Tomita K, Suzuki T, Oshikawa T, Yokoyama H, Shimamura K, et al. A high-cholesterol diet exacerbates liver fibrosis in mice via accumulation of free cholesterol in hepatic stellate cells. Gastroenterology. 2012;142: 152–164.e10.
64. Tomita K, Teratani T, Suzuki T, Shimizu M, Sato H, Narimatsu K, et al. Free cholesterol accumulation in hepatic stellate cells: mechanism of liver fibrosis aggravation in nonalcoholic steatohepatitis in mice. Hepatology. 2014;59: 154–169.
65. Lee WM. Etiologies of acute liver failure. Semin Liver Dis. 2008;28: 142–152.
66. Onakpoya IJ, Heneghan CJ, Aronson JK. Post-marketing withdrawal of 462 medicinal products because of adverse drug reactions: a systematic review of the world literature. BMC Med. 2016;14: 10.
67. Kaplowitz N. Biochemical and cellular mechanisms of toxic liver injury. Semin Liver Dis. 2002;22: 137–144.

68. Stanaway JD, Flaxman AD, Naghavi M, Fitzmaurice C, Vos T, Abubakar I, et al. The global burden of viral hepatitis from 1990 to 2013: findings from the Global Burden of Disease Study 2013. The Lancet. 2016. pp. 1081–1088.
69. Rehermann B. Pathogenesis of chronic viral hepatitis: differential roles of T cells and NK cells. Nat Med. 2013;19: 859–868.
70. Guidotti LG, Chisari FV. Immunobiology and pathogenesis of viral hepatitis. Annu Rev Pathol. 2006;1: 23–61.
71. Trey C, Davidson CS. The management of fulminant hepatic failure. Prog Liver Dis. 1970;3: 282–298.
72. Bernal W, Wendon J. Acute liver failure. N Engl J Med. 2013;369: 2525–2534.
73. Reuben A, Koch DG, Lee WM, Acute Liver Failure Study Group. Drug-induced acute liver failure: results of a U.S. multicenter, prospective study. Hepatology. 2010;52: 2065–2076.
74. D'Amico G, Garcia-Tsao G, Pagliaro L. Natural history and prognostic indicators of survival in cirrhosis: a systematic review of 118 studies. J Hepatol. 2006;44: 217–231.
75. Popper H. Pathologic aspects of cirrhosis. A review. Am J Pathol. 1977;87: 228–264.
76. Fleming KM, Aithal GP, Card TR, West J. All-cause mortality in people with cirrhosis compared with the general population: a population-based cohort study. Liver Int. 2012;32: 79–84.
77. D'Amico G, Pasta L, Morabito A, D'Amico M, Caltagirone M, Malizia G, et al. Competing risks and prognostic stages of cirrhosis: a 25-year inception cohort study of 494 patients. Aliment Pharmacol Ther. 2014;39: 1180–1193.
78. Heidelbaugh JJ, Bruderly M. Cirrhosis and chronic liver failure: part I. Diagnosis and evaluation. Am Fam Physician. 2006;74: 756–762.
79. Cancer of the Liver and Intrahepatic Bile Duct - Cancer Stat Facts. In: SEER [Internet]. [cited 6 Sep 2019]. Available: https://seer.cancer.gov/statfacts/html/livibd.html
80. Welzel TM, Graubard BI, Quraishi S, Zeuzem S, Davila JA, El-Serag HB, et al. Population-attributable fractions of risk factors for hepatocellular carcinoma in the United States. Am J Gastroenterol. 2013;108: 1314–1321.
81. de Martel C, Maucort-Boulch D, Plummer M, Franceschi S. World-wide relative contribution of hepatitis B and C viruses in hepatocellular carcinoma. Hepatology. 2015;62: 1190–1200.
82. Wong RJ, Cheung R, Ahmed A. Nonalcoholic steatohepatitis is the most rapidly growing indication for liver transplantation in patients with hepatocellular carcinoma in the U.S. Hepatology. 2014;59: 2188–2195.
83. Sánchez Alvarado A. Regeneration in the metazoans: why does it happen? Bioessays. 2000;22: 578–590.
84. Morgan TH. Experimental studies of the regeneration of Planaria maculata [Internet]. Archiv für Entwickelungsmechanik der Organismen. 1898. pp. 364–397. doi:10.1007/bf02161491
85. Muneoka K, Allan CH, Yang X, Lee J, Han M. Mammalian regeneration and regenerative medicine. Birth Defects Res C Embryo Today. 2008;84: 265–280.
86. Michalopoulos GK, DeFrances MC. Liver regeneration. Science. 1997;276: 60–66.
87. Power C, Rasko JEJ. Whither Prometheus' Liver? Greek Myth and the Science of Regeneration. Ann Intern Med. 2008;149: 421.
88. Francavilla A, Ove P, Polimeno L, Coetzee M, Makowka L, Barone M, et al. Regulation of liver size and regeneration: importance in liver transplantation. Transplant Proc. 1988;20: 494–497.
89. Farber E. Similarities in the sequence of early histological changes induced in the liver of the rat by ethionine, 2-acetylamino-fluorene, and 3'-methyl-4-dimethylaminoazobenzene. Cancer Res. 1956;16: 142–148.
90. Stöcker E, Wullstein HK, Bräu G. [Capacity of regeneration in liver epithelia of juvenile, repeated partially hepatectomized rats. Autoradiographic studies after continous infusion of 3H-thymidine (author's transl)]. Virchows Arch B Cell Pathol. 1973;14: 93–103.
91. Overturf K, al-Dhalimy M, Ou CN, Finegold M, Grompe M. Serial transplantation reveals the stem-cell-like regenerative potential of adult mouse hepatocytes. Am J Pathol. 1997;151: 1273–1280.

92. Kam I, Lynch S, Svanas G, Todo S, Polimeno L, Francavilla A, et al. Evidence that host size determines liver size: studies in dogs receiving orthotopic liver transplants. Hepatology. 1987;7: 362–366.
93. Madrahimov N, Dirsch O, Broelsch C, Dahmen U. Marginal Hepatectomy in the Rat. Ann Surg. 2006;244: 89–98.
94. Higgins GM, Anderson RM. Experimental pathology of liver: restoration of liver in white rat following partial surgical removal. Arch pathol. 1931;12: 186–202.
95. Taub R. Liver regeneration: from myth to mechanism [Internet]. Nature Reviews Molecular Cell Biology. 2004. pp. 836–847. doi:10.1038/nrm1489
96. Fausto N. Liver regeneration. J Hepatol. 2000;32: 19–31.
97. Grisham JW. A morphologic study of deoxyribonucleic acid synthesis and cell proliferation in regenerating rat liver; autoradiography with thymidine-H3. Cancer Res. 1962;22: 842–849.
98. Krawitt EL, Betel I, Potter VR. A study of the cytidine kinase pathway of nucleotide biosynthesis in regenerating rat liver. Biochim Biophys Acta. 1969;174: 763–765.
99. Fausto N, Campbell JS, Riehle KJ. Liver regeneration. Hepatology. 2006;43: S45–53.
100. Palmes D, Spiegel H-U. Animal models of liver regeneration. Biomaterials. 2004;25: 1601–1611.
101. Kim PTW, Testa G. Living donor liver transplantation in the USA. Hepatobiliary Surg Nutr. 2016;5: 133–140.
102. Michalopoulos GK. Liver regeneration after partial hepatectomy: critical analysis of mechanistic dilemmas. Am J Pathol. 2010;176: 2–13.
103. Jaeschke H. Molecular mechanisms of hepatic ischemia-reperfusion injury and preconditioning. Am J Physiol Gastrointest Liver Physiol. 2003;284: G15–26.
104. Jaeschke H, Farhood A. Neutrophil and Kupffer cell-induced oxidant stress and ischemia-reperfusion injury in rat liver. Am J Physiol. 1991;260: G355–62.
105. Zwacka RM, Zhou W, Zhang Y, Darby CJ, Dudus L, Halldorson J, et al. Redox gene therapy for ischemia/reperfusion injury of the liver reduces AP1 and NF-kappaB activation. Nat Med. 1998;4: 698–704.
106. Pritchard MT, Apte U. Models to Study Liver Regeneration [Internet]. Liver Regeneration. 2015. pp. 15–40. doi:10.1016/b978-0-12-420128-6.00002-6
107. Colletti LM, Remick DG, Burtch GD, Kunkel SL, Strieter RM, Campbell DA Jr. Role of tumor necrosis factor-alpha in the pathophysiologic alterations after hepatic ischemia/reperfusion injury in the rat. J Clin Invest. 1990;85: 1936–1943.
108. Lentsch AB, Yoshidome H, Kato A, Warner RL, Cheadle WG, Ward PA, et al. Requirement for interleukin-12 in the pathogenesis of warm hepatic ischemia/reperfusion injury in mice. Hepatology. 1999;30: 1448–1453.
109. Jaeschke H, Farhood A, Smith CW. Neutrophils contribute to ischemia/reperfusion injury in rat liver in vivo. FASEB J. 1990;4: 3355–3359.
110. Lentsch AB, Yoshidome H, Cheadle WG, Miller FN, Edwards MJ. Chemokine involvement in hepatic ischemia/reperfusion injury in mice: roles for macrophage inflammatory protein-2 and KC. Hepatology. 1998;27: 1172–1177.
111. Kountouras J, Billing BH, Scheuer PJ. Prolonged bile duct obstruction: a new experimental model for cirrhosis in the rat. Br J Exp Pathol. 1984;65: 305–311.
112. Polimeno L, Azzarone A, Zeng QH, Panella C, Subbotin V, Carr B, et al. Cell proliferation and oncogene expression after bile duct ligation in the rat: evidence of a specific growth effect on bile duct cells. Hepatology. 1995;21: 1070–1078.
113. Michalopoulos GK, Barua L, Bowen WC. Transdifferentiation of rat hepatocytes into biliary cells after bile duct ligation and toxic biliary injury. Hepatology. 2005;41: 535–544.
114. Keppler DO, Pausch J, Decker K. Selective uridine triphosphate deficiency induced by D-galactosamine in liver and reversed by pyrimidine nucleotide precursors. Effect on ribonucleic acid synthesis. J Biol Chem. 1974;249: 211–216.
115. Liehr H, Grün M, Seelig HP, Seelig R, Reutter W, Heine WD. On the pathogenesis of galactosamine hepatitis. Indications of extrahepatocellular mechanisms responsible for liver cell death. Virchows Arch B Cell Pathol. 1978;26: 331–344.

116. Kuhlmann WD, Peschke P. Hepatic progenitor cells, stem cells, and AFP expression in models of liver injury. Int J Exp Pathol. 2006;87: 343–359.
117. Abdul-Hussain SK, Mehendale HM. Ongoing hepatocellular regeneration and resiliency toward galactosamine hepatotoxicity. Arch Toxicol. 1992;66: 729–742.
118. Badger DA, Sauer JM, Hoglen NC, Jolley CS, Sipes IG. The role of inflammatory cells and cytochrome P450 in the potentiation of CCl4-induced liver injury by a single dose of retinol. Toxicol Appl Pharmacol. 1996;141: 507–519.
119. Kim SG, Chung HC, Cho JY. Molecular mechanism for alkyl sulfide-modulated carbon tetrachloride-induced hepatotoxicity: the role of cytochrome P450 2E1, P450 2B and glutathione S-transferase expression. J Pharmacol Exp Ther. 1996;277: 1058–1066.
120. Wong FW, Chan WY, Lee SS. Resistance to carbon tetrachloride-induced hepatotoxicity in mice which lack CYP2E1 expression. Toxicol Appl Pharmacol. 1998;153: 109–118.
121. Brattin WJ, Glende EA Jr, Recknagel RO. Pathological mechanisms in carbon tetrachloride hepatotoxicity. J Free Radic Biol Med. 1985;1: 27–38.
122. Armendariz-Borunda J, Katai H, Jones CM, Seyer JM, Kang AH, Raghow R. Transforming growth factor beta gene expression is transiently enhanced at a critical stage during liver regeneration after CCl4 treatment. Lab Invest. 1993;69: 283–294.
123. Rockey DC, Weisiger RA. Endothelin induced contractility of stellate cells from normal and cirrhotic rat liver: implications for regulation of portal pressure and resistance. Hepatology. 1996;24: 233–240.
124. Iredale JP, Benyon RC, Pickering J, McCullen M, Northrop M, Pawley S, et al. Mechanisms of spontaneous resolution of rat liver fibrosis. Hepatic stellate cell apoptosis and reduced hepatic expression of metalloproteinase inhibitors. J Clin Invest. 1998;102: 538–549.
125. Fitzhugh OG, Nelson AA. Liver Tumors in Rats Fed Thiourea or Thioacetamide. Science. 1948;108: 626–628.
126. Gupta DN. Acute changes in the liver after administration of thioacetamide. J Pathol Bacteriol. 1956;72: 183–192.
127. Müller A, Machnik F, Zimmermann T, Schubert H. Thioacetamide-induced cirrhosis-like liver lesions in rats--usefulness and reliability of this animal model. Exp Pathol. 1988;34: 229–236.
128. Wang T, Shankar K, Ronis MJ, Mehendale HM. Potentiation of thioacetamide liver injury in diabetic rats is due to induced CYP2E1. J Pharmacol Exp Ther. 2000;294: 473–479.
129. Kang JS, Wanibuchi H, Morimura K, Wongpoomchai R, Chusiri Y, Gonzalez FJ, et al. Role of CYP2E1 in thioacetamide-induced mouse hepatotoxicity. Toxicol Appl Pharmacol. 2008;228: 295–300.
130. Hunter AL, Holscher MA, Neal RA. Thioacetamide-induced hepatic necrosis. I. Involvement of the mixed-function oxidase enzyme system. J Pharmacol Exp Ther. 1977;200: 439–448.
131. Gallagher CH, Gupta DN, Judah JD, Rees KR. Biochemical changes in liver in acute thioacetamide intoxication. J Pathol Bacteriol. 1956;72: 193–201.
132. Díez-Fernández C, Sanz N, Alvarez AM, Zaragoza A, Cascales M. Influence of aminoguanidine on parameters of liver injury and regeneration induced in rats by a necrogenic dose of thioacetamide. Br J Pharmacol. 1998;125: 102–108.
133. Theocharis SE, Margeli AP, Agapitos EV, Mykoniatis MG, Kittas CN, Davaris PS. Effect of hepatic stimulator substance administration on tissue regeneration due to thioacetamide-induced liver injury in rats. Scand J Gastroenterol. 1998;33: 656–663.
134. Díez-Fernández C, Boscá L, Fernández-Simón L, Alvarez A, Cascales M. Relationship between genomic DNA ploidy and parameters of liver damage during necrosis and regeneration induced by thioacetamide. Hepatology. 1993;18: 912–918.
135. Lee WM, Squires RH Jr, Nyberg SL, Doo E, Hoofnagle JH. Acute liver failure: Summary of a workshop. Hepatology. 2008;47: 1401–1415.
136. Cummings AJ, King ML, Martin BK. A kinetic study of drug elimination: the excretion of paracetamol and its metabolites in man. Br J Pharmacol Chemother. 1967;29: 150–157.
137. Potter WZ, Davis DC, Mitchell JR, Jollow DJ, Gillette JR, Brodie BB. Acetaminophen-induced hepatic necrosis. 3. Cytochrome P-450-mediated covalent binding in vitro. J Pharmacol Exp Ther. 1973;187: 203–210.

138. Jollow DJ, Mitchell JR, Potter WZ, Davis DC, Gillette JR, Brodie BB. Acetaminophen-induced hepatic necrosis. II. Role of covalent binding in vivo. J Pharmacol Exp Ther. 1973;187: 195–202.
139. Nakagawa H, Maeda S, Hikiba Y, Ohmae T, Shibata W, Yanai A, et al. Deletion of apoptosis signal-regulating kinase 1 attenuates acetaminophen-induced liver injury by inhibiting c-Jun N-terminal kinase activation. Gastroenterology. 2008;135: 1311–1321.
140. Bajt ML, Farhood A, Lemasters JJ, Jaeschke H. Mitochondrial bax translocation accelerates DNA fragmentation and cell necrosis in a murine model of acetaminophen hepatotoxicity. J Pharmacol Exp Ther. 2008;324: 8–14.
141. Mitchell JR, Jollow DJ, Potter WZ, Davis DC, Gillette JR, Brodie BB. Acetaminophen-induced hepatic necrosis. I. Role of drug metabolism. J Pharmacol Exp Ther. 1973;187: 185–194.
142. Jaeschke H, Bajt ML. Intracellular signaling mechanisms of acetaminophen-induced liver cell death. Toxicol Sci. 2006;89: 31–41.
143. Dalhoff K, Laursen H, Bangert K, Poulsen HE, Anderson ME, Grunnet N, et al. Autoprotection in acetaminophen intoxication in rats: the role of liver regeneration. Pharmacol Toxicol. 2001;88: 135–141.
144. Zieve L, Anderson WR, Dozeman R, Draves K, Lyftogt C. Acetaminophen liver injury: sequential changes in two biochemical indices of regeneration and their relationship to histologic alterations. J Lab Clin Med. 1985;105: 619–624.
145. Grompe M, al-Dhalimy M, Finegold M, Ou CN, Burlingame T, Kennaway NG, et al. Loss of fumarylacetoacetate hydrolase is responsible for the neonatal hepatic dysfunction phenotype of lethal albino mice. Genes Dev. 1993;7: 2298–2307.
146. Kelsey G, Ruppert S, Beermann F, Grund C, Tanguay RM, Schütz G. Rescue of mice homozygous for lethal albino deletions: implications for an animal model for the human liver disease tyrosinemia type 1. Genes Dev. 1993;7: 2285–2297.
147. Lindblad B, Lindstedt S, Steen G. On the enzymic defects in hereditary tyrosinemia. Proc Natl Acad Sci U S A. 1977;74: 4641–4645.
148. Jorquera R, Tanguay RM. The mutagenicity of the tyrosine metabolite, fumarylacetoacetate, is enhanced by glutathione depletion. Biochem Biophys Res Commun. 1997;232: 42–48.
149. Jorquera R, Tanguay RM. Cyclin B-dependent kinase and caspase-1 activation precedes mitochondrial dysfunction in fumarylacetoacetate-induced apoptosis. FASEB J. 1999;13: 2284–2298.
150. Kvittingen EA, Brodtkorb E. The pre- and post-natal diagnosis of tyrosinemia type I and the detection of the carrier state by assay of fumarylacetoacetase. Scand J Clin Lab Invest Suppl. 1986;184: 35–40.
151. Uhlen M, Zhang C, Lee S, Sjöstedt E, Fagerberg L, Bidkhori G, et al. A pathology atlas of the human cancer transcriptome. Science. 2017;357. doi:10.1126/science.aan2507
152. Russo PA, Mitchell GA, Tanguay RM. Tyrosinemia: a review. Pediatr Dev Pathol. 2001;4: 212–221.
153. Laberge C. Hereditary tyrosinemia in a French Canadian isolate. Am J Hum Genet. 1969;21: 36–45.
154. De Braekeleer M, Larochelle J. Genetic epidemiology of hereditary tyrosinemia in Quebec and in Saguenay-Lac-St-Jean. Am J Hum Genet. 1990;47: 302–307.
155. Heyer E. One founder/one gene hypothesis in a new expanding population: Saguenay (Quebec, Canada). Hum Biol. 1999;71: 99–109.
156. St-Louis M, Tanguay RM. Mutations in the fumarylacetoacetate hydrolase gene causing hereditary tyrosinemia type I: overview. Hum Mutat. 1997;9: 291–299.
157. Kvittingen EA. Hereditary tyrosinemia type I--an overview. Scand J Clin Lab Invest Suppl. 1986;184: 27–34.
158. Russo P, O'Regan S. Visceral pathology of hereditary tyrosinemia type I. Am J Hum Genet. 1990;47: 317–324.
159. Larochelle J, Privé L, Saidi M, Bélanger M, Tremblay M, Claveau JC, et al. [Hereditary tyrosinemia with tyrosiluria. Study of 44 cases in infants]. Union Med Can. 1968;97: 762–772.
160. Larochelle J, Privé L, Bélanger M, Bélanger L, Tremblay M, Claveau JC, et al. [Hereditary

tyrosinemia. I. Clinical and biological study of 62 cases]. Pediatrie. 1973;28: 5–18.
161. Dehner LP, Snover DC, Sharp HL, Ascher N, Nakhleh R, Day DL. Hereditary tyrosinemia type I (chronic form): pathologic findings in the liver. Hum Pathol. 1989;20: 149–158.
162. van Spronsen FJ, Berger R, Smit GP, de Klerk JB, Duran M, Bijleveld CM, et al. Tyrosinaemia type I: orthotopic liver transplantation as the only definitive answer to a metabolic as well as an oncological problem. J Inherit Metab Dis. 1989;12 Suppl 2: 339–342.
163. Weinberg AG, Mize CE, Worthen HG. The occurrence of hepatoma in the chronic form of hereditary tyrosinemia. J Pediatr. 1976;88: 434–438.
164. Haber BA, Chuang E, Lee W, Taub R. Variable gene expression within human tyrosinemia type 1 liver may reflect region-specific dysplasia. Hepatology. 1996;24: 65–71.
165. Kvittingen EA, Talseth T, Halvorsen S, Jakobs C, Hovig T, Flatmark A. Renal failure in adult patients with hereditary tyrosinaemia type I. J Inherit Metab Dis. 1991;14: 53–62.
166. Mitchell G, Larochelle J, Lambert M, Michaud J, Grenier A, Ogier H, et al. Neurologic crises in hereditary tyrosinemia. N Engl J Med. 1990;322: 432–437.
167. Perry TL. Tyrosinemia associated with hypermethioninemia and islet cell hyperplasia. Can Med Assoc J. 1967;97: 1067–1075.
168. Esquivel CO, Mieles L, Marino IR, Todo S, Makowka L, Ambrosino G, et al. Liver transplantation for hereditary tyrosinemia in the presence of hepatocellular carcinoma. Transplant Proc. 1989;21: 2445–2446.
169. Paradis K, Weber A, Seidman EG, Larochelle J, Garel L, Lenaerts C, et al. Liver transplantation for hereditary tyrosinemia: the Quebec experience. Am J Hum Genet. 1990;47: 338–342.
170. Lock EA, Ellis MK, Gaskin P, Robinson M, Auton TR, Provan WM, et al. From toxicological problem to therapeutic use: the discovery of the mode of action of 2-(2-nitro-4-trifluoromethylbenzoyl)-1,3-cyclohexanedione (NTBC), its toxicology and development as a drug. J Inherit Metab Dis. 1998;21: 498–506.
171. Holme E, Lindstedt S. Tyrosinaemia type I and NTBC (2-(2-nitro-4-trifluoromethylbenzoyl)-1,3-cyclohexanedione). J Inherit Metab Dis. 1998;21: 507–517.
172. Barkaoui E, Debray D, Habès D, Ogier H, Bernard O. [Favorable outcome of treatment with NTBC of acute liver insufficiency disclosing hereditary tyrosinemia type I]. Arch Pediatr. 1999;6: 540–544.
173. Ellis MK, Whitfield AC, Gowans LA, Auton TR, Provan WM, Lock EA, et al. Inhibition of 4-hydroxyphenylpyruvate dioxygenase by 2-(2-nitro-4-trifluoromethylbenzoyl)-cyclohexane-1,3-dione and 2-(2-chloro-4-methanesulfonylbenzoyl)-cyclohexane-1,3-dione. Toxicol Appl Pharmacol. 1995;133: 12–19.
174. Grompe M, Lindstedt S, al-Dhalimy M, Kennaway NG, Papaconstantinou J, Torres-Ramos CA, et al. Pharmacological correction of neonatal lethal hepatic dysfunction in a murine model of hereditary tyrosinaemia type I. Nat Genet. 1995;10: 453–460.
175. Endo F, Awata H, Katoh H, Matsuda I. A nonsense mutation in the 4-hydroxyphenylpyruvic acid dioxygenase gene (Hpd) causes skipping of the constitutive exon and hypertyrosinemia in mouse strain III. Genomics. 1995;25: 164–169.
176. Overturf K, Al-Dhalimy M, Tanguay R, Brantly M, Ou CN, Finegold M, et al. Hepatocytes corrected by gene therapy are selected in vivo in a murine model of hereditary tyrosinaemia type I. Nat Genet. 1996;12: 266–273.
177. Overturf K, Al-Dhalimy M, Manning K, Ou CN, Finegold M, Grompe M. Ex vivo hepatic gene therapy of a mouse model of Hereditary Tyrosinemia Type I. Hum Gene Ther. 1998;9: 295–304.
178. Overturf K, al-Dhalimy M, Ou CN, Finegold M, Tanguay R, Lieber A, et al. Adenovirus-mediated gene therapy in a mouse model of hereditary tyrosinemia type I. Hum Gene Ther. 1997;8: 513–521.
179. Paulk NK, Wursthorn K, Wang Z, Finegold MJ, Kay MA, Grompe M. Adeno-associated virus gene repair corrects a mouse model of hereditary tyrosinemia in vivo. Hepatology. 2010;51: 1200–1208.

180. Montini E, Held PK, Noll M, Morcinek N, Al-Dhalimy M, Finegold M, et al. In vivo correction of murine tyrosinemia type I by DNA-mediated transposition. Mol Ther. 2002;6: 759–769.
181. Yin H, Xue W, Chen S, Bogorad RL, Benedetti E, Grompe M, et al. Genome editing with Cas9 in adult mice corrects a disease mutation and phenotype. Nat Biotechnol. 2014;32: 551–553.
182. Wangensteen KJ, Wilber A, Keng VW, He Z, Matise I, Wangensteen L, et al. A facile method for somatic, lifelong manipulation of multiple genes in the mouse liver. Hepatology. 2008;47: 1714–1724.
183. Wang AW, Wangensteen KJ, Wang YJ, Zahm AM, Moss NG, Erez N, et al. TRAP-seq identifies cystine/glutamate antiporter as a driver of recovery from liver injury. J Clin Invest. 2018;128: 2297–2309.
184. Wuestefeld T, Pesic M, Rudalska R, Dauch D, Longerich T, Kang T-W, et al. A Direct in vivo RNAi screen identifies MKK4 as a key regulator of liver regeneration. Cell. 2013;153: 389–401.
185. Wangensteen KJ, Zhang S, Greenbaum LE, Kaestner KH. A genetic screen reveals Foxa3 and TNFR1 as key regulators of liver repopulation. Genes Dev. 2015;29: 904–909.
186. Wangensteen KJ, Wang YJ, Dou Z, Wang AW, Mosleh-Shirazi E, Horlbeck MA, et al. Combinatorial genetics in liver repopulation and carcinogenesis with a in vivo CRISPR activation platform. Hepatology. 2018;68: 663–676.
187. Zahm AM, Wang AW, Wang YJ, Schug J, Wangensteen KJ, Kaestner KH. A high-content in vivo screen to identify microRNA epistasis in the repopulating mouse liver [Internet]. doi:10.1101/664847
188. Kjeldgaard NO, Ploug J. Urokinase an activator of plasminogen from human urine. II. Mechanism of plasminogen activation. Biochim Biophys Acta. 1957;24: 283–289.
189. Heckel JL, Sandgren EP, Degen JL, Palmiter RD, Brinster RL. Neonatal bleeding in transgenic mice expressing urokinase-type plasminogen activator. Cell. 1990;62: 447–456.
190. Sandgren EP, Palmiter RD, Heckel JL, Daugherty CC, Brinster RL, Degen JL. Complete hepatic regeneration after somatic deletion of an albumin-plasminogen activator transgene. Cell. 1991;66: 245–256.
191. Rhim JA, Sandgren EP, Degen JL, Palmiter RD, Brinster RL. Replacement of diseased mouse liver by hepatic cell transplantation. Science. 1994;263: 1149–1152.
192. Rhim JA, Sandgren EP, Palmiter RD, Brinster RL. Complete reconstitution of mouse liver with xenogeneic hepatocytes. Proc Natl Acad Sci U S A. 1995;92: 4942–4946.
193. Mercer DF, Schiller DE, Elliott JF, Douglas DN, Hao C, Rinfret A, et al. Hepatitis C virus replication in mice with chimeric human livers. Nat Med. 2001;7: 927–933.
194. Tateno C, Yoshizane Y, Saito N, Kataoka M, Utoh R, Yamasaki C, et al. Near completely humanized liver in mice shows human-type metabolic responses to drugs. Am J Pathol. 2004;165: 901–912.
195. Dandri M, Burda MR, Török E, Pollok JM, Iwanska A, Sommer G, et al. Repopulation of mouse liver with human hepatocytes and in vivo infection with hepatitis B virus. Hepatology. 2001;33: 981–988.
196. Wilson JW, Leduc EH. Role of cholangioles in restoration of the liver of the mouse after dietary injury. J Pathol Bacteriol. 1958;76: 441–449.
197. Demetris AJ, Seaberg EC, Wennerberg A, Ionellie J, Michalopoulos G. Ductular reaction after submassive necrosis in humans. Special emphasis on analysis of ductular hepatocytes. Am J Pathol. 1996;149: 439–448.
198. Grisham JW, Porta EA. ORIGIN AND FATE OF PROLIFERATED HEPATIC DUCTAL CELLS IN THE RAT: ELECTRON MICROSCOPIC AND AUTORADIOGRAPHIC STUDIES. Exp Mol Pathol. 1964;3: 242–261.
199. Gerber MA, Thung SN, Shen S, Stromeyer FW, Ishak KG. Phenotypic characterization of hepatic proliferation. Antigenic expression by proliferating epithelial cells in fetal liver, massive hepatic necrosis, and nodular transformation of the liver. Am J Pathol. 1983;110: 70–74.
200. Peraino C, Fry RJ, Staffeldt E. Reduction and enhancement by phenobarbital of hepatocarcinogenesis induced in the rat by 2-acetylaminofluorene. Cancer Res. 1971;31: 1506–1512.

201. Tatematsu M, Ho RH, Kaku T, Ekem JK, Farber E. Studies on the proliferation and fate of oval cells in the liver of rats treated with 2-acetylaminofluorene and partial hepatectomy. Am J Pathol. 1984;114: 418–430.
202. DeBaun JR, Rowley JY, Miller EC, Miller JA. Sulfotransferase activation of N-hydroxy-2-acetylaminofluorene in rodent livers susceptible and resistant to this carcinogen. Proc Soc Exp Biol Med. 1968;129: 268–273.
203. Evarts RP, Nagy P, Marsden E, Thorgeirsson SS. A precursor-product relationship exists between oval cells and hepatocytes in rat liver. Carcinogenesis. 1987;8: 1737–1740.
204. Petersen BE, Zajac VF, Michalopoulos GK. Hepatic oval cell activation in response to injury following chemically induced periportal or pericentral damage in rats. Hepatology. 1998;27: 1030–1038.
205. Tephly TR, Gibbs AH, De Matteis F. Studies on the mechanism of experimental porphyria produced by 3,5-diethoxycarbonyl-1,4-dihydrocollidine. Role of a porphyrin-like inhibitor of protohaem ferro-lyase. Biochem J. 1979;180: 241–244.
206. Preisegger KH, Factor VM, Fuchsbichler A, Stumptner C, Denk H, Thorgeirsson SS. Atypical ductular proliferation and its inhibition by transforming growth factor beta1 in the 3,5-diethoxycarbonyl-1,4-dihydrocollidine mouse model for chronic alcoholic liver disease. Lab Invest. 1999;79: 103–109.
207. Faktor VM, Engel'gardt NV, Iazova AK, Lazareva MN, Poltoranina VS, Rudinskaia TD. [Common antigens of oval cells and cholangiocytes in the mouse. Their detection by using monoclonal antibodies]. Ontogenez. 1990;21: 625–632.
208. Lemire JM, Shiojiri N, Fausto N. Oval cell proliferation and the origin of small hepatocytes in liver injury induced by D-galactosamine. Am J Pathol. 1991;139: 535–552.
209. Okabe M, Tsukahara Y, Tanaka M, Suzuki K, Saito S, Kamiya Y, et al. Potential hepatic stem cells reside in EpCAM+ cells of normal and injured mouse liver. Development. 2009;136: 1951–1960.
210. Sackett SD, Li Z, Hurtt R, Gao Y, Wells RG, Brondell K, et al. Foxl1 is a marker of bipotential hepatic progenitor cells in mice. Hepatology. 2009;49: 920–929.
211. Shin S, Walton G, Aoki R, Brondell K, Schug J, Fox A, et al. Foxl1-Cre-marked adult hepatic progenitors have clonogenic and bilineage differentiation potential. Genes Dev. 2011;25: 1185–1192.
212. Shinozuka H, Lombardi B, Sell S, Iammarino RM. Early histological and functional alterations of ethionine liver carcinogenesis in rats fed a choline-deficient diet. Cancer Res. 1978;38: 1092–1098.
213. Akhurst B, Croager EJ, Farley-Roche CA, Ong JK, Dumble ML, Knight B, et al. A modified choline-deficient, ethionine-supplemented diet protocol effectively induces oval cells in mouse liver. Hepatology. 2001;34: 519–522.
214. Yao ZM, Vance DE. The active synthesis of phosphatidylcholine is required for very low density lipoprotein secretion from rat hepatocytes. J Biol Chem. 1988;263: 2998–3004.
215. Aoyama Y, Yasui H, Ashida K. Effect of dietary protein and amino acids in a choline-deficient diet on lipid accumulation in rat liver. J Nutr. 1971;101: 739–745.
216. Lombardi B. Effects of choline deficiency on rat hepatocytes. Fed Proc. 1971;30: 139–142.
217. Norbury C, Nurse P. Animal cell cycles and their control. Annu Rev Biochem. 1992;61: 441–470.
218. Vermeulen K, Van Bockstaele DR, Berneman ZN. The cell cycle: a review of regulation, deregulation and therapeutic targets in cancer. Cell Prolif. 2003;36: 131–149.
219. Koff A, Cross F, Fisher A, Schumacher J, Leguellec K, Philippe M, et al. Human cyclin E, a new cyclin that interacts with two members of the CDC2 gene family. Cell. 1991;66: 1217–1228.
220. Lew DJ, Dulić V, Reed SI. Isolation of three novel human cyclins by rescue of G1 cyclin (Cln) function in yeast. Cell. 1991;66: 1197–1206.
221. Xiong Y, Connolly T, Futcher B, Beach D. Human D-type cyclin. Cell. 1991;65: 691–699.
222. Lehner CF, O'Farrell PH. Expression and function of Drosophila cyclin A during embryonic cell cycle progression. Cell. 1989;56: 957–968.

223. Pines J, Hunter T. Isolation of a human cyclin cDNA: evidence for cyclin mRNA and protein regulation in the cell cycle and for interaction with p34cdc2. Cell. 1989;58: 833–846.
224. Rabes HM, Iseler G, Czichos S, Tuczek HV. Synchronization of hepatocellular DNA synthesis in regenerating rat liver by continuous infusion of hydroxyurea. Cancer Res. 1977;37: 1105–1111.
225. Webber EM, Godowski PJ, Fausto N. In vivo response of hepatocytes to growth factors requires an initial priming stimulus. Hepatology. 1994;19: 489–497.
226. Mead JE, Braun L, Martin DA, Fausto N. Induction of replicative competence ("priming") in normal liver. Cancer Res. 1990;50: 7023–7030.
227. Fausto N. Growth factors in liver development, regeneration and carcinogenesis. Prog Growth Factor Res. 1991;3: 219–234.
228. Fausto N, Laird AD, Webber EM. Liver regeneration. 2. Role of growth factors and cytokines in hepatic regeneration. The FASEB Journal. 1995;9: 1527–1536.
229. Michalopoulos GK. Liver regeneration: molecular mechanisms of growth control. FASEB J. 1990;4: 176–187.
230. Decker K. Biologically active products of stimulated liver macrophages (Kupffer cells). Eur J Biochem. 1990;192: 245–261.
231. Akerman P, Cote P, Yang SQ, McClain C, Nelson S, Bagby GJ, et al. Antibodies to tumor necrosis factor-alpha inhibit liver regeneration after partial hepatectomy. Am J Physiol. 1992;263: G579–85.
232. Cressman DE, Greenbaum LE, DeAngelis RA, Ciliberto G, Furth EE, Poli V, et al. Liver failure and defective hepatocyte regeneration in interleukin-6-deficient mice. Science. 1996;274: 1379–1383.
233. Webber EM, Bruix J, Pierce RH, Fausto N. Tumor necrosis factor primes hepatocytes for DNA replication in the rat. Hepatology. 1998;28: 1226–1234.
234. Yamada Y, Kirillova I, Peschon JJ, Fausto N. Initiation of liver growth by tumor necrosis factor: deficient liver regeneration in mice lacking type I tumor necrosis factor receptor. Proc Natl Acad Sci U S A. 1997;94: 1441–1446.
235. Kirillova I, Chaisson M, Fausto N. Tumor necrosis factor induces DNA replication in hepatic cells through nuclear factor kappaB activation. Cell Growth Differ. 1999;10: 819–828.
236. Geiger T, Andus T, Klapproth J, Hirano T, Kishimoto T, Heinrich PC. Induction of rat acute-phase proteins by interleukin 6 in vivo. Eur J Immunol. 1988;18: 717–721.
237. Wuestefeld T, Klein C, Streetz KL, Betz U, Lauber J, Buer J, et al. Interleukin-6/glycoprotein 130-dependent pathways are protective during liver regeneration. J Biol Chem. 2003;278: 11281–11288.
238. Thompson NL, Mead JE, Braun L, Goyette M, Shank PR, Fausto N. Sequential protooncogene expression during rat liver regeneration. Cancer Res. 1986;46: 3111–3117.
239. Greenbaum LE, Li W, Cressman DE, Peng Y, Ciliberto G, Poli V, et al. CCAAT enhancer-binding protein beta is required for normal hepatocyte proliferation in mice after partial hepatectomy. J Clin Invest. 1998;102: 996–1007.
240. Haber BA, Mohn KL, Diamond RH, Taub R. Induction patterns of 70 genes during nine days after hepatectomy define the temporal course of liver regeneration. J Clin Invest. 1993;91: 1319–1326.
241. Li W, Liang X, Leu JI, Kovalovich K, Ciliberto G, Taub R. Global changes in interleukin-6-dependent gene expression patterns in mouse livers after partial hepatectomy. Hepatology. 2001;33: 1377–1386.
242. Matsumoto T, O'Malley K, Efron PA, Burger C, McAuliffe PF, Scumpia PO, et al. Interleukin-6 and STAT3 protect the liver from hepatic ischemia and reperfusion injury during ischemic preconditioning. Surgery. 2006;140: 793–802.
243. Bruccoleri A, Gallucci R, Germolec DR, Blackshear P, Simeonova P, Thurman RG, et al. Induction of early-immediate genes by tumor necrosis factor alpha contribute to liver repair following chemical-induced hepatotoxicity. Hepatology. 1997;25: 133–141.

244. Katz A, Chebath J, Friedman J, Revel M. Increased sensitivity of IL-6-deficient mice to carbon tetrachloride hepatotoxicity and protection with an IL-6 receptor-IL-6 chimera. Cytokines Cell Mol Ther. 1998;4: 221–227.
245. Chiu H, Gardner CR, Dambach DM, Durham SK, Brittingham JA, Laskin JD, et al. Role of tumor necrosis factor receptor 1 (p55) in hepatocyte proliferation during acetaminophen-induced toxicity in mice. Toxicol Appl Pharmacol. 2003;193: 218–227.
246. James LP, Lamps LW, McCullough S, Hinson JA. Interleukin 6 and hepatocyte regeneration in acetaminophen toxicity in the mouse. Biochem Biophys Res Commun. 2003;309: 857–863.
247. Fujita J, Marino MW, Wada H, Jungbluth AA, Mackrell PJ, Rivadeneira DE, et al. Effect of TNF gene depletion on liver regeneration after partial hepatectomy in mice. Surgery. 2001;129: 48–54.
248. Hayashi H, Nagaki M, Imose M, Osawa Y, Kimura K, Takai S, et al. Normal liver regeneration and liver cell apoptosis after partial hepatectomy in tumor necrosis factor-alpha-deficient mice. Liver Int. 2005;25: 162–170.
249. Sakamoto T, Liu Z, Murase N, Ezure T, Yokomuro S, Poli V, et al. Mitosis and apoptosis in the liver of interleukin-6-deficient mice after partial hepatectomy. Hepatology. 1999;29: 403–411.
250. Blindenbacher A, Wang X, Langer I, Savino R, Terracciano L, Heim MH. Interleukin 6 is important for survival after partial hepatectomy in mice. Hepatology. 2003;38: 674–682.
251. McGowan JA, Strain AJ, Bucher NL. DNA synthesis in primary cultures of adult rat hepatocytes in a defined medium: effects of epidermal growth factor, insulin, glucagon, and cyclic-AMP. J Cell Physiol. 1981;108: 353–363.
252. Brenner DA, Koch KS, Leffert HL. Transforming growth factor-alpha stimulates proto-oncogene c-jun expression and a mitogenic program in primary cultures of adult rat hepatocytes. DNA. 1989;8: 279–285.
253. Mead JE, Fausto N. Transforming growth factor alpha may be a physiological regulator of liver regeneration by means of an autocrine mechanism. Proc Natl Acad Sci U S A. 1989;86: 1558–1562.
254. Strain AJ, Ismail T, Tsubouchi H, Arakaki N, Hishida T, Kitamura N, et al. Native and recombinant human hepatocyte growth factors are highly potent promoters of DNA synthesis in both human and rat hepatocytes. J Clin Invest. 1991;87: 1853–1857.
255. Breider MA, Bleavins MR, Reindel JF, Gough AW, de la Iglesia FA. Cellular hyperplasia in rats following continuous intravenous infusion of recombinant human epidermal growth factor. Vet Pathol. 1996;33: 184–194.
256. Roos F, Ryan AM, Chamow SM, Bennett GL, Schwall RH. Induction of liver growth in normal mice by infusion of hepatocyte growth factor/scatter factor. Am J Physiol. 1995;268: G380–6.
257. Webber EM, Wu JC, Wang L, Merlino G, Fausto N. Overexpression of transforming growth factor-alpha causes liver enlargement and increased hepatocyte proliferation in transgenic mice. Am J Pathol. 1994;145: 398–408.
258. Skov Olsen P, Boesby S, Kirkegaard P, Therkelsen K, Almdal T, Poulsen SS, et al. Influence of epidermal growth factor on liver regeneration after partial hepatectomy in rats. Hepatology. 1988;8: 992–996.
259. Mars WM, Zarnegar R, Michalopoulos GK. Activation of hepatocyte growth factor by the plasminogen activators uPA and tPA. Am J Pathol. 1993;143: 949–958.
260. Schirmacher P, Geerts A, Jung W, Pietrangelo A, Rogler CE, Dienes HP. The role of Ito cells in the biosynthesis of HGF-SF in the liver. EXS. 1993;65: 285–299.
261. Naldini L, Tamagnone L, Vigna E, Sachs M, Hartmann G, Birchmeier W, et al. Extracellular proteolytic cleavage by urokinase is required for activation of hepatocyte growth factor/scatter factor. EMBO J. 1992;11: 4825–4833.
262. Lindroos PM, Zarnegar R, Michalopoulos GK. Hepatocyte growth factor (hepatopoietin A) rapidly increases in plasma before DNA synthesis and liver regeneration stimulated by partial hepatectomy and carbon tetrachloride administration. Hepatology. 1991;13: 743–750.

263. Naldini L, Vigna E, Narsimhan RP, Gaudino G, Zarnegar R, Michalopoulos GK, et al. Hepatocyte growth factor (HGF) stimulates the tyrosine kinase activity of the receptor encoded by the proto-oncogene c-MET. Oncogene. 1991;6: 501–504.
264. Tomiya T, Ogata I, Yamaoka M, Yanase M, Inoue Y, Fujiwara K. The mitogenic activity of hepatocyte growth factor on rat hepatocytes is dependent upon endogenous transforming growth factor-alpha. Am J Pathol. 2000;157: 1693–1701.
265. Diehl AM, Rai RM. Liver regeneration 3: Regulation of signal transduction during liver regeneration. FASEB J. 1996;10: 215–227.
266. Brenner DA. Signal transduction during liver regeneration [Internet]. Journal of Gastroenterology and Hepatology. 1998. pp. S93–S95. doi:10.1111/jgh.1998.13.s1.93
267. Shimizu M, Hara A, Okuno M, Matsuno H, Okada K, Ueshima S, et al. Mechanism of retarded liver regeneration in plasminogen activator-deficient mice: impaired activation of hepatocyte growth factor after Fas-mediated massive hepatic apoptosis. Hepatology. 2001;33: 569–576.
268. Burr AW, Toole K, Chapman C, Hines JE, Burt AD. Anti-hepatocyte growth factor antibody inhibits hepatocyte proliferation during liver regeneration. J Pathol. 1998;185: 298–302.
269. Borowiak M, Garratt AN, Wüstefeld T, Strehle M, Trautwein C, Birchmeier C. Met provides essential signals for liver regeneration. Proc Natl Acad Sci U S A. 2004;101: 10608–10613.
270. Huh C-G, Factor VM, Sánchez A, Uchida K, Conner EA, Thorgeirsson SS. Hepatocyte growth factor/c-met signaling pathway is required for efficient liver regeneration and repair. Proc Natl Acad Sci U S A. 2004;101: 4477–4482.
271. Elder JB, Williams G, Lacey E, Gregory H. Cellular localisation of human urogastrone/epidermal growth factor. Nature. 1978;271: 466–467.
272. Olsen PS, Poulsen SS, Kirkegaard P. Adrenergic effects on secretion of epidermal growth factor from Brunner's glands. Gut. 1985;26: 920–927.
273. Argast GM, Campbell JS, Brooling JT, Fausto N. Epidermal growth factor receptor transactivation mediates tumor necrosis factor-induced hepatocyte replication. J Biol Chem. 2004;279: 34530–34536.
274. Gruppuso PA, Mead JE, Fausto N. Transforming growth factor receptors in liver regeneration following partial hepatectomy in the rat. Cancer Res. 1990;50: 1464–1469.
275. UniProt Consortium. UniProt: a worldwide hub of protein knowledge. Nucleic Acids Res. 2019;47: D506–D515.
276. Scheving LA, Stevenson MC, Taylormoore JM, Traxler P, Russell WE. Integral role of the EGF receptor in HGF-mediated hepatocyte proliferation. Biochem Biophys Res Commun. 2002;290: 197–203.
277. Russell WE, Kaufmann WK, Sitaric S, Luetteke NC, Lee DC. Liver regeneration and hepatocarcinogenesis in transforming growth factor-alpha-targeted mice. Mol Carcinog. 1996;15: 183–189.
278. Natarajan A, Wagner B, Sibilia M. The EGF receptor is required for efficient liver regeneration. Proc Natl Acad Sci U S A. 2007;104: 17081–17086.
279. Nagy P, Evarts RP, McMahon JB, Thorgeirsson SS. Role of TGF-beta in normal differentiation and oncogenesis in rat liver. Mol Carcinog. 1989;2: 345–354.
280. Hyytiäinen M, Taipale J, Heldin CH, Keski-Oja J. Recombinant latent transforming growth factor beta-binding protein 2 assembles to fibroblast extracellular matrix and is susceptible to proteolytic processing and release. J Biol Chem. 1998;273: 20669–20676.
281. Bissell DM, Roulot D, George J. Transforming growth factor beta and the liver. Hepatology. 2001;34: 859–867.
282. Braun L, Mead JE, Panzica M, Mikumo R, Bell GI, Fausto N. Transforming growth factor beta mRNA increases during liver regeneration: a possible paracrine mechanism of growth regulation. Proc Natl Acad Sci U S A. 1988;85: 1539–1543.
283. Chari RS, Price DT, Sue SR, Meyers WC, Jirtle RL. Down-regulation of transforming growth factor beta receptor type I, II, and III during liver regeneration. Am J Surg. 1995;169: 126–31; discussion 131–2.
284. Houck KA, Michalopoulos GK. Altered responses of regenerating hepatocytes to norepinephrine and transforming growth factor type beta. J Cell Physiol. 1989;141: 503–509.

285. Houck KA, Cruise JL, Michalopoulos G. Norepinephrine modulates the growth-inhibitory effect of transforming growth factor-beta in primary rat hepatocyte cultures. J Cell Physiol. 1988;135: 551–555.
286. Macías-Silva M, Abdollah S, Hoodless PA, Pirone R, Attisano L, Wrana JL. MADR2 is a substrate of the TGFbeta receptor and its phosphorylation is required for nuclear accumulation and signaling. Cell. 1996;87: 1215–1224.
287. Zhang Y, Feng X, We R, Derynck R. Receptor-associated Mad homologues synergize as effectors of the TGF-beta response. Nature. 1996;383: 168–172.
288. Reynisdóttir I, Polyak K, Iavarone A, Massagué J. Kip/Cip and Ink4 Cdk inhibitors cooperate to induce cell cycle arrest in response to TGF-beta. Genes Dev. 1995;9: 1831–1845.
289. Koff A, Ohtsuki M, Polyak K, Roberts JM, Massagué J. Negative regulation of G1 in mammalian cells: inhibition of cyclin E-dependent kinase by TGF-beta. Science. 1993;260: 536–539.
290. Polyak K, Kato JY, Solomon MJ, Sherr CJ, Massague J, Roberts JM, et al. p27Kip1, a cyclin-Cdk inhibitor, links transforming growth factor-beta and contact inhibition to cell cycle arrest. Genes Dev. 1994;8: 9–22.
291. Carr BI, Hayashi I, Branum EL, Moses HL. Inhibition of DNA synthesis in rat hepatocytes by platelet-derived type beta transforming growth factor. Cancer Res. 1986;46: 2330–2334.
292. Russell WE, Coffey RJ Jr, Ouellette AJ, Moses HL. Type beta transforming growth factor reversibly inhibits the early proliferative response to partial hepatectomy in the rat. Proc Natl Acad Sci U S A. 1988;85: 5126–5130.
293. Sanderson N, Factor V, Nagy P, Kopp J, Kondaiah P, Wakefield L, et al. Hepatic expression of mature transforming growth factor beta 1 in transgenic mice results in multiple tissue lesions. Proc Natl Acad Sci U S A. 1995;92: 2572–2576.
294. Oe S, Lemmer ER, Conner EA, Factor VM, Levéen P, Larsson J, et al. Intact signaling by transforming growth factor beta is not required for termination of liver regeneration in mice. Hepatology. 2004;40: 1098–1105.
295. Yasuda H, Mine T, Shibata H, Eto Y, Hasegawa Y, Takeuchi T, et al. Activin A: an autocrine inhibitor of initiation of DNA synthesis in rat hepatocytes. J Clin Invest. 1993;92: 1491–1496.
296. Kogure K, Omata W, Kanzaki M, Zhang YQ, Yasuda H, Mine T, et al. A single intraportal administration of follistatin accelerates liver regeneration in partially hepatectomized rats. Gastroenterology. 1995;108: 1136–1142.
297. Lichtsteiner S, Wuarin J, Schibler U. The interplay of DNA-binding proteins on the promoter of the mouse albumin gene. Cell. 1987;51: 963–973.
298. Costa RH, Grayson DR, Xanthopoulos KG, Darnell JE Jr. A liver-specific DNA-binding protein recognizes multiple nucleotide sites in regulatory regions of transthyretin, alpha 1-antitrypsin, albumin, and simian virus 40 genes. Proc Natl Acad Sci U S A. 1988;85: 3840–3844.
299. Mischoulon D, Rana B, Bucher NL, Farmer SR. Growth-dependent inhibition of CCAAT enhancer-binding protein (C/EBP alpha) gene expression during hepatocyte proliferation in the regenerating liver and in culture. Mol Cell Biol. 1992;12: 2553–2560.
300. Greenbaum LE, Cressman DE, Haber BA, Taub R. Coexistence of C/EBP alpha, beta, growth-induced proteins and DNA synthesis in hepatocytes during liver regeneration. Implications for maintenance of the differentiated state during liver growth. J Clin Invest. 1995;96: 1351–1365.
301. Umek RM, Friedman AD, McKnight SL. CCAAT-enhancer binding protein: a component of a differentiation switch. Science. 1991;251: 288–292.
302. Timchenko NA, Wilde M, Nakanishi M, Smith JR, Darlington GJ. CCAAT/enhancer-binding protein alpha (C/EBP alpha) inhibits cell proliferation through the p21 (WAF-1/CIP-1/SDI-1) protein. Genes Dev. 1996;10: 804–815.
303. Timchenko NA, Harris TE, Wilde M, Bilyeu TA, Burgess-Beusse BL, Finegold MJ, et al. CCAAT/enhancer binding protein alpha regulates p21 protein and hepatocyte proliferation in newborn mice. Mol Cell Biol. 1997;17: 7353–7361.
304. Timchenko NA, Wilde M, Darlington GJ. C/EBPalpha regulates formation of S-phase-specific E2F-p107 complexes in livers of newborn mice. Mol Cell Biol. 1999;19: 2936–2945.

305. Timchenko NA, Wilde M, Iakova P, Albrecht JH, Darlington GJ. E2F/p107 and E2F/p130 complexes are regulated by C/EBPalpha in 3T3-L1 adipocytes. Nucleic Acids Res. 1999;27: 3621–3630.
306. Wang H, Iakova P, Wilde M, Welm A, Goode T, Roesler WJ, et al. C/EBPalpha arrests cell proliferation through direct inhibition of Cdk2 and Cdk4. Mol Cell. 2001;8: 817–828.
307. Wang H, Goode T, Iakova P, Albrecht JH, Timchenko NA. C/EBPalpha triggers proteasome-dependent degradation of cdk4 during growth arrest. EMBO J. 2002;21: 930–941.
308. Johnson PF. Molecular stop signs: regulation of cell-cycle arrest by C/EBP transcription factors. J Cell Sci. 2005;118: 2545–2555.
309. Soriano HE, Kang DC, Finegold MJ, Hicks MJ, Wang ND, Harrison W, et al. Lack of C/EBP alpha gene expression results in increased DNA synthesis and an increased frequency of immortalization of freshly isolated mice [correction of rat] hepatocytes. Hepatology. 1998;27: 392–401.
310. Flodby P, Barlow C, Kylefjord H, Ahrlund-Richter L, Xanthopoulos KG. Increased hepatic cell proliferation and lung abnormalities in mice deficient in CCAAT/enhancer binding protein alpha. J Biol Chem. 1996;271: 24753–24760.
311. Harvey KF, Pfleger CM, Hariharan IK. The Drosophila Mst ortholog, hippo, restricts growth and cell proliferation and promotes apoptosis. Cell. 2003;114: 457–467.
312. Udan RS, Kango-Singh M, Nolo R, Tao C, Halder G. Hippo promotes proliferation arrest and apoptosis in the Salvador/Warts pathway. Nat Cell Biol. 2003;5: 914–920.
313. Dong J, Feldmann G, Huang J, Wu S, Zhang N, Comerford SA, et al. Elucidation of a universal size-control mechanism in Drosophila and mammals. Cell. 2007;130: 1120–1133.
314. Zhao B, Wei X, Li W, Udan RS, Yang Q, Kim J, et al. Inactivation of YAP oncoprotein by the Hippo pathway is involved in cell contact inhibition and tissue growth control. Genes Dev. 2007;21: 2747–2761.
315. Wang C, Zhang L, He Q, Feng X, Zhu J, Xu Z, et al. Differences in Yes-associated protein and mRNA levels in regenerating liver and hepatocellular carcinoma. Mol Med Rep. 2012;5: 410–414.
316. Grijalva JL, Huizenga M, Mueller K, Rodriguez S, Brazzo J, Camargo F, et al. Dynamic alterations in Hippo signaling pathway and YAP activation during liver regeneration. Am J Physiol Gastrointest Liver Physiol. 2014;307: G196–204.
317. Camargo FD, Gokhale S, Johnnidis JB, Fu D, Bell GW, Jaenisch R, et al. YAP1 increases organ size and expands undifferentiated progenitor cells. Curr Biol. 2007;17: 2054–2060.
318. Zhou D, Conrad C, Xia F, Park J-S, Payer B, Yin Y, et al. Mst1 and Mst2 maintain hepatocyte quiescence and suppress hepatocellular carcinoma development through inactivation of the Yap1 oncogene. Cancer Cell. 2009;16: 425–438.
319. Apte U, Gkretsi V, Bowen WC, Mars WM, Luo J-H, Donthamsetty S, et al. Enhanced liver regeneration following changes induced by hepatocyte-specific genetic ablation of integrin-linked kinase. Hepatology. 2009;50: 844–851.
320. Donthamsetty S, Bowen W, Mars W, Bhave V, Luo J-H, Wu C, et al. Liver-specific ablation of integrin-linked kinase in mice results in enhanced and prolonged cell proliferation and hepatomegaly after phenobarbital administration. Toxicol Sci. 2010;113: 358–366.
321. Liu B, Bell AW, Paranjpe S, Bowen WC, Khillan JS, Luo J-H, et al. Suppression of liver regeneration and hepatocyte proliferation in hepatocyte-targeted glypican 3 transgenic mice. Hepatology. 2010;52: 1060–1067.
322. Lin C-W, Mars WM, Paranjpe S, Donthamsetty S, Bhave VS, Kang L-I, et al. Hepatocyte proliferation and hepatomegaly induced by phenobarbital and 1,4-bis [2-(3,5-dichloropyridyloxy)] benzene is suppressed in hepatocyte-targeted glypican 3 transgenic mice. Hepatology. 2011;54: 620–630.
323. Assy N, Spira G, Paizi M, Shenkar L, Kraizer Y, Cohen T, et al. Effect of vascular endothelial growth factor on hepatic regenerative activity following partial hepatectomy in rats. J Hepatol. 1999;30: 911–915.

324. Ding B-S, Nolan DJ, Butler JM, James D, Babazadeh AO, Rosenwaks Z, et al. Inductive angiocrine signals from sinusoidal endothelium are required for liver regeneration. Nature. 2010;468: 310–315.
325. Scher CD, Stone ME, Stiles CD. Platelet-derived growth factor prevents G0 growth arrest. Nature. 1979;281: 390–392.
326. Nakamura T, Nawa K, Ichihara A. Partial purification and characterization of hepatocyte growth factor from serum of hepatectomized rats. Biochem Biophys Res Commun. 1984;122: 1450–1459.
327. Housley RM, Morris CF, Boyle W, Ring B, Biltz R, Tarpley JE, et al. Keratinocyte growth factor induces proliferation of hepatocytes and epithelial cells throughout the rat gastrointestinal tract. J Clin Invest. 1994;94: 1764–1777.
328. Strain AJ, McGuinness G, Rubin JS, Aaronson SA. Keratinocyte growth factor and fibroblast growth factor action on DNA synthesis in rat and human hepatocytes: modulation by heparin. Exp Cell Res. 1994;210: 253–259.
329. Ito N, Kawata S, Tamura S, Kiso S, Tsushima H, Damm D, et al. Heparin-binding EGF-like growth factor is a potent mitogen for rat hepatocytes. Biochem Biophys Res Commun. 1994;198: 25–31.
330. Huang W, Ma K, Zhang J, Qatanani M, Cuvillier J, Liu J, et al. Nuclear receptor-dependent bile acid signaling is required for normal liver regeneration. Science. 2006;312: 233–236.
331. Lesurtel M, Graf R, Aleil B, Walther DJ, Tian Y, Jochum W, et al. Platelet-derived serotonin mediates liver regeneration. Science. 2006;312: 104–107.
332. Bucher ML, Swaffield MN. Regulation of hepatic regeneration in rats by synergistic action of insulin and glucagon. Proc Natl Acad Sci U S A. 1975;72: 1157–1160.
333. Starzl TE, Watanabe K, Porter KA, Putnam CW. Effects of insulin, glucagon, and insuling/glucagon infusions on liver morphology and cell division after complete portacaval shunt in dogs. Lancet. 1976;1: 821–825.
334. Cruise JL, Houck KA, Michalopoulos GK. Induction of DNA synthesis in cultured rat hepatocytes through stimulation of alpha 1 adrenoreceptor by norepinephrine. Science. 1985;227: 749–751.
335. Cruise JL, Knechtle SJ, Bollinger RR, Kuhn C, Michalopoulos G. Alpha 1-adrenergic effects and liver regeneration. Hepatology. 1987;7: 1189–1194.
336. Mastellos D, Papadimitriou JC, Franchini S, Tsonis PA, Lambris JD. A novel role of complement: mice deficient in the fifth component of complement (C5) exhibit impaired liver regeneration. J Immunol. 2001;166: 2479–2486.
337. Colletti LM, Green M, Burdick MD, Kunkel SL, Strieter RM. Proliferative effects of CXC chemokines in rat hepatocytes in vitro and in vivo. Shock. 1998;10: 248–257.
338. Hogaboam CM, Bone-Larson CL, Steinhauser ML, Lukacs NW, Colletti LM, Simpson KJ, et al. Novel CXCR2-dependent liver regenerative qualities of ELR-containing CXC chemokines. FASEB J. 1999;13: 1565–1574.
339. Tan X, Behari J, Cieply B, Michalopoulos GK, Monga SPS. Conditional deletion of beta-catenin reveals its role in liver growth and regeneration. Gastroenterology. 2006;131: 1561–1572.
340. Sekine S, Gutiérrez PJA, Lan BY-A, Feng S, Hebrok M. Liver-specific loss of beta-catenin results in delayed hepatocyte proliferation after partial hepatectomy. Hepatology. 2007;45: 361–368.
341. Köhler C, Bell AW, Bowen WC, Monga SP, Fleig W, Michalopoulos GK. Expression of Notch-1 and its ligand Jagged-1 in rat liver during liver regeneration. Hepatology. 2004;39: 1056–1065.
342. Walesky C, Apte U. Mechanisms of Termination of Liver Regeneration [Internet]. Liver Regeneration. 2015. pp. 103–111. doi:10.1016/b978-0-12-420128-6.00007-5
343. Imai T, Jiang M, Kastner P, Chambon P, Metzger D. Selective ablation of retinoid X receptor alpha in hepatocytes impairs their lifespan and regenerative capacity. Proc Natl Acad Sci U S A. 2001;98: 4581–4586.

344. Anderson SP, Yoon L, Richard EB, Dunn CS, Cattley RC, Corton JC. Delayed liver regeneration in peroxisome proliferator-activated receptor-alpha-null mice. Hepatology. 2002;36: 544–554.
345. Rao MS, Peters JM, Gonzalez FJ, Reddy JK. Hepatic regeneration in peroxisome proliferator-activated receptor alpha-null mice after partial hepatectomy. Hepatol Res. 2002;22: 52–57.
346. Dai G, He L, Bu P, Wan Y-JY. Pregnane X receptor is essential for normal progression of liver regeneration. Hepatology. 2008;47: 1277–1287.
347. Turmelle YP, Shikapwashya O, Tu S, Hruz PW, Yan Q, Rudnick DA. Rosiglitazone inhibits mouse liver regeneration. FASEB J. 2006;20: 2609–2611.
348. Yamamoto Y, Ono T, Dhar DK, Yamanoi A, Tachibana M, Tanaka T, et al. Role of peroxisome proliferator-activated receptor-gamma (PPARgamma) during liver regeneration in rats. J Gastroenterol Hepatol. 2008;23: 930–937.
349. Bonzo JA, Ferry CH, Matsubara T, Kim J-H, Gonzalez FJ. Suppression of hepatocyte proliferation by hepatocyte nuclear factor 4α in adult mice. J Biol Chem. 2012;287: 7345–7356.
350. Song G, Sharma AD, Roll GR, Ng R, Lee AY, Blelloch RH, et al. MicroRNAs control hepatocyte proliferation during liver regeneration. Hepatology. 2010;51: 1735–1743.
351. Kuboki S, Shin T, Huber N, Eismann T, Galloway E, Schuster R, et al. Hepatocyte signaling through CXC chemokine receptor-2 is detrimental to liver recovery after ischemia/reperfusion in mice. Hepatology. 2008;48: 1213–1223.
352. Van Sweringen HL, Sakai N, Tevar AD, Burns JM, Edwards MJ, Lentsch AB. CXC chemokine signaling in the liver: impact on repair and regeneration. Hepatology. 2011;54: 1445–1453.
353. Yamada Y, Webber EM, Kirillova I, Peschon JJ, Fausto N. Analysis of liver regeneration in mice lacking type 1 or type 2 tumor necrosis factor receptor: requirement for type 1 but not type 2 receptor. Hepatology . 1998. pp. 959–970.
354. Vogel G. Development. Two unexpected players add twists to liver's comeback story. Science. 2006. p. 178.
355. Español-Suñer R, Carpentier R, Van Hul N, Legry V, Achouri Y, Cordi S, et al. Liver progenitor cells yield functional hepatocytes in response to chronic liver injury in mice. Gastroenterology. 2012;143: 1564–1575.e7.
356. Huch M, Dorrell C, Boj SF, van Es JH, Li VSW, van de Wetering M, et al. In vitro expansion of single Lgr5+ liver stem cells induced by Wnt-driven regeneration. Nature. 2013;494: 247–250.
357. Yanger K, Knigin D, Zong Y, Maggs L, Gu G, Akiyama H, et al. Adult hepatocytes are generated by self-duplication rather than stem cell differentiation. Cell Stem Cell. 2014;15: 340–349.
358. Lu W-Y, Bird TG, Boulter L, Tsuchiya A, Cole AM, Hay T, et al. Hepatic progenitor cells of biliary origin with liver repopulation capacity. Nat Cell Biol. 2015;17: 971–983.
359. Shin S, Upadhyay N, Greenbaum LE, Kaestner KH. Ablation of Foxl1-Cre-labeled hepatic progenitor cells and their descendants impairs recovery of mice from liver injury. Gastroenterology. 2015;148: 192–202.e3.
360. Raven A, Lu W-Y, Man TY, Ferreira-Gonzalez S, O'Duibhir E, Dwyer BJ, et al. Cholangiocytes act as facultative liver stem cells during impaired hepatocyte regeneration. Nature. 2017;547: 350–354.
361. Grompe M, Laconi E, Shafritz DA. Principles of therapeutic liver repopulation. Semin Liver Dis. 1999;19: 7–14.
362. Nicolas CT, Hickey RD, Chen HS, Mao SA, Lopera Higuita M, Wang Y, et al. Concise Review: Liver Regenerative Medicine: From Hepatocyte Transplantation to Bioartificial Livers and Bioengineered Grafts. Stem Cells. 2017;35: 42–50.
363. Lelli KM, Slattery M, Mann RS. Disentangling the many layers of eukaryotic transcriptional regulation. Annu Rev Genet. 2012;46: 43–68.
364. Istrail S, Davidson EH. Logic functions of the genomic cis-regulatory code. Proc Natl Acad Sci U S A. 2005;102: 4954–4959.

365. Gill G. Regulation of the initiation of eukaryotic transcription. Essays Biochem. 2001;37: 33–43.
366. Narlikar GJ, Fan H-Y, Kingston RE. Cooperation between complexes that regulate chromatin structure and transcription. Cell. 2002;108: 475–487.
367. Xu L, Glass CK, Rosenfeld MG. Coactivator and corepressor complexes in nuclear receptor function. Curr Opin Genet Dev. 1999;9: 140–147.
368. Courey AJ. Cooperativity in transcriptional control. Curr Biol. 2001;11: R250–2.
369. Moretti R, Ansari AZ. Expanding the specificity of DNA targeting by harnessing cooperative assembly. Biochimie. 2008;90: 1015–1025.
370. Badis G, Berger MF, Philippakis AA, Talukder S, Gehrke AR, Jaeger SA, et al. Diversity and complexity in DNA recognition by transcription factors. Science. 2009;324: 1720–1723.
371. Benayoun BA, Veitia RA. A post-translational modification code for transcription factors: sorting through a sea of signals. Trends Cell Biol. 2009;19: 189–197.
372. Luger K, Mäder AW, Richmond RK, Sargent DF, Richmond TJ. Crystal structure of the nucleosome core particle at 2.8 A resolution. Nature. 1997;389: 251–260.
373. Jenuwein T, Allis CD. Translating the histone code. Science. 2001;293: 1074–1080.
374. Felsenfeld G, Groudine M. Controlling the double helix. Nature. 2003;421: 448–453.
375. Bai L, Morozov AV. Gene regulation by nucleosome positioning. Trends Genet. 2010;26: 476–483.
376. Wang X, Bai L, Bryant GO, Ptashne M. Nucleosomes and the accessibility problem. Trends Genet. 2011;27: 487–492.
377. Bhutani N, Burns DM, Blau HM. DNA demethylation dynamics. Cell. 2011;146: 866–872.
378. Bártová E, Krejcí J, Harnicarová A, Galiová G, Kozubek S. Histone modifications and nuclear architecture: a review. J Histochem Cytochem. 2008;56: 711–721.
379. Zorn C, Cremer C, Cremer T, Zimmer J. Unscheduled DNA synthesis after partial UV irradiation of the cell nucleus. Distribution in interphase and metaphase. Exp Cell Res. 1979;124: 111–119.
380. Vaquerizas JM, Akhtar A, Luscombe NM. Large-scale nuclear architecture and transcriptional control. Subcell Biochem. 2011;52: 279–295.
381. Krivega I, Dean A. Enhancer and promoter interactions-long distance calls. Curr Opin Genet Dev. 2012;22: 79–85.
382. Agelopoulos M, McKay DJ, Mann RS. Developmental regulation of chromatin conformation by Hox proteins in Drosophila. Cell Rep. 2012;1: 350–359.
383. Noordermeer D, Leleu M, Splinter E, Rougemont J, De Laat W, Duboule D. The dynamic architecture of Hox gene clusters. Science. 2011;334: 222–225.
384. Schoenfelder S, Sexton T, Chakalova L, Cope NF, Horton A, Andrews S, et al. Preferential associations between co-regulated genes reveal a transcriptional interactome in erythroid cells. Nat Genet. 2010;42: 53–61.
385. Dekker J, Rippe K, Dekker M, Kleckner N. Capturing chromosome conformation. Science. 2002;295: 1306–1311.
386. Jones SA, Shim S-H, He J, Zhuang X. Fast, three-dimensional super-resolution imaging of live cells. Nat Methods. 2011;8: 499–508.
387. Darnell JE Jr. Variety in the level of gene control in eukaryotic cells. Nature. 1982;297: 365–371.
388. Greengard O, Federman M, Knox WE. Cytomorphometry of developing rat liver and its application to enzymic differentiation. J Cell Biol. 1972;52: 261–272.
389. Jungermann K, Katz N. Functional hepatocellular heterogeneity. Hepatology. 1982;2: 385–395.
390. Derman E, Krauter K, Walling L, Weinberger C, Ray M, Darnell JE Jr. Transcriptional control in the production of liver-specific mRNAs. Cell. 1981;23: 731–739.
391. Ott MO, Sperling L, Herbomel P, Yaniv M, Weiss MC. Tissue-specific expression is conferred by a sequence from the 5' end of the rat albumin gene. EMBO J. 1984;3: 2505–2510.
392. Ciliberto G, Dente L, Cortese R. Cell-specific expression of a transfected human alpha 1-antitrypsin gene. Cell. 1985;41: 531–540.

393. Costa RH, Lai E, Darnell JE Jr. Transcriptional control of the mouse prealbumin (transthyretin) gene: both promoter sequences and a distinct enhancer are cell specific. Mol Cell Biol. 1986;6: 4697–4708.
394. Cereghini S, Raymondjean M, Carranca AG, Herbomel P, Yaniv M. Factors involved in control of tissue-specific expression of albumin gene. Cell. 1987;50: 627–638.
395. Cohen AB. Interrelationships between the human alveolar macrophage and alpha-1-antitrypsin. J Clin Invest. 1973;52: 2793–2799.
396. Green PH, Lefkowitch JH, Glickman RM, Riley JW, Quinet E, Blum CB. Apolipoprotein localization and quantitation in the human intestine. Gastroenterology. 1982;83: 1223–1230.
397. Dickson PW, Aldred AR, Marley PD, Bannister D, Schreiber G. Rat choroid plexus specializes in the synthesis and the secretion of transthyretin (prealbumin). Regulation of transthyretin synthesis in choroid plexus is independent from that in liver. J Biol Chem. 1986;261: 3475–3478.
398. Baumhueter S, Mendel DB, Conley PB, Kuo CJ, Turk C, Graves MK, et al. HNF-1 shares three sequence motifs with the POU domain proteins and is identical to LF-B1 and APF. Genes Dev. 1990;4: 372–379.
399. Kuo CJ, Conley PB, Hsieh CL, Francke U, Crabtree GR. Molecular cloning, functional expression, and chromosomal localization of mouse hepatocyte nuclear factor 1. Proc Natl Acad Sci U S A. 1990;87: 9838–9842.
400. Drewes T, Senkel S, Holewa B, Ryffel GU. Human hepatocyte nuclear factor 4 isoforms are encoded by distinct and differentially expressed genes. Mol Cell Biol. 1996;16: 925–931.
401. Coffinier C, Barra J, Babinet C, Yaniv M. Expression of the vHNF1/HNF1beta homeoprotein gene during mouse organogenesis. Mech Dev. 1999;89: 211–213.
402. De Simone V, Cortese R. Transcriptional regulation of liver-specific gene expression. Curr Opin Cell Biol. 1991;3: 960–965.
403. Costa RH, Grayson DR, Darnell JE Jr. Multiple hepatocyte-enriched nuclear factors function in the regulation of transthyretin and alpha 1-antitrypsin genes. Mol Cell Biol. 1989;9: 1415–1425.
404. Herbst RS, Friedman N, Darnell JE Jr, Babiss LE. Positive and negative regulatory elements in the mouse albumin enhancer. Proc Natl Acad Sci U S A. 1989;86: 1553–1557.
405. Courtois G, Morgan JG, Campbell LA, Fourel G, Crabtree GR. Interaction of a liver-specific nuclear factor with the fibrinogen and alpha 1-antitrypsin promoters. Science. 1987;238: 688–692.
406. Lemaigre FP, Durviaux SM, Rousseau GG. Identification of regulatory sequences and protein-binding sites in the liver-type promoter of a gene encoding 6-phosphofructo-2-kinase/fructose-2,6-bisphosphatase. Mol Cell Biol. 1991;11: 1099–1106.
407. Cereghini S, Blumenfeld M, Yaniv M. A liver-specific factor essential for albumin transcription differs between differentiated and dedifferentiated rat hepatoma cells. Genes Dev. 1988;2: 957–974.
408. Coffinier C, Thépot D, Babinet C, Yaniv M, Barra J. Essential role for the homeoprotein vHNF1/HNF1beta in visceral endoderm differentiation. Development. 1999;126: 4785–4794.
409. Rey-Campos J, Chouard T, Yaniv M, Cereghini S. vHNF1 is a homeoprotein that activates transcription and forms heterodimers with HNF1. EMBO J. 1991;10: 1445–1457.
410. Mendel DB, Hansen LP, Graves MK, Conley PB, Crabtree GR. HNF-1 alpha and HNF-1 beta (vHNF-1) share dimerization and homeo domains, but not activation domains, and form heterodimers in vitro. Genes Dev. 1991;5: 1042–1056.
411. Reber M, Cereghini S. Variant hepatocyte nuclear factor 1 expression in the mouse genital tract. Mech Dev. 2001;100: 75–78.
412. Frain M, Swart G, Monaci P, Nicosia A, Stämpfli S, Frank R, et al. The liver-specific transcription factor LF-B1 contains a highly diverged homeobox DNA binding domain. Cell. 1989;59: 145–157.
413. Hayashi Y, Wang W, Ninomiya T, Nagano H, Ohta K, Itoh H. Liver enriched transcription factors and differentiation of hepatocellular carcinoma. Mol Pathol. 1999;52: 19–24.

414. Courtois G, Baumhueter S, Crabtree GR. Purified hepatocyte nuclear factor 1 interacts with a family of hepatocyte-specific promoters. Proc Natl Acad Sci U S A. 1988;85: 7937–7941.
415. Kuo CJ, Mendel DB, Hansen LP, Crabtree GR. Independent regulation of HNF-1 alpha and HNF-1 beta by retinoic acid in F9 teratocarcinoma cells. EMBO J. 1991;10: 2231–2236.
416. Mendel DB, Khavari PA, Conley PB, Graves MK, Hansen LP, Admon A, et al. Characterization of a cofactor that regulates dimerization of a mammalian homeodomain protein. Science. 1991;254: 1762–1767.
417. Jose-Estanyol M, Danan JL. A liver-specific factor and nuclear factor I bind to the rat alpha-fetoprotein promoter. J Biol Chem. 1988;263: 10865–10871.
418. Chambaz J, Cardot P, Pastier D, Zannis VI, Cladaras C. Promoter elements and factors required for hepatic transcription of the human ApoA-II gene. J Biol Chem. 1991;266: 11676–11685.
419. Brooks AR, Levy-Wilson B. Hepatocyte nuclear factor 1 and C/EBP are essential for the activity of the human apolipoprotein B gene second-intron enhancer. Mol Cell Biol. 1992;12: 1134–1148.
420. Odom DT, Zizlsperger N, Gordon DB, Bell GW, Rinaldi NJ, Murray HL, et al. Control of pancreas and liver gene expression by HNF transcription factors. Science. 2004;303: 1378–1381.
421. Coffinier C, Gresh L, Fiette L, Tronche F, Schütz G, Babinet C, et al. Bile system morphogenesis defects and liver dysfunction upon targeted deletion of HNF1beta. Development. 2002;129: 1829–1838.
422. Cereghini S, Ott MO, Power S, Maury M. Expression patterns of vHNF1 and HNF1 homeoproteins in early postimplantation embryos suggest distinct and sequential developmental roles. Development. 1992;116: 783–797.
423. Ott MO, Rey-Campos J, Cereghini S, Yaniv M. vHNF1 is expressed in epithelial cells of distinct embryonic origin during development and precedes HNF1 expression. Mech Dev. 1991;36: 47–58.
424. Nagy P, Bisgaard HC, Thorgeirsson SS. Expression of hepatic transcription factors during liver development and oval cell differentiation. J Cell Biol. 1994;126: 223–233.
425. Pontoglio M, Barra J, Hadchouel M, Doyen A, Kress C, Bach JP, et al. Hepatocyte nuclear factor 1 inactivation results in hepatic dysfunction, phenylketonuria, and renal Fanconi syndrome. Cell. 1996;84: 575–585.
426. Barbacci E, Reber M, Ott MO, Breillat C, Huetz F, Cereghini S. Variant hepatocyte nuclear factor 1 is required for visceral endoderm specification. Development. 1999;126: 4795–4805.
427. Lokmane L, Haumaitre C, Garcia-Villalba P, Anselme I, Schneider-Maunoury S, Cereghini S. Crucial role of vHNF1 in vertebrate hepatic specification. Development. 2008;135: 2777–2786.
428. Yamagata K, Oda N, Kaisaki PJ, Menzel S, Furuta H, Vaxillaire M, et al. Mutations in the hepatocyte nuclear factor-1alpha gene in maturity-onset diabetes of the young (MODY3). Nature. 1996;384: 455–458.
429. Horikawa Y, Iwasaki N, Hara M, Furuta H, Hinokio Y, Cockburn BN, et al. Mutation in hepatocyte nuclear factor-1 beta gene (TCF2) associated with MODY. Nat Genet. 1997;17: 384–385.
430. Lai E, Prezioso VR, Smith E, Litvin O, Costa RH, Darnell JE Jr. HNF-3A, a hepatocyte-enriched transcription factor of novel structure is regulated transcriptionally. Genes Dev. 1990;4: 1427–1436.
431. Lai E, Prezioso VR, Tao WF, Chen WS, Darnell JE Jr. Hepatocyte nuclear factor 3 alpha belongs to a gene family in mammals that is homologous to the Drosophila homeotic gene fork head. Genes Dev. 1991;5: 416–427.
432. Pani L, Overdier DG, Porcella A, Qian X, Lai E, Costa RH. Hepatocyte nuclear factor 3 beta contains two transcriptional activation domains, one of which is novel and conserved with the Drosophila fork head protein. Mol Cell Biol. 1992;12: 3723–3732.
433. Lai E, Clark KL, Burley SK, Darnell JE Jr. Hepatocyte nuclear factor 3/fork head or “winged helix” proteins: a family of transcription factors of diverse biologic function. Proc Natl Acad Sci U S A. 1993;90: 10421–10423.

434. Kaestner KH, Knochel W, Martinez DE. Unified nomenclature for the winged helix/forkhead transcription factors. Genes Dev. 2000;14: 142–146.
435. Sund NJ, Ang SL, Sackett SD, Shen W, Daigle N, Magnuson MA, et al. Hepatocyte nuclear factor 3beta (Foxa2) is dispensable for maintaining the differentiated state of the adult hepatocyte. Mol Cell Biol. 2000;20: 5175–5183.
436. Friedman JR, Kaestner KH. The Foxa family of transcription factors in development and metabolism. Cell Mol Life Sci. 2006;63: 2317–2328.
437. Clark KL, Halay ED, Lai E, Burley SK. Co-crystal structure of the HNF-3/fork head DNA-recognition motif resembles histone H5. Nature. 1993;364: 412–420.
438. Qian X, Costa RH. Analysis of hepatocyte nuclear factor-3 beta protein domains required for transcriptional activation and nuclear targeting. Nucleic Acids Res. 1995;23: 1184–1191.
439. Marsden I, Jin C, Liao X. Structural changes in the region directly adjacent to the DNA-binding helix highlight a possible mechanism to explain the observed changes in the sequence-specific binding of winged helix proteins 1 1Edited by P. E. Wright. J Mol Biol. 1998;278: 293–299.
440. Liu JK, DiPersio CM, Zaret KS. Extracellular signals that regulate liver transcription factors during hepatic differentiation in vitro. Mol Cell Biol. 1991;11: 773–784.
441. Groupp ER, Crawford N, Locker J. Characterization of the distal alpha-fetoprotein enhancer, a strong, long distance, liver-specific activator. J Biol Chem. 1994;269: 22178–22187.
442. Schrem H. Liver-Enriched Transcription Factors in Liver Function and Development. Part I: The Hepatocyte Nuclear Factor Network and Liver-Specific Gene Expression. Pharmacol Rev. 2002;54: 129–158.
443. Lemaigre FP, Durviaux SM, Rousseau GG. Liver-specific factor binding to the liver promoter of a 6-phosphofructo-2-kinase/fructose-2,6-bisphosphatase gene. J Biol Chem. 1993;268: 19896–19905.
444. Cirillo LA, McPherson CE, Bossard P, Stevens K, Cherian S, Shim EY, et al. Binding of the winged-helix transcription factor HNF3 to a linker histone site on the nucleosome. EMBO J. 1998;17: 244–254.
445. Monaghan AP, Kaestner KH, Grau E, Schütz G. Postimplantation expression patterns indicate a role for the mouse forkhead/HNF-3 alpha, beta and gamma genes in determination of the definitive endoderm, chordamesoderm and neuroectoderm. Development. 1993;119: 567–578.
446. Kaestner KH, Katz J, Liu Y, Drucker DJ, Schütz G. Inactivation of the winged helix transcription factor HNF3alpha affects glucose homeostasis and islet glucagon gene expression in vivo. Genes Dev. 1999;13: 495–504.
447. Ang S-L, Rossant J. HNF-3β is essential for node and notochord formation in mouse development. Cell. 1994;78: 561–574.
448. Weinstein DC, Ruiz i Altaba A, Chen WS, Hoodless P, Prezioso VR, Jessell TM, et al. The winged-helix transcription factor HNF-3 beta is required for notochord development in the mouse embryo. Cell. 1994;78: 575–588.
449. Zhang L, Rubins NE, Ahima RS, Greenbaum LE, Kaestner KH. Foxa2 integrates the transcriptional response of the hepatocyte to fasting. Cell Metab. 2005;2: 141–148.
450. Li Z, White P, Tuteja G, Rubins N, Sackett S, Kaestner KH. Foxa1 and Foxa2 regulate bile duct development in mice. J Clin Invest. 2009;119: 1537–1545.
451. Kaestner KH, Hiemisch H, Schütz G. Targeted disruption of the gene encoding hepatocyte nuclear factor 3gamma results in reduced transcription of hepatocyte-specific genes. Mol Cell Biol. 1998;18: 4245–4251.
452. Shen W, Scearce LM, Brestelli JE, Sund NJ, Kaestner KH. Foxa3 (hepatocyte nuclear factor 3gamma) is required for the regulation of hepatic GLUT2 expression and the maintenance of glucose homeostasis during a prolonged fast. J Biol Chem. 2001;276: 42812–42817.
453. Qian X, Samadani U, Porcella A, Costa RH. Decreased expression of hepatocyte nuclear factor 3 alpha during the acute-phase response influences transthyretin gene transcription. Mol Cell Biol. 1995;15: 1364–1376.

454. Nakamura T, Akiyoshi H, Shiota G, Isono M, Nakamura K, Moriyama M, et al. Hepatoprotective action of adenovirus-transferred HNF-3gamma gene in acute liver injury caused by CCl(4). FEBS Lett. 1999;459: 1–4.
455. Wang W, Yao L-J, Shen W, Ding K, Shi P-M, Chen F, et al. FOXA2 alleviates CCl-induced liver fibrosis by protecting hepatocytes in mice. Sci Rep. 2017;7: 15532.
456. O'Leary NA, Wright MW, Brister JR, Ciufo S, Haddad D, McVeigh R, et al. Reference sequence (RefSeq) database at NCBI: current status, taxonomic expansion, and functional annotation. Nucleic Acids Res. 2016;44: D733–45.
457. Thomas H, Jaschkowitz K, Bulman M, Frayling TM, Mitchell SM, Roosen S, et al. A distant upstream promoter of the HNF-4alpha gene connects the transcription factors involved in maturity-onset diabetes of the young. Hum Mol Genet. 2001;10: 2089–2097.
458. Huang J, Levitsky LL, Rhoads DB. Novel P2 promoter-derived HNF4α isoforms with different N-terminus generated by alternate exon insertion. Exp Cell Res. 2009;315: 1200–1211.
459. Sladek FM, Zhong WM, Lai E, Darnell JE. Liver-enriched transcription factor HNF-4 is a novel member of the steroid hormone receptor superfamily. Genes Dev. 1990;4: 2353–2365.
460. Mangelsdorf DJ, Thummel C, Beato M, Herrlich P, Schütz G, Umesono K, et al. The nuclear receptor superfamily: the second decade. Cell. 1995;83: 835–839.
461. Hertz R, Magenheim J, Berman I, Bar-Tana J. Fatty acyl-CoA thioesters are ligands of hepatic nuclear factor-4α. Nature. 1998;392: 512–516.
462. Yuan X, Ta TC, Lin M, Evans JR, Dong Y, Bolotin E, et al. Identification of an endogenous ligand bound to a native orphan nuclear receptor. PLoS One. 2009;4: e5609.
463. Hadzopoulou-Cladaras M, Kistanova E, Evagelopoulou C, Zeng S, Cladaras C, Ladias JA. Functional domains of the nuclear receptor hepatocyte nuclear factor 4. J Biol Chem. 1997;272: 539–550.
464. Jiang G, Nepomuceno L, Hopkins K, Sladek FM. Exclusive homodimerization of the orphan receptor hepatocyte nuclear factor 4 defines a new subclass of nuclear receptors. Mol Cell Biol. 1995;15: 5131–5143.
465. Jiang G, Sladek FM. The DNA binding domain of hepatocyte nuclear factor 4 mediates cooperative, specific binding to DNA and heterodimerization with the retinoid X receptor alpha. J Biol Chem. 1997;272: 1218–1225.
466. Babeu J-P, Boudreau F. Hepatocyte nuclear factor 4-alpha involvement in liver and intestinal inflammatory networks. World J Gastroenterol. 2014;20: 22–30.
467. Taraviras S, Monaghan AP, Schütz G, Kelsey G. Characterization of the mouse HNF-4 gene and its expression during mouse embryogenesis. Mech Dev. 1994;48: 67–79.
468. Fang B, Mane-Padros D, Bolotin E, Jiang T, Sladek FM. Identification of a binding motif specific to HNF4 by comparative analysis of multiple nuclear receptors. Nucleic Acids Res. 2012;40: 5343–5356.
469. Ginsburg GS, Ozer J, Karathanasis SK. Intestinal apolipoprotein AI gene transcription is regulated by multiple distinct DNA elements and is synergistically activated by the orphan nuclear receptor, hepatocyte nuclear factor 4. J Clin Invest. 1995;96: 528–538.
470. Ladias JA, Hadzopoulou-Cladaras M, Kardassis D, Cardot P, Cheng J, Zannis V, et al. Transcriptional regulation of human apolipoprotein genes ApoB, ApoCIII, and ApoAII by members of the steroid hormone receptor superfamily HNF-4, ARP-1, EAR-2, and EAR-3. J Biol Chem. 1992;267: 15849–15860.
471. Costa RH, Van Dyke TA, Yan C, Kuo F, Darnell JE Jr. Similarities in transthyretin gene expression and differences in transcription factors: liver and yolk sac compared to choroid plexus. Proc Natl Acad Sci U S A. 1990;87: 6589–6593.
472. Schaeffer E, Guillou F, Part D, Zakin MM. A different combination of transcription factors modulates the expression of the human transferrin promoter in liver and Sertoli cells. J Biol Chem. 1993;268: 23399–23408.
473. Erdmann D, Heim J. Orphan nuclear receptor HNF-4 binds to the human coagulation factor VII promoter. J Biol Chem. 1995;270: 22988–22996.

474. Duncan SA, Manova K, Chen WS, Hoodless P, Weinstein DC, Bachvarova RF, et al. Expression of transcription factor HNF-4 in the extraembryonic endoderm, gut, and nephrogenic tissue of the developing mouse embryo: HNF-4 is a marker for primary endoderm in the implanting blastocyst. Proceedings of the National Academy of Sciences. 1994;91: 7598–7602.
475. Chen WS, Manova K, Weinstein DC, Duncan SA, Plump AS, Prezioso VR, et al. Disruption of the HNF-4 gene, expressed in visceral endoderm, leads to cell death in embryonic ectoderm and impaired gastrulation of mouse embryos. Genes Dev. 1994;8: 2466–2477.
476. Duncan SA, Nagy A, Chan W. Murine gastrulation requires HNF-4 regulated gene expression in the visceral endoderm: tetraploid rescue of Hnf-4(-/-) embryos. Development. 1997;124: 279–287.
477. Battle MA, Konopka G, Parviz F, Gaggl AL, Yang C, Sladek FM, et al. Hepatocyte nuclear factor 4alpha orchestrates expression of cell adhesion proteins during the epithelial transformation of the developing liver. Proc Natl Acad Sci U S A. 2006;103: 8419–8424.
478. Parviz F, Matullo C, Garrison WD, Savatski L, Adamson JW, Ning G, et al. Hepatocyte nuclear factor 4alpha controls the development of a hepatic epithelium and liver morphogenesis. Nat Genet. 2003;34: 292–296.
479. Hayhurst GP, Lee YH, Lambert G, Ward JM, Gonzalez FJ. Hepatocyte nuclear factor 4alpha (nuclear receptor 2A1) is essential for maintenance of hepatic gene expression and lipid homeostasis. Mol Cell Biol. 2001;21: 1393–1403.
480. Yamagata K, Furuta H, Oda N, Kaisaki PJ, Menzel S, Cox NJ, et al. Mutations in the hepatocyte nuclear factor-4alpha gene in maturity-onset diabetes of the young (MODY1). Nature. 1996;384: 458–460.
481. Ktistaki E, Ktistakis NT, Papadogeorgaki E, Talianidis I. Recruitment of hepatocyte nuclear factor 4 into specific intranuclear compartments depends on tyrosine phosphorylation that affects its DNA-binding and transactivation potential. Proceedings of the National Academy of Sciences. 1995;92: 9876–9880.
482. Soutoglou E, Katrakili N, Talianidis I. Acetylation Regulates Transcription Factor Activity at Multiple Levels. Mol Cell. 2000;5: 745–751.
483. Lemaigre FP, Durviaux SM, Truong O, Lannoy VJ, Hsuan JJ, Rousseau GG. Hepatocyte nuclear factor 6, a transcription factor that contains a novel type of homeodomain and a single cut domain. Proc Natl Acad Sci U S A. 1996;93: 9460–9464.
484. Rider MH, Bertrand L, Vertommen D, Michels PA, Rousseau GG, Hue L. 6-phosphofructo-2-kinase/fructose-2,6-bisphosphatase: head-to-head with a bifunctional enzyme that controls glycolysis. Biochem J. 2004;381: 561–579.
485. Lannoy VJ, Bürglin TR, Rousseau GG, Lemaigre FP. Isoforms of hepatocyte nuclear factor-6 differ in DNA-binding properties, contain a bifunctional homeodomain, and define the new ONECUT class of homeodomain proteins. J Biol Chem. 1998;273: 13552–13562.
486. Blochlinger K, Bodmer R, Jack J, Jan LY, Jan YN. Primary structure and expression of a product from cut, a locus involved in specifying sensory organ identity in Drosophila. Nature. 1988;333: 629–635.
487. Neufeld EJ, Skalnik DG, Lievens PM, Orkin SH. Human CCAAT displacement protein is homologous to the Drosophila homeoprotein, cut. Nat Genet. 1992;1: 50–55.
488. Samadani U, Costa RH. The transcriptional activator hepatocyte nuclear factor 6 regulates liver gene expression. Mol Cell Biol. 1996;16: 6273–6284.
489. Landry C, Clotman F, Hioki T, Oda H, Picard JJ, Lemaigre FP, et al. HNF-6 is expressed in endoderm derivatives and nervous system of the mouse embryo and participates to the cross-regulatory network of liver-enriched transcription factors. Dev Biol. 1997;192: 247–257.
490. Rausa F, Samadani U, Ye H, Lim L, Fletcher CF, Jenkins NA, et al. The cut-homeodomain transcriptional activator HNF-6 is coexpressed with its target gene HNF-3 beta in the developing murine liver and pancreas. Dev Biol. 1997;192: 228–246.
491. Lannoy VJ, Decaux JF, Pierreux CE, Lemaigre FP, Rousseau GG. Liver glucokinase gene expression is controlled by the onecut transcription factor hepatocyte nuclear factor-6. Diabetologia. 2002;45: 1136–1141.

492. Clotman F, Lannoy VJ, Reber M, Cereghini S, Cassiman D, Jacquemin P, et al. The onecut transcription factor HNF6 is required for normal development of the biliary tract. Development. 2002;129: 1819–1828.
493. Vanderpool C, Sparks EE, Huppert KA, Gannon M, Means AL, Huppert SS. Genetic interactions between hepatocyte nuclear factor-6 and Notch signaling regulate mouse intrahepatic bile duct development in vivo. Hepatology. 2012;55: 233–243.
494. Zhang Y, Fang B, Damle M, Guan D, Li Z, Kim YH, et al. HNF6 and Rev-erbα integrate hepatic lipid metabolism by overlapping and distinct transcriptional mechanisms. Genes Dev. 2016;30: 1636–1644.
495. Tan Y, Yoshida Y, Hughes DE, Costa RH. Increased expression of hepatocyte nuclear factor 6 stimulates hepatocyte proliferation during mouse liver regeneration. Gastroenterology. 2006;130: 1283–1300.
496. Lahuna O, Fernandez L, Karlsson H, Maiter D, Lemaigre FP, Rousseau GG, et al. Expression of hepatocyte nuclear factor 6 in rat liver is sex-dependent and regulated by growth hormone. Proc Natl Acad Sci U S A. 1997;94: 12309–12313.
497. Lahuna O, Rastegar M, Maiter D, Thissen JP, Lemaigre FP, Rousseau GG. Involvement of STAT5 (signal transducer and activator of transcription 5) and HNF-4 (hepatocyte nuclear factor 4) in the transcriptional control of the hnf6 gene by growth hormone. Mol Endocrinol. 2000;14: 285–294.
498. Pierreux CE, Stafford J, Demonte D, Scott DK, Vandenhaute J, O'Brien RM, et al. Antiglucocorticoid activity of hepatocyte nuclear factor-6. Proc Natl Acad Sci U S A. 1999;96: 8961–8966.
499. Graves BJ, Johnson PF, McKnight SL. Homologous recognition of a promoter domain common to the MSV LTR and the HSV tk gene. Cell. 1986;44: 565–576.
500. Johnson PF, Landschulz WH, Graves BJ, McKnight SL. Identification of a rat liver nuclear protein that binds to the enhancer core element of three animal viruses. Genes Dev. 1987;1: 133–146.
501. Landschulz WH, Johnson PF, Adashi EY, Graves BJ, McKnight SL. Isolation of a recombinant copy of the gene encoding C/EBP. Genes Dev. 1988;2: 786–800.
502. Takiguchi M. The C/EBP family of transcription factors in the liver and other organs. Int J Exp Pathol. 1998;79: 369–391.
503. Diehl AM. Roles of CCAAT/enhancer-binding proteins in regulation of liver regenerative growth. J Biol Chem. 1998;273: 30843–30846.
504. Akira S, Isshiki H, Sugita T, Tanabe O, Kinoshita S, Nishio Y, et al. A nuclear factor for IL-6 expression (NF-IL6) is a member of a C/EBP family. EMBO J. 1990;9: 1897–1906.
505. Roman C, Platero JS, Shuman J, Calame K. Ig/EBP-1: a ubiquitously expressed immunoglobulin enhancer binding protein that is similar to C/EBP and heterodimerizes with C/EBP. Genes Dev. 1990;4: 1404–1415.
506. Cooper C, Henderson A, Artandi S, Avitahl N, Calame K. Ig/EBP (C/EBP gamma) is a transdominant negative inhibitor of C/EBP family transcriptional activators. Nucleic Acids Res. 1995;23: 4371–4377.
507. Williams SC, Cantwell CA, Johnson PF. A family of C/EBP-related proteins capable of forming covalently linked leucine zipper dimers in vitro. Genes Dev. 1991;5: 1553–1567.
508. Agre P, Johnson PF, McKnight SL. Cognate DNA binding specificity retained after leucine zipper exchange between GCN4 and C/EBP. Science. 1989;246: 922–926.
509. Landschulz WH, Johnson PF, McKnight SL. The DNA binding domain of the rat liver nuclear protein C/EBP is bipartite. Science. 1989;243: 1681–1688.
510. Ron D, Habener JF. CHOP, a novel developmentally regulated nuclear protein that dimerizes with transcription factors C/EBP and LAP and functions as a dominant-negative inhibitor of gene transcription. Genes Dev. 1992;6: 439–453.
511. Osada S, Yamamoto H, Nishihara T, Imagawa M. DNA binding specificity of the CCAAT/enhancer-binding protein transcription factor family. J Biol Chem. 1996;271: 3891–3896.

512. Park EA, Roesler WJ, Liu J, Klemm DJ, Gurney AL, Thatcher JD, et al. The role of the CCAAT/enhancer-binding protein in the transcriptional regulation of the gene for phosphoenolpyruvate carboxykinase (GTP). Mol Cell Biol. 1990;10: 6264–6272.
513. Kim JW, Ahn YH. CCAAT/enhancer binding protein regulates the promoter activity of the rat GLUT2 glucose transporter gene in liver cells. Biochem J. 1998;336 (Pt 1): 83–90.
514. Nolten LA, van Schaik FM, Steenbergh PH, Sussenbach JS. Expression of the insulin-like growth factor I gene is stimulated by the liver-enriched transcription factors C/EBP alpha and LAP. Mol Endocrinol. 1994;8: 1636–1645.
515. Boccia LM, Lillicrap D, Newcombe K, Mueller CR. Binding of the Ets factor GA-binding protein to an upstream site in the factor IX promoter is a critical event in transactivation. Mol Cell Biol. 1996;16: 1929–1935.
516. Lee YH, Alberta JA, Gonzalez FJ, Waxman DJ. Multiple, functional DBP sites on the promoter of the cholesterol 7 alpha-hydroxylase P450 gene, CYP7. Proposed role in diurnal regulation of liver gene expression. J Biol Chem. 1994;269: 14681–14689.
517. Croniger C, Trus M, Lysek-Stupp K, Cohen H, Liu Y, Darlington GJ, et al. Role of the isoforms of CCAAT/enhancer-binding protein in the initiation of phosphoenolpyruvate carboxykinase (GTP) gene transcription at birth. J Biol Chem. 1997;272: 26306–26312.
518. Friedman JR, Larris B, Le PP, Peiris TH, Arsenlis A, Schug J, et al. Orthogonal analysis of C/EBPbeta targets in vivo during liver proliferation. Proc Natl Acad Sci U S A. 2004;101: 12986–12991.
519. Ray A, Ray BK. Serum amyloid A gene expression under acute-phase conditions involves participation of inducible C/EBP-beta and C/EBP-delta and their activation by phosphorylation. Mol Cell Biol. 1994;14: 4324–4332.
520. Yiangou M, Paraskeva E, Hsieh CC, Markou E, Victoratos P, Scouras Z, et al. Induction of a subgroup of acute phase protein genes in mouse liver by hyperthermia. Biochim Biophys Acta. 1998;1396: 191–206.
521. Ramji DP, Foka P. CCAAT/enhancer-binding proteins: structure, function and regulation. Biochem J. 2002;365: 561–575.
522. Shiojiri N, Takeshita K, Yamasaki H, Iwata T. Suppression of C/EBP alpha expression in biliary cell differentiation from hepatoblasts during mouse liver development. J Hepatol. 2004;41: 790–798.
523. Wang ND, Finegold MJ, Bradley A, Ou CN, Abdelsayed SV, Wilde MD, et al. Impaired energy homeostasis in C/EBP alpha knockout mice. Science. 1995;269: 1108–1112.
524. Bosma PJ, Seppen J, Goldhoorn B, Bakker C, Oude Elferink RP, Chowdhury JR, et al. Bilirubin UDP-glucuronosyltransferase 1 is the only relevant bilirubin glucuronidating isoform in man. J Biol Chem. 1994;269: 17960–17964.
525. Lee YH, Sauer B, Johnson PF, Gonzalez FJ. Disruption of the c/ebp alpha gene in adult mouse liver. Mol Cell Biol. 1997;17: 6014–6022.
526. Trautwein C, Rakemann T, Malek NP, Plümpe J, Tiegs G, Manns MP. Concanavalin A-induced liver injury triggers hepatocyte proliferation. J Clin Invest. 1998;101: 1960–1969.
527. Kuo CJ, Conley PB, Chen L, Sladek FM, Darnell JE Jr, Crabtree GR. A transcriptional hierarchy involved in mammalian cell-type specification. Nature. 1992;355: 457–461.
528. Nagaki M, Moriwaki H. Transcription factor HNF and hepatocyte differentiation. Hepatol Res. 2008;38: 961–969.
529. Griffo G, Hamon-Benais C, Angrand PO, Fox M, West L, Lecoq O, et al. HNF4 and HNF1 as well as a panel of hepatic functions are extinguished and reexpressed in parallel in chromosomally reduced rat hepatoma-human fibroblast hybrids. J Cell Biol. 1993;121: 887–898.
530. Späth GF, Weiss MC. Hepatocyte nuclear factor 4 expression overcomes repression of the hepatic phenotype in dedifferentiated hepatoma cells. Mol Cell Biol. 1997;17: 1913–1922.
531. Späth GF, Weiss MC. Hepatocyte Nuclear Factor 4 Provokes Expression of Epithelial Marker Genes, Acting As a Morphogen in Dedifferentiated Hepatoma Cells. J Cell Biol. 1998;140: 935–946.

532. Heiman M, Kulicke R, Fenster RJ, Greengard P, Heintz N. Cell type-specific mRNA purification by translating ribosome affinity purification (TRAP). Nat Protoc. 2014;9: 1282–1291.
533. Mo A, Mukamel EA, Davis FP, Luo C, Henry GL, Picard S, et al. Epigenomic Signatures of Neuronal Diversity in the Mammalian Brain. Neuron. 2015;86: 1369–1384.
534. Buenrostro JD, Giresi PG, Zaba LC, Chang HY, Greenleaf WJ. Transposition of native chromatin for fast and sensitive epigenomic profiling of open chromatin, DNA-binding proteins and nucleosome position. Nat Methods. 2013;10: 1213–1218.
535. Miura N, Tanaka K. Analysis of the rat hepatocyte nuclear factor (HNF) 1 gene promoter: synergistic activation by HNF4 and HNF1 proteins. Nucleic Acids Res. 1993;21: 3731–3736.
536. Kritis AA, Ktistaki E, Barda D, Zannis VI, Talianidis I. An indirect negative autoregulatory mechanism involved in hepatocyte nuclear factor-1 gene expression. Nucleic Acids Res. 1993;21: 5882–5889.
537. Ktistaki E, Talianidis I. Modulation of hepatic gene expression by hepatocyte nuclear factor 1. Science. 1997;277: 109–112.
538. Hiemisch H, Schütz G, Kaestner KH. Transcriptional regulation in endoderm development: characterization of an enhancer controlling Hnf3g expression by transgenesis and targeted mutagenesis. EMBO J. 1997;16: 3995–4006.
539. Duncan SA, Navas MA, Dufort D, Rossant J, Stoffel M. Regulation of a transcription factor network required for differentiation and metabolism. Science. 1998;281: 692–695.
540. Samadani U, Porcella A, Pani L, Johnson PF, Burch JB, Pine R, et al. Cytokine regulation of the liver transcription factor hepatocyte nuclear factor-3 beta is mediated by the C/EBP family and interferon regulatory factor 1. Cell Growth Differ. 1995;6: 879–890.

CHAPTER 2

TRAP-SEQ IDENTIFIES CYSTINE/GLUTAMATE ANTIPORTER AS A DRIVER OF RECOVERY FROM LIVER INJURY

Parts of this chapter were adapted with permission from TRAP-seq identifies cystine/glutamate antiporter as a driver of recovery from liver injury. Wang AW, Wangensteen KJ*, Wang YJ, Zahm AM, Moss NG, Erez N, Kaestner KH. The Journal of Clinical Investigation. 2018;128(6):2297-2309. doi:10.1172/JCI95120.*

ABSTRACT

Understanding the molecular basis of the regenerative response following hepatic injury holds promise for improved treatment of liver diseases. Here, we report an innovative method to profile gene expression specifically in the hepatocytes that regenerate the liver following toxic injury. We used the *Fah*$^{-/-}$ mouse, a model of hereditary tyrosinemia, which conditionally undergoes severe liver injury unless fumarylacetoacetate hydrolase (FAH) expression is reconstituted ectopically. We used translating ribosome affinity purification followed by high-throughput RNA sequencing (TRAP-seq) to isolate mRNAs specific to repopulating hepatocytes. We uncovered upstream regulators and important signaling pathways that are highly enriched in genes changed in regenerating hepatocytes. Specifically, we found that glutathione metabolism, particularly the gene *Slc7a11* encoding the cystine/glutamate antiporter (xCT), is massively upregulated during liver regeneration. Furthermore, we show that *Slc7a11* overexpression in hepatocytes enhances, and its suppression inhibits, repopulation following toxic injury. TRAP-seq allows cell type-specific expression profiling in repopulating hepatocytes and identified xCT, a factor that supports antioxidant responses during liver regeneration. xCT has potential as a therapeutic target for enhancing liver regeneration in response to liver injury.

INTRODUCTION

The liver is the main metabolic organ in the body; it is the nexus for homeostasis of carbohydrates, proteins, and lipids, and it eliminates waste products by oxidation and reduction, conjugation, and excretion into the bile. As such, the liver is exposed to environmental toxins that can severely damage hepatocytes and cause acute liver failure [1]. Animals have conserved the ability to regenerate the liver parenchyma upon damage [2] and to restore full mass and function even with the loss of up to 75% of hepatocytes [3].

Liver cells in adult animals are normally quiescent and divide infrequently. With acute tissue damage, however, mature hepatocytes and cholangiocytes enter the cell cycle and divide [4]. In addition, hepatocyte proliferation occurs after partial hepatectomy (PHx), a noninflammatory liver regeneration model in which up to two-thirds of the liver is removed [5]. In rodents, this leads to cell division in most hepatocytes within hours and expansion of the remnant organ over the course of 1 to 2 weeks, until the entire mass of the liver is restored. Because PHx is relatively easily carried out in rodents, it has been used to study liver regeneration in mice for decades [5,6]. In fact, many studies have profiled changes in gene expression during regeneration, and a number of important genes and pathways have been identified [7–9]. The common theme from these studies is that cell-cycle genes are upregulated and metabolic genes are downregulated as hepatocytes divide to recover from PHx.

Other paradigms to study liver regeneration utilize injury models involving treatment of animals with hepatotoxins to examine the expression changes of injured liver tissue taken *en bloc* [10–12]. However, until now there has been no methodology to distinguish the responses of the healthy, repopulating liver cells from those of damaged hepatocytes and inflammatory cells. In clinically relevant hepatic injury, a minority of cells may be protected from the initial insult and thus poised to drive repopulation [13,14]. It is therefore important to establish which genes in the repopulating hepatocyte drive regeneration in the setting of widespread injury.

The mouse model of hereditary tyrosinemia, an inborn error of tyrosine metabolism caused by a deficiency of fumarylacetoacetate hydrolase (FAH) enzyme [14], is useful for studying the

mechanisms of liver regeneration, since repopulating hepatocytes can be labeled as they divide to restore liver function after injury. Homozygous null (*Fah*$^{-/-}$) mice die at birth with hepatic dysfunction from toxic metabolites but can be maintained in a healthy state by the drug 2-(2-nitro-4-trifluoromethylbenzoyl)-1,3-cyclohexanedione (NTBC) [14]. Alternatively, gene therapy that restores FAH expression can normalize tyrosine catabolism within hepatocytes and allow liver repopulation by the corrected cells upon NTBC removal [15]. Our previous work also demonstrated that transgenes can be coexpressed with FAH and can be used to genetically trace repopulating hepatocytes over time [15,16].

Here, we use translating ribosome affinity purification (TRAP) [17] followed by high-throughput RNA sequencing (TRAP-seq) to profile the gene expression pattern specific to repopulating hepatocytes. *Slc7a11*, encoding the cystine/glutamate antiporter (xCT), was massively activated in regenerating hepatocytes. xCT imports cystine as a precursor for glutathione (GSH) synthesis [18,19]. We show that ectopic expression of xCT promotes liver repopulation, whereas CRISPR/Cas9-mediated mutation of *Slc7a11* causes a decrease in replicating hepatocytes. These findings indicate the functional significance of xCT and suggest that activation of *Slc7a11* could be used clinically to support therapeutic liver regeneration in the setting of acute liver injury.

RESULTS

TRAP enables lineage-tracing of repopulating hepatocytes

With the goal of specifically isolating repopulating hepatocytes from the injured liver to perform RNA-seq, we initially set out to lineage trace repopulating hepatocytes with GFP and isolate tagged cells by FACS for expression analysis. However, we encountered several problems. First, the fragility of hepatocytes undergoing repopulation led to poor recovery following liver perfusion. Second, the large size of the repopulating hepatocytes hampered the yield and purity of isolated cells by sorting. Finally, the process from organ harvest to cell isolation took more than 2 h, which may have altered the expression profile.

Next, we turned to TRAP-seq (Figure 2.1A), which enables the immunoprecipitation of ribosome-bound, translating mRNA from cells that express a fusion protein of the ribosomal protein L10a and GFP (GFP-L10a) [17]. The fusion protein was subcloned into the coexpression vector pKT2/Fah-mCa//SB [15] to construct pKT2/Fah-Gfp-L10a//SB (TRAP vector), which expresses FAH together with GFP-L10a. The TRAP vector utilizes the Sleeping Beauty transposon system for stable plasmid integration into the hepatocyte genome [15]. The TRAP vector was hydrodynamically injected into *Fah*$^{-/-}$ mice, and NTBC was withdrawn to induce liver injury and create pressure for the selection of hepatocytes that stably express FAH to repopulate the liver. An estimated 0.1% to 1% of hepatocytes integrated the plasmid stably into their genomes [20]. Tissue was harvested 1 or 4 weeks after injection, and GFP-tagged polysomes were extracted to isolate translating mRNAs specifically from repopulating hepatocytes (Figure 2.1B). No RNA was recovered from mice that were not injected with the TRAP vector, indicating the specificity of TRAP isolation. Three mice in the four-week regeneration group had a greater degree of weight loss (Figure 2.2), which was suggestive of more severe injury. Indeed, livers from these mice had large areas lacking GFP staining, indicating a reduced level of initial plasmid uptake (Figure 2.1C). Hence, we grouped these mice into a separate category termed “4-week regeneration after severe injury.” Immunofluorescence (IF) analysis of liver sections confirmed that the majority of proliferating hepatocytes also expressed GFP (Figure 2.1C). Thus, TRAP allows for mRNA

isolation selectively from hepatocytes repopulating the injured liver, without contamination from dying hepatocytes or inflammatory cells.

TRAP allows hepatocyte-specific RNA isolation from the quiescent liver

To obtain mRNA from quiescent hepatocytes as a reference for TRAP-seq, we used the *Rosa*$^{LSL\text{-}GFP\text{-}L10a}$ mouse, in which expression of GFP-L10a can be activated following Cre expression [21]. We injected *Rosa*$^{LSL\text{-}GFP\text{-}L10a}$ mice with hepatocyte-specific AAV8-TBG-Cre [22,23] and performed TRAP to isolate hepatocyte mRNA 1 week later (Figure 2.1A). IHC of liver tissue from these mice confirmed that GFP expression was only found in hepatocytes following AAV8-TBG-Cre injection (Figure 2.1C). GFP and Ki67 colabeling revealed very few actively dividing hepatocytes (Figure 2.1C), consistent with the quiescent liver state.

High-throughput sequencing of cDNA libraries derived from 16 samples of TRAP-isolated mRNA obtained, on average, 5.8 million uniquely mapped reads (Supplementary Digital Table 2.1). As expected in pure hepatic mRNA, the 10 most abundant transcripts in the quiescent animals were specific to hepatocytes (Table 2.1) [24–26]. Hepatocyte-specific genes such as Alb and Ttr were highly abundant in hepatocytes from all samples, whereas the biliary epithelium markers CK19, CK7, CFTR, and PKD2, as well as transcripts from other cell types in the liver, were nearly undetectable (Table 2.2) [27,28], demonstrating the exquisite specificity of the TRAP method.

TRAP-seq detects differentially expressed genes in repopulating hepatocytes

Differential gene expression analysis identified 6,745 genes that change in expression in repopulating compared with quiescent hepatocytes (Supplementary Digital Table 2.2); 3,418 were significantly upregulated and 3,380 downregulated (FDR ≤ 5%) (Figure 2.3A). Hierarchical clustering of the differentially expressed genes showed a distinct separation between quiescent and repopulating hepatocytes (Figure 2.3B). Notably, the 4-week regeneration group clustered closer to the 1-week regeneration group, demonstrating that TRAP-seq allows identification of different levels of liver regeneration. To establish whether the differentially expressed genes fall into defined regulatory networks, we used pathway analysis and focused on the highly validated

Kyoto Encyclopedia of Genes and Genomes (KEGG) network collection [29,30] (Figure 2.3C). Pathways controlling replication and growth were overrepresented among the upregulated genes, including those regulating the cell cycle and DNA replication, indicating that genes involved in cell replication were activated during liver repopulation, as expected. Strikingly, the GSH metabolic pathway was strongly activated in regenerating hepatocytes, aligning with previous studies showing that control of oxidative stress plays a crucial role in the regenerative response following toxic liver injury [31]. Interestingly, metabolic pathways were enriched in both activated and inhibited genes, reflecting the important metabolic regulation of hepatocytes, although the genes at play were different in the 2 groups (Supplementary Digital Table 2.3). Upregulated metabolic genes included redox processes, whereas repressed genes regulate lipid biosynthesis, corroborating previous findings that hepatocytes limit the activity of metabolic networks to conserve energy for rapid cell replication and DNA synthesis during regeneration [6].

The key regulatory nodes enriched in differentially expressed genes were analyzed with Ingenuity Pathway Analysis, which takes into account the degree of change of each gene to generate putative regulatory networks and predict activation or inhibition of the pathways. We identified 227 upstream regulators, of which 24 met the following additional filters: (a) significant Z-scores (≥2 for predicted activation and ≤2 for predicted inhibition); (b) at least a 2-fold change in expression; and (c) congruence between the observed fold change and predicted state categories (Table 2.3). MYC, the most enriched regulator, is a proto-oncogene activated as early as 1 h after PHx [32] and is also upregulated in liver regeneration induced by carbon tetrachloride and galactosamine [33]. Previous work had identified MYC as the strongest driver of liver repopulation in *Fah*$^{-/-}$ mice in a cDNA overexpression screen of more than 40 genes [16], and its overexpression also induces spontaneous hepatocellular carcinoma (HCC) development in the *Fah*$^{-/-}$ mouse model within 8 weeks [34]. A second upstream regulator of the proliferative response is the transcription factor FOXM1, which was previously shown to enhance liver repopulation [35]. These results indicate that we were indeed able to profile the translating mRNA signature specifically in

repopulating hepatocytes and demonstrate that TRAP-seq is a robust methodology for identifying enriched pathways and upstream regulators.

Fah$^{-/-}$ and PHx regeneration models share common genetic pathways

Next, we set out to compare the transcriptional changes of regenerating hepatocytes in *Fah*$^{-/-}$ mice recovering from toxic injury with those occurring following PHx, a paradigm of noninjury regeneration. First, we reanalyzed previous RNA-seq data from whole-liver homogenates after PHx [36] and identified 2,321 differentially expressed genes, 1,449 of which were activated and 872 inhibited (Figure 2.3D). Hierarchical clustering showed a distinct separation of gene regulation at various time points after PHx (Figure 2.3E). Interestingly, gene expression at 1 h clustered closer with quiescent hepatocytes, indicating that at this very early time point only a few early-response genes were transcriptionally regulated. Pathway analysis [29,30] showed enrichment of genes regulating cell-cycle and DNA synthesis pathways among the upregulated genes and those regulating immune and metabolic pathways among the downregulated genes (Figure 2.3F).

We compared the gene expression changes between the *Fah*$^{-/-}$ and PHx models, defining congruent genes as those regulated in the same direction in both models for at least 1 time point. We identified a total of 1,236 congruent genes, 790 of which were activated and 446 repressed (Figure 2.4A). Gene expression changes that occurred at all time points in the *Fah*$^{-/-}$ repopulation mice were most similar to the changes observed in the PHx model at later time points (36 or 48 h after PHx), as shown by the high percentage of congruence. Additionally, we found that the percentage of congruence was higher among the upregulated genes, indicating a more similar gene activation pattern in the 2 regeneration models. We discovered that the top upregulated congruent genes — ranked by mean fold change in *Fah*$^{-/-}$ mice and subsequently retrieved from the PHx data set — were associated with GSH metabolism, including the genes *Slc7a11* and *Gsta1* (Supplementary Digital Table 2.4) [18]. This was confirmed by pathway analysis, in which GSH metabolism was highly enriched in the congruently upregulated genes, along with cell-cycle, DNA replication, and DNA repair pathways (Figure 2.4C). Immune response and metabolic pathways

were enriched among the congruently downregulated genes (Figure 2.4D). Interestingly, the majority of the congruent genes did not show a significant change 1 h after PHx (Supplementary Digital Table 2.4), as at this stage, hepatocytes still resembled quiescent hepatocytes, with activation of only a few immediate early genes [2].

Of note, 2 of the top congruently upregulated genes, *Ly6d* and *Pbk*, are not typically expressed in hepatocytes. The average fragments per kilobase of transcript per million mapped (FPKM) reads for these genes in the quiescent hepatocytes were 2.7 and 0.01, but increased to 504.4 and 6.6 in regenerating hepatocytes, respectively (Supplementary Digital Table 2.2). *Ly6d* expression has been shown to be associated with HCC and liver regeneration after injury [37,38], while *Pbk* has been detected in HCC and cholangiocarcinoma [39,40]. This further demonstrates the sensitivity and specificity of TRAP-seq in detecting expression changes in a unique subpopulation of the liver — that of the regenerating hepatocytes.

Additionally, we identified genes that were only changed in 1 model but not the other (unique genes), of which 5,510 were unique to *Fah*$^{-/-}$ mice, and 1,033 were unique to the PHx model (Figure 2.4B). Of note, in both models, the percentage of unique genes compared with the total number of differentially expressed genes was approximately 81%. However, in the *Fah*$^{-/-}$ mice, up- and downregulated genes each constituted 50% of the unique genes, whereas in the PHx model, the upregulated and downregulated genes made up 64% and 36% of the unique genes, respectively. To further identify the biological pathways specific to each model, pathway enrichment analysis was performed on the unique genes [29,30], and overrepresented networks were identified (Figure 2.4, C and D). In *Fah*$^{-/-}$ mice, liver injury response categories such as alcoholism and viral carcinogenesis were uniquely activated, while immune response and metabolic pathways were uniquely inhibited. On the other hand, no significant pathway activation was unique to the PHx model, whereas the pancreatic secretion and protein and fat digestion/absorption pathways were uniquely inhibited. The striking difference in enriched pathways demonstrates the gene expression signatures that differentiate the 2 regeneration paradigms, in which injury response and immune modulation are unique to *Fah*$^{-/-}$ mice and nutrient redistribution is integral to the PHx model.

Recently, single-molecule RNA-FISH combined with single-cell RNA-seq (scRNA-seq) has been applied to reconstruct the spatial heterogeneity and identify novel zonal signature genes within the quiescent liver [41]. While TRAP-seq utilizes bulk RNA-seq and therefore cannot inform a spatial resolution of transcriptional changes during regeneration, we compared the expression profiles of quiescent hepatocytes from TRAP-seq with the scRNA-seq data. We reasoned that since all hepatocytes express GFP-L10a in the quiescent liver (Figure 2.1C), the isolated transcripts from TRAPseq should have an equal representation of the genes identified from the 9 different subpopulations by scRNA-seq. As expected, we found significant overlap between TRAP-seq and all 9 layers of scRNA-seq, with an average of 10,405 common genes, constituting 90.7% of the genes detected by TRAP-seq (Figure 2.5). Thus, TRAP-seq enables unbiased RNA isolation from all layers of hepatocytes.

Slc7a11 is massively upregulated in regenerating hepatocytes

The comparison of the *Fah*$^{-/-}$ and PHx models revealed *Slc7a11* as the most significantly activated gene in both paradigms, with a remarkable increase of 900-fold in the former and 200-fold in the latter (Supplementary Digital Table 2.4). *Slc7a11* encodes xCT, a sodium-independent transporter for cystine import and glutamate export [19]. After entering the cell, cystine is rapidly reduced to cysteine, a precursor for GSH synthesis necessary for cellular defense against oxidative stress [18]. Previous studies indicated that deficiency of glutamate-cysteine ligase, the rate-limiting enzyme in GSH synthesis, leads to decreased hepatocyte proliferation in vitro and delayed regeneration after PHx [42,43]. However, the role of xCT in liver regeneration has not been studied. We hypothesized that xCT upregulation supports actively repopulating hepatocytes to defend against increased oxidative stress during injury and regeneration (Figure 2.6A).

To evaluate the role of xCT in liver regeneration, we first validated our observations from RNA-seq with quantitative real-time reverse transcription PCR (qRT-PCR) on TRAP-purified mRNA and confirmed a significant upregulation of *Slc7a11* and *Gsta1* transcripts in repopulating hepatocytes (Figure 2.7A). Western blot analysis showed an increase in xCT protein in repopulating

livers (Figure 2.7B). Of note, there was low xCT expression in the quiescent liver, albeit no mRNA transcripts were present in hepatocytes. One possibility is that whole-liver homogenate was used for the protein analysis, and thus xCT protein from other cell types such as macrophages was detected [19]. Alternatively, the protein stability of *Slc7a11* could exceed its RNA turnover rate. Regardless, the expression of *Slc7a11* was significantly activated in the regenerating liver.

We next sought to investigate whether oxidative stress is increased in *Fah*$^{-/-}$ livers during regeneration. We used immunohistochemical methods to detect markers of lipid peroxidation (malondialdehyde and 4-hydroxynonenal) and protein nitration (nitrotyrosine). We observed an accumulation of redox metabolites in the injured livers compared with healthy, quiescent livers (Figure 2.7C). These results indicate that *Slc7a11* mRNA expression and xCT protein levels are highly enriched in repopulating hepatocytes in the presence of increased reactive oxygen and nitrogen species, suggesting a functional role of *Slc7a11* in the regulation of liver regeneration.

Ectopic *Slc7a11* expression promotes liver regeneration

To examine the functional importance of xCT activation in regenerating hepatocytes, we constructed plasmids coexpressing Fah and overexpressing *Slc7a11* (Fah-Slc7a11) or *Gfp* (Fah-Gfp). We performed a competition assay, in which equimolar amounts of Fah-Gfp and Fah-Slc7a11 were injected into *Fah*$^{-/-}$ mice, followed by NTBC withdrawal (Figure 2.6B). After 4 weeks of repopulation, we observed a 2.5-fold enrichment of Fah-Slc7a11 plasmid relative to the Fah-Gfp control plasmid by qPCR of extracted liver genomic DNA (Figure 2.6C) as well as overrepresentation of HA-tagged, xCT-expressing hepatocytes compared with GFP-expressing cells (Figure 2.6D). These results demonstrate a positive selection for hepatocytes overexpressing xCT, even above the already striking activation of endogenous *Slc7a11*.

To test whether *Slc7a11* is required for liver regeneration, we used CRISPR/Cas9 to inactivate *Slc7a11* specifically in the repopulating hepatocytes. We coexpressed FAH with either 10 single-guide RNAs (sgRNAs) targeting *Slc7a11* exons (Fah-sgSlc7a11) or 10 control sgRNAs targeting luciferase (Fah-gCtl) and performed hydrodynamic tail-vein injection of these sgRNAs,

together with adeno-associated virus 8 (AAV8) expressing Staphylococcus aureus Cas9 (SaCas9) to allow for hepatocyte-specific expression of the SaCas9 nuclease [44], which efficiently introduces indels comparable to those of Cas9 from *S. pyogenes* [45] (Figure 2.6E). Liver repopulation was then carried out for 4 weeks. To quantify and characterize the mutations induced by CRISPR/Cas9, we extracted genomic DNA from the repopulating livers, PCR amplified exon 1 for Sanger sequencing, and performed tracking of indels by decomposition (TIDE) analysis [46]. We found that the 2 sgRNAs targeting the first exon of *Slc7a11* exhibited different mutation efficiency: 29.5% and 51.6%, respectively (Figure 2.8, A and B). Furthermore, the main mutation introduced by SaCas9 in either sgRNA was a 5-nucleotide deletion, with an efficacy of 27.9% and 51.6%, respectively. The difference in mutation rate could be due to the slight difference in the protospacer-associated motif (PAM) sequence (NNGRRT) of the 2 sgRNAs, CTGAGT and AAGGGT [44]. Nonetheless, TIDE analysis demonstrated that *Slc7a11* was mutated through the expression of SaCas9 in the hepatocytes.

We measured weight changes over the 4-week period of liver repopulation and found no significant weight differences in mice treated with *Slc7a11* sgRNAs compared with those treated with control sgRNAs (Figure 2.8C). Likewise, we detected no significant difference in the liver weight to body weight ratio by the end of the 4-week period (Figure 2.8D). However, sgSlc7a11-treated mice had smaller FAH repopulation nodules and fewer Ki67/FAH double-positive hepatocytes compared with sgCtl-treated mice (Figure 2.6F), indicating that *Slc7a11* mutation inhibits replication of FAH-expressing cells during liver injury. It should be noted that these results are probably an underrepresentation of the true effect of *Slc7a11* mutation, as only hepatocytes homozygous, not those that are heterozygous, for inactivation of *Slc7a11* are expected to be at a growth disadvantage. Furthermore, redundant pathways could compensate for the loss of *Slc7a11* [47]. Together, these studies demonstrate the functional importance of xCT during liver repopulation and show that *Slc7a11* overexpression is sufficient to accelerate repopulation, whereas *Slc7a11* inactivation, while not completely abrogating regeneration, hinders hepatocyte replication.

Slc7a11 is transcriptionally activated by ATF4

Finally, we investigated the mechanism of xCT activation during liver repopulation. Several transcription factors have been shown to regulate *Slc7a11* expression in different contexts: nuclear factor E2-related factor 2 (NRF2) activates xCT during redox stress [48], activating transcription factor 4 (ATF4) upregulates xCT under ER stress, octamer-binding transcription factor (OCT1) disinhibits *Slc7a11* following ethanol exposure [49], and p53 inhibits xCT under normal tumor suppression conditions [50]. Additionally, ATF4 is suggested to regulate the basal levels of *Slc7a11* expression [51].

We first performed unbiased chromatin accessibility profiling to identify regulatory elements at the *Slc7a11* locus in hepatocytes in the basal and repopulating state. We used the isolation of nuclei-tagged in specific cell types (INTACT) system to label the nuclei of regenerating hepatocytes [52]. Specifically, the nuclear envelope protein SUN1 was tagged with GFP [53], and the resulting fragment was subcloned into the FAH coexpression construct (Fah-Sun1-Gfp). One week after the $Fah^{-/-}$ mice were repopulated with Fah-Sun1-Gfp, livers were harvested and sorted for GFP-positive nuclei (Figure 2.9A). As a quiescent control, we injected $Rosa^{LSL\text{-}Sun1\text{-}GFP}$ mice with AAV8-TBG-Cre and sorted hepatocytes after 1 week (Figure 2.9A). We used the assay for transposase accessible chromatin using sequencing (ATAC-seq) [54,55] to profile the chromatin landscape changes after 1 week of regeneration. Remarkably, the *Slc7a11* promoter is highly accessible in the regenerating hepatocytes, as indicated by the strong peak present 1 week after regeneration (Figure 2.9B). In comparison, we observed no peak at the promoter in the quiescent liver, demonstrating a heterochromatic state in healthy liver cells. This observation coincides with our TRAP-seq analysis, in which no *Slc7a11* transcripts were detected in quiescent hepatocytes, but became highly abundant in regenerating hepatocytes (Figure 2.7A).

Next, to determine how *Slc7a11* is activated, we performed a motif search at the open chromatin region of the activated promoter and identified a potential NRF2-binding site 39 bases and 2 potential ATF4-binding sites 39 and 66 bases upstream of the transcriptional start site (Figure 2.9C). To assess whether ATF4 or NRF2 binds to the *Slc7a11* promoter during liver repopulation,

we carried out ChIP-qPCR in quiescent and 4-week regenerating livers. We detected a significant 4-fold enrichment of bound ATF4 at the *Slc7a11* promoter in regenerating hepatocytes relative to that seen in quiescent controls. In contrast, NRF2 binding was undetected in either condition (Figure 2.9D), suggesting that ATF4, but not NRF2, activates *Slc7a11* transcription during liver repopulation.

TABLES

Table 2.1. Top ten abundant transcripts identified in quiescent livers.

Gene	Quiescent	1-week regeneration	4-week regeneration	4-week regeneration after severe injury
Apoc3	22258.99	8284.08	16707.52	10378.8
Apoa2	18465.14	8906.01	8600.62	10388.86
Fabp1	14824	15222.48	10529.91	1586.67
Apoc1	12632.39	14177.49	6945.49	15360.81
Apoe	12418.85	6753.43	5936.13	10505.54
Apoc1	11083.99	12446.11	6094.25	13496.84
Alb	10481.08	5141.19	2962.66	9602.19
Trf	6906.36	1267.84	1930.87	3292.12
Gpx1	6150.21	4540.07	5258.64	5562.72
Apoc4	5028.13	4193.01	4623.31	2596.7

Numbers represent the average fragments per kilobase of transcript per million (FPKM) reads in each regeneration group.

Table 2.2. FPKM of cell type-specific transcripts detected by TRAP-seq.

Gene	Quiescent	1-week regeneration	4-week regeneration	4-week regeneration after severe injury	Cell type
Alb	10481.08	5141.19	2962.66	9602.19	Hepatocyte
Ttr	2639.6	3072.59	1212.62	5454.57	Hepatocyte
Cyp2e1	2424.01	588.72	1418.17	380.48	Hepatocyte
Asgr1	1190.04	865.69	1375.35	654.07	Hepatocyte
Krt19	0.18	0.16	0.15	1.97	Biliary epithelium
Pkd2	1.28	0.71	0.79	1.56	Biliary epithelium
Krt7	0.22	0	0.22	0.89	Biliary epithelium
Cftr	0	0	0.02	0	Biliary epithelium
Des	1.09	0.33	0.43	0.86	Stellate cell
Acta2	0.41	0.35	0.27	0.34	Stellate cell
Col1a1	0.04	0.42	0.26	1.22	Stellate cell
Cd68	0.92	0.71	0.36	5.9	Kupffer cell
Emr1	0.67	0.28	0.27	0.84	Kupffer cell
Cd163l1	0	0	0	0	Kupffer cell
Clec5a	0	0	0.02	0.05	Kupffer cell

Table 2.3. Upstream regulators predicted by Ingenuity Pathway Analysis.

Upstream regulator	Fold change	Molecule type	Predicted state	Z-score	*P* value
MYC	3.08	Transcription regulator	Activated	4.73	1.15E-24
SREBF1	0.26	Transcription regulator	Inhibited	-3.97	3.32E-16
THRB	0.50	Nuclear receptor	Inhibited	-2.28	4.26E-10
E2F1	2.53	Transcription regulator	Activated	2.59	2.06E-09
FOXM1	15.67	Transcription regulator	Activated	3.23	4.79E-09
EGR1	0.33	Transcription regulator	Inhibited	-2.09	4.33E-08
HBB-B1	0.11	Transporter	Inhibited	-2.07	7.41E-08
SPARC	0.30	Other	Inhibited	-3.62	1.43E-07
CSF1	0.48	Cytokine	Inhibited	-2.95	2.63E-07
HBB-B2	0.11	Other	Inhibited	-2.68	5.31E-07
ERF2	4.85	Transcription regulator	Activated	2.75	9.10E-07
USF2	0.35	Transcription regulator	Inhibited	-2.49	2.40E-06
AGTR1	0.40	GPCR	Inhibited	-2.70	6.04E-06
LMNB1	6.69	Other	Activated	2.56	6.26E-06
CCNE1	3.7	Transcription regulator	Activated	2.07	2.14E-05
MLXIPL	0.40	Transcription regulator	Inhibited	-3.70	3.19E-05
TFEB	0.35	Transcription regulator	Inhibited	-2.05	3.33E-04
S100A6	2.92	Transporter	Activated	2.85	1.20E-03
CTGF	0.44	Growth factor	Inhibited	-2.04	1.26E-03
TAS1R3	0.42	GPCR	Inhibited	-2.14	2.02E-03
IL15	0.37	Cytokine	Inhibited	-2.70	3.28E-03
FASN	0.14	Enzyme	Inhibited	-2.11	1.77E-02
TNK1	0.46	Kinase	Inhibited	-2.83	2.03E-02
MLYCD	0.50	Enzyme	Inhibited	-2.00	2.06E-02

Filter criteria: (a) significant *Z*-scores (≥2 for predicted activation and ≤2 for predicted inhibition); (b) at least 2-fold change in expression; and (c) congruence between the observed fold change and predicted state categories.

FIGURES

Figure 2.1. Translating ribosome affinity purification (TRAP) enables cell type-specific isolation of RNA from quiescent and repopulating hepatocytes.

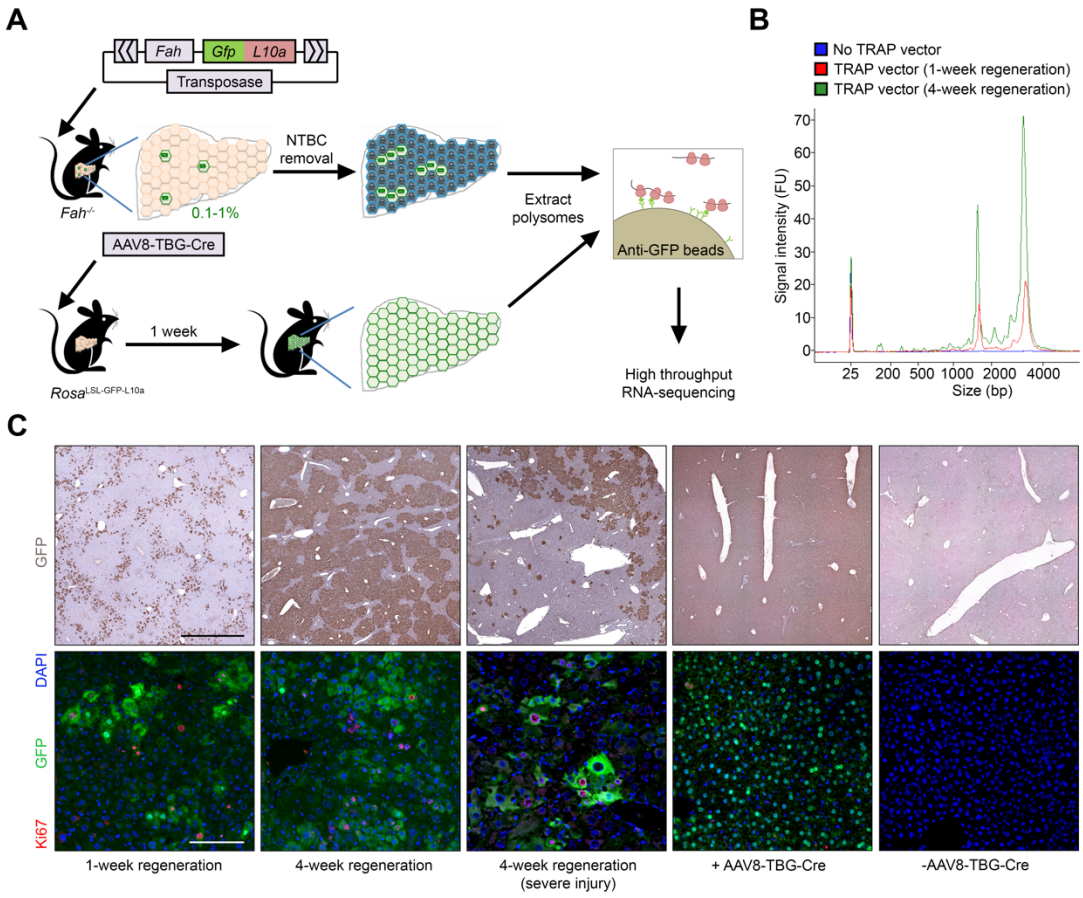

(**A**) The approach for isolating repopulating hepatocyte RNA with the *Fah*$^{-/-}$ model involves use of the FAH expression construct to mediate liver repopulation and the GFP-tagged ribosomal protein L10a (GFP-L10a) to specifically isolate translating mRNAs with TRAP. Injection of the RosaLSL-GFP-L10a mouse with the AAV8-TBG-Cre virus, which has a tropism for hepatocytes and has a hepatocyte-specific promoter driving Cre expression in nearly all hepatocytes, allows for immunoprecipitation of translating mRNA from quiescent hepatocytes. (**B**) Bioanalyzer tracings of affinity-purified RNA from mice treated with or without the TRAP vector. FU, fluorescence units. (**C**) Representative (n = 3) IHC images of GFP show progressive repopulation over time in *Fah*$^{-/-}$ mice as well as complete labeling of quiescent hepatocytes in *Rosa*$^{LSL\text{-}GFP\text{-}L10a}$ mice 1 week after injection

of AAV8-TBG-Cre. No GFP expression was observed in livers from the uninjected mice. IF of Ki67 and GFP confirmed successful liver repopulation in *Fah*$^{-/-}$mice injected with the TRAP vector, as all Ki67-positive hepatocytes express GFP. IF costaining also showed global GFP-expressing and rare Ki67-positive hepatocytes, indicating that the control tissue was truly quiescent. Note that a subset of mice showed only partial repopulation at 4 weeks (4-week regeneration after severe injury). Scale bars: 1 mm (top) and 100 μm (bottom).

Figure 2.2. Mice in the 4-week regeneration after severe injury group exhibit significant weight loss.

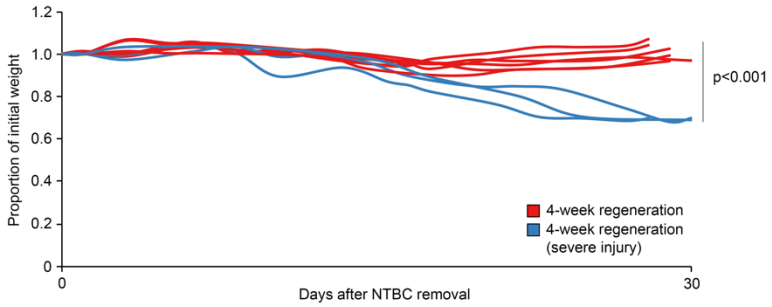

The proportion of weight loss was normalized to the initial weight prior to plasmid injection and NTBC removal. Bodyweight was monitored three times per week after induction of liver injury and regeneration. After four weeks of injury and regeneration, three mice lost ~30% of the starting weight (blue), significantly different from mice in the 4-week regeneration group that underwent initial weight loss but restored body weight after four weeks (red). A two-sided, two-tailed Student's t-test was used to compare the proportion of body weight in the 4-week regeneration (n=6) and 4-week regeneration after severe injury (n=3) groups.

Figure 2.3. TRAP-seq identifies differentially expressed genes specific to repopulating hepatocytes in the *Fah*$^{-/-}$ model.

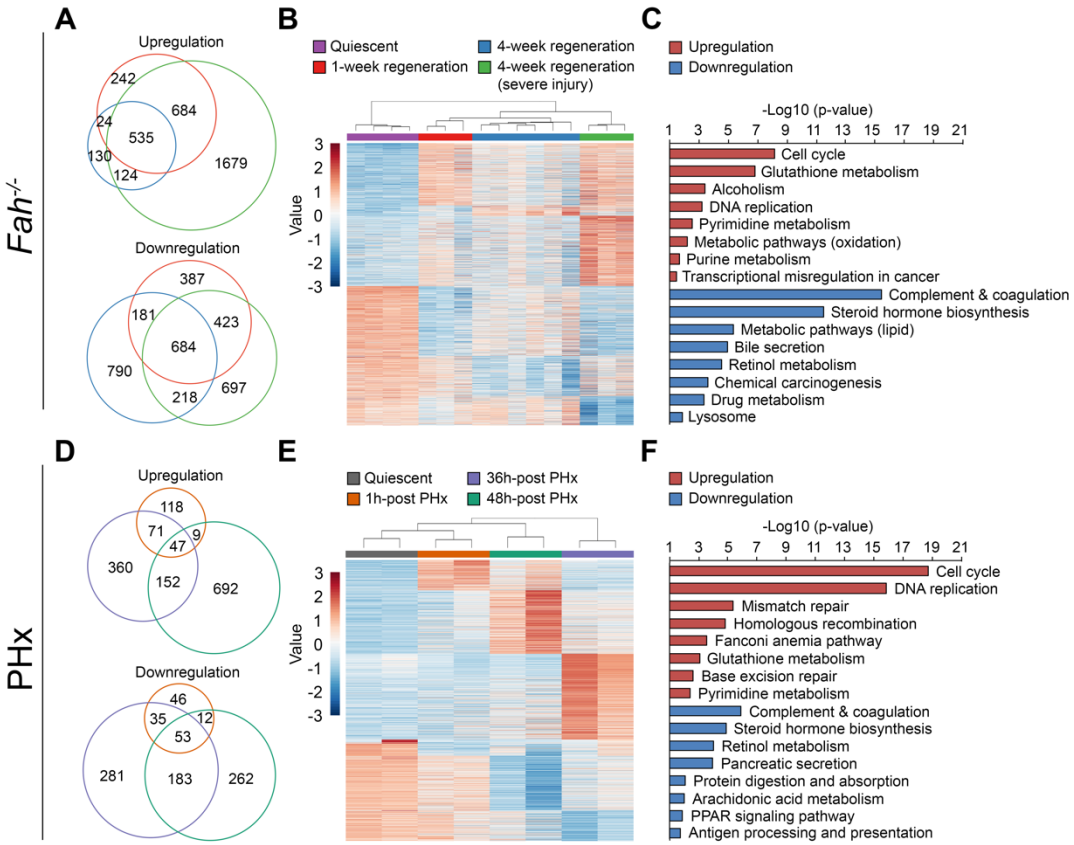

(**A** and **D**) Differential expression analysis identified 6,745 (3,418 upregulated and 3,380 downregulated) and 2,321 (1,449 upregulated and 872 downregulated) genes as being significantly altered in repopulating hepatocytes in the *Fah*$^{-/-}$ (**A**) and PHx (**D**) models (36), respectively, compared with quiescent controls. Red, 1-week *Fah*$^{-/-}$ regeneration and 1 h after PHx; blue, 4-week *Fah*$^{-/-}$ regeneration and 36 h after PHx; green, 4-week *Fah*$^{-/-}$ regeneration after severe injury and 48 h after PHx. (**B** and **E**) Hierarchical clustering of differentially expressed genes of quiescent and repopulating hepatocytes at different time points. (**C** and **F**) KEGG pathways significantly enriched for the sets of activated and repressed genes, respectively, in the *Fah*$^{-/-}$ (**C**) and PHx (**F**) data sets.

Figure 2.4. Comparison of the *Fah*$^{-/-}$ TRAP-seq data with RNA-seq data from the PHx model identifies common and unique characteristics of liver repopulation paradigms.

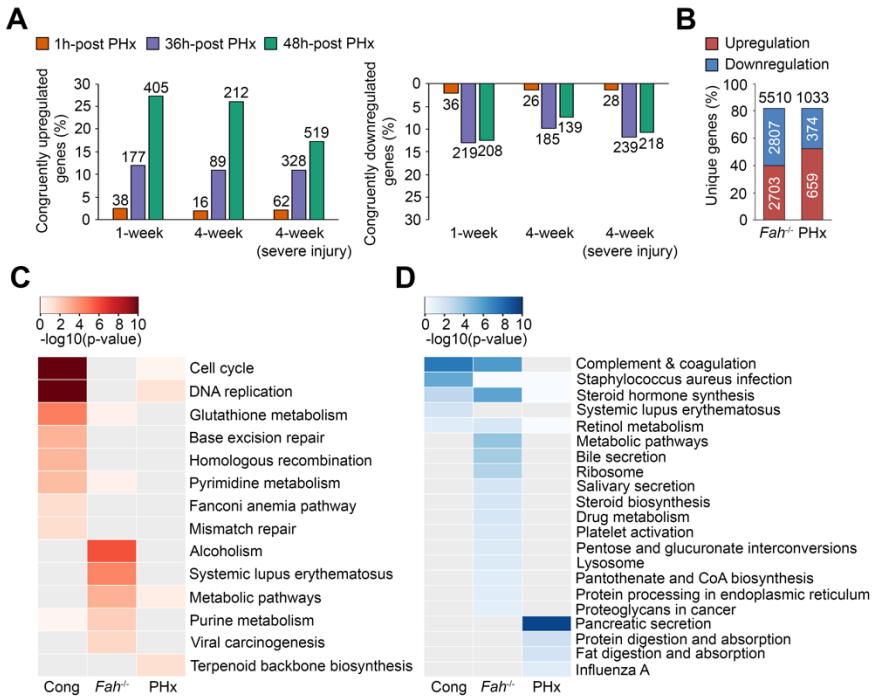

(**A**) A total of 1,236 genes were significantly altered in the same direction in both models [36] for at least 1 time point (congruent genes). Of these genes, 790 were activated and 446 inhibited. Labels indicate the number of congruent genes at each time point. (**B**) A total of 5,510 and 1,033 genes were uniquely changed in the *Fah*$^{-/-}$ and PHx models, respectively. (**C** and **D**) Comparison of the KEGG pathways enriched for genes upregulated (**C**) and downregulated (**D**) in the congruent (Cong) and unique gene sets.

Figure 2.5. Comparison of identified transcripts from single-cell RNA-seq (scRNA-seq) [41] shows significant overlap between TRAP-seq and all nine layers of scRNA-seq.

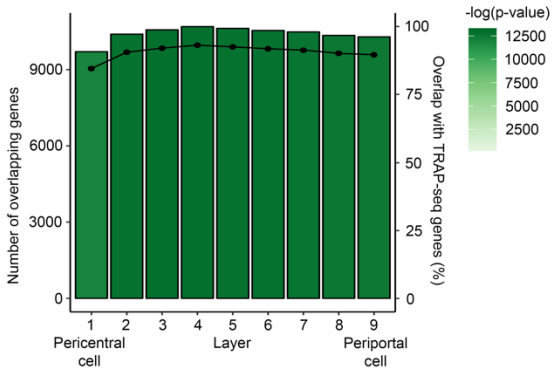

Genes identified in the quiescent samples from TRAP-seq was compared to that from scRNA-seq. Bar height indicates the number of overlapping genes identified in two techniques. Line and data points indicate the percentage overlap from each scRNA-seq layer compared to TRAP-seq. A hypergeometric test was used to calculate the significance of overlapping genes from the two sequencing methods.

Figure 2.6. *Slc7a11* enhances hepatocyte repopulation.

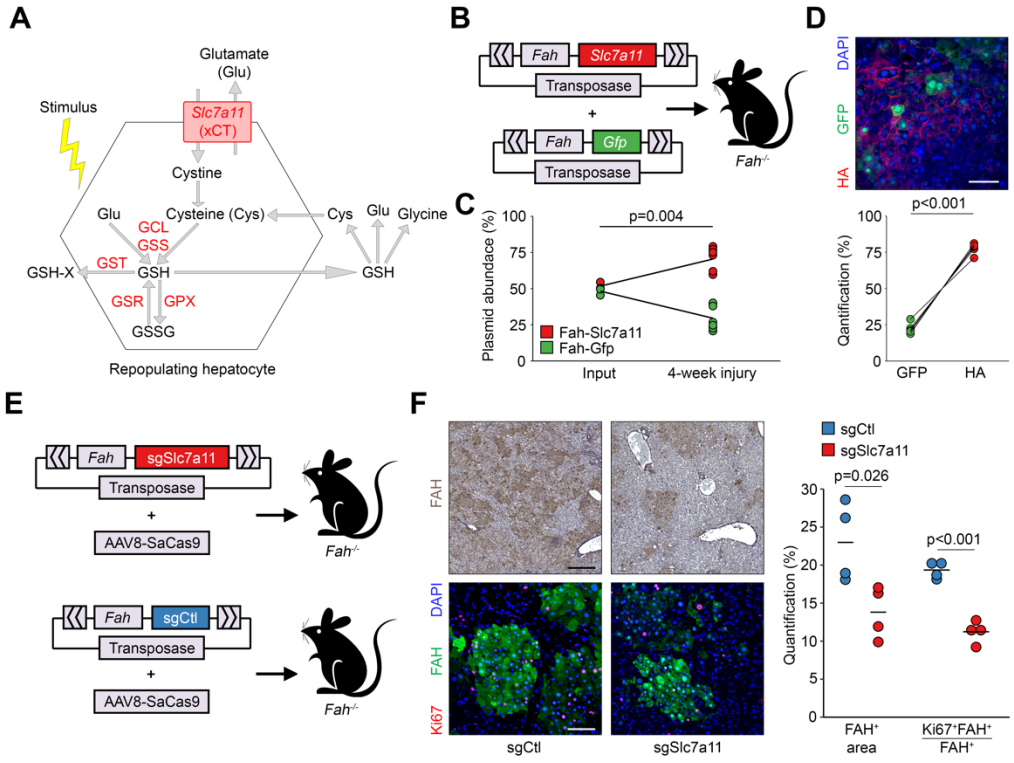

(**A**) The *Slc7a11* gene product (xCT) imports cystine, which is used for GSH synthesis to alleviate oxidative stress. Several GSH metabolic enzymes were significantly (FDR ≤ 5%) upregulated (red) in repopulating hepatocytes from *Fah*$^{-/-}$ mice. GSSG, glutathione disulfide; GCL, glutamate-cysteine ligase; GSS, glutathione synthetase; GST, glutathione S-transferase; GSR, glutathione reductase; GPX, glutathione peroxidase. (**B**) Schematic of the competition assay to determine the effects of *Slc7a11* overexpression on repopulation. (**C**) The Fah-Slc7a11 plasmid was significantly enriched after 4 weeks of repopulation. A 1-sample, 2-tailed Student's t-test was used to compare the ratio of 2 plasmids before and after repopulation (n = 8). (**D**) Representative IF staining and quantification showing a significant increase in xCT-positive hepatocytes. A paired, 2-tailed Student's t-test was used to compare HA- and GFP-expressing hepatocytes (n = 5). Scale bar: 100 μm. (**E**) Schematic of the CRISPR/Cas9 system used to inactivate *Slc7a11* in *Fah*$^{-/-}$ mice. sgCtl, sgRNAs targeting firefly luciferase. (**F**) Representative IHC and IF images and quantification showing a significant reduction in repopulation nodules and replicating hepatocytes in mice treated

with sgRNAs targeting *Slc7a11* (sgSlc7a11) compared with control mice treated with sgCtl. A 2-sample, 2-tailed Student's t-test was used to compare groups (n = 4 each). Scale bars: 300 μm (top) and 100 μm (bottom).

Figure 2.7. *Slc7a11* is activated at the transcript and protein levels under increased oxidative stress during liver regeneration.

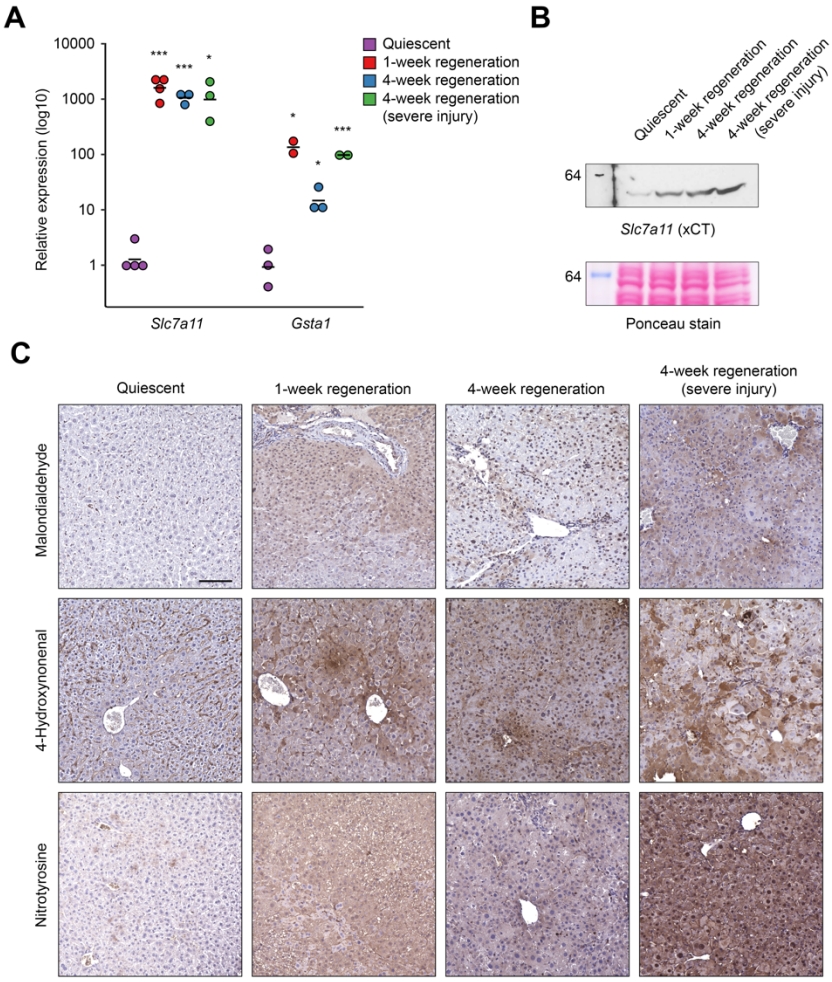

(**A**) Real-time reverse transcription PCR (qRT-PCR) analysis showed continuous upregulation of *Slc7a11* and *Gsta1*, both involved in GSH metabolism, in repopulating hepatocytes. A two-sample, two-tailed Student's t-test was used to compare repopulating and quiescent hepatocytes. * $p<0.05$, *** $p<0.001$ (n=4, quiescent and 1-week regeneration; n=3, 4-week regeneration and 4-week regeneration after severe injury). (**B**) Western blot analysis confirmed the activation of xCT in the regenerating liver. (**C**) IHC staining of lipid peroxidation markers (malondialdehyde and 4-hydroxynonenal) and protein nitration (nitrotyrosine) showed accumulation of redox metabolites in the injured, repopulating liver compared to healthy, quiescent livers. Scale bar: 100μm.

Figure 2.8. No significant differences in the weight of mice with *Slc7a11* inhibition compared to control after 4 weeks of repopulation.

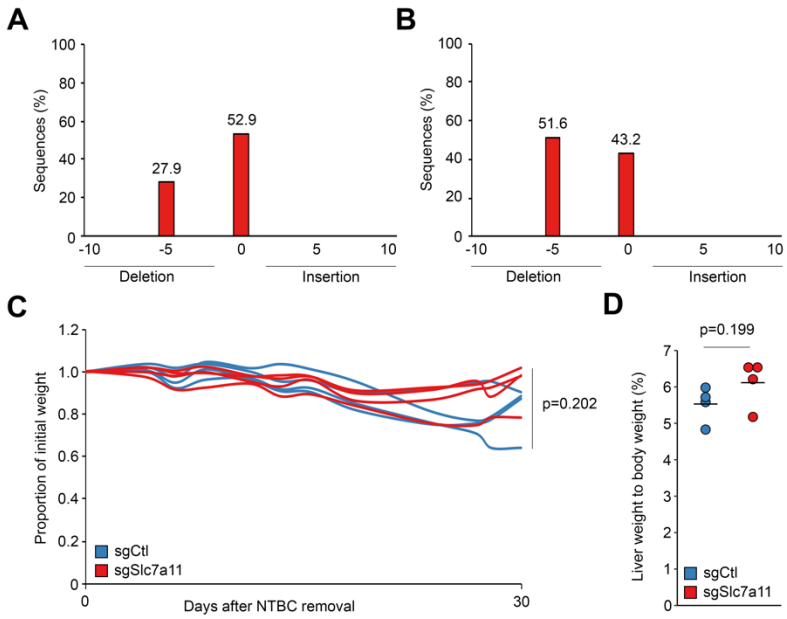

(**A** and **B**) Mutation analysis of *Slc7a11* exon one identified differential indel rates introduced by two single guide RNAs (sgRNA), sgSlc7a11-1 (**A**) and sgSlc7a11-2 (**B**). The x-axis indicates the number of nucleotides that were inserted or deleted and the y-axis indicates the percentage of mutation. (**C**) No weight differences during and after 4 weeks of repopulation and no changes in liver weight to body weight ratio (**D**) in mice treated with sgRNA against *Slc7a11* (n=4) compared to control mice (n=4). A two-sample, two-tailed Student's t-test was used to compare mice treated with *Slc7a11* and control sgRNAs.

Figure 2.9. *Slc7a11* is activated by ATF4 during liver repopulation.

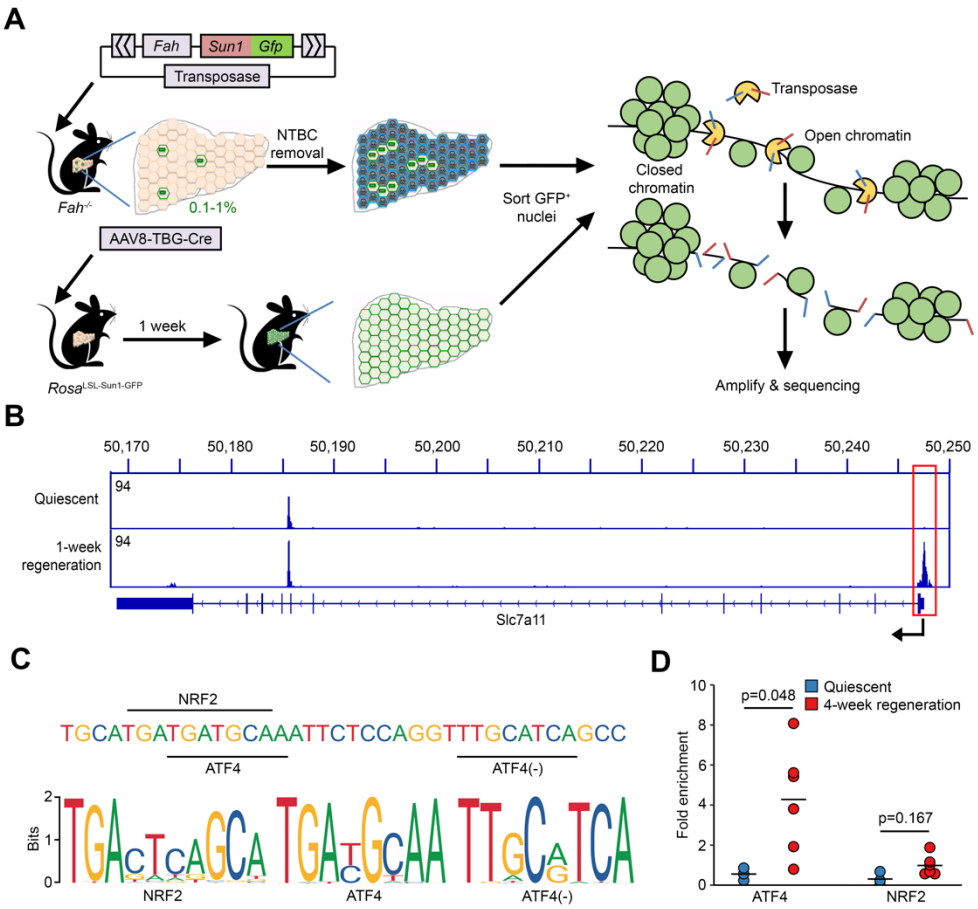

(**A**) Schematic of our approach utilizing the GFP-labeled nuclear envelope protein SUN1 to isolate hepatocyte nuclei [53], followed by ATAC-seq [54,55] analysis. (**B)** ATAC-seq identified an open chromatin state at the promoter region of *Slc7a11* specifically in regenerating hepatocytes (n = 2, quiescent; n = 4, 1-week regeneration). (**C**) The open chromatin region of the *Slc7a11* promoter contains binding motifs for NRF2 and ATF4. (**D**) ChIP-qPCR showed a 4-fold enrichment of ATF4 binding to the *Slc7a11* promoter after 4 weeks of liver regeneration, while no enrichment in NRF2 binding was observed. The Wilcoxon rank-sum test was used to compare the differential binding in regenerating and quiescent livers (n = 3, quiescent; n = 6, 4-week regeneration).

DISCUSSION

Here, we performed what we believe to be the first expression profile specific to repopulating hepatocytes by integrating the TRAP assay with the *Fah*$^{-/-}$ mouse model. We identified important signaling networks and regulators, including upregulation of the cell-cycle and GSH metabolic pathways, and several activated transcription factors such as MYC and FOXM1. Bioinformatics analysis comparing the gene expression of *Fah*$^{-/-}$ and PHx regeneration models identified pathways common to both models, i.e., cell cycle and GSH metabolism pathway genes among the congruently activated genes, and immune response pathway genes among the congruently inhibited genes. We also observed that liver damage pathways are uniquely upregulated in *Fah*$^{-/-}$ mice, while altered biosynthetic activity is a main theme in the PHx model.

A recent study utilizing single-cell technology to reconstruct the spatial heterogeneity of the liver had identified 9 distinct layers of gene expression profiles in quiescent hepatocytes [41]. We showed that transcripts identified from TRAP-seq significantly overlapped with those found in scRNA-seq, regardless of the layer, demonstrating the sensitivity and specificity of TRAP-seq in isolating transcripts from pure hepatocytes. Nonetheless, there are several differences between the 2 techniques. First, TRAP-seq utilizes bulk RNA-seq and therefore could not capture the zonal information by scRNA-seq. Second, TRAP-seq isolates mRNA bound to the ribosomal subunit L10a and hence only captures the actively translating mRNA. Third, TRAP-seq does not require cell sorting and therefore bypasses the time-consuming sample preprocessing required for scRNA-seq. Previous efforts to isolate intact regenerating hepatocytes after hydrodynamic injection has been unsuccessful, rendering TRAP-seq a valuable alternative. Future work could apply cell layer-specific expression of GFP-L10a to shed light on the zonal responses to liver injury and regeneration.

Previous work has demonstrated the importance of controlling oxidative stress during liver regeneration to allow hepatocyte replication, as an elevation of ROS induces a compensatory upregulation of GSH to inhibit irreversible cell damage and promote hepatic replication [56]. In support of the central role of GSH in liver regeneration, inhibition or deficiency of glutamate-cysteine

ligase, the rate-limiting enzyme in GSH synthesis, leads to downregulation of cyclin expression, decreased hepatocyte proliferation in vitro, and delayed regeneration after PHx [42,43]. Furthermore, GSH is depleted in acetaminophen-induced liver injury by the toxic metabolite NAPQI [57], pointing to the importance of GSH detoxification and ROS homeostasis in various regenerative paradigms.

Importantly, our results indicate that *Slc7a11* becomes dramatically activated in repopulating hepatocytes, and we further show that ectopic expression of xCT concomitantly with the onset of liver injury promotes regeneration, probably by shielding repopulating hepatocytes from oxidative stress. These results highlight the therapeutic potential of activating *Slc7a11* as a treatment for acute liver injury. We did not observe any health complications in mice overexpressing *Slc7a11* during the 4-week period of repopulation in the *Fah*$^{-/-}$ mouse. However, determining whether this approach is beneficial in managing chronic liver injury and whether long term xCT activation is safe will require further examination.

Recent studies have found *Slc7a11* to be highly expressed in HCC, breast cancer cells, and gastrointestinal tumors [58–60] and have shown that pharmacological xCT inhibition induces growth arrest in cancer cells and decreases tumor size in mouse models [59,60]. Therefore, it is possible that regenerating hepatocytes experience metabolic requirements similar to those seen in cancer cells to increase GSH availability. This raises the question of the safety of using xCT antagonists in patients with HCC, as both the growth of cancer cells and regenerating hepatocytes would be inhibited. Interestingly, in our gene inactivation studies, while a decrease in replicating hepatocytes during regeneration was observed, *Slc7a11* inhibition did not completely abrogate liver repopulation, and the mice treated with sgRNAs against *Slc7a11* were still able to restore full body weight after 4 weeks of regeneration. This observation is consistent with recent findings that xCT deficiency alone is not sufficient to induce liver injury but exacerbates injury when combined with secondary stress such as a high-iron diet [61] or inhibition of the transsulfuration pathway [62]. In addition, as discussed above, *Slc7a11* was probably not inactivated for both alleles in all regenerating hepatocyte clones. Furthermore, genetic redundancy has been proposed to underlie

liver regeneration, as loss of any single gene rarely leads to complete inhibition of the regenerative process [3].

In conclusion, this study demonstrates the feasibility of TRAP-seq for cell type-specific mRNA isolation of hepatocytes and identifies *Slc7a11* as a driver that promotes recovery after acute liver injury. Likewise, TRAP could be used to label other cell types in the liver to study their roles in acute liver injury. For instance, by combining the *Rosa*$^{LSL\text{-}GFP\text{-}L10a}$ mouse with a biliary-specific Cre or stellate cell-specific Cre transgene, it will be possible to profile the cell type-specific gene expression for these cells during injury and regeneration.

MATERIALS AND METHODS

All primer sequences are listed in Supplementary Digital Table 2.5.

Plasmid construction

The plasmid C2-EGFP-L10a was provided by Nathaniel Heintz (The Rockefeller University, New York, NY, USA). The GFP-L10a coding sequence was amplified by PCR using the primers L10a-R-BsiWI and MfeI-EGFP-F and subcloned into the vector pKT2/Fah-mCa//SB [15] at the EcoRI and BsiWI restriction sites. The vector utilizes the *Sleeping Beauty* (SB) transposon system to enable the integration of transgene sequences into the genome. The *Slc7a11* cDNA was purchased (MG225346, OriGene) and amplified by PCR with the primers Slc7a11_clone_F1 and Slc7a11_psmd_bcd-R or Slc7a11-HA_bcd-R to include the HA tag. For the CRISPR/Cas9 studies, the vector pKT2/Fah-SpCas9//SB [34] was used to replace the SpCas9 with the SaCas9 sgRNA scaffold and introduce the subcloning site for further sgRNA subcloning using the oligonucleotides SaCas-9Ins-F and -R and the restriction enzymes SapI and EcoRI to generate the vector pKT2/Fah-SaCas9//SB. Next, 10 sgRNAs targeting the exon regions of *Slc7a11* were designed with the online CRISPR RGEN Tools [63] and DESKGEN Cloud [64]. Ten sgRNAs against luciferase were designated as the control, and the oligonucleotides were subcloned into the pKT2/Fah-SaCas9//SB vector at the SapI restriction sites. For the ATAC-seq study, SUN1-GFP fragments with EcoRI and BsiWI restriction sites were amplified from the SUN1-GFP plasmid (a gift of Jeremy Nathans, Johns Hopkins University, Baltimore, MD, USA) with the primers MfeI-Sun1-F and BsiW1-Sun1-R and subcloned into the vector pKT2/Fah-mCa//SB to generate pKT2/Fah-Sun1-Gfp//SB. Endotoxin-free Maxi-scale DNA extraction and purification were performed with the GenElute HP Plasmid Maxiprep Kit (MilliporeSigma).

Mouse experiments

Fah$^{-/-}$ mice were maintained on NTBC (Swedish Orphan Biovitrum) in the drinking water (7.5 mg/l) until hydrodynamic tail-vein injection [15] of 10 μg plasmid, as specified below. For the TRAP-seq study, pKT2/Fah-Gfp-L10a//SB was injected, and the mice were euthanized 1 week (n

= 3) or 4 weeks (n = 9) after injection. Likewise, for the overexpression assay, mice were injected with equimolar amounts of the plasmids pKT2/Fah-Gfp//SB and pKT2/Fah-Slc7a11//SB (n = 3) or pKT2/Fah-Slc7a11-HA//SB (n = 5) and euthanized 4 weeks after injection. For the CRISPR/Cas9 studies, Mice were injected with either a mixture of 10 pKT2/Fah-sgSlc7a11//SB (n = 4) or pKT2/Fah-sgCtl//SB (n = 4) in conjunction with 110^{12} genome copies of AAV8.SaCas9 (Penn Vector Core [65]) for 4 weeks of repopulation. For the ATAC-seq assay, mice were injected with pKT2/Fah-Sun1-Gfp//SB (n = 4). One week after plasmid injection, the livers were harvested, and GFP-positive nuclei were isolated by FACS. Mouse weights were measured 3 times per week over the course of the repopulation period to ensure successful liver regeneration. *Rosa*$^{LSL\text{-}GFP\text{-}L10a}$ mice were purchased from The Jackson Laboratory and used as a healthy control (n = 4) in the TRAP-seq study, and the *Rosa*$^{LSL\text{-}GFP\text{-}L10a}$ mice were provided by Mitchell Lazar (University of Pennsylvania, Philadelphia, PA, USA) as a quiescent control in the ATAC-seq (n = 2) experiments. AAV8.TBG.PI.Cre.rBG (Penn Vector Core [65]) was injected into the tail vein of mice at 110^{11} virus particles per mouse. Mice were euthanized after 1 week of injection, and the livers were harvested. All animal studies were performed in 8- to 12-week-old female mice.

Translating RNA isolation

RNA specific for repopulating hepatocytes was isolated by TRAP [17]. Briefly, 200 mg liver tissue was taken en bloc from mice injected with the TRAP construct and from *Rosa*$^{LSL\text{-}GFP\text{-}L10a}$ mice, homogenized with lysis buffer, and incubated with magnetic beads that were conjugated with anti-GFP antibodies (clones Htz-GFP-19F7 and Htz-GFP-19C8, Memorial Sloan-Kettering Monoclonal Antibody Facility, New York, New York, USA) to affinity purify RNA that was bound by the GFP-L10a fusion protein.

IHC and IF

Liver lobes were dissected from mice and fixed with 4% paraformaldehyde, embedded in paraffin, and sectioned. For IHC, slides were rehydrated and subjected to antigen retrieval in

sodium citrate (pH 6.0). H_2O_2 (30%) was used for quenching endogenous peroxidases, and avidin D and biotin (Vector Laboratories) were used for blocking before incubation with primary antibodies overnight at 4 °C. The slides were then incubated with biotin-conjugated secondary antibody at 37 °C for 30 min. The avidin-peroxidase complex was incubated at 37 °C for 30 min (VECTASTAIN Elite Kit, Vector Laboratories). A DAB Substrate Kit for Peroxidase (Vector Laboratories) was used for development and hematoxylin for counterstaining. For IF, slides were prepared as described above. Incubation with primary antibodies was done overnight at 4 °C in a humid chamber, followed by secondary antibody incubation for 2 h at room temperature.

Antibodies

GFP was detected with goat anti-GFP antibody (ab6673, 1:100, Abcam) for IHC and chicken anti-GFP antibody (GFP-1020, 1:300, Aves Labs) for IF staining. We used rabbit anti-mouse Ki67 antibody (SP6, 1:300, Thermo Fisher Scientific) and anti-mouse Ki67 antibody (550609, 1:200, BD Biosciences) to detect proliferating cells, rabbit anti-HA antibody (sc-805, 1:100, Santa Cruz Biotechnology) for Slc7a11-HA-positive hepatocytes, rabbit anti-mouse FAH antibody (ab81087, 1:500 for IHC and 1:200 for IF, Abcam), and DAPI for nuclear staining.

RNA-seq

RNA integrity was measured using an Agilent RNA 6000 Bioanalyzer (Agilent Technologies). cDNA libraries were made from isolated RNA with a NEBNext Ultra RNA Library Prep Kit for Illumina (New England BioLabs) according to the manufacturer's instructions. Library quality was measured with an Agilent High Sensitivity DNA Bioanalyzer, and cDNA libraries were purified and qPCR quantified (Kapa Biosystems). Twenty samples of equimolar libraries were pooled and sequenced with an Illumina HiSeq 2500.

RNA-seq data analysis

Fastq files of RNA-seq were processed using the RUM algorithm [66], with support from the University of Pennsylvania's Next Generation Sequencing Core [67]. Differential gene expression analysis was performed using the package edgeR [68] in R software. Differentially expressed genes were identified with a cutoff of greater than 2-fold change and an FDR of less than 5%. Congruent genes in *Fah*$^{-/-}$ and PHx models were defined as genes regulated in the same direction for at least 1 time point in both models. Quantile-normalized reads were used for generating the heatmaps with the R package aheatmap, and Venn diagrams were created using Vennerable. Gene ontology was performed using the Database for Annotation, Visualization, and Integrated Discovery (DAVID) [29,30]. The top 3,000 upregulated and downregulated genes were uploaded to DAVID and analyzed using the functional annotation tool. A list of enriched KEGG pathways was obtained from the functional annotation chart report. The top-10 most significantly enriched KEGG pathways were selected and sorted according to the Bonferroni-corrected p-value. In addition, all differentially expressed genes, along with their corresponding fold change, were uploaded into the Ingenuity Pathway Analysis tool, and functional analysis was performed using the Core Analysis function. The upstream regulators predicted by Ingenuity Pathway Analysis were further filtered by (a) genes that were also changed in the RNA-seq analysis by at least 2-fold, (b) a significant Z-score (≥2 for predicted activation and ≤2 for predicted inhibition), and (c) congruence between the observed fold change and the predicted activation or inhibition.

Quantitative reverse-transcription with polymerase chain reaction (qRT-PCR)

Extracted RNAs were reverse transcribed to cDNA with SuperScript II Reverse Transcriptase (Invitrogen, Thermo Fisher Scientific), and qRT-PCR was performed with *Slc7a11* primers (Slc7a11-qRTPCR-F and -R), *Gsta1* primers (Gsta1-qRTPCR-F and -R), and Tbp primers (Tbp-qRTPCR-F and -R). Relative expression levels were normalized to Tbp.

Quantitative PCR (qPCR)

Genomic DNA was extracted from mice injected with equimolar amounts of pKT2/Fah-Gfp//SB (Fah-Gfp) and pKT2/Fah-Slc7a11-HA//SB (Fah-Slc7a11-HA) over a 4-week period with a DNeasy Blood and Tissue Kit (QIAGEN), followed by ethanol precipitation. qPCR was performed with PrimeTime primer sets (IDT DNA) *Slc7a11* (Slc7a11-qPCR-F, -R, and -P) and *Gfp* (Gfp-qPCR-F, -R, and -P). Standard curves were generated by performing a serial dilution of the input plasmid with equimolar amounts of Fah-Gfp and Fah-Slc7a11-HA.

Western blotting

Proteins were extracted from whole-liver homogenate with lysis buffer containing 50 mM Tris, pH 7.5, 0.5 mM EDTA, 150 mM NaCl, 10% glycerol, 1% NP-40, and 1% SDS, supplemented with 1:100 Halt Protease Inhibitor Cocktail (Thermo Fisher Scientific). The lysates were sonicated at 30-second intervals for 5 min and electrophoresed on 4% to 12% NuPAGE Precast Gels (Life Technologies, Thermo Fisher Scientific). A nitrocellulose membrane was used for transfer, and 5% milk in TBST (TBS plus 0.1% Tween-20) was used to block the membrane at room temperature for 1 h. The anti-mouse xCT antibody (sc-79360, 1:200, Santa Cruz Biotechnology) was diluted in 5% BSA in TBST and incubated overnight at 4 °C. The membrane was washed with TBST 3 times for 10 min, followed by an HRP-conjugated secondary antibody in 5% milk in TBST for 1 h, and then exposed to film.

Hepatocyte nuclei isolation and sorting

Livers were harvested and nuclei isolation was performed as previously described [69]. Briefly, liver was dounced in a pestle tissue grinder in 10 ml hypotonic buffer (10 mM Tris-HCl, pH7.5, 2 mM MgCl2, 3 mM CaCl2) on ice. The homogenate was passed through a 100-μm filter and sedimented at 400 g at 4 °C for 10 min. The pellet was resuspended in 10 ml hypotonic buffer with 10% glycerol, and 10 ml lysis buffer (hypotonic buffer, 10% glycerol, 1% IGEPAL CA-630) was

added dropwise. After 5 min of incubation, the solution was centrifuged at 600 g for 5 min at 4 °C. The isolated nuclei were washed again in lysis buffer, and nuclei were counted in a hemocytometer.

Isolated hepatocyte nuclei were labeled with an Alexa Fluor 647 anti-GFP antibody (338006, clone FM264G, 1:25, BioLegend). Immediately before cell sorting, the nuclei suspension was stained with 2 μg/ml DAPI. GFP– and AF647–double-positive nuclei were sorted using a BD FACSAria II, after gating for DAPI-positive nuclei. Because of the polyploidy state of the hepatocytes, only 4n nuclei were collected.

ATAC-seq

Sorted hepatocyte nuclei were tagmented and PCR amplified according to a previously published ATAC-seq protocol [54,55]. Briefly, 25,000 nuclei were aliquoted, and transposition was performed at 37 °C for 30 min. The transposition reaction was stopped by Buffer ERC (QIAGEN), and DNA was purified using the QIAGEN MinElute Reaction Cleanup Kit. Genomic fragments were preamplified for 5 cycles, and the final amplification cycle was determined by qPCR. The libraries were size selected with Agencourt AMPure XP beads (Beckman Coulter) and sequenced with an Illumina HiSeq 4000. ATAC-seq data analysis. Fastq files from ATAC-seq were analyzed with the pipeline developed by Anshul Kundaje (Stanford University, Stanford, CA, USA) [70]. Briefly, for each sample, adapters were trimmed and aligned to the genome mm9 with Bowtie. The aligned bam files of biological replicates were then merged and subjected to peak calling of open chromatin regions. The parameters for the analysis were -auto_detect_adapter -enable_idr -filt_bam-sample1 -filt_bam-sample2 … -filt_bam-sampleN.

ChIP-qPCR

The *Slc7a11* promoter was analyzed, and potential NRF2- and ATF4-binding motifs were identified with JASPAR [71]. Liver chromatin was prepared as previously described [72]. Briefly, 100 mg liver was fixed and sonicated with a Bioruptor (Diagenode) for 2 rounds of 7.5 min each. Sheared DNA (10 μg) was then incubated with anti-ATF4 antibody (D4B8, 1:200, Cell Signaling

Technology) and NRF2 antibodies (D1Z9C, 1:100, Cell Signaling Technology). Immunoprecipitated DNA was then isolated with phenol:chloroform extraction and subjected to qPCR analysis with the primers Slc7a11-Nrf2/Atf4-ChIP-qPCR-2F and -2R. Fold enrichment was calculated by normalization to the average Ct value of Ins (Ins-ChIP-qPCR-F and -R) and Arbp (Arbp-ChIP-qPCR-F and -R) compared with input DNA. Sequencing data download. TRAP-seq and ATAC-seq data have been deposited according to MINSEQE standards in the NCBI's Gene Expression Omnibus database (GEO GSE109466) [73]. RNA-seq data from PHx are available in the ArrayExpress database (accession no.E-MTAB-1612).

Statistics

Unless otherwise indicated, a 2-tailed, 2-sample Student's t-test was used to analyze the experimental and control groups in all assays performed in this study. A 2-tailed, 1-sample Student's t-test was used to compare the ratio of Fah-Slc7a11 to Fah-Gfp plasmids after liver repopulation with the injected plasmid mix. A hypergeometric test was used to analyze the overlapping genes in the scRNA-seq and TRAP-seq experiments. The Wilcoxon rank-sum test was used to compare the differential binding of NRF2 and ATF4 in the repopulating and quiescent livers. A P value or FDR of less than 0.05 was considered significant. Individual data are presented as dot plots, with the mean shown as a horizontal line. Study approval. All animal studies were reviewed and approved by the IACUC of the Penn Office of Animal Welfare (University of Pennsylvania).

REFERENCES

1. Lee WM. Etiologies of Acute Liver Failure. Semin Liver Dis. 2008;28: 142–152.
2. Taub R. Liver regeneration: from myth to mechanism. Nat Rev Mol Cell Biol. 2004;5: 836.
3. Michalopoulos GK, DeFrances MC. Liver regeneration. Science. 1997;276: 60–66.
4. Malato Y, Naqvi S, Schürmann N, Ng R, Wang B, Zape J, et al. Fate tracing of mature hepatocytes in mouse liver homeostasis and regeneration. J Clin Invest. 2011;121: 4850–4860.
5. Michalopoulos GK. Liver regeneration after partial hepatectomy: critical analysis of mechanistic dilemmas. Am J Pathol. 2010;176: 2–13.
6. Fausto N. Liver regeneration and repair: hepatocytes, progenitor cells, and stem cells. Hepatology. 2004;39: 1477–1487.
7. White P, Brestelli JE, Kaestner KH, Greenbaum LE. Identification of transcriptional networks during liver regeneration. J Biol Chem. 2005;280: 3715–3722.
8. Locker J, Tian J, Carver R, Concas D, Cossu C, Ledda-Columbano GM, et al. A common set of immediate-early response genes in liver regeneration and hyperplasia. Hepatology. 2003;38: 314–325.
9. Arai M, Yokosuka O, Chiba T, Imazeki F, Kato M, Hashida J, et al. Gene expression profiling reveals the mechanism and pathophysiology of mouse liver regeneration. J Biol Chem. 2003;278: 29813–29818.
10. Jung J-W, Park J-S, Hwang J-W, Kang K-S, Lee Y-S, Song B-S, et al. Gene expression analysis of peroxisome proliferators- and phenytoin-induced hepatotoxicity using cDNA microarray. J Vet Med Sci. 2004;66: 1329–1333.
11. Craig A, Sidaway J, Holmes E, Orton T, Jackson D, Rowlinson R, et al. Systems toxicology: integrated genomic, proteomic and metabonomic analysis of methapyrilene induced hepatotoxicity in the rat. J Proteome Res. 2006;5: 1586–1601.
12. Blomme EAG, Yang Y, Waring JF. Use of toxicogenomics to understand mechanisms of drug-induced hepatotoxicity during drug discovery and development. Toxicol Lett. 2009;186: 22–31.
13. Duncan AW, Hanlon Newell AE, Bi W, Finegold MJ, Olson SB, Beaudet AL, et al. Aneuploidy as a mechanism for stress-induced liver adaptation. J Clin Invest. 2012;122: 3307–3315.
14. Grompe M, al-Dhalimy M, Finegold M, Ou CN, Burlingame T, Kennaway NG, et al. Loss of fumarylacetoacetate hydrolase is responsible for the neonatal hepatic dysfunction phenotype of lethal albino mice. Genes Dev. 1993;7: 2298–2307.
15. Wangensteen KJ, Wilber A, Keng VW, He Z, Matise I, Wangensteen L, et al. A facile method for somatic, lifelong manipulation of multiple genes in the mouse liver. Hepatology. 2008;47: 1714–1724.
16. Wangensteen KJ, Zhang S, Greenbaum LE, Kaestner KH. A genetic screen reveals Foxa3 and TNFR1 as key regulators of liver repopulation. Genes Dev. 2015;29: 904–909.
17. Heiman M, Kulicke R, Fenster RJ, Greengard P, Heintz N. Cell type-specific mRNA purification by translating ribosome affinity purification (TRAP). Nat Protoc. 2014;9: 1282–1291.
18. Lu SC. Regulation of glutathione synthesis. Mol Aspects Med. 2009;30: 42–59.
19. Lo M, Wang Y-Z, Gout PW. The x(c)- cystine/glutamate antiporter: a potential target for therapy of cancer and other diseases. J Cell Physiol. 2008;215: 593–602.
20. Montini E, Held PK, Noll M, Morcinek N, Al-Dhalimy M, Finegold M, et al. In vivo correction of murine tyrosinemia type I by DNA-mediated transposition. Mol Ther. 2002;6: 759–769.
21. Liu J, Krautzberger AM, Sui SH, Hofmann OM, Chen Y, Baetscher M, et al. Cell-specific translational profiling in acute kidney injury. J Clin Invest. 2014;124: 1242–1254.
22. Yanger K, Knigin D, Zong Y, Maggs L, Gu G, Akiyama H, et al. Adult hepatocytes are generated by self-duplication rather than stem cell differentiation. Cell Stem Cell. 2014;15: 340–349.

23. Shin S, Wangensteen KJ, Teta-Bissett M, Wang YJ, Mosleh-Shirazi E, Buza EL, et al. Genetic lineage tracing analysis of the cell of origin of hepatotoxin-induced liver tumors in mice. Hepatology. 2016;64: 1163–1177.
24. Huang P, He Z, Ji S, Sun H, Xiang D, Liu C, et al. Induction of functional hepatocyte-like cells from mouse fibroblasts by defined factors. Nature. 2011;475: 386–389.
25. Liu Q, Yuan B, Lo KA, Patterson HC, Sun Y, Lodish HF. Adiponectin regulates expression of hepatic genes critical for glucose and lipid metabolism. Proc Natl Acad Sci U S A. 2012;109: 14568–14573.
26. Severgnini M, Sherman J, Sehgal A, Jayaprakash NK, Aubin J, Wang G, et al. A rapid two-step method for isolation of functional primary mouse hepatocytes: cell characterization and asialoglycoprotein receptor based assay development. Cytotechnology. 2012;64: 187–195.
27. Takahara Y, Takahashi M, Wagatsuma H, Yokoya F, Zhang Q-W, Yamaguchi M, et al. Gene expression profiles of hepatic cell-type specific marker genes in progression of liver fibrosis. World J Gastroenterol. 2006;12: 6473–6499.
28. Ju C, Tacke F. Hepatic macrophages in homeostasis and liver diseases: from pathogenesis to novel therapeutic strategies. Cell Mol Immunol. 2016;13: 316–327.
29. Huang DW, Sherman BT, Lempicki RA. Systematic and integrative analysis of large gene lists using DAVID bioinformatics resources. Nat Protoc. 2009;4: 44–57.
30. Huang DW, Sherman BT, Lempicki RA. Bioinformatics enrichment tools: paths toward the comprehensive functional analysis of large gene lists. Nucleic Acids Res. 2009;37: 1–13.
31. Marí M, Colell A, Morales A, von Montfort C, Garcia-Ruiz C, Fernández-Checa JC. Redox control of liver function in health and disease. Antioxid Redox Signal. 2010;12: 1295–1331.
32. Columbano A, Shinozuka H. Liver regeneration versus direct hyperplasia. FASEB J. 1996;10: 1118–1128.
33. Schmiedeberg P, Biempica L, Czaja MJ. Timing of protooncogene expression varies in toxin-induced liver regeneration. J Cell Physiol. 1993;154: 294–300.
34. Wangensteen KJ, Wang YJ, Dou Z, Wang AW, Mosleh-Shirazi E, Horlbeck MA, et al. Combinatorial genetics in liver repopulation and carcinogenesis with a in vivo CRISPR activation platform. Hepatology. 2018;68: 663–676.
35. Xiang D, Liu C-C, Wang M-J, Li J-X, Chen F, Yao H, et al. Non-viral FoxM1 gene delivery to hepatocytes enhances liver repopulation. Cell Death Dis. 2014;5: e1252.
36. Schug J, McKenna LB, Walton G, Hand N, Mukherjee S, Essuman K, et al. Dynamic recruitment of microRNAs to their mRNA targets in the regenerating liver. BMC Genomics. 2013;14: 264.
37. He G, Dhar D, Nakagawa H, Font-Burgada J, Ogata H, Jiang Y, et al. Identification of liver cancer progenitors whose malignant progression depends on autocrine IL-6 signaling. Cell. 2013;155: 384–396.
38. Guo L, Fang H, Collins J, Fan X-H, Dial S, Wong A, et al. Differential gene expression in mouse primary hepatocytes exposed to the peroxisome proliferator-activated receptor alpha agonists. BMC Bioinformatics. 2006;7 Suppl 2: S18.
39. He F, Yan Q, Fan L, Liu Y, Cui J, Wang J, et al. PBK/TOPK in the differential diagnosis of cholangiocarcinoma from hepatocellular carcinoma and its involvement in prognosis of human cholangiocarcinoma. Hum Pathol. 2010;41: 415–424.
40. Yang Y-F, Pan Y-H, Cao Y, Fu J, Yang X, Zhang M-F, et al. PDZ binding kinase, regulated by FoxM1, enhances malignant phenotype via activation of β-Catenin signaling in hepatocellular carcinoma. Oncotarget. 2017;8: 47195–47205.
41. Halpern KB, Shenhav R, Matcovitch-Natan O, Toth B, Lemze D, Golan M, et al. Single-cell spatial reconstruction reveals global division of labour in the mammalian liver. Nature. 2017;542: 352–356.
42. Huang ZZ, Chen C, Zeng Z, Yang H, Oh J, Chen L, et al. Mechanism and significance of increased glutathione level in human hepatocellular carcinoma and liver regeneration. FASEB J. 2001;15: 19–21.

43. Riehle KJ, Haque J, McMahan RS, Kavanagh TJ, Fausto N, Campbell JS. Sustained Glutathione Deficiency Interferes with the Liver Response to TNF-α and Liver Regeneration after Partial Hepatectomy in Mice. J Liver Disease Transplant. 2013;1. Available: https://www.ncbi.nlm.nih.gov/pubmed/24611135
44. Yang Y, Wang L, Bell P, McMenamin D, He Z, White J, et al. A dual AAV system enables the Cas9-mediated correction of a metabolic liver disease in newborn mice. Nat Biotechnol. 2016;34: 334–338.
45. Ran FA, Cong L, Yan WX, Scott DA, Gootenberg JS, Kriz AJ, et al. In vivo genome editing using Staphylococcus aureus Cas9. Nature. 2015;520: 186–191.
46. Brinkman EK, Chen T, Amendola M, van Steensel B. Easy quantitative assessment of genome editing by sequence trace decomposition. Nucleic Acids Res. 2014;42: e168.
47. Michalopoulos GK. Liver regeneration. J Cell Physiol. 2007;213: 286–300.
48. Sasaki H, Sato H, Kuriyama-Matsumura K, Sato K, Maebara K, Wang H, et al. Electrophile response element-mediated induction of the cystine/glutamate exchange transporter gene expression. J Biol Chem. 2002;277: 44765–44771.
49. Lin X, Yang H, Zhang H, Zhou L, Guo Z. A novel transcription mechanism activated by ethanol: induction of Slc7a11 gene expression via inhibition of the DNA-binding activity of transcriptional repressor octamer-binding transcription factor 1 (OCT-1). J Biol Chem. 2013;288: 14815–14823.
50. Jiang L, Kon N, Li T, Wang S-J, Su T, Hibshoosh H, et al. Ferroptosis as a p53-mediated activity during tumour suppression. Nature. 2015;520: 57–62.
51. Lewerenz J, Maher P. Basal levels of eIF2alpha phosphorylation determine cellular antioxidant status by regulating ATF4 and xCT expression. J Biol Chem. 2009;284: 1106–1115.
52. Deal RB, Henikoff S. A simple method for gene expression and chromatin profiling of individual cell types within a tissue. Dev Cell. 2010;18: 1030–1040.
53. Mo A, Mukamel EA, Davis FP, Luo C, Henry GL, Picard S, et al. Epigenomic Signatures of Neuronal Diversity in the Mammalian Brain. Neuron. 2015;86: 1369–1384.
54. Buenrostro JD, Giresi PG, Zaba LC, Chang HY, Greenleaf WJ. Transposition of native chromatin for fast and sensitive epigenomic profiling of open chromatin, DNA-binding proteins and nucleosome position. Nat Methods. 2013;10: 1213–1218.
55. Ackermann AM, Wang Z, Schug J, Naji A, Kaestner KH. Integration of ATAC-seq and RNA-seq identifies human alpha cell and beta cell signature genes. Mol Metab. 2016;5: 233–244.
56. Huang ZZ, Li H, Cai J, Kuhlenkamp J, Kaplowitz N, Lu SC. Changes in glutathione homeostasis during liver regeneration in the rat. Hepatology. 1998;27: 147–153.
57. Bunchorntavakul C, Reddy KR. Acetaminophen-related hepatotoxicity. Clin Liver Dis. 2013;17: 587–607, viii.
58. Kinoshita H, Okabe H, Beppu T, Chikamoto A, Hayashi H, Imai K, et al. Cystine/glutamic acid transporter is a novel marker for predicting poor survival in patients with hepatocellular carcinoma. Oncol Rep. 2013;29: 685–689.
59. Ishimoto T, Nagano O, Yae T, Tamada M, Motohara T, Oshima H, et al. CD44 variant regulates redox status in cancer cells by stabilizing the xCT subunit of system xc(-) and thereby promotes tumor growth. Cancer Cell. 2011;19: 387–400.
60. Timmerman LA, Holton T, Yuneva M, Louie RJ, Padró M, Daemen A, et al. Glutamine sensitivity analysis identifies the xCT antiporter as a common triple-negative breast tumor therapeutic target. Cancer Cell. 2013;24: 450–465.
61. Wang H, An P, Xie E, Wu Q, Fang X, Gao H, et al. Characterization of ferroptosis in murine models of hemochromatosis. Hepatology. 2017;66: 449–465.
62. Kang ES, Lee J, Homma T, Kurahashi T, Kobayashi S, Nabeshima A, et al. xCT deficiency aggravates acetaminophen-induced hepatotoxicity under inhibition of the transsulfuration pathway. Free Radic Res. 2017;51: 80–90.
63. Bae S, Park J, Kim J-S. Cas-OFFinder: a fast and versatile algorithm that searches for potential off-target sites of Cas9 RNA-guided endonucleases. Bioinformatics. 2014;30: 1473–1475.

64. Hough SH, Ajetunmobi A, Brody L, Humphryes-Kirilov N, Perello E. Desktop Genetics. Per Med. 2016;13: 517–521.
65. University of Pennsylvania Gene Therapy Program. Vector Core [Internet]. [cited 24 Aug 2019]. Available: http://gtp.med.upenn.edu/core-laboratories-public/vector-core
66. Grant GR, Farkas MH, Pizarro AD, Lahens NF, Schug J, Brunk BP, et al. Comparative analysis of RNA-Seq alignment algorithms and the RNA-Seq unified mapper (RUM). Bioinformatics. 2011;27: 2518–2528.
67. University of Pennsylvania Next-Generation Sequencing Core [Internet]. [cited 24 Aug 2019]. Available: https://ngsc.med.upenn.edu
68. Robinson MD, McCarthy DJ, Smyth GK. edgeR: a Bioconductor package for differential expression analysis of digital gene expression data. Bioinformatics. 2010;26: 139–140.
69. Kim YH, Marhon SA, Zhang Y, Steger DJ, Won K-J, Lazar MA. Rev-erbα dynamically modulates chromatin looping to control circadian gene transcription. Science. 2018;359: 1274–1277.
70. Kundaje Lab. atac_dnase_pipelines. In: GitHub [Internet]. [cited 24 Aug 2019]. Available: https://github.com/kundajelab/atac_dnase_pipelines
71. Khan A, Fornes O, Stigliani A, Gheorghe M, Castro-Mondragon JA, van der Lee R, et al. JASPAR 2018: update of the open-access database of transcription factor binding profiles and its web framework. Nucleic Acids Res. 2018;46: D1284.
72. Bochkis IM, Schug J, Ye DZ, Kurinna S, Stratton SA, Barton MC, et al. Genome-wide location analysis reveals distinct transcriptional circuitry by paralogous regulators Foxa1 and Foxa2. PLoS Genet. 2012;8: e1002770.
73. Edgar R, Domrachev M, Lash AE. Gene Expression Omnibus: NCBI gene expression and hybridization array data repository. Nucleic Acids Res. 2002;30: 207–210.

CHAPTER 3

CELL TYPE-SPECIFIC EXPRESSION PROFILING IN THE MOUSE LIVER

Parts of this chapter were adapted with permission from Cell type-specific gene expression profiling in the mouse liver. Wang AW, Zahm AM, Wangensteen KJ. The Journal of Visualized Experiments. 2019;151:e60242.doi:10.3791/60242.

ABSTRACT

Liver repopulation after injury is a crucial feature of mammals which prevents immediate organ failure and death after exposure to environmental toxins. A deeper understanding of the changes in gene expression that occur during the regenerative process could help identify therapeutic targets to promote the restoration of liver function in the setting of injuries. Nonetheless, methods to isolate specifically the repopulating hepatocytes are inhibited by a lack of cell markers, limited cell numbers, and the fragility of these cells. The development of the translating ribosome affinity purification (TRAP) method in conjunction with the *Fah*$^{-/-}$ mouse model to recapitulate repopulation in the setting of liver injury allows gene expression profiling of the repopulating hepatocytes. With TRAP, cell type-specific translating mRNA is rapidly and efficiently isolated. We developed a method that utilizes TRAP with affinity-based isolation of translating mRNA from hepatocytes that selectively express the green fluorescent protein (GFP)-tagged ribosomal protein (RP) L10A, GFP:RPL10A. TRAP circumvents the long time period required for fluorescence-activated cell sorting (FACS) that could change the gene expression profile. Furthermore, since only the repopulating hepatocytes express the GFP:RPL10A fusion protein, the isolated mRNA is devoid of contamination from the surrounding injured hepatocytes and other cell types in the liver. The affinity-purified mRNA is of high quality and enables downstream PCR- or high-throughput sequencing-based analysis of gene expression.

INTRODUCTION

As the main metabolic organ in vertebrates, the liver is responsible for glucose homeostasis, serum protein synthesis, bile acid secretion, and xenobiotic metabolism and detoxification. The liver possesses an extraordinary capacity to regenerate the injured parenchyma upon exposure to toxins to prevent immediate liver dysfunction [1]. However, failure of regeneration can occur in the setting of acetaminophen or alcohol overconsumption, which can lead to acute liver failure [2]. Furthermore, chronic liver injury caused by viral hepatitis infection, fatty liver disease, and steatohepatitis frequently result in liver fibrosis, cirrhosis, and hepatocellular carcinoma [3]. The only available curative treatment for end-stage liver disease is transplantation but is currently limited by organ shortage, preventing efficient treatment for all patients [4]. A better understanding of the recovery process after toxic liver injury is therefore crucial for the development of treatments to stimulate regeneration sufficient to rescue function in the diseased organ.

The most broadly-applied model system for the study of liver regeneration is partial hepatectomy in rodents, in which a large proportion of the liver is resected to stimulate rapid hepatocyte expansion [5]. However, partial hepatectomy does not recapitulate hepatocyte expansion following toxic liver injury due to the lack of immune cell infiltration and hepatocyte cell necrosis often observed in the setting of acute liver injury in humans [6]. A more suitable system to model this form of organ renewal is the *Fah*$^{-/-}$ mouse, which lacks functional fumarylacetoacetate hydrolase (FAH) required for proper tyrosine catabolism, and develops severe liver damage leading to death [7]. These mice can be maintained in a healthy state indefinitely by treatment with the drug nitisinone in the drinking water. Alternatively, FAH expression can be restored by transgene delivery to a subset of hepatocytes, which will expand to repopulate the liver upon nitisinone removal [8].

To profile the gene expression changes of repopulating hepatocytes, a tool to specifically isolate these cells in the *Fah*$^{-/-}$ mouse without contamination from the neighboring injured hepatocytes and other cell types is required. Unfortunately, fluorescence-assisted cell sorting (FACS) of hepatocytes is difficult since (1) the fragility of repopulating cells leads to poor recovery

after liver perfusion, (2) replicating hepatocytes are highly variable in size, making isolation of a pure population by FACS difficult, and (3) the procedure time from liver perfusion to RNA isolation is greater than 2 h, hence gene expression profiles may undergo substantial artificial changes prior to sample acquisition [9].

Alternatively, the expression of epitope-tagged ribosomes specifically in repopulating hepatocytes enables the rapid isolation of actively translating mRNA bound by ribosomes using affinity purification immediately after organ harvest with bulk liver tissue lysates. Here, we describe a protocol to perform translating-ribosome affinity purification (TRAP) [10] followed by high-throughput RNA-sequencing (TRAP-seq) to specifically isolate and profile mRNA in repopulating hepatocytes in the *Fah*$^{-/-}$ mouse [9]. Coexpression of green fluorescent protein (GFP)-tagged ribosomal protein (RP) L10A (GFP:RPL10A) with FAH allows affinity purification of translating mRNA bound by polysomes containing GFP:RPL10A. This method avoids any cell dissociation steps, such as liver perfusion to isolate fragile repopulating hepatocytes. Instead, TRAP utilizes whole organ tissue lysis and antibodies to rapidly extract the RNA specifically from target cells. Finally, isolation of abundant, high-quality mRNA via TRAP-seq enables downstream applications such as sequencing analysis to profile the dynamic change of gene expression during the repopulation process.

PROTOCOL

All methods that involve the use of mice are consistent with the guidelines provided by the Institutional Animal Care and Use Committee (IACUC) of the Penn Office of Animal Welfare at the University of Pennsylvania.

1. Reagent preparation

1.1. Cycloheximide. To make 500 µl of 0.1 g/ml cycloheximide, suspend 50 mg of cycloheximide in 500 µl of methanol. Cycloheximide can be stored at 4 °C for up to 1 day.

NOTE: Cycloheximide inhibits translation.

CAUTION: cycloheximide is extremely toxic to the environment and can cause congenital malformation. All wastes and buffers containing cycloheximide should be collected for proper disposal.

1.2. DTT. To make 1 ml of 1M DTT, suspend 0.15 g of DTT powder in RNase-free water. DTT can be stored at -20 °C. It is recommended to store 1M DTT in single-use aliquots of 50 µl.

NOTE: DTT is a detergent.

CAUTION: DTT can cause irritation to the skin, eye, and respiratory tract.

1.3. Deoxycholate (DOC). To make 10% DOC, suspend 1 g of DOC in a 50 ml conical tube and add RNase-free water up to 10 ml. Shake vigorously until the powder is dissolved. The 10% DOC solution is slightly yellow and can be stored at RT for up to 1 year.

NOTE: DOC is used for nuclear lysis.

1.4. GFP antibodies. Aliquot GFP antibodies when using for the first time. Snap freeze the aliquots and store at -80 °C. It is recommended to store 50 µg of GFP antibodies in single-use aliquots.

1.5. Biotinylated protein L. Resuspend biotinylated protein L in 1X PBS to make the final concentration 1 µg/µl. The resuspended solution can be stored at -20 °C for up to 6 months.

2. Buffer preparation

2.1. BSA buffer. To make 50 ml of 3% BSA buffer, add 1.5 g of IgG- and protease-free BSA powder into 40 ml of PBS followed by a quick vortex. After the BSA is dissolved, add PBS to a final volume of 50 ml. The BSA buffer can be stored at 4 °C for up to 6 months.

2.2. Dissection buffer. To make 50 ml of dissection buffer stock, combine 5 ml of 10X HBSS, 125 µl of 1M HEPES, 1750 µl of 1M glucose, and 200 µl of 1M $NaHCO_3$. Add RNase-free water to a final volume of 50 ml. The dissection buffer stock can be stored at 4 °C for up to 6 months. Immediately prior to use, add 100 µg/ml of 0.1 g/ml cycloheximide and keep on ice.

2.3. High-salt buffer. To make 50 ml of high-salt buffer stock, add 1 ml of 1M HEPES, 8.75 ml 2M KCl, 500 µl 1M $MgCl_2$, and 500 µl 100% branched octylphenoxy poly(ethyleneoxy)ethanol (IGEPAL) to RNase-free water. The high-salt buffer stock can be stored at 4 °C for up to 6 months. Immediately prior to use, add 0.5 µl/ml of 1M DTT and 1 µl/ml of 0.1 g/ml cycloheximide. Keep the fresh high-salt buffer on ice.

2.4. Low-salt buffer. To make 50 ml of low-salt buffer stock, add 1 ml of 1M 4-(2-hydroxyethyl)-1-piperazineethanesulfonic acid (HEPES), 3.75 ml of 2M KCl, 500 µl of 1M $MgCl_2$, and 500 µl of 100% IGEPAL to 44.25 ml RNase-free water. The low-salt buffer stock can be stored at 4 °C up to 6 months. Add 0.5 µl/ml of 1M DTT and 1 µl/ml of 0.1 g/ml cycloheximide prior to use. Keep the fresh low-salt buffer on ice.

2.5. Tissue lysis buffer. To make 50 ml of tissue lysis buffer stock, combine 1 ml of 1M HEPES, 3.75 ml of 2M KCl, and 500 µl of 1M MgCl2. Add RNase-free water to a final of 50 ml. The dissection buffer stock can be stored at 4 °C up to 6 months. Add 1 tab/ml of EDTA-free protease inhibitor, 1 µl/ml of 0.1 g/ml cycloheximide, 10 µl/ml of RNase inhibitors each immediately prior to use. Keep the fresh tissue lysis buffer on ice.

3. Conjugation of antibodies to magnetic beads

3.1. Antibodies

3.1.1. Calculate the amount of GFP antibodies required for all samples and prepare for one extra sample. For each sample, 50 µg of each GFP antibody is required.

3.1.2. Thaw GFP antibodies on ice and spin at maximum speed (> 13,000 x g) for 10 min at 4 °C and transfer supernatants to a new Eppendorf.

NOTE: The antibody preparation step can be performed prior to bead preparation and the thawed antibodies can be kept on ice. Alternatively, this step can be performed during incubation of magnetic beads with biotinylated protein L.

3.2. Resuspend magnetic beads

3.2.1. Resuspend magnetic beads by gentle pipetting. For each sample, 150 µl of magnetic bead is used. Calculate the volume of magnetic bead required for all samples and prepare one extra.

3.2.2. Transfer the resuspended magnetic beads to a 1.5 or 2 ml Eppendorf. If more than 1 ml is required for an experiment, split the total amount into equal volumes.

3.2.3. Collect beads on a magnetic stand for > 1 min and remove the supernatant. Remove Eppendorf from the magnetic stand and add 1 ml PBS followed by pipetting up and down to wash the beads. Collect beads on a magnetic stand for > 1 min and remove PBS.

3.3. Preparation of protein L-coated beads

3.3.1. Take the amount of biotinylated protein L required for all samples and prepare one extra. For each sample, 60 µl of biotinylated protein L is used. If protein L is previously resuspended and stored at -20 °C, thaw on ice.

3.3.2. Add the calculated volume of biotinylated protein L to the resuspended and washed magnetic beads. Add 1X PBS to make the final volume 1 ml if using a 1.5 ml Eppendorf, or 1.5 ml if using a 2 ml Eppendorf. Incubate magnetic beads with biotinylated protein L for 35 min at RT on a tube rotator.

NOTE: Antibodies can be prepared at this step during bead incubation with protein L.

3.3.3. Collect protein L-coated beads on a magnetic stand for > 1 min and remove the supernatant. Remove the Eppendorf tube from the magnetic stand and add 1 ml of 3% BSA buffer followed by gentle pipetting for 5 times to wash the protein L-coated beads.

3.3.4. Collect coated beads on a magnetic stand for > 1 min and remove the supernatant. Repeat the washing steps with 3% BSA for another 4 times (a total of 5 times).

3.4. Antibody binding

3.4.1. Add the calculated amount of GFP antibodies into the protein L-coated beads and incubate for 1 h at 4 °C on a tube rotator.

NOTE: After antibody incubation, take special care to not vortex or vigorously shake the affinity matrix as it could disrupt the binding of biotinylated protein L to the magnetic beads.

3.4.2. During incubation, prepare low-salt buffer by calculating the total volume required for all samples and add 0.5 µl/ml of 1M DTT and 1 µl/ml of 0.1 g/ml cycloheximide to low-salt buffer stock prior to use. 3 ml of low-salt buffer for washing each tube of GFP-conjugated beads and 200 µl/sample for resuspension of the GFP-conjugated beads are required. Fresh low-salt buffer can be kept on ice for a couple of hours.

3.4.3. Collect the affinity matrix on a magnetic stand for > 1 min and remove the supernatant. Add 1 ml of low-salt buffer and gently pipette up and down to wash the affinity matrix.

3.4.4. Collect the affinity matrix on a magnetic stand for > 1 min and remove low-salt buffer. Repeat the washing steps with low-salt buffer for another 2 times (a total of 3 times).

3.4.5. Resuspend the beads in low-salt buffer so that each sample has 200 µl of affinity matrix.

3.4.6. The affinity matrix can be stored in 0.02% NaN_3 at 4 °C for up to 2 weeks. The affinity matrix should be quickly washed in low-salt buffer 3 times and resuspended gently on a tube rotator at 4 °C for at least 10 min if the affinity matrix is prepared within 1 week or overnight if the affinity matrix is stored for over 1 week.

CAUTION: Sodium azide is extremely toxic to the environment. Contact with acids produces toxic gas. All wastes should be collected for proper disposal.

NOTE: The protocol can be paused after this step.

4. Liver tissue lysis

4.1. Buffer preparation and equipment setup

4.1.1. Calculate the number of Eppendorf tubes required, label and chill on ice. Usually, 7 1.5 ml Eppendorf tubes are required for each sample. 1 for the remaining dissected liver, 4 for 4 ml of homogenized liver lysate, and 2 for transferring supernatants.

4.1.2. Prepare fresh dissection buffer by calculating the total volume required for all samples and add 1 µl/ml of 0.1 g/ml cycloheximide. Place the fresh dissection buffer on ice to keep cold throughout the experiment. For each sample, 10 ml of dissection buffer is required.

4.1.3. Prepare fresh lysis buffer by calculating the total volume required for all samples and add 1 tab/10 ml of EDTA-free protease inhibitor, 1 µl/ml of 0.1 g/ml cycloheximide, and 10 µl/ml of RNase inhibitors each. Keep the lysis buffer on ice throughout the experiment. For each sample, 4 ml of lysis buffer is required.

4.1.4. Setup the homogenizer apparatus so that the Teflon-glass tubes can be placed on ice during homogenization of liver pieces. Put 4 ml of cold lysis buffer in the Teflon-glass tubes.

4.2. Repopulating liver homogenization

4.2.1. Euthanize 8-12-week-old *Fah*$^{-/-}$ mice injected with the TRAP vector and repopulated for one to four weeks with anesthesia and cervical dislocation according to approved animal experimental guidelines.

4.2.2. Place mice on a dissection board and spray the abdomen with 70% ethanol. Tent the skin and peritoneum using forceps and use scissors to make a transverse incision low in the abdomen and continue to cut with the scissors to make a wide U-shaped peritoneal flap, with care to not cut the viscera. Flip the peritoneal flap over the sternum to expose the liver.

4.2.3. Carefully remove the liver with scissors and forceps and quickly place the tissue in cold dissection buffer to rinse. To homogenize frozen tissues, quickly move the desired amount of liver tissue into Teflon-glass tubes with cold lysis buffer without the tissue thawing.

NOTE: The dissected tissue can be flash-frozen and stored at -80 °C after it is washed with dissection buffer. The protocol can be paused after this step.

4.2.4. Weigh the liver on a Petri dish, Isolate 200-500 mg of liver, and transfer to the Teflon-glass tubes. Place the remaining tissue into a pre-chilled microcentrifuge tube and flash freeze.

NOTE: The amount of tissue used is based on the abundance of the cell type of interest.

4.2.5. Homogenize the tissue in a motor-driven homogenizer starting at 300 rpm to dissociate hepatocytes from the liver structure for at least 5 strokes. Lower the glass tube each time but take care to not let the pestle rise above the solution to prevent aeration that could cause protein denaturation.

4.2.6. Raise the speed to 900 rpm to fully homogenize the liver tissues for at least 12 full strokes.

4.2.7. Transfer the lysate into labeled and pre-chilled Eppendorf tubes, with no more than 1 ml of lysate per 1.5 ml tube. If 4 ml of lysis buffer is used, keep 1 tube and flash freeze the remaining 3 tubes.

NOTE: The lysates can be kept on ice for up to 1 h while dissecting the next animal and preparing fresh lysates. The homogenized liver can be flash-frozen after the lysis step and stored at -80 °C. There could be a 50% decrease in isolated RNA if frozen lysates are used. The protocol can be paused after this step.

4.3. Nuclear lysis

4.3.1. Centrifuge the liver lysate at 2,000 x g at 4 °C for 10 min and transfer the supernatant to a new, prechilled Eppendorf on ice.

4.3.2. Add 1/9 of the supernatant volume of 10% IGEPAL to make a final concentration of 1% and mix by gently inverting the Eppendorf tubes.

4.3.3. Quickly spin down the Eppendorf tubes and add 1/9 of the sample volume of 10% DOC to make a final concentration of 1% and mix by gently inverting the Eppendorf tubes. Quickly spin down the Eppendorf tubes and incubate on ice for 5 min.

4.3.4. Centrifuge the nuclear lysate at 20,000 x g at 4 °C for 10 min and transfer the supernatant to a new, prechilled Eppendorf on ice.

NOTE: The mitochondria-depleted supernatant can be placed on ice for a couple of hours while the remaining samples are being collected.

5. Immunoprecipitation

5.1. For each sample, take out 1% of the total volume of the mitochondria-depleted supernantant as a pre-immunoprecipitation control to compare target enrichment after incubation with the affinity matrix. Place the pre-immunoprecipitation controls on a tube rotator at 4 °C overnight, the same way as the immunoprecipitated samples are processed.

5.2. Add 200 µl of affinity matrix to each sample. Take extra care to resuspend the beads by gentle pipetting prior to adding the affinity matrix to each sample. Incubate the lysates with affinity matrix at 4 °C overnight with gentle mixing on a tube rotator.

NOTE: The protocol can be paused for up to a day after this step.

6. RNA isolation

6.1. Removal of unbound background noise

6.1.1. Place the magnetic rack at 4 °C for at least 30 min to pre-chill and keep the rack on ice throughout the experiment.

6.1.2. Calculate the number of Eppendorf tubes required and pre-chill on ice or at 4 °C. Usually, each sample requires 1 Eppendorf tube for the final purified RNA.

6.1.3. Quickly spin down the supernant incubated with the affinity matrix and collect the beads by placing on the magnetic rack for at least 1 min. Collect or discard the supernatant that contains the unbound fraction in additional Eppendorf tubes.

NOTE: The collected supernatant can be flash-frozen and stored at -80 °C to compare with the bound fraction for transcript enrichment after purification.

6.1.4. Prepare high-salt buffer by adding 0.5 µl/ml of 1M DTT and 1 µl/ml of 0.1 g/ml cycloheximide to high-salt buffer stock. 5 ml of high-salt buffer is required for each sample.

6.1.5. Add 1 ml of fresh high-salt buffer to each tube followed by gentle pipetting for at least 5 times without introducing bubbles.

NOTE: Insufficient washing could introduce backgrounds of unbound transcripts while the introduction of bubbles could accelerate RNA degradation.

6.1.6. Collect beads on a magnetic stand for > 1 min and remove the supernatant. Repeat the washing steps with high-salt buffer for another 4 times (a total of 5 times).

6.1.7. Remove remaining high-salt buffer and remove Eppendorf tubes from the magnetic stand and place at RT for 5 min to warm up.

6.2. RNA isolation with column-based kits

6.2.1. Resuspend the beads in 100 µl of lysis buffer with β-mercaptoethanol, both provided in the RNA isolation kit.

NOTE: Any RNA isolation and purification kit that contains the denaturant guanidine thiocyanate in the lysis buffer can be used to release bound RNA from the affinity matrix. RNA extraction should be processed at room temperature since guanidine thiocyanate can crystallize at low temperatures.

6.2.2. Vortex the beads and buffer for at least 5 sec at the highest speed, quickly spin down to collect the buffer on the side of the Eppendorf and incubate the beads at RT for 10 min to release the bead-bound RNA into the lysis buffer.

6.2.3. Collect beads on a magnetic stand for > 1 min and collect the supernatant to proceed immediately to RNA cleanup according to the RNA purification protocol as specified in the kit.

NOTE: The supernatant containing the eluted RNA in lysis buffer can also be stored at -80 °C for up to 1 month prior to cleanup. To proceed after storage, warm up the tubes to RT upon thawing.

6.2.4. To achieve maximum quality of the isolated RNA, perform all optional steps including DNase digestion and all RNA elution steps. Heat up the elution buffer provided by the RNA isolation kit or RNase-free water to 60 °C for maximum RNA recovery.

NOTE: The isolated RNA can be stored at -20 °C for up to 1 month or -80 °C for several years. The protocol can be paused after this step.

7. Optional RNA quality analysis (recommended)

7.1. Assess RNA quality using a Bioanalyzer and quantity with a Nanodrop to determine if repeating the immunoprecipitation process is required to obtain ample and high-quality RNA.

NOTE: The optimal RNA quality for high-throughput sequencing should follow protocols specified by individual library preparation kits and sequencing platforms.

8. Downstream applications

NOTE: Total RNA isolated by the TRAP protocol can be used in a number of standard downstream applications, including RNA-seq (TRAP-seq) and reverse transcription and quantitative PCR (RT-qPCR).

8.1. RNA-seq. Prepare cDNA sequencing libraries using commercial RNA-seq kits with oligo d(T)-based enrichment of polyadenylated (poly(A)) transcripts. Alternatively, if the total RNA quality is lower than recommended for poly(A) enrichment, use rRNA depletion modules. However, expect to see more rRNA alignment after sequencing.

8.2. RT-qPCR. Standard reverse transcription and quantitative PCR protocols can be used following TRAP.

REPRESENTATIVE RESULTS

To profile gene expression in repopulating hepatocytes of the *Fah*$^{-/-}$ mouse, *Gfp:Rpl10a* fusion and *Fah* transgenes are co-delivered within a transposon-containing plasmid [8] (TRAP vector) to livers by hydrodynamic injection (Figure 3.1A). The removal of nitisinone induces a toxic liver injury that creates a selection pressure for hepatocytes stably expressing FAH to repopulate the injured parenchyma [9]. Immunofluorescence staining confirms the co-expression of FAH and the GFP:RPL10A fusion protein in repopulating hepatocytes after two weeks of liver repopulation (Figure 3.1B).

In the following representative experiment, TRAP-seq was performed using quiescent and repopulating mouse hepatocytes. First, to obtain GFP-tagged ribosomes from quiescent hepatocytes, transgenic *Rosa*$^{LSL\text{-}GFP\text{-}L10A}$ mice were injected with AAV8-TBG-Cre 7 days prior to sacrifice to induce GFP:RPL10A expression in all hepatocytes [11]. We also processed a liver sample collected from a wild type mouse as a negative control to ensure isolation of translating mRNA was specific, meaning RNA could only be extracted from mice expressing GFP:RPL10A. The concentration of isolated RNA correlated with the number of cells expressing the fusion protein; the quiescent sample displays the highest yield since all hepatocytes express GFP:RPL10A after AAV8-TBG-Cre injection (Figure 3.2A). Conversely, barely any RNA was detectable in wild type controls that did not possess the GFP:RPL10A transgene, indicating the TRAP procedure is highly specific and has a low background. When TRAP was used on liver tissues undergoing repopulation with GFP:RPL10A-transduced hepatocytes, abundant, high-quality RNA was obtained while no RNA trace was detected via Bioanalyzer for the negative control sample (Figure 3.2B).

Downstream gene expression analysis can be carried out via RT-qPCR or RNA-seq on TRAP-isolated RNA. *Gsta1* encodes glutathione S-transferase that plays an important role in the metabolism of glutathione, the main detoxifying peptide to protect cellular oxidative stress damage [12]. *Gsta1* expression is induced by over 10-fold in repopulating hepatocytes as compared to quiescent hepatocytes, while no CT cycle was detected with TRAP-isolated RNA from the wild type mouse due to the lack of input RNA (Figure 3.3A). Note that RNA quality can greatly impact gene

expression analysis. In the case of RNA-seq experiments, assessment of RNA quality should be performed according to the recommendations of the library preparation kit and the sequencing platform (Figure 3.3B). A Bioanalyzer is often used to determine the RNA integrity number (RIN), with a high RIN correlating with a higher rate of mRNA alignments to the genome (Figure 3.3B, left), whereas a lower RIN leading to a higher rate of ribosomal reads, indicating mRNA degradation (Figure 3.3B, right). Figures 3.3C and D demonstrate that TRAP-seq can identify differential gene expression in quiescent and repopulating hepatocytes. For instance, *Alb* expression is inhibited and *Afp* expression is activated during liver repopulation, reflecting that the regenerating hepatocytes assume a less differentiated state to inhibit liver metabolic functions during repopulation [9,13].

TABLES

Table 3.1. Materials for the TRAP-seq protocol.

Name of Material/ Equipment	Company	Catalog Number
10 ml Tissue Grinder, Potter-Elv, Coated	DWK Life Sciences (Wheaton)	358007
Absolutely RNA Miniprep Kit	Agilent	400800
Anti-GFP antibodies	Memorial Sloan-Kettering Antibody & Bioresource Core	GFP Ab #19C8 and GFP Ab #19F7
Bovine Serum Albumin, IgG-Free, Protease-Free	Jackson ImmunoResearch	001-000-162
cOmplete, Mini, EDTA-free Protease Inhibitor Cocktail	Roche	11836170001
Cycloheximide	Millipore Sigma	C7698
D-Glucose, Dextrose	Fisher Scientific	D16
Deoxycholic acid, DOC	Millipore Sigma	D2510
DL-Dithiothreitol	Millipore Sigma	D9779
Dynabeads MyOne Streptavidin T1	Thermo Fisher Scientific	65602
Fisherbrand Petri Dishes with Clear Lid	Fisher Scientific	FB0875712
HBSS (10X), calcium, magnesium, no phenol red	Thermo Fisher Scientific	14065-056
HEPES, 1M Solution, pH 7.3, Molecular Biology Grade, Ultrapure, Thermo Scientific	Thermo Fisher Scientific	AAJ16924AE
IGEPAL CA-630 (Octylphenoxy poly(ethyleneoxy)ethanol, branched)	Millipore Sigma	I8896
Magnesium chloride, MgCl2	Millipore Sigma	M8266
Methanol	Fisher Scientific	A452
NanoDrop 2000/2000c Spectrophotometer	Thermo Fisher Scientific	VV-83061-00
NEBNext Poly(A) mRNA Magnetic Isolation Module	New England BioLabs	E7490S
NEBNext Ultra RNA Library Prep Kit for Illumina	New England BioLabs	E7530S
Nuclease-Free Water, not DEPC-Treated	Ambion	AM9932
Overhead Stirrer	DWK Life Sciences (Wheaton)	903475
PBS Buffer (10X), pH 7.4	Ambion	AM9625
Pierce Recombinant Protein L, Biotinylated	Thermo Fisher Scientific	29997
Potassium chloride, KCl	Millipore Sigma	P4504
RNaseZap RNase Decontamination Solution	Invitrogen	AM9780
RNasin Ribonuclease Inhibitors	Promega	N2515
RNA 6000 Pico Kit & Reagents	Agilent	5067-1513
Sodium azide, NaN3	Millipore Sigma	S2002
Sodium bicarbonate, NaHCO3	Millipore Sigma	S6297
SUPERase·In RNase Inhibitor	Invitrogen	AM2694

FIGURES

Figure 3.1. Implementation of translating ribosome affinity purification (TRAP) with *Fah*$^{-/-}$ to profile gene expression change of repopulating hepatocytes.

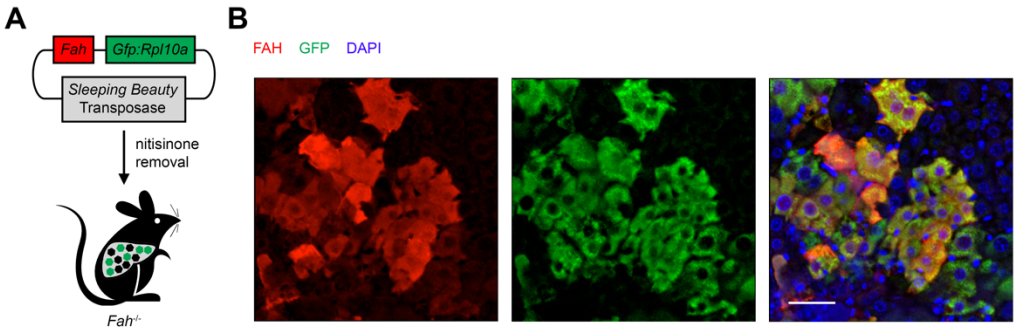

(**A**) Schematic of expressing the green fluorescent protein (GFP)-tagged ribosome protein (RP) subunit L10A (GFP:RPL10A) with FAH in the *Sleeping Beauty* transposon system followed by injection into the *Fah*$^{-/-}$ mouse. Green hexagons indicate repopulating hepatocytes with stable expression of FAH and GFP:RPL10A, whereas black hexagons represent injured, dying hepatocytes. (**B**) Representative immunofluorescence staining demonstrates coexpression of FAH (red) and GFP-tagged ribosomal protein L10A (green) in the repopulating hepatocytes. Scale bar, 50 μm.

Figure 3.2. TRAP enables cell type-specific isolation of high-quality RNA.

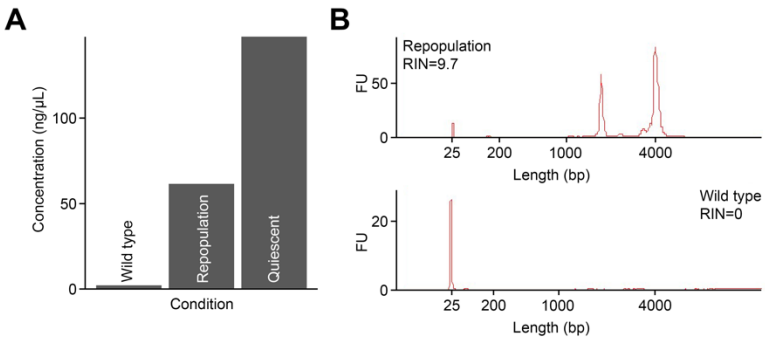

(**A**) The yield of RNA is positively correlated with the number of hepatocytes expressing GFP:RPL10A. The low yield of RNA from a wild type mouse demonstrates the specificity of TRAP from sources without the expression of GFP:RPL10A. (**B**) Bioanalyzer traces of total RNA isolated from repopulating livers expressing GFP:RPL10A and from wild type livers demonstrate the specificity of TRAP. Total RNA isolated from wild type liver tissue devoid of the GFP:RPL10A transgene shows that minimal RNA has been collected, whereas transgene-expressing tissues provide ample high-quality RNA. Note that ribosomal RNA peaks are present following successful TRAP [10]. FU, Fluorescence unit. RIN, RNA integrity number.

Figure 3.3. TRAP-isolated RNA can be used for downstream gene expression analysis.

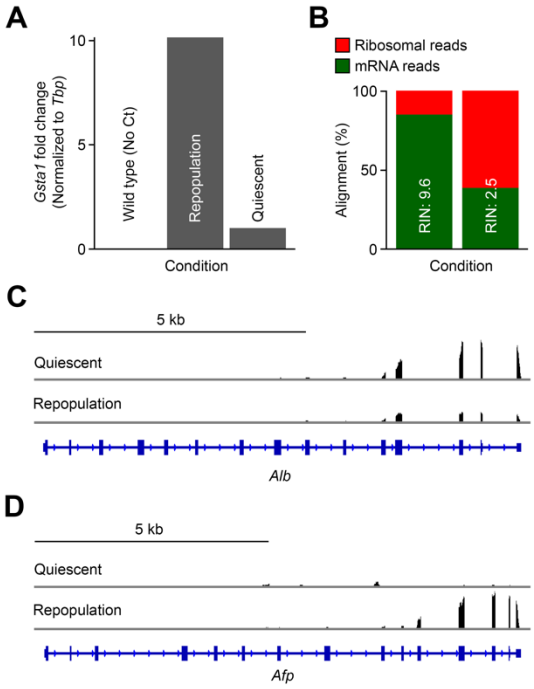

(**A**) Representative reverse transcription and quantitative PCR (RT-qPCR) results of *Gsta1* in quiescent and repopulating hepatocytes. No Ct value was detected with RNA isolated from wild type animals. (**B**) Alignment analysis of isolated RNA after high-throughput sequencing, demonstrating the importance of determining RNA integrity after isolation. High-quality RNA results in a higher percentage of mRNA reads (green), while low-quality RNA leads to a much higher percentage of ribosome reads (red), as most mRNA is degraded. RIN, RNA integrity number. (**C**) and (**D**) IGV tracks of RNA-sequencing reads of mRNA affinity-purified from quiescent and repopulating hepatocytes at the (**C**) *Alb* and (**D**) *Afp* loci. Note the 3' read bias is typical of a polyadenylated (poly(A)) selection pipeline.

DISCUSSION

TRAP-seq is a technique for cell type-specific isolation of translating mRNA via epitope-tagged ribosomes and presents an alternative to FACS approaches, as it circumvents limitations such as time requirements of FACS [9]. Instead, TRAP allows rapid and efficient isolation of RNA directly from bulk tissues, helping to avoid any alterations in gene expression. TRAP-seq is especially well-suited for use in the repopulating *Fah*$^{-/-}$ mouse liver, as hepatocyte expansion following removal of nitisinone is cell-autonomous and enables gene expression profiling of the subset of hepatocytes with integrated transgenes. The TRAP vector can also be coexpressed with gene-activating or -silencing molecules [14], including cDNA, short-hairpin RNA, and guide RNA, to study the effects on global gene expression of activation or inhibition of a specific gene. Alternatively, the *Rosa*$^{LSL\text{-}GFP\text{-}L10A}$ transgenic mouse provides the ability to profile gene expression in any cell with Cre recombinase activity. Since GFP:RPL10A can be specifically expressed in any cells that express Cre, the role of other cell types in the liver during liver injury and repopulation could be studied. For instance, crossing the CK19-Cre mouse with the TRAP transgenic mouse could be used to express GFP:RPL10A in cholangiocytes followed by TRAP-seq to study the change of gene expression in the biliary epithelium during the repopulation process.

To ensure accurate profiling of gene expression, it is critical to prepare all buffers and the affinity matrix prior to tissue dissection. All steps should be performed on ice with cold buffers unless otherwise specified to ensure polysome stabilization [10] and prevent RNA degradation. All buffers should be prepared with RNase-free reagents and the TRAP-seq protocol should be carried out in an RNase-free environment to prevent RNA degradation and low yield of immunoprecipitated RNA. The affinity matrix can be prepared up to 2 weeks prior to use with gentle resuspension on a tube rotator overnight. Special care should be taken to not vigorously shake the matrix to prevent disruption of the antibody-conjugated, protein L-coated magnetic beads. The methods to prepare the affinity matrix includes conjugation of magnetic beads to biotinylated protein L followed by incubation with anti-GFP antibodies. However, commercially available protein A/G magnetic beads can be substituted; if used, skip the initial conjugation step and proceed directly to antibody binding.

Furthermore, alternative epitope tags are presumably feasible with the above protocol with appropriate modification.

There are various points in which the RNA isolation and purification step can be paused (see protocol above). However, once liver samples have been harvested, continuing to the immunoprecipitation is recommended, as the yield of isolated RNA could drop by ~50% with freezing at this step [10]. Tissues should be quickly rinsed with dissection buffer that contains cycloheximide to inhibit mRNA translation. Insufficient tissue lysis could also contribute to low RNA yield. It is critical to homogenize tissues on ice until no tissue chunks are visible with the motor homogenizer while ensuring minimal aeration [10]. Additionally, sufficient washing with high-salt buffer is crucial to ensure removal of nonspecific binding of ribosomal proteins to the affinity matrix. Including a wild type mouse as a negative control helps to assess the specificity of the immunoprecipitation and the efficiency of the wash steps. Additionally, using a commercial RNA purification kit that includes RNase-free DNase treatment will increase RNA purity.

Moreover, it is recommended to verify the expression and abundance of the GFP:RPL10A fusion protein and assess the amount of tissue required to obtain ample RNA for downstream analysis. Tissue sections or lysates could be used for immuno-based detection methods to validate the expression of GFP:RPL10A. The amount of RNA isolated can vary by: (1) the number of cells expressing GFP:RPL10A, (2) the expression level of the transgene, and (3) the size and ploidy of the cells expressing the transgene. A pilot experiment using half and double the amount of the recommended amount of tissue could be useful in determining the optimal input lysate for TRAP-seq. In our hands, we could obtain ~150 ng of RNA with as little as 1-2% of hepatocytes expressing GFP:RPL10A from 200 mg of the repopulating *Fah*$^{-/-}$ liver, representing ~2x10^{5} polyploid hepatocytes with transgene expression [9].

The TRAP-seq methodology isolates ribosome-bound mRNA to profile a cell's translating mRNA pool. The resulting sequencing reads, therefore, correspond to the 'translatome' rather than the transcriptome. Note that translating ribosome footprints will not be collected, as TRAP is performed on native rather than cross-linked complexes. If footprinting analyses are desired, the

above protocol should be modified with relevant cross-linking followed by immunoprecipitation (CLIP) methodologies [15]. Another limitation of TRAP is the requirement of a sufficient amount of cells expressing the GFP:RPL10A fusion protein. For experiments in which the cell type of interest is small, combining multiple biological samples may be required to isolate sufficient RNA to enable RNA-seq [16]. Furthermore, TRAP-seq requires the presence of GFP:RPL10A in the cell type of interest. This could pose a challenge if there is no specific delivery system to the cells or if a cell-type specific promoter to drive Cre expression is not available.

The recent development of single-cell RNA-seq (scRNA-seq) technology has allowed direct sequencing followed by *in silico* identification of various cell types, enabling sequencing without sorting for specific cell types of interests [17–19]. However, scRNA-seq still requires dissociation of cells from the organ. In the case of the *Fah*$^{-/-}$ repopulation model, liver perfusion and hepatocyte isolation are extremely difficult and inefficient due to the fragility of both the injured and replicating hepatocytes. In fact, we have not yet been able to isolate sufficient hepatocytes from *Fah*$^{-/-}$ mice undergoing repopulation after hydrodynamic injection of FAH plasmids. Additionally, in the time it takes to process tissues, gene expression levels could change. Protocols for liver perfusion take up to 30 minutes of warm ischemia time. Future methodologies to optimize liver perfusion to decrease the processing time and increase isolation efficiency could allow scRNA-seq integration to the *Fah*$^{-/-}$ mouse model system and possibly to other injury and repopulation models. This would also support the study of all liver cell types.

In conclusion, the integration of TRAP-seq with the *Fah*$^{-/-}$ mouse enables specific isolation and gene expression profiling of regenerating hepatocytes to identify therapeutic targets that could promote liver repopulation. This method can be implemented to study other cell types in the liver and other organ systems for disease-specific identification of gene expression changes to identify potential drug targets or biomarkers. An analogous technique can be used to collect nuclei from repopulating hepatocytes using affinity purification, followed by epigenetic analysis of these specific cells [13].

REFERENCES

1. Taub R. Liver regeneration: from myth to mechanism. Nat Rev Mol Cell Biol. 2004;5: 836–847.
2. Lee WM. Etiologies of acute liver failure. Semin Liver Dis. 2008;28: 142–152.
3. Sanyal AJ, Yoon SK, Lencioni R. The etiology of hepatocellular carcinoma and consequences for treatment. Oncologist. 2010;15 Suppl 4: 14–22.
4. Jadlowiec CC, Taner T. Liver transplantation: Current status and challenges. World J Gastroenterol. 2016;22: 4438–4445.
5. Michalopoulos GK, DeFrances MC. Liver regeneration. Science. 1997;276: 60–66.
6. Michalopoulos GK. Liver regeneration after partial hepatectomy: critical analysis of mechanistic dilemmas. Am J Pathol. 2010;176: 2–13.
7. Grompe M, al-Dhalimy M, Finegold M, Ou CN, Burlingame T, Kennaway NG, et al. Loss of fumarylacetoacetate hydrolase is responsible for the neonatal hepatic dysfunction phenotype of lethal albino mice. Genes Dev. 1993;7: 2298–2307.
8. Wangensteen KJ, Wilber A, Keng VW, He Z, Matise I, Wangensteen L, et al. A facile method for somatic, lifelong manipulation of multiple genes in the mouse liver. Hepatology. 2008;47: 1714–1724.
9. Wang AW, Wangensteen KJ, Wang YJ, Zahm AM, Moss NG, Erez N, et al. TRAP-seq identifies cystine/glutamate antiporter as a driver of recovery from liver injury. J Clin Invest. 2018;128: 2297–2309.
10. Heiman M, Kulicke R, Fenster RJ, Greengard P, Heintz N. Cell type-specific mRNA purification by translating ribosome affinity purification (TRAP). Nat Protoc. 2014;9: 1282–1291.
11. Liu J, Krautzberger AM, Sui SH, Hofmann OM, Chen Y, Baetscher M, et al. Cell-specific translational profiling in acute kidney injury. J Clin Invest. 2014;124: 1242–1254.
12. Lu SC. Regulation of glutathione synthesis. Mol Aspects Med. 2009;30: 42–59.
13. Wang AW, Wang YJ, Zahm AM, Morgan AR, Wangensteen KJ, Kaestner KH. The dynamic chromatin architecture of the regenerating liver [Internet]. doi:10.1101/664862
14. Zahm AM, Wang AW, Wang YJ, Schug J, Wangensteen KJ, Kaestner KH. A high-content in vivo screen to identify microRNA epistasis in the repopulating mouse liver [Internet]. doi:10.1101/664847
15. Stork C, Zheng S. Genome-Wide Profiling of RNA-Protein Interactions Using CLIP-Seq. Methods Mol Biol. 2016;1421: 137–151.
16. Zhao X, Lorent K, Wilkins BJ, Marchione DM, Gillespie K, Waisbourd-Zinman O, et al. Glutathione antioxidant pathway activity and reserve determine toxicity and specificity of the biliary toxin biliatresone in zebrafish. Hepatology. 2016;64: 894–907.
17. Halpern KB, Shenhav R, Matcovitch-Natan O, Toth B, Lemze D, Golan M, et al. Single-cell spatial reconstruction reveals global division of labour in the mammalian liver. Nature. 2017;542: 352–356.
18. Camp JG, Sekine K, Gerber T, Loeffler-Wirth H, Binder H, Gac M, et al. Multilineage communication regulates human liver bud development from pluripotency. Nature. 2017;546: 533–538.
19. Wang YJ, Kaestner KH. Single-Cell RNA-Seq of the Pancreatic Islets—a Promise Not yet Fulfilled?. Cell Metab. 2019;3: 539–544.

CHAPTER 4

THE DYNAMIC CHROMATIN ARCHITECTURE OF THE REGENERATING LIVER

Parts of this chapter were adapted with permission from The dynamic chromatin architecture of the regenerating liver. Wang AW, Yue YJ, Zahm AM, Morgan AR, Wangensteen KJ, Kaestner KH. Cellular and Molecular Gastroenterology and Hepatology. 2019. In press.

ABSTRACT

The adult liver is the main detoxification organ and is routinely exposed to environmental insults but retains the ability to restore its mass and function upon tissue damage. However, extensive injury can lead to liver failure, and chronic injury causes fibrosis, cirrhosis, and hepatocellular carcinoma (HCC). Currently, the transcriptional regulation of organ repair in the adult liver is incompletely understood. We isolated nuclei from quiescent as well as repopulating hepatocytes in a mouse model of hereditary tyrosinemia, which recapitulates the injury and repopulation seen in toxic liver injury in humans. We then performed the 'assay for transposase accessible chromatin with high-throughput sequencing' (ATAC-seq) specifically in repopulating hepatocytes to identify differentially accessible chromatin regions and nucleosome positioning. Additionally, we employed motif analysis to predict differential transcription factor occupancy and validated the *in silico* results with chromatin immunoprecipitation followed by sequencing (ChIP-seq) for hepatocyte nuclear factor 4α (HNF4α) and CCCTC-binding factor (CTCF). Chromatin accessibility in repopulating hepatocytes was increased in the regulatory regions of genes promoting proliferation and decreased in the regulatory regions of genes involved in metabolism. The epigenetic changes at promoters and liver enhancers correspond with the regulation of gene expression, with enhancers of many liver function genes displaying a less accessible state during the regenerative process. Our analysis of hepatocyte-specific epigenomic changes during liver repopulation identified CTCF and HNF4α as key regulators of hepatocyte proliferation and regulation of metabolic programs. Moreover, increased CTCF occupancy at promoters and decreased HNF4α binding at enhancers implicate these factors as key drivers of the transcriptomic changes in replicating hepatocytes that enable liver repopulation. Thus, liver repopulation in the setting of toxic injury makes use of both general transcription factors (CTCF) for promoter activation, and reduced binding by a hepatocyte-enriched factor (HNF4α) to temporarily limit enhancer activity.

INTRODUCTION

As the central metabolic organ in vertebrates, the liver regulates carbohydrate, protein, and lipid homeostasis, metabolizes nutrients, wastes, and xenobiotics, and synthesizes bile, amino acids, coagulation factors, and serum proteins [1]. To prevent acute liver failure upon exposure of harmful toxins, the liver has maintained an extraordinary ability to effectively restore its mass and function, in which the normally quiescent mature hepatocytes rapidly re-enter the cell cycle and divide [2]. Nonetheless, failure of regeneration can occur after exposure to harmful metabolites and environmental toxins, as often seen with the overconsumption of acetaminophen and alcohol [3]. Hence, understanding the genetic networks regulating the regenerative process can have an immense impact on the development of novel therapeutic strategies to treat acute liver failure.

The *Fah* null mouse model of human hereditary tyrosinemia type I provides a unique system to study the hepatocyte replication process after acute liver injury. Lack of the fumarylacetoacetate hydrolase (FAH) enzyme, essential for normal tyrosine catabolism, results in the accumulation of toxic intermediates followed by hepatocyte cell death [4,5]. *Fah*$^{-/-}$ mice can be maintained in a healthy state by supplementation with the drug 2-(2-nitro-4-trifluoromethylbenzoyl)-1,3-cyclohexanedione (NTBC) which inhibits an upstream enzymatic step that prevents toxin production [4]. Alternatively, gene therapy that utilizes hydrodynamic tail-vein injection and the *Sleeping Beauty* transposon system to restore *Fah* expression in hepatocytes can rescue these mice [6,7]. When a small fraction (0.1-1%) of hepatocytes express FAH following removal of NTBC, these hepatocytes competitively repopulate the liver in the context of injury through clonal expansion. Furthermore, this method allows lineage-tracing of repopulating hepatocytes since only those with stable FAH expression can expand and repopulate the injured parenchyma [7,8].

Eukaryotic DNA is highly organized and structured into compact chromatin to allow tight transcriptional control. Transcriptional regulation can be broadly categorized into two integrated layers: (1) transcription factors and the transcriptional machinery, and (2) chromatin structure and its regulatory proteins [9]. Expression of genes targeted by transcription factors depends on their binding affinity to specific target DNA recognition sequences, combinatorial assembly with other

cofactors, the concentration of the transcription factor, and post-translational modifications that affect protein localization [10]. The chromatin landscape is governed by DNA methylation, nucleosome properties, histone modifications, and intra- and interchromosomal interactions [10]. Establishing the relationship of chromatin structure, transcriptional regulators, and the effects on gene expression is therefore vital in elucidating the transcriptional control governing the regenerative process. To date, most studies have relied on transcriptomic studies to document gene expression changes in the regenerating liver [11–15] while two others focused on histone modifications [16,17]. However, these processes are downstream of chromatin reorganization and therefore do not capture the dynamic crosstalk of chromatin accessibility and transcriptional regulation. To identify transcriptomic changes specific to repopulating hepatocytes, we previously employed the translating ribosome affinity purification (TRAP) [18] to isolate translating mRNAs only from repopulating hepatocytes [15]. To discern the dynamic chromatin patterns that underlie liver repopulation, we now implement the 'isolation of nuclei tagged in specific cell types' (INTACT) [19] approach to isolate nuclei only from repopulating hepatocytes. This is achieved by expressing the GFP-tagged nuclear envelope protein SUN1-GFP together with FAH in *Fah*$^{-/-}$ mice, followed by the sorting of GFP-positive nuclei from repopulating hepatocytes and ATAC-seq [20]. We identify promoter accessibility changes corresponding to upregulation of cell cycle genes and downregulation of metabolic pathways, consistent with previous gene expression studies [12,15]. Integrative expression level and chromatin accessibility analysis suggests that gene activation is primarily associated with increased promoter accessibility, while inactivation is correlated with the closure of select promoters and enhancers. We propose a model in which a more accessible promoter allows increased transcription factor binding and gene activation, whereas decreased enhancer accessibility prevents binding of hepatocyte-enriched DNA binding proteins followed by inhibition of liver function genes so that the repopulating liver assumes a less differentiated state to promote cell growth and proliferation.

RESULTS

Adaptation of INTACT in the *Fah*$^{-/-}$ model allows for isolation of repopulating hepatocyte nuclei

Liver cells in humans and mice rarely undergo division in homeostatic conditions [2]. However, with injury and repopulation, hepatocytes become facultative stem cells and divide to replenish liver mass and restore liver function [2]. We hypothesized that this change from quiescence to replication is accompanied by substantial and specific changes to chromatin accessibility. To analyze the chromatin specific to repopulating hepatocytes, we adapted the INTACT [19] method to the *Fah*$^{-/-}$ model to label hepatocytes with the GFP-tagged nuclear envelope protein, SUN1-GFP, and performed fluorescence-activated cell sorting (FACS) to isolate nuclei from whole liver at selected time points (Figure 1). The SUN1-GFP fragment was subcloned into a FAH expression plasmid [7] so that all repopulating hepatocytes express GFP on the nuclear envelope. Following hydrodynamic injection of the FAH-SUN1-GFP plasmid into *Fah*$^{-/-}$ mice, NTBC was removed and liver repopulation was allowed to proceed for one or four weeks (Figure 1A). As a control for healthy, quiescent hepatocytes, *Rosa*$^{\text{LSL-SUN1-GFP}}$ transgenic mice [19] were injected with AAV8-TBG-Cre [21] to label all hepatocytes. Nuclei were isolated from repopulating hepatocytes exclusively at the selected time points by FACS-sorting with an anti-GFP antibody (Figure 1B). ATAC-seq [20] was then performed on the sorted nuclei to profile the changes in the chromatin regulatory landscape that occur during liver repopulation.

Immunofluorescence labeling demonstrated expression of GFP-tagged nuclear envelopes in FAH-positive cells (Figure 1C), illustrating the specificity of using SUN1-GFP^{+} nuclei as a marker to identify repopulating hepatocytes. Interestingly, FAH and GFP signals were not homogeneous across all replicating cells, possibly due to the different copy numbers of plasmids taken in after hydrodynamic tail-vein injection of the SUN1-GFP construct [22]. In addition, since the *Sleeping Beauty* transposon system displays little insertion site preference [23], the loci in which the DNA fragments are integrated can affect expression levels of FAH and SUN1-GFP [24].

ATAC-seq detects differentially accessible chromatin regions

All ATAC-seq libraries were sequenced to ~100 million reads to ensure ample coverage across the genome followed by quality assessment to verify the robustness of the data (Table 4.1). We observed consistent ATAC-seq signals across various loci such as the *Alb* gene, which showed a progressive decrease in accessibility at the enhancer region during repopulation (Figure 4.1A). To identify differentially accessible chromatin regions, fragments below 150 bp, termed 'nucleosome-free reads', were used for peak calling. We identified 16,043 differentially accessible regions between quiescent and repopulating hepatocytes (Figure 4.1B, Supplementary Digital Table 4.1), of which 5,359 displayed increased accessibility in 1-week and 5,102 in 4-week repopulating hepatocytes, while 3,580 regions showed decreased accessibility in week 1 and 5,304 in week 4. Hierarchical clustering of the differentially accessible sites showed a clear separation of repopulating and quiescent hepatocytes (Figure 4.2C), corroborating previous transcriptome studies that 1-week and 4-week repopulating hepatocytes have a similar expression profile distinct from quiescent hepatocytes [15]. Replicates also clustered within the same condition, illustrating the reproducibility between biological replicates. Comparing accessibility regulated in the same direction in both time points ('congruent'), 1,241 peaks were congruently increased and 2,033 congruently decreased (Figure 4.2B). Of note, only 28 regions exhibit accessibility changes in opposite directions in week 1 and week 4 ('incongruent'), reflecting the similarity in the chromatin profile between the two repopulation time points.

Next, we focused on differentially accessible promoter elements. Differential ATAC-seq regions within 1 kb up- and downstream of the transcription start sites (TSS) were determined and KEGG pathway [25] analysis was performed (Figure 4.2D). As expected, pathways involved in cell growth and proliferation were enriched among the genes with increased accessibility in the promoter regions during repopulation, including MAPK signaling [26] and cancer pathways. Interestingly, purine and pyrimidine metabolism were only enriched in genes with increased promoter accessibility at week 1 but not at week 4, suggesting early activation of DNA synthesis immediately after liver injury in early stages of repopulation. This observation is consistent with

previous comparison of the *Fah*$^{-/-}$ and partial hepatectomy (PHx) models showing that the transcriptome of 1-week repopulating hepatocytes in the *Fah*$^{-/-}$ mouse is closest to that of 36 and 48 h post-PHx [15], at which the highest rate of DNA synthesis occurs in this model [27]. On the other hand, genes involved in hepatocyte functions such as complement and coagulation and metabolic pathways displayed significantly decreased promoter accessibility at both regeneration time points. Our pathway enrichment analysis substantiates prior studies of gene expression profiles and extends the findings to chromatin accessibility in that proliferation pathways are activated while liver functions are inhibited during repopulation [12,15].

Integration of chromatin accessibility and gene activity infers regulatory mechanisms

To evaluate the association of chromatin landscape and gene expression, we utilized our prior TRAP-seq study [15] as a dataset of transcriptomic changes in repopulating hepatocytes. Genes with ATAC-seq signals and TRAP-seq reads that changed in the same direction at the same time point were identified as 'concordant genes' (Figure 4.3A, Supplementary Digital Table 4.2). We observed significant overlap of the concordant genes with ATAC-seq and TRAP-seq ($p<1E-16$ for all 1-week concordant genes and 4-week concordantly activated genes. $p=0.03$ for 4-week concordantly inhibited genes), while there was no significant overlap of genes with increased expression in 1 week and decreased chromatin accessibility at 4 weeks ($p=0.39$). KEGG pathway [25] analysis suggested enrichment of cell growth and replication in the week 1 concordantly activated genes, and overrepresentation of biosynthesis and metabolism in both week 1 and week 4 concordantly inhibited genes (Figures 3B, C). In addition, pathway enrichment supported previous observations that activation of the glutathione metabolic network is essential for reactive oxygen species removal after PHx or recovery following toxic liver injury [15,28,29]. We conclude that changes to the chromatin structure underlie the upregulation of genes involved in cell proliferation and downregulation of genes associated with metabolic processes.

Next, we sought to investigate co-regulatory networks in repopulating hepatocytes. All ATAC-seq peaks identified were first separated into increased, decreased, or unchanged

accessibility, with a cutoff of absolute fold change ≥1.5 and false discovery rate (FDR) ≤0.05, followed by subdivision into regulatory regions of promoters, liver-specific enhancers, or cerebellum-specific enhancers as a negative control [30]. Promoter peaks were annotated to the nearest genes and the corresponding transcript levels at the same time point were extracted from TRAP-seq data [15]. We then compared the gene expression levels in the differentially accessible promoters to those in the unchanged promoters (Figures 4.3D, E). The normalized $\log_2$ fold change was positive (p=7.47E-03 in week 1 and 3.81E-02 in week 4) with increased and negative (p=1.06E-06 in week 1 and 1.38E-03 in week 4) with decreased promoter accessibility at both time points, demonstrating a significant association of promoter openness and transcriptional activity. Differentially accessible liver enhancer peaks were similarly categorized, putative enhancer-regulated genes extrapolated [30], corresponding target gene expression extracted [15], and the transcript level changes compared to those of genes with unchanged enhancer accessibility. Interestingly, decreased liver enhancer accessibility was highly correlated with decreased gene activity (p=1.89E-20 in week 1 and 1.19E-07 in week 4), while no significant expression changes (p=0.22 in week 1 and 0.88 in week 4) were associated with increased enhancer openness. While the exact mechanism explaining this lack of correlation requires further evaluation, we posit that target genes regulated by enhancers in the quiescent liver are already highly expressed in mature, differentiated hepatocytes [12,15]. An increase in liver enhancer accessibility hence does not further elevate the expression of these genes significantly. Another likely explanation for the lack of significant association between increased liver enhancer accessibility and activation of target genes could be the recruitment of repressors instead of activators to the regulatory elements to decrease expression [31–33]. Finally, refinement of the computationally predicted enhancer-promoter pairs with experimental approaches could result in a more accurate correlation of enhancer accessibility and transcriptional activity. Importantly, cerebellum enhancers exhibited no significant correlation with the changes in transcript levels and chromatin accessibility in the repopulating liver, as expected (Figures 4.3D, E, right). Our integrated ATAC-seq and TRAP-seq analysis reveal that gene activation is regulated by increased promoter accessibility, presumably

allowing recruitment of transcriptional activators and RNA polymerase II to the TSS, whereas gene inhibition may be governed by both decreased promoter and enhancer openness, preventing long-range enhancer-promoter interactions [34].

Differential chromatin accessibility predicts transcription factors involved in liver repopulation

Dynamic coordination of chromatin structure and transcription factors is required to fine-tune gene expression. Chromatin organization influences access of the transcriptional apparatus by regulating binding sequence accessibility [35] and transcription factor binding stability [36]; conversely, transcription factors affect access of remodelers to the chromatin [35] and histones [37]. To identify DNA binding transcription factors that connect differential chromatin accessibility and gene expression, we carried out *de novo* motif profiling at differentially accessible promoters and liver enhancers [30].

We found enrichment of the ETS transcription factor ELK1 motif in promoters with increased accessibility in both 1-week (FDR=1E-76) and 4-week (FDR=1E-41) repopulating hepatocytes (Figure 4.4A, B, Supplemental Digital Table 4.3). ELK1 binds to the serum response element upon MAPK phosphorylation [38] to activate immediate early genes such as *Fos* and components of the basal transcriptional machinery [39]. Furthermore, ELK1 supports cell cycle entry during liver regeneration as *Elk1*$^{-/-}$ mice show reduced hepatocyte proliferation after PHx [40]. We postulate that promoters became more accessible after acute liver injury to permit increased ELK1 occupancy, enabling hepatocyte repopulation.

Among the regions with increased accessibility during liver repopulation, surprisingly, the CTCF motif was highly enriched (FDR=1E-78 in week 1 and 1E-49 in week 4) (Figures 4.4C, D). CTCF plays numerous roles in transcriptional regulation to function as a transcriptional activator [41] or repressor [42], insulator to block enhancer-promoter interactions [43], chromatin structure organizer to form topologically-associated domains [44] modulator of long-range chromatin looping [45], and even mediator of local RNA polymerase II pausing to regulate alternative exon usage [46].

CTCF is recruited to the *Axin1* promoter as a transcriptional repressor by the 'long noncoding RNA associated with liver regeneration' (lncRNA-LALR1) after PHx, leading to activation of Wnt/β-catenin signaling to promote hepatocyte proliferation [47]. However, the function of CTCF in liver regeneration is not fully understood.

In addition, we found the HNF4α binding motif to be significantly associated with liver enhancers with decreased accessibility during liver regeneration (FDR=1E-146 in week 1 and 1E-186 in week 4) (Figures 4.4E, F). HNF4α is a master regulator atop the transcriptional cascade of hepatocyte differentiation [48,49] and a crucial factor that maintains hepatocytes in the differentiated state [50]. Importantly, HNF4α suppresses liver proliferation, as mice with conditional deletion of *Hnf4a* demonstrate increased hepatocyte BrdU incorporation and Ki67 expression [51]. HNF4α also directly inhibits cell growth and replication pathways, as illustrated by the upregulation of cell cycle and proliferation genes upon acute HNF4α loss [51,52]. Moreover, motifs of other liver-enriched transcription factors were also overrepresented at enhancers that became less accessible in repopulating hepatocytes, including hepatocyte nuclear factor 1β (HNF1β) and hepatocyte nuclear factor 6 (HNF6) [53] (Figures 4.4E, F). We examined the locations for CTCF and HNF4α motifs within regions of dynamic chromatin accessibility and found that they are present in the center of these regions with CTCF at those with increased (p=2.70E-04 in week 1 and 1.97E-13 in week 4), and HNF4α at those with decreased accessibility (p=0.59 in week 1 and 2.48E-03 in week 4) (Figure 4.4G, H).

In summary, *de novo* motif analysis of differentially accessible ATAC-seq regions suggests increased occupancy of ELK1 and CTCF at chromatin regions that become more accessible, and decreased binding of liver-enriched transcription factors at liver enhancers that become less accessible during repopulation.

HNF4α occupancy is decreased in liver-specific enhancers during repopulation

We postulated that decreased HNF4α binding allows repopulating hepatocytes to assume a less differentiated and pro-proliferative state and carried out ChIP-seq on quiescent and 4-week

repopulating livers to examine genome-wide HNF4α occupancy during the repopulation process. We observed 508 peaks with decreased and only 14 peaks with increased occupancy in repopulating livers (Figure 4.5A, Supplemental Digital Table 4.4). Remarkably, 42% (214) of lost HNF4α occupancy occurred within previously-defined liver enhancers [30], while 23% (119) fell into distal intergenic regions, and 10% (52) were within 1 kb up- and downstream of the TSS ('promoter') (Figure 4.5B). These data corroborate the differentially accessible chromatin analysis of transcription factor motifs that had identified enrichment of the HNF4α consensus sequence at enhancers with decreased accessibility in repopulating hepatocytes (Figure 4.4H).

Next, we integrated ATAC-seq, ChIP-seq, and TRAP-seq datasets [15], and identified hepatocyte-enriched genes crucial for establishing liver functions including complement and coagulation (*Cfb*, *F2*), biosynthesis (*Itih1*, *Acsl1*, *Pgrmc1*), and metabolism (*Ugt1a5*, *Mthfs*, *Rdh10*) [54] as correlated with decreased HNF4α enhancer occupancy during regeneration (Figure 4.5C, E). To explore the mechanism responsible for decreased HNF4α occupancy during liver repopulation, we next turned to the TRAP-seq dataset [15] to inspect *Hnf4a* expression levels in quiescent and replicating hepatocytes. Remarkably, we found a 50% reduction of *Hnf4a* transcripts in 4-week repopulating hepatocytes (FDR=4.16E-3) compared to the quiescent liver (Figure 4.5D, Table 4.2). Taken together, these results implicate decreased chromatin accessibility and reduced *Hnf4a* expression as contributors to the suppression of hepatocyte-specific genes and downregulation of liver biosynthetic functions during repopulation.

CTCF promoter occupancy is increased in the repopulating liver

In order to extend the computational finding of enriched CTCF motif at promoters with increased accessibility, we performed ChIP-seq in quiescent and 4-week repopulating livers. CTCF occupancy was increased at 1,382 sites in the repopulating liver, while only 2 peaks showed decreased binding (Figure 4.6A, Supplemental Digital Table 4.5). To characterize the role of increased CTCF occupancy during liver repopulation, we first evaluated its potential insulator function by calculating an 'insulator strength score' [55] at all gained binding sites. Genomic regions

with increased CTCF occupancy with divergent flanking promoters within 50 kb were identified and the normalized expression levels corresponding to the genes were extracted from our TRAP-seq data (Figure 4.6B) [15]. Surprisingly, gene pairs with increased CTCF binding were not significantly more enriched for differential gene expression than random gene pairs (p=0.9) (Figure 4.6C), suggesting that CTCF is unlikely to act as an insulator during liver repopulation.

Remarkably, the vast majority (1,026, 74%) of the gained CTCF peaks fell within 1 kb up- and downstream of the TSS ('promoter') (Figure 4.6D). To examine the targets of increased CTCF occupancy, all differentially bound peaks were annotated to the nearest genes and their corresponding expression changes were obtained from our TRAP-seq dataset [15,25,56]. We found 545 (39%) peaks associated with chromatin modification, transcription regulation, and cancer (Figure 4.6E), while 656 (47%) sites with increased CTCF binding were associated with inhibition of genes in cell death regulation, stress response, and morphogenesis. Together, our network analysis suggests a diverse role for CTCF in transcriptional regulation in which increased CTCF occupancy supports hepatocyte replication and prevents cell death during liver repopulation, possibly by enabling binding of both activating and repressing cofactors.

CTCF is known to exhibit divergent roles in activating and repressing transcription by recruiting various protein partners in a context-dependent manner [57]. To identify these cofactors, we performed motif analysis for the regions differentially bound by CTCF (Figure 4.6F). As expected, the CTCF motif was highly enriched (FDR=1E-26) at all differential binding sites, confirming the specificity of the anti-CTCF antibody for immunoprecipitation. At sites where CTCF binding corresponded to gene activation, we observed significant enrichment for the 'zinc finger and BTB domain-containing protein 3' (ZBTB3) (FDR=1E-10) and nuclear transcription factor Y (NF-Y) (FDR=1E-10) binding motifs (Figure 4.6F). ZBTB3 is considered a likely factor binding 5' of CTCF due to its frequent enrichment ~10 bp upstream of CTCF motifs in the human genome [58]. Furthermore, expression of ZBTB3 is induced by the accumulation of reactive oxygen species to promote cancer cell growth and prevent apoptosis via the activation of antioxidant gene expression in cell lines [59]. Whether CTCF directly interacts with or indirectly recruits ZBTB3 is yet unclear,

but the proteins are likely to interact based on their close proximity at promoters. NF-Y binds to the CCAAT box present at ~30% of the promoters [60] and is required for cell cycle progression, DNA synthesis, and proliferation in mouse embryonic fibroblasts [61]. Additionally, reconstituted *in vitro* transcription reactions demonstrated that binding of NF-Y disrupts nucleosome structure at promoters containing the NF-Y recognition sequence [62]. Recruitment of NF-Y could hence induce local nucleosome repositioning to allow increased accessibility of the transcriptional apparatus to activate gene expression.

On the other hand, the Yin Yang 1 (YY1) binding motif was enriched (FDR=1E-13) at sites where increased CTCF occupancy corresponded with decreased gene expression (Figure 4.6F). YY1 regulates embryogenesis, cell differentiation, and tumorigenesis [63,64], as well as enhancer-promoter interactions analogous to long-range chromatin looping mediated by CTCF [65]. YY1 functions as a transcriptional repressor via recruitment of the polycomb repressor complex, resulting in trimethylation of histone H3 lysine 27 [66,67]. It is also a cofactor of CTCF in regulating X chromosome inactivation, although the exact mechanism remains unclear [68]. Given these observations, it is likely that direct or indirect co-binding of CTCF and YY1 at promoters induces transcriptional repression or disrupts enhancer to promoter interactions to downregulate target genes.

When examining gene expression, we found the levels of ZBTB3 and YY1 not significantly changed in repopulating hepatocytes (Table 4.2). Three NF-Y proteins exhibited varying changes in transcript levels, with unchanged NF-YA, downregulated NF-YB in 1-week, and downregulated NF-YC in 4-week repopulating hepatocytes, albeit all with modest changes of less than 2-fold. These observations do not rule out the possibility of post-translational modifications that might alter the abundance or localization of transcription factors.

To analyze if transcription factors colocalize to CTCF-occupied promoters with differential gene expression during liver regeneration, we performed ZBTB3 and YY1 ChIP-qPCR on quiescent and 4-week repopulating livers. We observed a significant increase of ZBTB3 occupancy at *Ctnna2* ($p=0.023$) and *Smad3* ($p=0.025$) promoters, two genes with increased promoter accessibility,

elevated CTCF binding, and upregulated expression during liver regeneration (Figure 4.6G, H). Regarding YY1 occupancy, there was a significant increase at the *Bcl2l11* (p=0.029) promoter, a gene with increased promoter accessibility, enhanced CTCF occupancy, and decreased transcript levels (Figure 4.6I). With the limited loci tested, we conclude that ZBTB3 is recruited to open chromatin regions occupied by CTCF to activate gene expression during liver regeneration. On the other hand, increased YY1 binding to select promoters with elevated CTCF binding could regulate transcriptional repression in repopulating hepatocytes. These results suggest that increased chromatin accessibility correlates with enhanced CTCF occupancy that recruits coactivators or corepressors to fine-tune target gene expression to induce replication and prevent apoptosis during liver repopulation (Figure 4.6J). Future experiments that utilize co-immunoprecipitation and high-throughput sequencing technologies to analyze interactions between CTCF and cofactors as well as genome-wide binding patterns of the coregulators will aid in the understanding of mechanisms underlying CTCF modulation.

Liver regeneration is accompanied by nucleosome remodeling

Most eukaryotic DNA is packaged around histone protein octamers into nucleosomes to regulate chromatin organization and transcriptional control. Nucleosome properties such as positioning and turn-over rates can affect the binding of transcription factors and access of the transcriptional machinery [69]. The nucleosome landscape adjacent to the TSS is of particular interest, as nucleosomes adopt a specific phasing pattern immediately up- and downstream [70]. Hence, nucleosome organization could act as an additional layer of transcriptional regulation in repopulating hepatocytes.

We inferred nucleosome positioning from nucleosome-containing sequences by extracting ATAC-seq reads longer than 150 bp (Figure 4.7A). Nucleosomes surrounding the TSS were defined as '-1 nucleosomes' within 350 bp upstream and '+1 nucleosomes' within 250 bp downstream, and the distance between the +1 to -1 nucleosomes was defined as the 'nucleosome-free region'. When compared to quiescent hepatocytes, there was a median downstream shift of 9

bp in 1-week (p=2.60E-13) and an upstream shift of 19 bp in 4-week (p<1E-15) repopulating hepatocytes for the -1 nucleosomes, while there was no significant shift in +1 nucleosome positioning (Figure 4.7B, Supplemental Digital Table 4.6). As a result, there was a global increase of promoter openness in 4-week repopulating hepatocytes as the distance between +1 to -1 nucleosomes increased, while the nucleosome-free region was shorter in 1-week regenerating liver compared to the quiescent state. The difference in genome-wide promoter openness in repopulating hepatocytes at various time points suggests that accessibility of divergent functional regions could be differentially regulated during liver regeneration. Indeed, the nucleosome-free region constitutes only 17.5% of regions with increased accessibility in week 1 but 45.6% in week 4 (Figure 4.7C), whereas 39.0% of week 1 and only 26.9% of week 4 regions that became more open fall into distal intergenic regions (Figure 4.7D). On the other hand, chromatin regions with decreased accessibility show a similar distribution between the nucleosome-free region and distal intergenic regions. These observations indicate that the increase of chromatin accessibility occurs mainly at distal genomic areas in 1-week and around the TSS in 4-week repopulating hepatocytes.

To evaluate the association of TSS accessibility and gene expression, we extracted the top 500 up- and downregulated genes in repopulation [15] and calculated the change in the length of the nucleosome-free region between quiescent and regenerating hepatocytes as a surrogate for differential TSS accessibility. We only observed a significant increase (p=1.15E-2) of +1 to -1 nucleosome distance in genes activated in week 4 when compared to quiescent hepatocytes, while no significant change in the nucleosome-free region was present in genes upregulated in week 1 or genes downregulated in week 1 and week 4 (Figure 4.7E, F). It is likely that eviction or repositioning of the -1 nucleosomes could expose transcription factor binding sequences and allow access of the transcriptional machinery to the TATA box for gene activation in regenerating hepatocytes [71]. Altogether, analysis of the nucleosome structure implies nucleosome reorganization could affect gene activation but not inhibition during liver repopulation.

TABLES

Table 4.1. ATAC-seq library sequencing summary.

Sample ID	Condition	Index	Cumulate reads
SUN1-GFP-1	Quiescent	CGAGGCTG	119,120,180
SUN1-GFP-2	Quiescent	AAGAGGCA	111,970,248
#3603	1-week repopulation	AATTCGTT	97,320,484
#3604	1-week repopulation	GGCGTCGA	135,005,202
#2383	4-week repopulation	GTAGAGGA	186,365,116
#2385	4-week repopulation	TGCTGGGT	236,418,952

Table 4.2. Gene expression of enriched transcription factor motifs.

Gene	Transcript	W1 log_2 fold change	W1 FDR	W4 log_2 fold change	W4 FDR
Elk1	NM_007922	0.23	0.83	0.05	0.96
Ctcf	NM_181322	-0.36	0.47	0.23	0.66
Hnf4a	NM_008261	-0.17	0.74	-1.12	0.00
Hnf1b	NM_009330	-0.15	0.85	-0.22	0.67
Hnf6	NM_008262	0.54	0.49	0.11	0.92
Zbtb3	NM_001098237	1.26	0.33	-0.64	0.73
Nfya	NM_001110832	0.23	0.85	0.03	1.00
Nfyb	NM_010914	-0.74	0.02	-0.20	0.64
Nfyc	NM_001048168	-0.67	0.10	-0.82	0.02
Yy1	NM_009537	-0.35	0.42	-0.12	0.79

Table 4.3. Primer sequences used in this study.

Primer name	Sequence	Use
MfeI-Sun1-F	GACTCAATTGGCGGCCGCACTACTGGCC	Plasmid construction
BsiW1-Sun1-R	GCTACGTACGTTAACCGCTACTATTAAGATC CTCCTCGGATATTAACTTCTGC	Plasmid construction
ZBTB3-ChIP-Ctnna2-qPCR-F1	TTTGTTCGATCACAGTGCCG	ZBTB3 ChIP-qPCR
ZBTB3-ChIP-Ctnna2-qPCR-R1	TGGGAGCAACAGTGGATGAA	ZBTB3 ChIP-qPCR
ZBTB3-ChIP-Smad3-qPCR-F2	AGACCTCCGTGCCTTTTCTA	ZBTB3 ChIP-qPCR
ZBTB3-ChIP-Smad3-qPCR-R2	GGCGGTTGAGTTTCACAGAG	ZBTB3 ChIP-qPCR
YY1-ChIP-Bcl2l11-qPCR-F1	CTCTTGTAGCGATCACCCCT	YY1 ChIP-qPCR
YY1-ChIP-Bcl2l11-qPCR-R1	CTGCCGTCCCAATCAATGTT	YY1 ChIP-qPCR
40S-F2	AGCGAGCTGTGCTGAAGTTT	ChIP-qPCR control
40S-R2	AGGCTGCTTGGATCTGGTTA	ChIP-qPCR control

FIGURES

Figure 4.1. Implementation of the 'isolation of nuclei tagged in specific cell types' (INTACT) [19] method with the *Fah*$^{-/-}$ mouse model allows isolation of repopulating hepatocyte nuclei.

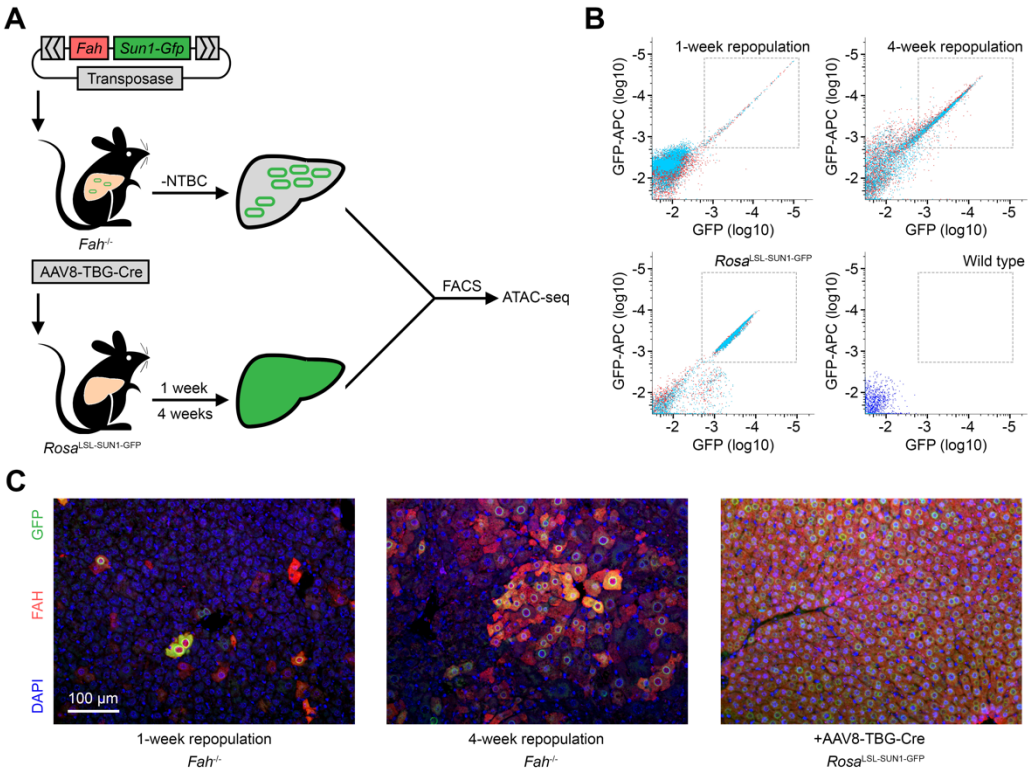

(**A**) Schematic of coexpression of the GFP-tagged nuclear envelope protein SUN1 (SUN1-GFP) with FAH to label repopulating hepatocytes for fluorescence-activated cell sorting (FACS) followed by the 'assay for transposase accessible chromatin with high-throughput sequencing' (ATAC-seq). (**B**) Representative images (n=2) of repopulating hepatocyte nuclei show specific isolation with anti-GFP antibody labeling. Gray boxes denote the sorting strategy to collect GFP^{+} nuclei. (**C**) Representative images (n=2) of immunofluorescent staining of GFP and FAH show coexpression of SUN1-GFP and FAH in repopulating hepatocytes of the *Fah*$^{-/-}$ mouse after 1 week (left) and 4 weeks (middle), and global expression of SUN1-GFP and FAH in all hepatocytes of the *Rosa*$^{LSL\text{-}SUN1\text{-}GFP}$ mouse 1 week after AAV8-TBG-Cre injection. FACS: fluorescence-activated cell sorting.

Figure 4.2. Chromatin accessibility changes during liver repopulation are related to cell growth activation and metabolic inhibition.

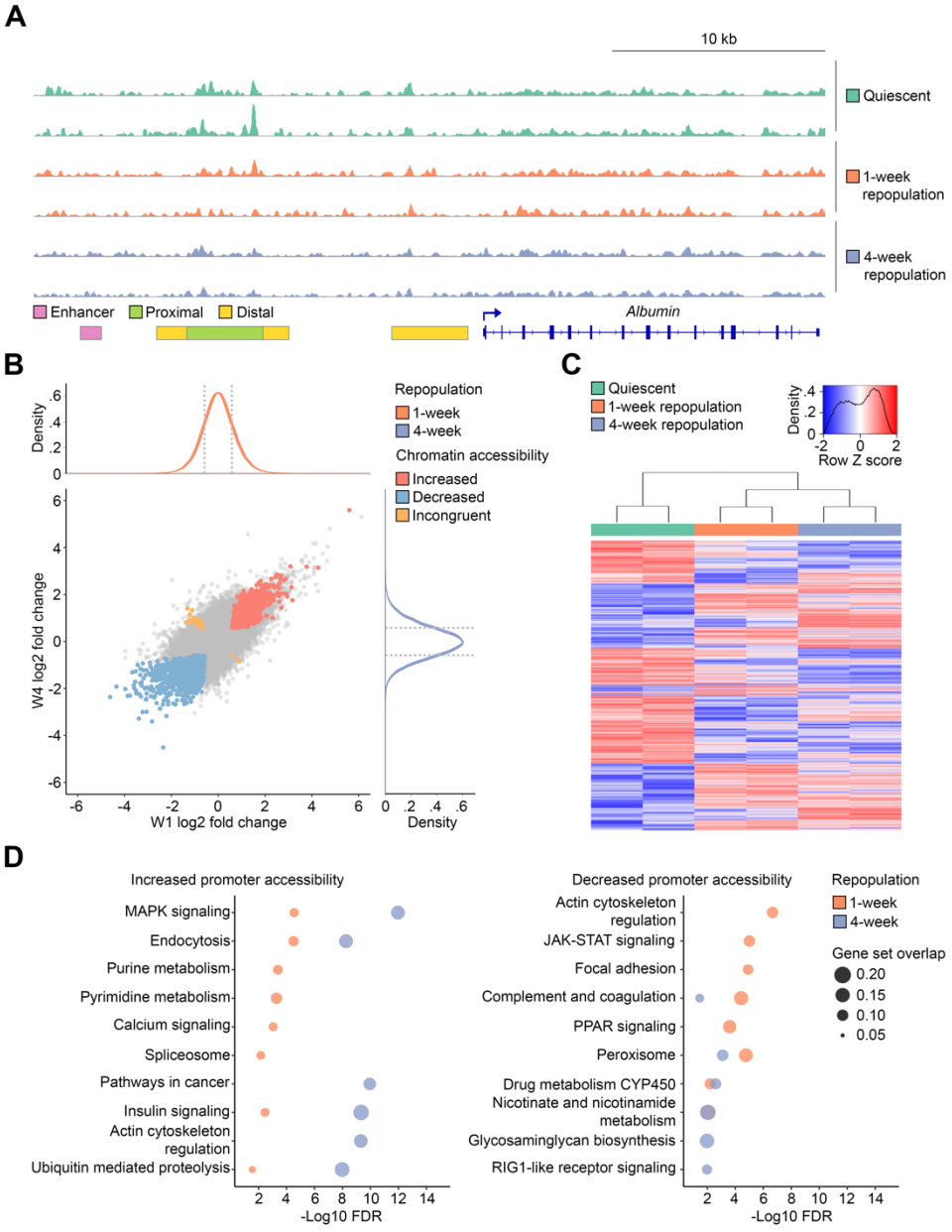

(**A**) ATAC-seq shows reproducible signals across biological replicates and a decrease of peak intensity in the proximal regulatory region [105] of the *Alb* locus. (**B**) 16,043 significantly differential accessible regions were identified in repopulating and quiescent hepatocytes (absolute fold change ≥1.5 and FDR ≤0.05). Comparison of differential accessible regions identified at different time

points during repopulation shows 3,273 that changed in the same direction ('congruent' peaks), of which 1,241 were congruently increased (red dots) and 2,033 congruently decreased (blue dots). (**C**) Hierarchical clustering of all differentially accessible regions shows that biological replicates have similar chromatin landscape. (**D**) KEGG pathway analysis of differentially accessible promoters with increased (left) and decreased (right) accessibility in repopulating hepatocytes. FDR: false discovery rate.

Figure 4.3. Association of expression levels and chromatin accessibility implicates divergent regulatory mechanisms for gene activation and inhibition.

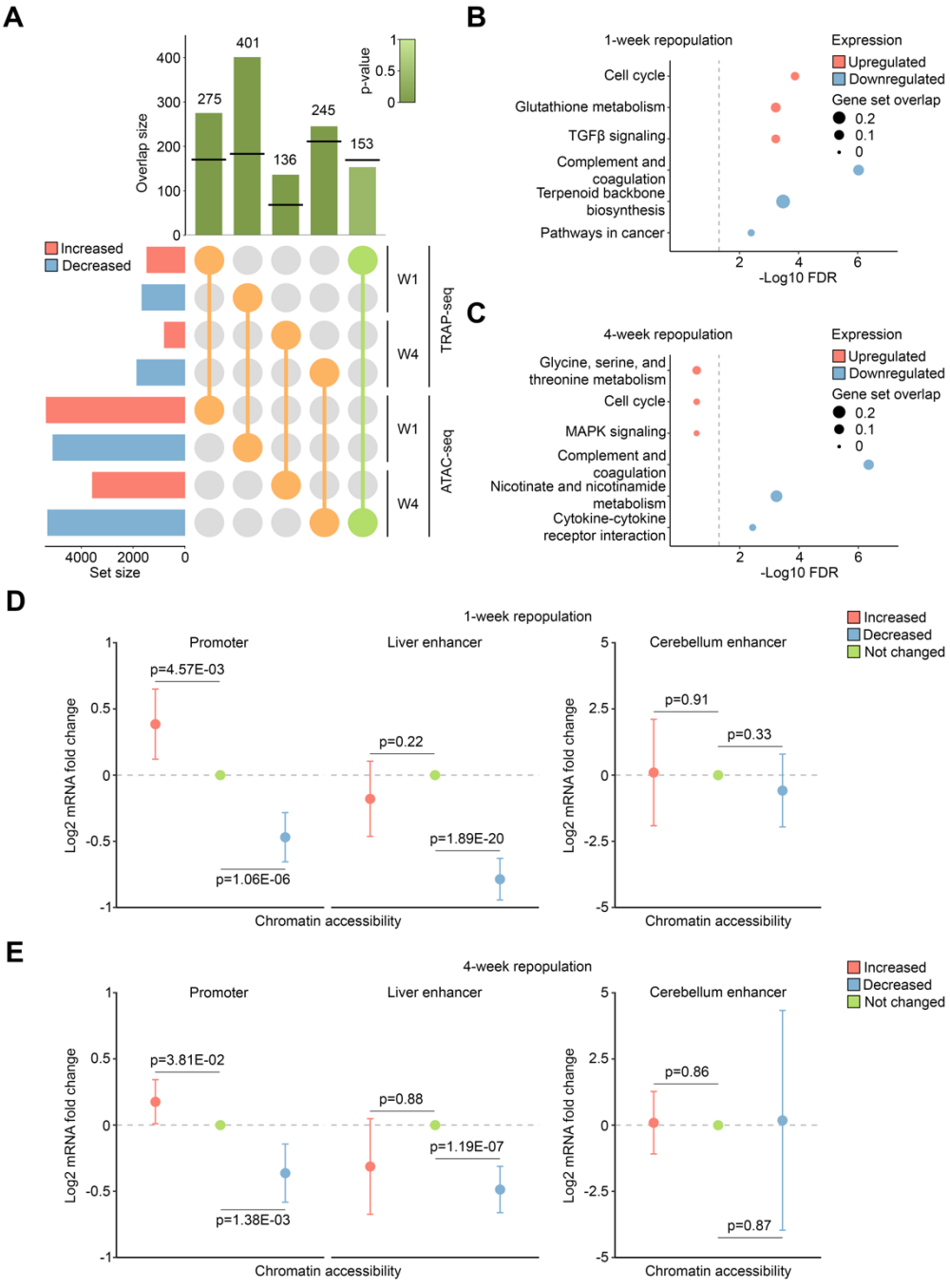

(**A**) Differential gene expression data were obtained from a previous study that implemented translating ribosome affinity purification followed by RNA-sequencing (TRAP-seq) [15]. 'Upset' plot

demonstrates overlap of ATAC-seq regions and TRAP-seq genes that are significantly changed in the same direction at the same time points ('concordant' genes) in repopulating hepatocytes. Fisher's exact test was performed to calculate the significance of overlapping targets. The horizontal black lines in the green bars of the top panel indicate the number of overlaps expected by chance. (**B** and **C**) KEGG pathway analysis of concordantly activated and repressed genes in (**B**) 1-week and (**C**) 4-week repopulating hepatocytes. Dashed lines denote FDR=0.05. (**D** and **E**) Association of changes in chromatin accessibility and gene expression in (**D**) 1-week and (**E**) 4-week repopulating hepatocytes indicates that promoter accessibility changes are related to both gene activation and inhibition, while only decreased liver enhancer accessibility is significantly correlated with decreased expression of putative target genes [30]. Cerebellum enhancers and their putative targets do not display any significant relationship to chromatin accessibility and gene expression changes in the liver. One-sample t-tests were carried out to identify the differences in normalized $\log_2$ fold change in differentially accessible and unchanged chromatin regions. Vertical lines denote the 95% confidence interval of normalized $\log_2$ fold change in peaks with increased and decreased accessibility.

Figure 4.4. Enrichment analysis identifies transcription factor motifs overrepresented at differential accessible promoters and enhancers [30].

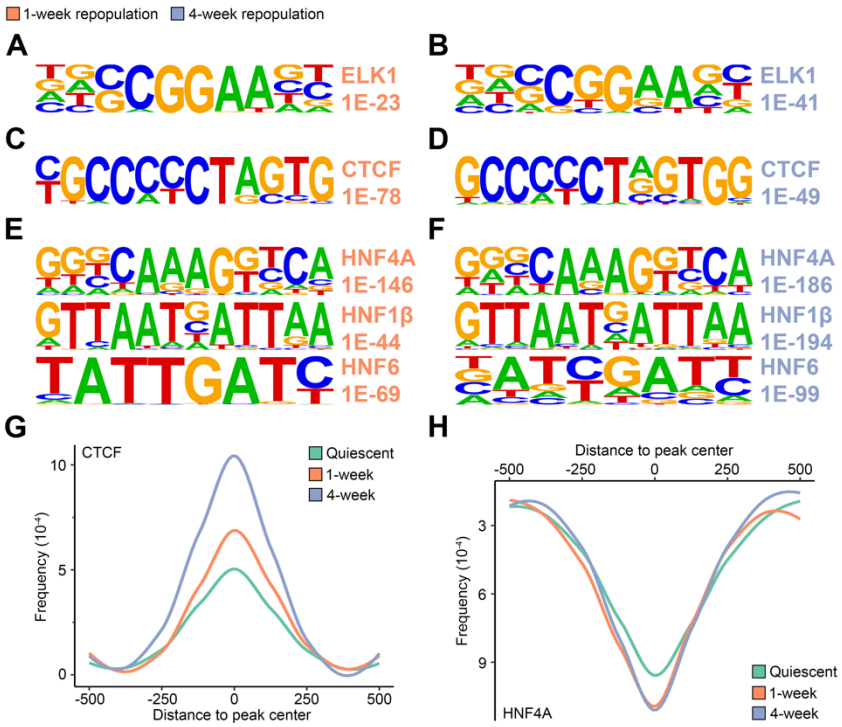

(**A** and **B**) The ELK1 motif is enriched in promoter regions that became more open in repopulating hepatocytes. (**C** and **D**) The CTCF motif is overrepresented in liver enhancers with increased accessibility in both (**C**) 1-week and (**D**) 4-week repopulating hepatocytes, respectively. (**E** and **F**) Motifs of liver-enriched transcription factors HNF4α, HNF1β, and HNF6 are enriched in enhancers with decreased accessibility during (**E**) 1-week and (**F**) 4-week liver repopulation. (**G** and **H**) Motif frequency of the differential accessible peaks for (**G**) CTCF and (**H**) HNF4α display enrichment of the transcription factor motifs at the enhancer peak center in repopulating hepatocytes. Numbers presented in (**A**-**F**) denote FDR.

Figure 4.5. HNF4α binding is decreased in the repopulating liver.

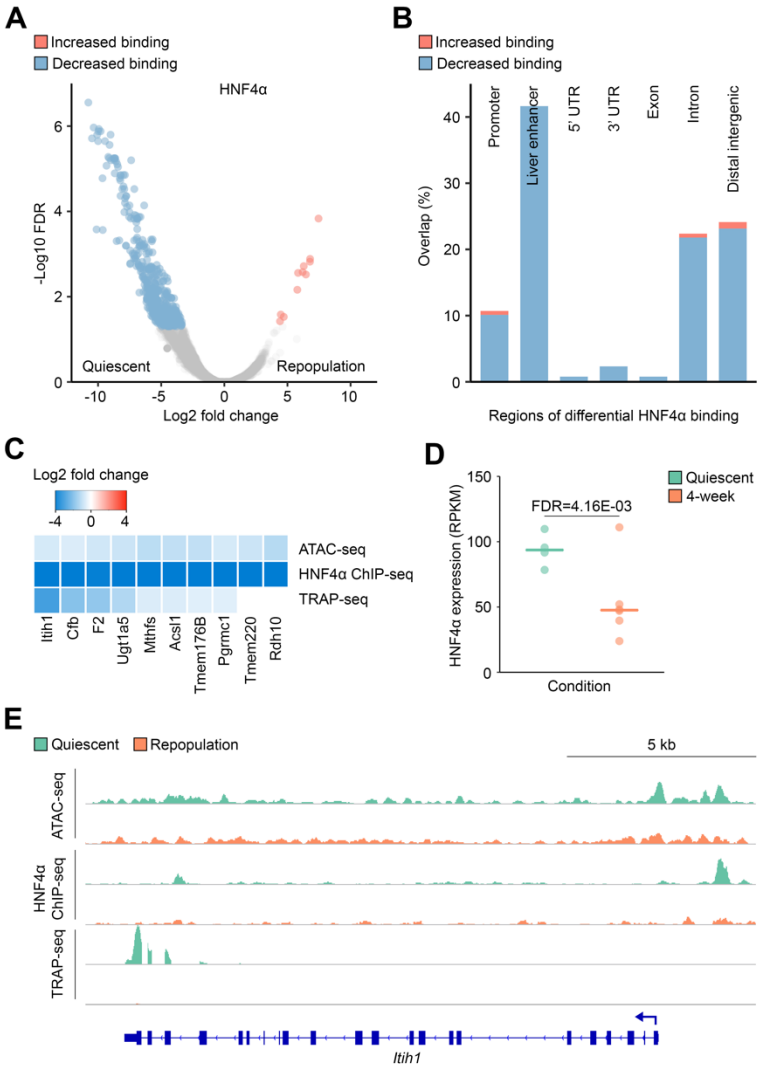

(**A**) 508 genomic regions display decreased and only 14 display increased HNF4α occupancy in the regenerating liver (**B**) 40% of peaks with decreased HNF4α binding overlap with liver-enriched enhancers ('liver enhancer') [30], and 25% fall in distal intergenic regions that contain ubiquitous enhancers ('distal intergenic'). (**C**) Integrative analysis of chromatin accessibility (ATAC-seq), HNF4α binding (ChIP-seq), and gene expression (TRAP-seq) [15] changes suggests the suppression of liver functions including complement, biosynthesis, and metabolic pathways during liver regeneration is associated with reduced HNF4α occupancy. (**D**) HNF4α expression is downregulated in repopulating hepatocytes (n=4 for quiescent and n=6 for repopulating

hepatocytes) [15]. (**E**) Representative tracks (n=2 for ATAC-seq and ChIP-seq, n=4 for TRAP-seq) of chromatin accessibility, HNF4α occupancy, and transcript levels at *Itih1*, the locus with the strongest decrease of HNF4α occupancy. RPKM: reads per kilobase of transcript, per million mapped.

Figure 4.6. CTCF binding is increased at promoters in the repopulating liver.

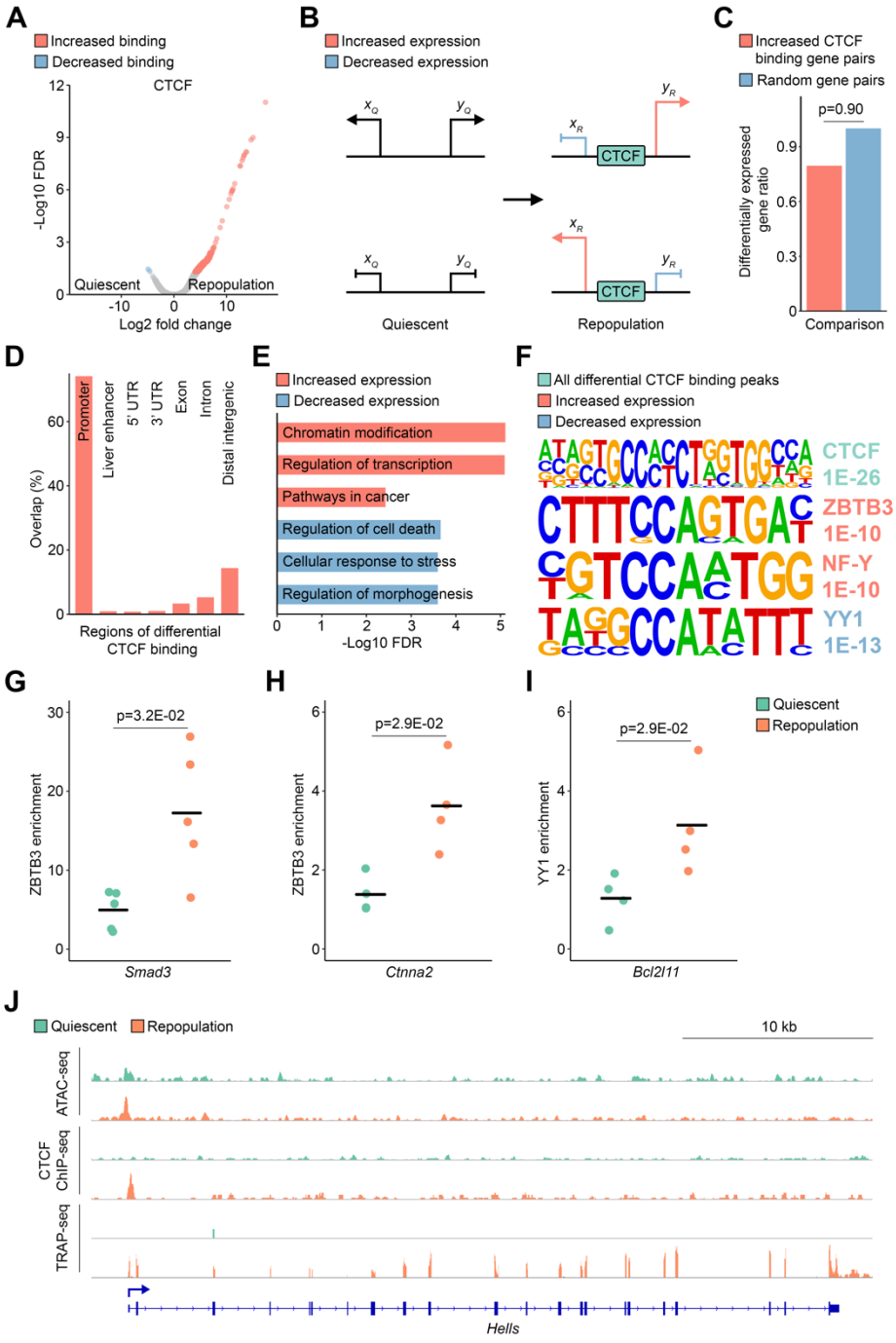

(**A**) 1,306 peaks show increased, while only 2 peaks show decreased CTCF occupancy during repopulation. (**B**) Schematic to test the insulator function of increased CTCF binding to differentially regulate expression of the flanking genes [55]. (**C**) Promoters flanking sites of increased CTCF

occupancy are not more enriched for differentially expressed genes compared to random gene pairs in the genome. A Fisher's exact test was used to examine the differentially expressed gene ratios from the two groups of gene pairs. (**D**) 75% of the genomic regions with increased CTCF binding are within 1 kb up- and downstream of the TSS ('promoter'), and only 13 peaks overlap with liver enhancers [30]. (**E**) Enriched pathways of increased chromatin accessibility, CTCF occupancy, and increased (red) or decreased (blue) gene expression during liver repopulation. (**F**) Motif enrichment analysis identifies an overrepresentation of CTCF motif in differentially-bound regions, the 'zinc finger and BTB domain-containing protein 3' (ZBTB3) and nuclear transcription factor Y (NF-Y) motifs at sites with increased CTCF occupancy associated with gene activation, and the Yin Yang 1 (YY1) motif at sites with increased CTCF occupancy associated with gene inhibition. Numbers denote FDR. (**G** and **H**) ZBTB3 occupancy is increased in the repopulating liver at the (**G**) *Smad3* and (**H**) *Ctnna2* promoters, two genes with increased CTCF occupancy and expression during regeneration. (**H**) YY1 occupancy is increased in the repopulating liver at the *Bcl2l11* promoter, a gene with elevated CTCF binding and decreased expression during regeneration. (**I**) Representative tracks (n=2 for ATAC-seq and ChIP-seq, n=4 for TRAP-seq) of chromatin accessibility, CTCF occupancy, and transcript levels at *Hells*, the locus with the strongest increase in CTCF binding.

Figure 4.7. Decreased nucleosome density is associated with increased gene expression [15] in repopulating hepatocytes.

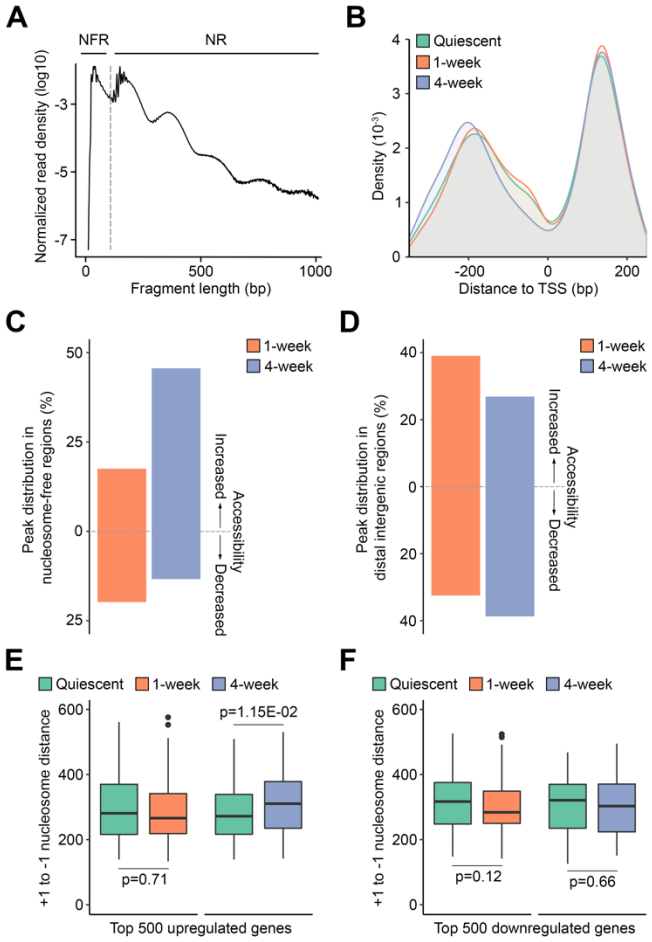

(**A**) Schematic for identifying nucleosome positioning information with NucleoATAC [104]. (**B**) Globally, -1 nucleosomes have an upstream shift away from the TSS in 4-week repopulating hepatocytes, while +1 nucleosomes positioning is constant during liver repopulation. (**C** and **D**) Distribution of regions with differential accessibility in (**C**) the nucleosome-free region that is within 350 bp upstream and 250 bp downstream of the TSS and (**D**) distal intergenic regions in 1- and 4-week repopulating hepatocytes. (**E**) The top 500 upregulated genes exhibit an increased +1 to -1 nucleosome distance in 4-week but not 1-week repopulating hepatocytes when compared to quiescent hepatocytes. (**F**) The top 500 downregulated genes are not significantly associated with changes in +1 to -1 nucleosome distance in repopulating compared to quiescent hepatocytes.

Permutation tests with 10,000 iterations were used to compare the nucleosome distance in repopulating and quiescent hepatocytes. NFR: nucleosome-free reads. NR: nucleosomal reads.

Figure 4.8. Model of transcriptional regulation in repopulating hepatocytes.

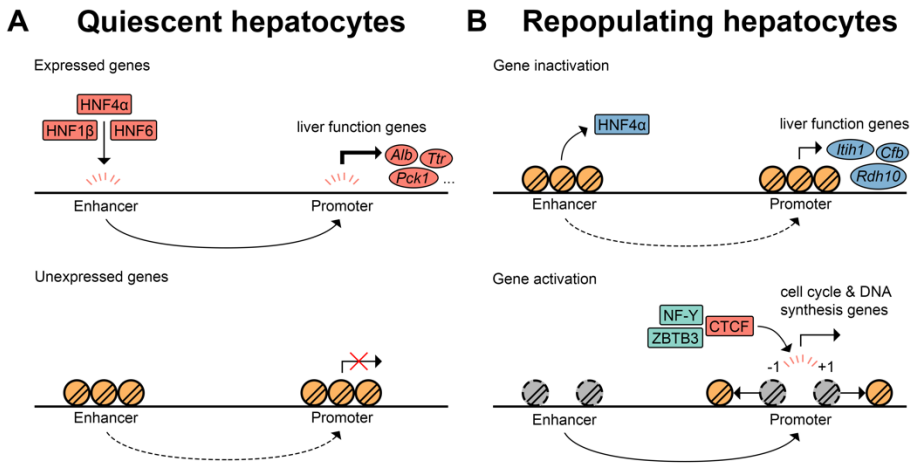

(**A**) Access to enhancers allows liver-enriched transcription factors to maintain quiescent hepatocytes in the differentiated state (top). In contrast, chromatin-dense enhancers and promoters prevent transcription factor binding to inhibit gene expression of cell cycle genes (bottom). (**B**) During liver repopulation, decreased accessibility of liver enhancers [30] in conjunction with more closed promoters prevents binding of transcription factor and assembly of the transcriptional machinery at hepatocyte-specific liver function genes, resulting in a less differentiated transcriptomic and epigenomic profile in the repopulating cells (top). Conversely, the promoter regions of cell cycle genes become more open, with increased +1 to -1 distance and increased CTCF occupancy at the promoter, allowing elevated expression of genes involved in the cell cycle and DNA synthesis pathways (bottom).

DISCUSSION

Gene regulation is tightly controlled by a complex network integrating transcription factor binding and transcriptional apparatus assembly, chromatin structure, epigenetic modifications, and even intra- and interchromosomal interactions [9,10]. In this study, we investigated the association of chromatin accessibility, nucleosome properties, transcription factor occupancy, and gene expression [15] to delineate the multidimensional framework of transcriptional regulation in the repopulating liver. By implementing the INTACT method [19] to express SUN1-GFP in the *Fah*$^{-/-}$ model, we successfully performed cell type-specific isolation of only repopulating hepatocyte nuclei followed by ATAC-seq to identify changes of the chromatin landscape (Figures 4.1, 4.2). Integration of TRAP-seq [15] with ATAC-seq determined that gene activation corresponds with increased promoter openness, while gene inhibition is linked to a decreased promoter and enhancer accessibility (Figure 4.3C). We also corroborated previous findings that cell cycle, DNA synthesis, proliferation, and glutathione metabolism are activated whereas complement and coagulation, biosynthesis, and metabolic pathways are inhibited during liver repopulation (Figures 4.2D and 4.3B, C) [12,15]. In addition, *de novo* motif analysis identified enrichment of CTCF and HNF4α binding sequences in regions with increased and decreased accessibility in repopulating hepatocytes, respectively (Figure 4.4). We further validated the differential occupancy of both factors in the repopulating liver with ChIP-seq and observed decreased HNF4α binding at liver enhancers [30] (Figure 4.5) and increased CTCF binding at promoters (Figure 4.6). Integrated ATAC-seq, ChIP-seq, and TRAP-seq analysis suggests that CTCF recruits cofactors to activate genes involved in chromatin organization and replication and inhibit genes in the regulation of cell death (Figure 4.6E-J). On the other hand, loss of HNF4α occupancy at liver enhancers decreases the expression of hepatocyte-enriched genes crucial in establishing liver homeostasis and function (Figure 4.5C-E).

In general, 40% of CTCF binding sites occur in intergenic regions distant to the TSS, while 35% of CTCF sites are found in promoters [30,44]. Interestingly, the vast majority (75%) of sites with increased CTCF occupancy are located within promoters in the repopulating liver (Figure

4.6D). In fact, CTCF can function as a direct transcriptional repressor at the *Myc* promoter [72] and as an activator of the amyloid precursor protein promoter [73], strengthening the notion that CTCF plays a more localized role as a transcriptional regulator in the repopulating liver via recruitment of cofactors. Upregulation of CTCF in liver cancer is associated with poor survival, likely through the activation of forkhead box M1 (FOXM1) to stimulate cell growth and tumor metastasis [74]. The CTCF-FOXM1 axis could be triggered during liver regeneration to promote hepatocyte proliferation [75]. Increased CTCF activity at the *Myc* promoter [76] or decreased CTCF repression at the *Myc* enhancer [77] have both been observed in cancer cells that lead to increased MYC expression. The high tumor mutational burden of CTCF results in abnormal occupancy [78,79], and thus the cofactors and targets of CTCF could be different in the regenerating liver and liver cancer. The multitude of CTCF functions warrants further investigation to understand its contribution to mediating chromatin structure and organization in the context of liver repopulation. Specifically, CTCF also acts as an insulator to block enhancer-promoter interactions [43], a factor that promotes long-range chromatin looping [45], and a TAD boundary protein that defines expression domains for tight transcriptional control [44]. Future experiments to detect changes in chromatin interactions via chromosome conformation capture [80] would be valuable in determining whether differential CTCF occupancy affects three-dimensional chromatin organization during liver repopulation.

The mechanisms of increased CTCF and decreased HNF4α binding in the repopulating liver are also not fully understood. In the current study, we infer that a more open chromatin state at specific promoters correlates with the accessibility of CTCF to its binding sites; however, we have not assessed causality. Previous work found that enrichment of thymidine (T) at the 18th position in the CTCF motif reduces its affinity, where low-affinity sites are more sensitive to loss of CTCF binding during mouse embryonic stem cell differentiation [55]. Additionally, it is likely that changes in DNA methylation influence differential CTCF occupancy, as methylated CpGs in the CTCF recognition site can prevent its binding [81,82]. Demethylation at specific promoter regions could, therefore, increase CTCF occupancy during liver repopulation. In the case of reduced HNF4α occupancy at liver-specific enhancers in the regenerating liver, part of this effect can be

explained by reduced expression of HNF4α itself. Furthermore, HNF4α could be regulated post-transcriptionally via phosphorylation by kinases such as protein kinase A and C, as well as AMP-activated protein kinase to decrease its DNA binding activity or nuclear localization [83]. Activation of the MAPK signaling pathway is also shown to inhibit *Hnf4a* expression via activation of the transcription factor JUN [83,84]. The fact that enrichment of DNA synthesis pathways is only observed in 1-week repopulating livers and that *Hnf4a* transcript level is unchanged in week 1 but reduced in week 4 hepatocytes strengthens the notion that activation of cell growth and proliferation occur early after the initiation of liver repopulation, followed by a later reduction of *Hnf4a* transcription. Future studies using, for instance, targeted degradation of CTCF [85] or HNF4α could be implemented to identify potential promoters and inhibitors of liver repopulation. Technologies such as cDNA [8] or clustered regularly interspaced short palindromic repeats (CRISPR) [86,87] screens could also be utilized to evaluate the effectors downstream of CTCF activation and HNF4α inhibition.

In summary, we propose the following model to explain the transcriptional adaptations that accompany liver repopulation (Figure 4.8): during hepatocyte replication, the promoters of selected genes become more open due to an increased distance between histones at +1 to -1, increasing accessibility for CTCF, transcription factor recruitment, and transcriptional machinery assembly to activate genes that regulate cell cycle, DNA synthesis, and proliferation pathways. On the other hand, decreased enhancer accessibility in conjunction with suppression of *Hnf4a* expression evicts or prevents HNF4α binding, and possibly that of other hepatocyte nuclear factors, to liver enhancers, resulting in repression of hepatocyte metabolic and biosynthetic function genes.

MATERIALS AND METHODS

All primer sequences are listed in Table 4.3.

Plasmid construction

The generation of the pKT2/Fah-Sun1-Gfp//SB plasmid was described previously [15]. The nuclear envelope SUN1-tagged GFP (SUN1-GFP) plasmid was a generous gift from Dr. Jeremy Nathans (Johns Hopkins University, Baltimore, MD, USA). We amplified the SUN1-GFP insert by PCR amplification with the primers MfeI-Sun1-F and BsiW1-Sun1-R and subcloned it into the vector pKT2/Fah-mCa//SB [7] to construct pKT2/Fah-Sun1-Gfp//SB. This construct utilizes the *Sleeping Beauty* (SB) transposase for stable transgene integration into the genome. The plasmid was prepared with the GenElute HP Plasmid Maxiprep Kit (NA0310-1KT, MilliporeSigma) for endotoxin-free maxi-scale DNA extraction and purification.

Mouse studies

Fah$^{-/-}$ mice were maintained on 7.5 mg/l 2-(2-nitro-4-trifluoromethylbenzoyl)-1,3-cyclohexanedione (NTBC) (Swedish Orphan Biovitrum) in the drinking water. Hydrodynamic tail-vein injection [86] of 10 µg of pKT2/Fah-Sun1-Gfp//SB was performed followed by NTBC withdrawal for 1 week (n=2) or 4 weeks (n=2) to induce liver repopulation [15]. The *Rosa*$^{LSL\text{-}Sun1\text{-}GFP}$ mice [19,88] were kindly provided by Dr. Jeremy Nathans (Johns Hopkins University, Baltimore, MD, USA) and were tail-vein injected with AAV8.TBG.PI.Cre.rBG (Penn Vector Core [89]) at 1 x 10^{11} virus particles per mouse to ablate the loxP-stop-loxP cassette only in hepatocytes. Livers from these mice were harvested 1 week after viral injection and served as quiescent controls. All studies were performed in 8 to 12-week-old mice.

Immunofluorescence staining

Liver lobes were isolated, fixed in 4% paraformaldehyde overnight at 4 °C, embedded in paraffin, and sectioned. Tissue sections were deparaffinized with xylene and rehydrated with serial incubation of 100%, 95%, 80%, and 75% ethanol followed by PBS. Antigen retrieval was carried

out in Tris/EDTA buffer (10mM Trix, 1mM EDTA, pH 9.2) in a pressure cooker (2100 Antigen Retriever, Aptum Biologics Ltd.) and cooled to room temperature. Slides were then blocked with blocking buffer (PBS, 1% BSA) for 1 h followed by overnight incubation of antibodies in the blocking buffer at 4 °C in a humidified chamber. Three washes of PBS were carried out the next day followed by incubation with secondary antibodies at room temperature for 2 h. Goat anti-GFP antibody (ab6673, 1:300, Abcam) and rabbit anti-FAH antibody (ab81087, 1:600, Abcam) were used to label repopulating hepatocytes from *Fah*$^{-/-}$ mice after one and four weeks of repopulation and all hepatocytes from *Rosa*$^{LSL\text{-}GFP\text{-}L10a}$ mice injected with AAV8-TBG-Cre. DAPI (B1098, 1:10,000, BioVision) was used to label nuclei.

Hepatocyte nuclei isolation

Liver was homogenized in 10 ml hypotonic buffer (10 mM Tris-HCL, pH 7.5, 2 mM $MgCl_2$, 3 mM $CaCl_2$) on ice. The homogenate was filtered with a 100 µm filter and sedimented at 400 g for 10 min at 4 °C. 10 ml of hypotonic buffer with 10% glycerol was used to resuspend the pellet followed by dropwise addition of 10 ml cell lysis buffer (hypotonic buffer, 10% glycerol, 1% IGEPAL CA-630). The homogenate was incubated for 5 min on ice and sedimented at 600 g for 5 min at 4 °C. Nuclei were washed with lysis buffer again and quantified in a hemocytometer. Isolated nuclei were labeled with an Alexa Fluor 647 anti-GFP antibody (338006, clone FM264G, 1:25, BioLegend, San Diego, CA) for 30 min and 2 µg/ml DAPI immediately prior to sorting. After gating for the DAPI-positive signal, nuclei double-positive for GFP and AF647 were sorted with a BD FACSAria II, and only tetraploid hepatocyte nuclei were collected for further experiments.

ATAC-seq library generation

ATAC-seq libraries were generated as previously described [20]. Briefly, transposition was performed on 25,000 sorted tetraploid nuclei at 37 °C for 30 min followed by DNA purification with the MinElute Reaction Cleanup Kit (28206, QIAGEN). DNA fragments were PCR preamplified for 5 cycles initially, and 1/10 of the volume (5 µl) was removed for qPCR amplification for 20 cycles.

A ‘R vs Cycle Number’ plot was generated and the number of cycles required to reach ⅓ of the maximum R determined for each sample. The preamplified ATAC-seq libraries were then amplified for the calculated additional cycles. Agencourt AMPure XP beads (A63881, Beckman Coulter) were used for size selection to generate the final libraries [90]. Library quality was assessed with an Agilent High Sensitivity DNA Bioanalyzer (5067-4626, Agilent Technologies), and quantity measured with KAPA Library Quantification Kits (KK4835, KAPA Biosystems).

ATAC-seq peak calling

ATAC-seq libraries were paired-end sequenced on an Illumina HiSeq 4000 (Illumina, San Diego, CA, USA) with 50, 75, or 100 reads. Reads were then trimmed to 50 bp with Cutadapt [91] and peaks called with the ATAC-Seq/DNase-Seq pipeline [92]. Briefly, the trimmed fastq files were aligned to the mouse genome (mm10) with Bowtie2 [93] followed by removal of PCR duplicates and mitochondrial reads. Bam files of the same biological sample from various technical replicates were then merged with Samtools [94] and duplicated reads removed. The filtered reads were shifted 5 bp for + strands and 4 bp for - strands to adjust for the transposase binding sites [20]. Nucleosome-free reads were identified with the R package ATACseqQC using a random forest classifier [95] followed by peak calling with MACS2 [96]. Artifact signals were then removed according to the mm10 empirical blacklist regions [97]. The irreproducible discovery rate (IDR) framework was used to compare all pairs of biological replicates to identify reproducible peaks that passed a threshold of 10% for all pairwise analyses. The conservative peak set for each sample was identified by selecting the longest peak list from all pairs that passed the 10% IDR cutoff.

ATAC-seq peak quality assessment

To ensure the ATAC-seq peaks generated from the sorted nuclei are of high quality, The R package ATACseqQC [95] was employed for assessment. We first visualized the insert size distribution to confirm the presence of distinct periodicity of ~175 bp associated with nucleosome patterning in all samples, indicating the DNA fragments are protected by integer multiples of

nucleosomes [20]. The signal intensity of nucleosome-free reads and nucleosomal reads was also averaged across all TSS to examine evidence that no over-fragmentation was introduced during hepatocyte nuclei isolation, sorting, or ATAC-seq library preparation.

ATAC-seq differential peak analysis

The R package ATACseqQC [95] was used to split the aligned bam files into nucleosome-free reads and nucleosomal reads. The R package DiffBind [98] was used to identify differential accessible peaks from the nucleosome-free reads. The overlapping regions from the ATAC-seq peak sets for each sample were identified and merged into non-overlapping regions. Read counts for each region were quantified with dba.count (score=DBA_SCORE_TMM_READS_FULL, fragmentSize=0, bScaleControl=F, filter=0, bRemoveDuplicates=F, bUseSummarizeOverlaps=T). Peaks identified in both biological replicates in the same conditions were used for differential analysis with dba.analyze (method=DBA_EDGER, bSubControl=F, bTagwise=T) in conjunction with edgeR [99]. Peaks with an absolute fold change ≥1.5 and FDR ≤0.05 were identified as significant differentially accessible regions.

Integrative analysis of TRAP-seq and ATAC-seq data

To identify chromatin accessibility and gene expression that changed in the same direction at the same time point (‘concordant genes’), the differentially accessible peaks were first annotated to the nearest TSS with the R package ChIPseeker [100]. Genes with differential expression during liver repopulation were obtained from a previous study that utilized translating-ribosome affinity purification followed by RNA-sequencing (TRAP-seq) [15]. The concordant ATAC-seq peaks and TRAP-seq genes were identified and the expected overlap and significance was calculated with a hypergeometric test. To evaluate the association of chromatin accessibility and gene expression changes, all chromatin regions were stratified into regions with increased, decreased, or unchanged accessibility, with the cutoff of an absolute fold change ≥1.5 and FDR ≤0.05. For promoter accessibility and gene activity association analysis, regions within 1 kb up- and

downstream of the TSS were identified and annotated to the nearest genes with the R package ChIPseeker [100]. The corresponding expression change at the same time point was extracted from TRAP-seq [15] and normalized by subtracting the mean $\log_2$ fold change of the unchanged from the increased and decreased chromatin accessibility groups. The normalized expression fold change of the nearest genes in the differentially accessible promoters was compared to that in the unchanged accessibility promoters with a one-sample t-test. For enhancer accessibility and gene expression association studies, liver- and cerebellum-specific enhancers and their putative targets were obtained from a previous study [30]. Briefly, regions with the presence of H3K4me1 but the absence of H3K4me3 ChIP-seq peaks were identified as putative enhancers and refined with a chromatin-signature based enhancer predictor. Enhancer-promoter units were identified by calculating the correlation of H3K4me1 and RNA polymerase II ChIP-seq peak strength along each chromosome. All possible promoter and enhancer pairs with a >0.23 Spearman correlation coefficient were identified as linked enhancer-promoter units. Gene expression fold changes were normalized as described above, and the normalized gene expression fold-change of the enhancer target genes in the differentially accessible enhancers was compared to that in the unchanged accessibility enhancers with a one-sample t-test.

Transcription factor motif enrichment analysis

ATAC-seq peaks are separated into promoter and liver enhancer [30] regions and Homer [101] is used to identify enrichment of *de novo* motifs with the function findMotifsGenome.pl (mm10 -size given). Motifs with a p-value of lower than 1E-12 are considered significant to reduce the number of false positives. FDR is also calculated with each significant motif. To ensure the identified motifs are enriched in ATAC-seq peaks with different accessibility, motif frequency surrounding 500 up- and downstream of the peak center from all identified IDR peaks in quiescent hepatocytes and differentially accessible regions in repopulating cells is extracted. The difference in motif frequency distribution of regenerating and quiescent samples was then calculated with a Kolmogorov-Smirnov test.

ChIP-seq library generation

100 mg of quiescent (n=2) and repopulating (n=2) liver tissue was finely chopped with a razor blade and cross-linked in 1% formaldehyde for 10 min followed by addition of 2.5 M glycine and incubation for 5 min at room temperature. Tissues were sedimented, washed with cold PBS, and Dounce-homogenized in cold ChIP cell lysis buffer (10 mM Tris-HCl pH 8.0, 10 mM NaCl, 3 mM MgCl2, 0.5% IGEPAL CA-630, protease inhibitor) on ice. After incubation at 4 °C for 5 min, nuclei were pelleted and resuspended in nuclear lysis buffer (50 mM Tris-HCl pH 8.1, 1% SDS, 5 mM EDTA, protease inhibitor). Nuclei were sonicated with a Bioruptor (Diagenode) for 2 rounds of 7.5 min each. 10 µg of sheared DNA was incubated with anti-CTCF (2 µg, 07-729, Millipore) or anti-HNF4α (2 µg, ab181604, Abcam) antibodies in dilution buffer (16.7 mM Tris-HCl pH 8.1, 167 mM NaCl, 0.01% SDS, 1.1% Triton-X 100, protease inhibitor) at 4 °C overnight. Protein-A agarose beads were also washed with cold dilution buffer three times and incubated with blocking buffer (10 mg/ml BSA, ChIP dilution buffer, protease inhibitor) at 4 °C overnight. Sheared DNA incubated with antibody and blocked protein-A agarose were incubated at 4 °C for 1 h the next day and washed at room temperature with buffers TSEI (20 mM Tris-HCl pH 8.1, 150 mM NaCl, 2 mM EDTA, 0.1% SDS, 1% Triton X-100), TSE II (20 mM Tris-HCl pH 8.1, 500 mM NaCl, 2 mM EDTA, 0.1% SDS, 1% Triton X-100), ChIP buffer III (10 mM Tris-HCl pH 8.1, 0.25M LiCl, 1 mM EDTA, 1% NP-40, 1% deoxycholate), and TE (10 mM Tris-HCl pH 8.1, 1 mM EDTA). Chromatin was eluted with elution buffer (1% SDS, 0.1 M $NaHCO_3$) twice and incubated with 0.2 M NaCl at 65 °C overnight to reverse the cross-links. Digestion was carried out with 10 mg/ml proteinase K in 40 mM Tris-HCl pH 7.5 and 10 mM EDTA to purify CTCF- or HNF4α-bound and input DNA. ChIP-seq libraries were prepared with the NEBNext Ultra II DNA Library Prep Kit for Illumina (E7645S, New England BioLabs) and Agencourt AMPure XP beads were used for size selection to generate the final libraries. Library quality was assessed with an Agilent High Sensitivity DNA Bioanalyzer (5067-4626, Agilent Technologies), and quantity measured with KAPA Library Quantification Kits (KK4835, KAPA Biosystems).

ChIP-seq data analysis

ChIP-seq libraries were sequenced on an Illumina HiSeq 4000 (Illumina) with 100 single-end reads and aligned to the mm10 genome with STAR [102]. Bam files from various technical replicates of the same biological sample were merged with Samtools [94]. Peak calling was performed with Homer [101] and differential occupancy analysis was carried out with the R package DiffBind [98]. Read counts for each peak were quantified with dba.count (score=DBA_SCORE_TMM_MINUS_FULL, bUseSummarizeOverlaps=TRUE) and differential analysis were identified with dba.analyze (method=DBA_EDGER, bSubControl=T, bTagwise=F) in conjunction with edgeR [99].

ChIP-qPCR

ChIP was performed with 5 µg of anti-ZBTB3 (ab106536, Abcam) and 2 µg of YY1 (ab109237, Abcam) antibodies with 10 µg of sheared DNA from quiescent and 4-week repopulating livers as described above. Input and immunoprecipitated DNA were purified with phenol-chloroform extraction followed by qPCR with primer sets ZBTB3-ChIP-Ctnna2-qPCR-F1 and -R1, ZBTB3-ChIP-Smad3-qPCR-F1 and -R1, YY1-ChIP-Bcl2l11-qPCR-F1 and -R1, YY1-ChIP-Igf2r-qPCR-F1 and -R1, and 40S-F2 and -R2.

CTCF differential expression insulator analysis

Increased CTCF occupancy during liver repopulation could prevent distal regulatory regions to activate only one of the flanking promoters surrounding a CTCF binding site, and therefore leading to a larger difference in gene expression levels. We define this ‘differential expression insulator’ function, in which a gene pair is either highly or lowly expressed without the presence of CTCF, but only one flanking gene exhibits a decrease in gene expression after binding of CTCF. An insulator strength score was calculated for all significantly gained (fold change ≥1.5, FDR ≤0.05) CTCF peaks in the repopulating liver as previously described [55]. Briefly, CTCF sites with divergent flanking promoters within 50 kb were identified and the corresponding gene

expression levels from quiescent and 4-week repopulating hepatocytes were extracted from published TRAP-seq [15].

Low-expressors, in which RPKM-normalized read counts are 0 across all samples, were filtered followed by calculation of a rank percentile based on RPKM for each gene. Let $x_Q$and $y_Q$be the expression percentile in the quiescent hepatocytes; $x_R$and $y_R$be the expression percentile in the 4-week repopulating hepatocytes. The insulator strength score is calculated by taking the maximum value of $x_Q \times y_Q \times x_R \times (1 - y_R)$ and $x_Q \times y_Q \times (1 - x_R) \times y_R$. A differential expression insulator function will have one of the following effects: (1) Increased $x_R$and decreased y_R: in this case, $x_Q \times y_Q \times x_R \times (1 - y_R)$ will be the largest. (2) Decreased $x_R$and increased y_R: in this case, $x_Q \times y_Q \times (1 - x_R) \times y_R$ will be the largest. Gained CTCF sites with the top 25% insulator strength scores were categorized as strong insulators. Random gene pairs not flanked by CTCF within 50 kb were used as controls and a differential expression insulator score for each gene pair was calculated as described above. The number of significant (FDR≤0.05) and non-significant (FDR>0.05) differential expression of the flanking genes were identified for all strong insulators from increased CTCF binding and random genomic regions. Finally, we used Fisher's exact test to examine the likelihood of gained CTCF sites to contain more significantly changed genes when compared to that of control regions.

Nucleosome location analysis with ATAC-seq

MAC2 (callpeak --keep-dup all, -B --SPMR, -q 0.05, --broad) [96] was used to identify broad peaks from all aligned bam files including nucleosome-free reads and nucleosome-containing reads from ATAC-seq. Broad peaks were then processed with BEDtools [103] to extend the peaks (bedtools slop -b 200), sorted by genomic positions (sort -k1,1 -k2,2n), and overlapping reads were merged (bedtools merge). Nucleosome position was identified with NucleoATAC [104] from the aligned bam and broad peak files. The closest nucleosomes with respect to TSS were identified, and those within 350 bp upstream and 250 bp downstream of the TSS were identified as the -1 and +1 nucleosomes, respectively.

Nucleosome positioning analysis

The distance of +1 to -1 nucleosomes was calculated for each transcript. We used the Kolmogorov-Smirnov test to compare the +1 and -1 nucleosome distribution differences between quiescent and repopulating hepatocytes, respectively. To analyze the association between gene activity and nucleosome positioning, transcriptomic changes in repopulating hepatocytes [15] were first stratified into three categories: top 500 upregulated (fold change ≥1.5, FDR ≤0.05), top 500 downregulated (fold change ≥1.5, FDR ≤0.05), and unchanged (absolute fold change <1.5 or FDR >0.05) genes. The distances between the +1 to -1 nucleosomes were calculated for each gene and differential positioning was carried out by comparing the distance in quiescent to regenerating hepatocytes in the upregulated, downregulated, and unchanged gene expression groups, respectively, with a permutation test (n=10,000).

Statistical analysis

EdgeR [99] was used for all high-throughput sequencing data analysis. For the integrative TRAP-seq and ATAC-seq analysis, a hypergeometric test was used for identifying the significance of overlapping gene sets, and a one-sample t-test was used to compare the difference between normalized gene expression fold change in differentially accessible promoter and enhancer regions, respectively. A Kolmogorov-Smirnov test was performed for global distribution change of +1 and -1 nucleosome positioning and a permutation test (n=10,000) was carried out to test the change in +1 to -1 nucleosome distance of genes with differential expression.

Study approval

The animal experiments carried out in this study were reviewed and approved by the IACUC of the Penn Office of Animal Welfare at the University of Pennsylvania.

REFERENCES

1. Trefts E, Gannon M, Wasserman DH. The liver. Curr Biol. 2017;27: R1147–R1151.
2. Michalopoulos GK, DeFrances MC. Liver regeneration. Science. 1997;276: 60–66.
3. Lee WM. Etiologies of Acute Liver Failure. Semin Liver Dis. 2008;28: 142–152.
4. Grompe M, al-Dhalimy M, Finegold M, Ou CN, Burlingame T, Kennaway NG, et al. Loss of fumarylacetoacetate hydrolase is responsible for the neonatal hepatic dysfunction phenotype of lethal albino mice. Genes Dev. 1993;7: 2298–2307.
5. Russo PA, Mitchell GA, Tanguay RM. Tyrosinemia: A Review. Pediatric and Developmental Pathology. 2001;3: 212–221.
6. Overturf K, Al-Dhalimy M, Tanguay R, Brantly M, Ou C-N, Finegold M, et al. Hepatocytes corrected by gene therapy are selected in vivo in a murine model of hereditary tyrosinaemia type I. Nature Genetics. 1996;3: 266–273.
7. Wangensteen KJ, Wilber A, Keng VW, He Z, Matise I, Wangensteen L, et al. A facile method for somatic, lifelong manipulation of multiple genes in the mouse liver. Hepatology. 2008;47: 1714–1724.
8. Wangensteen KJ, Zhang S, Greenbaum LE, Kaestner KH. A genetic screen reveals Foxa3 and TNFR1 as key regulators of liver repopulation. Genes Dev. 2015;29: 904–909.
9. Lee TI, Young RA. Transcriptional Regulation and Its Misregulation in Disease. Cell. 2013;152: 1237–1251.
10. Lelli KM, Slattery M, Mann RS. Disentangling the many layers of eukaryotic transcriptional regulation. Annu Rev Genet. 2012;46: 43–68.
11. Su AI, Guidotti LG, Pezacki JP, Chisari FV, Schultz PG. Gene expression during the priming phase of liver regeneration after partial hepatectomy in mice. Proc Natl Acad Sci U S A. 2002;99: 11181–11186.
12. White P, Brestelli JE, Kaestner KH, Greenbaum LE. Identification of transcriptional networks during liver regeneration. J Biol Chem. 2005;280: 3715–3722.
13. Yang D, Liu Q, Yang M, Wu H, Wang Q, Xiao J, et al. RNA-seq liver transcriptome analysis reveals an activated MHC-I pathway and an inhibited MHC-II pathway at the early stage of vaccine immunization in zebrafish. BMC Genomics. 2012;13: 319.
14. Min JS, DeAngelis RA, Reis ES, Gupta S, Maurya MR, Evans C, et al. Systems Analysis of the Complement-Induced Priming Phase of Liver Regeneration. J Immunol. 2016;197: 2500–2508.
15. Wang AW, Wangensteen KJ, Wang YJ, Zahm AM, Moss NG, Erez N, et al. TRAP-seq identifies cystine/glutamate antiporter as a driver of recovery from liver injury. J Clin Invest. 2018;128: 2297–2309.
16. Huang J, Schriefer AE, Yang W, Cliften PF, Rudnick DA. Identification of an epigenetic signature of early mouse liver regeneration that is disrupted by Zn-HDAC inhibition. Epigenetics. 2014;9: 1521–1531.
17. Sato Y, Katoh Y, Matsumoto M, Sato M, Ebina M, Itoh-Nakadai A, et al. Regulatory signatures of liver regeneration distilled by integrative analysis of mRNA, histone methylation, and proteomics. J Biol Chem. 2017;292: 8019–8037.
18. Heiman M, Kulicke R, Fenster RJ, Greengard P, Heintz N. Cell type-specific mRNA purification by translating ribosome affinity purification (TRAP). Nat Protoc. 2014;9: 1282–1291.
19. Mo A, Mukamel EA, Davis FP, Luo C, Henry GL, Picard S, et al. Epigenomic Signatures of Neuronal Diversity in the Mammalian Brain. Neuron. 2015;86: 1369–1384.
20. Buenrostro JD, Giresi PG, Zaba LC, Chang HY, Greenleaf WJ. Transposition of native chromatin for fast and sensitive epigenomic profiling of open chromatin, DNA-binding proteins and nucleosome position. Nat Methods. 2013;10: 1213–1218.
21. Shin S, Wangensteen KJ, Teta-Bissett M, Wang YJ, Mosleh-Shirazi E, Buza EL, et al. Genetic lineage tracing analysis of the cell of origin of hepatotoxin-induced liver tumors in mice. Hepatology. 2016;64: 1163–1177.

22. Bell JB, Podetz-Pedersen KM, Aronovich EL, Belur LR, McIvor RS, Hackett PB. Preferential delivery of the Sleeping Beauty transposon system to livers of mice by hydrodynamic injection. Nat Protoc. 2007;2: 3153–3165.
23. Aronovich EL, McIvor RS, Hackett PB. The Sleeping Beauty transposon system: a non-viral vector for gene therapy. Hum Mol Genet. 2011;20: R14–20.
24. Garrison BS, Yant SR, Mikkelsen JG, Kay MA. Postintegrative gene silencing within the Sleeping Beauty transposition system. Mol Cell Biol. 2007;27: 8824–8833.
25. Kanehisa M, Sato Y, Kawashima M, Furumichi M, Tanabe M. KEGG as a reference resource for gene and protein annotation. Nucleic Acids Res. 2016;44: D457–62.
26. Zhang W, Liu HT. MAPK signal pathways in the regulation of cell proliferation in mammalian cells. Cell Res. 2002;12: 9–18.
27. Weglarz TC, Sandgren EP. Timing of hepatocyte entry into DNA synthesis after partial hepatectomy is cell autonomous. Proc Natl Acad Sci U S A. 2000;97: 12595–12600.
28. Huang ZZ, Li H, Cai J, Kuhlenkamp J, Kaplowitz N, Lu SC. Changes in glutathione homeostasis during liver regeneration in the rat. Hepatology. 1998;27: 147–153.
29. Riehle KJ, Haque J, McMahan RS, Kavanagh TJ, Fausto N, Campbell JS. Sustained Glutathione Deficiency Interferes with the Liver Response to TNF-α and Liver Regeneration after Partial Hepatectomy in Mice. J Liver Disease Transplant. 2013;1. Available: https://www.ncbi.nlm.nih.gov/pubmed/24611135
30. Shen Y, Yue F, McCleary DF, Ye Z, Edsall L, Kuan S, et al. A map of the cis-regulatory sequences in the mouse genome. Nature. 2012;488: 116–120.
31. Park K, Atchison ML. Isolation of a candidate repressor/activator, NF-E1 (YY-1, delta), that binds to the immunoglobulin kappa 3' enhancer and the immunoglobulin heavy-chain mu E1 site. Proc Natl Acad Sci U S A. 1991;88: 9804–9808.
32. Walton KM, Rehfuss RP, Chrivia JC, Lochner JE, Goodman RH. A dominant repressor of cyclic adenosine 3',5'-monophosphate (cAMP)-regulated enhancer-binding protein activity inhibits the cAMP-mediated induction of the somatostatin promoter in vivo. Mol Endocrinol. 1992;6: 647–655.
33. Spitz F, Furlong EEM. Transcription factors: from enhancer binding to developmental control. Nat Rev Genet. 2012;13: 613–626.
34. Daugherty AC, Yeo RW, Buenrostro JD, Greenleaf WJ, Kundaje A, Brunet A. Chromatin accessibility dynamics reveal novel functional enhancers in. Genome Res. 2017;27: 2096–2107.
35. Li M, Hada A, Sen P, Olufemi L, Hall MA, Smith BY, et al. Dynamic regulation of transcription factors by nucleosome remodeling. Elife. 2015;4. doi:10.7554/eLife.06249
36. Ballaré C, Castellano G, Gaveglia L, Althammer S, González-Vallinas J, Eyras E, et al. Nucleosome-driven transcription factor binding and gene regulation. Mol Cell. 2013;49: 67–79.
37. Strenkert D, Schmollinger S, Sommer F, Schulz-Raffelt M, Schroda M. Transcription factor-dependent chromatin remodeling at heat shock and copper-responsive promoters in Chlamydomonas reinhardtii. Plant Cell. 2011;23: 2285–2301.
38. Besnard A, Galan-Rodriguez B, Vanhoutte P, Caboche J. Elk-1 a transcription factor with multiple facets in the brain. Front Neurosci. 2011;5: 35.
39. Boros J, Donaldson IJ, O'Donnell A, Odrowaz ZA, Zeef L, Lupien M, et al. Elucidation of the ELK1 target gene network reveals a role in the coordinate regulation of core components of the gene regulation machinery. Genome Res. 2009;19: 1963–1973.
40. Wuestefeld T, Pesic M, Rudalska R, Dauch D, Longerich T, Kang T-W, et al. A Direct in vivo RNAi screen identifies MKK4 as a key regulator of liver regeneration. Cell. 2013;153: 389–401.
41. Klenova EM, Nicolas RH, Paterson HF, Carne AF, Heath CM, Goodwin GH, et al. CTCF, a conserved nuclear factor required for optimal transcriptional activity of the chicken c-myc gene, is an 11-Zn-finger protein differentially expressed in multiple forms. Mol Cell Biol. 1993;13: 7612–7624.

42. Lobanenkov VV, Nicolas RH, Adler VV, Paterson H, Klenova EM, Polotskaja AV, et al. A novel sequence-specific DNA binding protein which interacts with three regularly spaced direct repeats of the CCCTC-motif in the 5'-flanking sequence of the chicken c-myc gene. Oncogene. 1990;5: 1743–1753.
43. Bell AC, West AG, Felsenfeld G. The protein CTCF is required for the enhancer blocking activity of vertebrate insulators. Cell. 1999;98: 387–396.
44. Dixon JR, Selvaraj S, Yue F, Kim A, Li Y, Shen Y, et al. Topological domains in mammalian genomes identified by analysis of chromatin interactions. Nature. 2012;485: 376–380.
45. Splinter E, Heath H, Kooren J, Palstra R-J, Klous P, Grosveld F, et al. CTCF mediates long-range chromatin looping and local histone modification in the beta-globin locus. Genes Dev. 2006;20: 2349–2354.
46. Shukla S, Kavak E, Gregory M, Imashimizu M, Shutinoski B, Kashlev M, et al. CTCF-promoted RNA polymerase II pausing links DNA methylation to splicing. Nature. 2011;479: 74–79.
47. Xu D, Yang F, Yuan J-H, Zhang L, Bi H-S, Zhou C-C, et al. Long noncoding RNAs associated with liver regeneration 1 accelerates hepatocyte proliferation during liver regeneration by activating Wnt/β-catenin signaling. Hepatology. 2013;58: 739–751.
48. Sladek FM, Zhong WM, Lai E, Darnell JE. Liver-enriched transcription factor HNF-4 is a novel member of the steroid hormone receptor superfamily. Genes Dev. 1990;4: 2353–2365.
49. Duncan SA, Manova K, Chen WS, Hoodless P, Weinstein DC, Bachvarova RF, et al. Expression of transcription factor HNF-4 in the extraembryonic endoderm, gut, and nephrogenic tissue of the developing mouse embryo: HNF-4 is a marker for primary endoderm in the implanting blastocyst. Proceedings of the National Academy of Sciences. 1994;91: 7598–7602.
50. Babeu J-P, Boudreau F. Hepatocyte nuclear factor 4-alpha involvement in liver and intestinal inflammatory networks. World J Gastroenterol. 2014;20: 22–30.
51. Bonzo JA, Ferry CH, Matsubara T, Kim J-H, Gonzalez FJ. Suppression of hepatocyte proliferation by hepatocyte nuclear factor 4α in adult mice. J Biol Chem. 2012;287: 7345–7356.
52. Walesky C, Gunewardena S, Terwilliger EF, Edwards G, Borude P, Apte U. Hepatocyte-specific deletion of hepatocyte nuclear factor-4α in adult mice results in increased hepatocyte proliferation. American Journal of Physiology-Gastrointestinal and Liver Physiology. 2013;1: G26–G37.
53. Schrem H, Klempnauer J, Borlak J. Liver-enriched transcription factors in liver function and development. Part I: the hepatocyte nuclear factor network and liver-specific gene expression. Pharmacol Rev. 2002;54: 129–158.
54. O'Leary NA, Wright MW, Brister JR, Ciufo S, Haddad D, McVeigh R, et al. Reference sequence (RefSeq) database at NCBI: current status, taxonomic expansion, and functional annotation. Nucleic Acids Res. 2016;44: D733–45.
55. Plasschaert RN, Vigneau S, Tempera I, Gupta R, Maksimoska J, Everett L, et al. CTCF binding site sequence differences are associated with unique regulatory and functional trends during embryonic stem cell differentiation. Nucleic Acids Res. 2014;42: 774–789.
56. Ashburner M, Ball CA, Blake JA, Botstein D, Butler H, Cherry JM, et al. Gene ontology: tool for the unification of biology. The Gene Ontology Consortium. Nat Genet. 2000;25: 25–29.
57. Zlatanova J, Caiafa P. CTCF and its protein partners: divide and rule? J Cell Sci. 2009;122: 1275–1284.
58. Boyle AP, Song L, Lee B-K, London D, Keefe D, Birney E, et al. High-resolution genome-wide in vivo footprinting of diverse transcription factors in human cells. Genome Res. 2011;21: 456–464.
59. Lim J-H. Zinc finger and BTB domain-containing protein 3 is essential for the growth of cancer cells. BMB Rep. 2014;47: 405–410.
60. Dolfini D, Gatta R, Mantovani R. NF-Y and the transcriptional activation of CCAAT promoters. Crit Rev Biochem Mol Biol. 2012;47: 29–49.

61. Bhattacharya A, Deng JM, Zhang Z, Behringer R, de Crombrugghe B, Maity SN. The B subunit of the CCAAT box binding transcription factor complex (CBF/NF-Y) is essential for early mouse development and cell proliferation. Cancer Res. 2003;63: 8167–8172.
62. Oldfield AJ, Yang P, Conway AE, Cinghu S, Freudenberg JM, Yellaboina S, et al. Histone-fold domain protein NF-Y promotes chromatin accessibility for cell type-specific master transcription factors. Mol Cell. 2014;55: 708–722.
63. Donohoe ME, Zhang X, McGinnis L, Biggers J, Li E, Shi Y. Targeted disruption of mouse Yin Yang 1 transcription factor results in peri-implantation lethality. Mol Cell Biol. 1999;19: 7237–7244.
64. Kurisaki K, Kurisaki A, Valcourt U, Terentiev AA, Pardali K, Ten Dijke P, et al. Nuclear factor YY1 inhibits transforming growth factor beta- and bone morphogenetic protein-induced cell differentiation. Mol Cell Biol. 2003;23: 4494–4510.
65. Weintraub AS, Li CH, Zamudio AV, Sigova AA, Hannett NM, Day DS, et al. YY1 Is a Structural Regulator of Enhancer-Promoter Loops. Cell. 2017;171: 1573–1588.e28.
66. Atchison L, Ghias A, Wilkinson F, Bonini N, Atchison ML. Transcription factor YY1 functions as a PcG protein in vivo. EMBO J. 2003;22: 1347–1358.
67. Wilkinson FH, Park K, Atchison ML. Polycomb recruitment to DNA in vivo by the YY1 REPO domain. Proc Natl Acad Sci U S A. 2006;103: 19296–19301.
68. Donohoe ME, Zhang L-F, Xu N, Shi Y, Lee JT. Identification of a Ctcf Cofactor, Yy1, for the X Chromosome Binary Switch. Molecular Cell. 2007;1: 43–56.
69. Bai L, Morozov AV. Gene regulation by nucleosome positioning. Trends in Genetics. 2010;11: 476–483.
70. Shivaswamy S, Bhinge A, Zhao Y, Jones S, Hirst M, Iyer VR. Dynamic remodeling of individual nucleosomes across a eukaryotic genome in response to transcriptional perturbation. PLoS Biol. 2008;6: e65.
71. Svaren J, Hörz W. Transcription factors vs nucleosomes: regulation of the PHO5 promoter in yeast. Trends Biochem Sci. 1997;22: 93–97.
72. Filippova GN, Fagerlie S, Klenova EM, Myers C, Dehner Y, Goodwin G, et al. An exceptionally conserved transcriptional repressor, CTCF, employs different combinations of zinc fingers to bind diverged promoter sequences of avian and mammalian c-myc oncogenes. Mol Cell Biol. 1996;16: 2802–2813.
73. Yang Y, Quitschke WW, Vostrov AA, Brewer GJ. CTCF is essential for up-regulating expression from the amyloid precursor protein promoter during differentiation of primary hippocampal neurons. J Neurochem. 1999;73: 2286–2298.
74. Zhang B, Zhang Y, Zou X, Chan AW, Zhang R, Lee TK-W, et al. The CCCTC-binding factor (CTCF)-forkhead box protein M1 axis regulates tumour growth and metastasis in hepatocellular carcinoma. J Pathol. 2017;243: 418–430.
75. Xiang D, Liu C-C, Wang M-J, Li J-X, Chen F, Yao H, et al. Non-viral FoxM1 gene delivery to hepatocytes enhances liver repopulation. Cell Death Dis. 2014;5: e1252.
76. Pu H, Zheng Q, Li H, Wu M, An J, Gui X, et al. CUDR promotes liver cancer stem cell growth through upregulating TERT and C-Myc. Oncotarget. 2015;6: 40775–40798.
77. Schuijers J, Manteiga JC, Weintraub AS, Day DS, Zamudio AV, Hnisz D, et al. Transcriptional Dysregulation of MYC Reveals Common Enhancer-Docking Mechanism. Cell Rep. 2018;23: 349–360.
78. Fujimoto A, Furuta M, Totoki Y, Tsunoda T, Kato M, Shiraishi Y, et al. Whole-genome mutational landscape and characterization of noncoding and structural mutations in liver cancer. Nat Genet. 2016;48: 500–509.
79. Umer HM, Cavalli M, Dabrowski MJ, Diamanti K, Kruczyk M, Pan G, et al. A Significant Regulatory Mutation Burden at a High-Affinity Position of the CTCF Motif in Gastrointestinal Cancers. Hum Mutat. 2016;37: 904–913.
80. Belton J-M, McCord RP, Gibcus JH, Naumova N, Zhan Y, Dekker J. Hi-C: a comprehensive technique to capture the conformation of genomes. Methods. 2012;58: 268–276.
81. Bell AC, Felsenfeld G. Methylation of a CTCF-dependent boundary controls imprinted expression of the Igf2 gene. Nature. 2000;405: 482–485.

82. Wang H, Maurano MT, Qu H, Varley KE, Gertz J, Pauli F, et al. Widespread plasticity in CTCF occupancy linked to DNA methylation. Genome Res. 2012;22: 1680–1688.
83. Vető B, Bojcsuk D, Bacquet C, Kiss J, Sipeki S, Martin L, et al. The transcriptional activity of hepatocyte nuclear factor 4 alpha is inhibited via phosphorylation by ERK1/2. PLoS One. 2017;12: e0172020.
84. Simó R, Barbosa-Desongles A, Hernandez C, Selva DM. IL1β down-regulation of sex hormone-binding globulin production by decreasing HNF-4α via MEK-1/2 and JNK MAPK pathways. Mol Endocrinol. 2012;26: 1917–1927.
85. Nora EP, Goloborodko A, Valton A-L, Gibcus JH, Uebersohn A, Abdennur N, et al. Targeted Degradation of CTCF Decouples Local Insulation of Chromosome Domains from Genomic Compartmentalization. Cell. 2017;169: 930–944.e22.
86. Wangensteen KJ, Wang YJ, Dou Z, Wang AW, Mosleh-Shirazi E, Horlbeck MA, et al. Combinatorial genetics in liver repopulation and carcinogenesis with a novel in vivo CRISPR activation platform. Hepatology. 2017; doi:10.1002/hep.29626
87. Kieckhaefer JE, Maina F, Wells RG, Wangensteen KJ. Liver Cancer Gene Discovery Using Gene Targeting, Sleeping Beauty, and CRISPR/Cas9. Semin Liver Dis. 2019;39: 261–274.
88. Luo C, Keown CL, Kurihara L, Zhou J, He Y, Li J, et al. Single-cell methylomes identify neuronal subtypes and regulatory elements in mammalian cortex. Science. 2017;357: 600–604.
89. University of Pennsylvania Gene Therapy Program. Vector Core [Internet]. [cited 25 Aug 2019]. Available: http://gtp.med.upenn.edu/core-laboratories-public/vector-core
90. Ackermann AM, Wang Z, Schug J, Naji A, Kaestner KH. Integration of ATAC-seq and RNA-seq identifies human alpha cell and beta cell signature genes. Mol Metab. 2016;5: 233–244.
91. Martin M. Cutadapt removes adapter sequences from high-throughput sequencing reads. EMBnet.journal. 2011;17: 10.
92. Kundaje Lab. atac_dnase_pipelines. In: GitHub [Internet]. [cited 25 Aug 2019]. Available: https://github.com/kundajelab/atac_dnase_pipelines
93. Langmead B, Salzberg SL. Fast gapped-read alignment with Bowtie 2. Nat Methods. 2012;9: 357–359.
94. Li H, Handsaker B, Wysoker A, Fennell T, Ruan J, Homer N, et al. The Sequence Alignment/Map format and SAMtools. Bioinformatics. 2009;25: 2078–2079.
95. Ou J, Liu H, Yu J, Kelliher MA, Castilla LH, Lawson ND, et al. ATACseqQC: a Bioconductor package for post-alignment quality assessment of ATAC-seq data. BMC Genomics. 2018;19: 169.
96. Zhang Y, Liu T, Meyer CA, Eeckhoute J, Johnson DS, Bernstein BE, et al. Model-based analysis of ChIP-Seq (MACS). Genome Biol. 2008;9: R137.
97. ENCODE Project Consortium. An integrated encyclopedia of DNA elements in the human genome. Nature. 2012;489: 57–74.
98. Ross-Innes CS, Stark R, Teschendorff AE, Holmes KA, Ali HR, Dunning MJ, et al. Differential oestrogen receptor binding is associated with clinical outcome in breast cancer. Nature. 2012;481: 389–393.
99. Robinson MD, McCarthy DJ, Smyth GK. edgeR: a Bioconductor package for differential expression analysis of digital gene expression data. Bioinformatics. 2010;26: 139–140.
100. Yu G, Wang L-G, He Q-Y. ChIPseeker: an R/Bioconductor package for ChIP peak annotation, comparison and visualization. Bioinformatics. 2015;31: 2382–2383.
101. Heinz S, Benner C, Spann N, Bertolino E, Lin YC, Laslo P, et al. Simple combinations of lineage-determining transcription factors prime cis-regulatory elements required for macrophage and B cell identities. Mol Cell. 2010;38: 576–589.
102. Dobin A, Davis CA, Schlesinger F, Drenkow J, Zaleski C, Jha S, et al. STAR: ultrafast universal RNA-seq aligner. Bioinformatics. 2013;29: 15–21.
103. Quinlan AR, Hall IM. BEDTools: a flexible suite of utilities for comparing genomic features. Bioinformatics. 2010;26: 841–842.

104. Schep AN, Buenrostro JD, Denny SK, Schwartz K, Sherlock G, Greenleaf WJ. Structured nucleosome fingerprints enable high-resolution mapping of chromatin architecture within regulatory regions. Genome Res. 2015;25: 1757–1770.
105. Zerbino DR, Achuthan P, Akanni W, Amode MR, Barrell D, Bhai J, et al. Ensembl 2018. Nucleic Acids Res. 2018;46: D754–D761.

CHAPTER 5

DISCUSSION

SUMMARY

This thesis work is the first to implement novel cell type-specific labeling technologies to mark repopulating hepatocytes *in vivo* to achieve unbiased profiling of transcriptomic and epigenomic alterations that occur during the regenerative process. With the utilization of innovative methodologies to exclusively track regenerating hepatocytes combined with extensive integrative multiomic analyses, I identified several factors and pathways with important biological implications followed by examining their functional significance in the regulation of liver regeneration. Additionally, the gene expression and chromatin accessibility datasets provide comprehensive information on the transcriptional regulation of repopulating hepatocytes.

By adopting translating ribosome affinity purification with high-throughput RNA-sequencing (TRAP-seq) for the isolation of mRNA from repopulating hepatocytes, I identified *Slc7a11*, encoding the cystine/glutamate antiporter, xCT, as a promoter of liver regeneration in the setting of acute liver injury. *Slc7a11* is upregulated for over 600- and 250-fold in repopulating hepatocytes after 1 week and 4 weeks of liver injury and regeneration. Nonetheless, activation of *Slc7a11* via ectopic expression at the time of injury still allowed hepatocytes with increased xCT expression to repopulate the injured liver more efficiently.

The implementation of hepatocyte nuclear isolation followed by the 'assay for transposase-accessible chromatin using sequencing' (ATAC-seq) allowed identification of the alterations in the chromatin landscape and investigation of the epigenomic regulation that occurs during liver repopulation. Multiomic data integration has enabled the detection of increased promoter accessibility that corresponds to enhanced CCCTC-binding factor (CTCF) occupancy followed by activation of proliferative genes. On the other hand, decreased liver-specific enhancer accessibility correlates with decreased hepatocyte nuclear factor 4α (HNF4α) binding and inhibition of liver function genes. These observations provide new insights into how mature hepatocytes assume a less differentiated state to enable cell growth and replication during acute injury followed by repopulation.

LIMITATIONS

Considerations of the quiescent and regeneration mouse models

In the studies aimed at understanding the genome-wide changes that occur during liver regeneration, I utilized two different transgenic mouse lines, i.e. *Rosa*$^{LSL\text{-}GFP\text{-}L10a}$ and *Rosa*$^{LSL\text{-}SUN1\text{-}GFP}$, as sources for quiescent hepatocytes, whereas *Fah*$^{-/-}$ mice were used to induce liver injury and isolate repopulating liver cells. While no phenotypic deficiencies have been observed between the *Rosa*$^{LSL\text{-}GFP\text{-}L10a}$ [1] and *Rosa*$^{LSL\text{-}SUN1\text{-}GFP}$ [2] mice, studies have yet to demonstrate that hepatocytes isolated from these transgenic lines after injection of AAV8-TBG-Cre exhibit similar transcriptomic and epigenomic profiles compared to hepatocytes isolated from wild type mice. A small portion of differentially expressed genes and divergent accessible regions identified in the current investigations could result from the expression of GFP-tagged proteins.

In addition, the *Fah*$^{-/-}$ repopulation mouse could be perceived as an artificial model. In patients with hereditary tyrosinemia type I (HTI), all hepatocytes are exposed to toxic metabolites and subject to an injurious environment during tyrosine catabolism. However, cells that receive the *Fah* transgene in the *Fah*$^{-/-}$ model are technically not injured. Moreover, mechanisms of injury specific to tyrosine metabolism could limit the interpretation and findings to expand upon other injury-induced liver repopulation conditions, further restricting the utility of potential therapeutic targets identified in the current work. Analysis of injured hepatocytes could elucidate the transcriptomic and epigenomic discrepancies between the liver cells in HTI patients and repopulating hepatocytes in *Fah*$^{-/-}$ mice. This comparison may also answer whether similar alterations in redox pathways are present in injured cells, similar to that observed in repopulating cells. Finally, investigation of injured hepatocytes could add to the knowledge on signaling from injured to repopulating hepatocytes to better understand the induction of liver regeneration.

TRAP-seq profiles the 'translatome'

It is worth noting that TRAP isolates translating mRNA bound to the ribosomal protein L10a. Therefore, the sequencing reads represent the 'translatome' rather than the 'transcriptome' of

repopulating hepatocytes. Future methods to enable the isolation of nascent mRNAs particularly from repopulating hepatocytes is likely to generate divergent datasets and will allow the comparison of transcriptome and translatome, as well as the calculation of translation efficiency [3] during liver regeneration.

Isolation of repopulating hepatocyte nuclei is time-consuming

While affinity-purification was successful in isolating mRNA from repopulating hepatocytes, no enrichment was detected with immunoprecipitation of repopulating hepatocyte nuclei expressing the SUN1-GFP fusion protein. This was attempted several times with various anti-GFP antibodies according to methods described previously [2,4]. The exact mechanism of failure to immunoprecipitate SUN1-GFP-labeled nuclei is unclear but we postulate that a combination of the fragility of repopulating hepatocyte nuclei and the small amount of repopulating cells hinder the affinity-purification of SUN1-GFP expressing hepatocytes. To address the technical difficulty of lack of enrichment of target nuclei with the 'isolation of nuclei-tagged in specific cell types' (INTACT) method [2], we turned to fluorescence-activated cell sorting (FACS) to isolate repopulating hepatocyte nuclei. However, FACS is a time-consuming process and depending on the percentage of regenerating cells, took up to over 4 hours. The lengthy process could introduce cellular stress and cause chromatin fragmentation. In my hands, samples that required sorting for over 4 hours exhibited low-quality ATAC-seq reads that significantly reduced the signal to noise ratio, hindering peak calling in downstream analysis to identify open chromatin regions.

Limitations of the ATAC-seq technology and bioinformatics analysis pipelines

ATAC-seq makes use of the Tn5 transposase that accesses the relatively 'open' chromatin to fragment and tag accessible chromatin regions, a process referred to as 'tagmentation' [5]. However, the Tn5 transposase displays sequence-specific binding preferences that induce bias during tagmentation [6]. Computational methods to model and correct for the transposition bias

have been proposed [7,8], but these have not been widely-adopted or experimentally validated to date.

Furthermore, ATAC-seq is limited to only examining euchromatic areas and thus generates mainly short fragments under 200 bp constituted of nucleosome-free or mono-nucleosomal reads. This limits our ability to investigate the regulation of heterochromatic regions during liver repopulation. Other methods that utilize sonication-resistant heterochromatin followed by a gradient separation to discriminate subtypes of histone 3 lysine 9 trimethylation (H3K9me3) and histone 3 lysine 27 trimethylation (H3K27me3) [9] could be implemented to elucidate transcriptional silencing and domain repression during liver regeneration.

The development of ATAC-seq to examine open chromatin regions is a relatively new technology [5] and hence no pipelines have been proposed as the gold standard for data analysis. The analysis utilized in this thesis includes a combination of the ATAC-seq pipeline for ENCODE data developed by Anshul Kundaje and the ENCODE Data Analysis Center [10], as well as in-house scripts developed specifically for the analysis of the present study. The use of alternative bioinformatics programs could, therefore, generate distinct results. Nevertheless, I presume that the highly significant regions with differential accessibility should remain the same or at least similar across various analysis platforms.

Finally, chromatin regions with differential accessibility identified by ATAC-seq only refer to the state of openness but do not infer the activity of the gene. A chromatin region could become more accessible to allow the binding of transcriptional repressors, leading to suppression of its target genes. Hence, ATAC-seq only provides a broad overview of the modifications in the chromatin landscape rather than specific directional changes of gene activity. Integration of additional genome-wide experiments such as ChIP-seq, promoter-enhancer interaction mapping by chromatin capture methods, or other functional manipulation is necessary to guide the understanding of the effects of altered chromatin accessibility. For instance, the integration of TRAP-seq to inform transcriptomic modifications in this thesis provides additional information to assess the consequences of chromatin accessibility changes.

Whole repopulating livers are used for chromatin immunoprecipitation (ChIP)

In both studies to profile the transcriptomic and epigenomic changes that occur during liver regeneration, ChIP experiments were carried out on whole quiescent and repopulating livers to elucidate the mechanism of *Slc7a11* activation as well as the occupancy of CTCF and HNF4α. Due to the large cell number required for typical ChIP assays (1-10 million) [11], the lack of sufficient repopulating hepatocytes isolated from the regenerating liver has prevented cell type-specific ChIP-seq. Thus, it is possible that the signals of increased activating transcription factor 4 (ATF4) binding at the *Slc7a11* promoter are detected from hepatocytes undergoing injury and repopulation, as well as other cell types in the liver. The lack of significantly increased occupancy of nuclear factor erythroid 2-related factor 2 (NRF2) at the *Slc7a11* locus could also be the result of chromatin dilution by injured hepatocytes in the regenerating liver. Similarly, CTCF and HNF4α ChIP-seq experiments were performed in whole-livers that underwent 4 weeks of repopulation in a non-cell type-specific manner. The changes in CTCF and HNF4α occupancy detected are therefore likely a mixture of signals from injured and regenerating hepatocytes. Changes in binding patterns specific to repopulating cells could also be diluted by other cell types and the surrounding dying hepatocytes.

Development of novel methods to utilize micrococcal nuclease-based native ChIP without cross-linking — including 'Occupied Regions of Genomes from Affinity-purified Naturally Isolated Chromatin (ORGANIC)' [12], 'Ultra-Low-Input micrococcal nuclease-based Native ChIP (ULI-NChIP)' [13], and 'Cleavage Under Targets & Release Using Nuclease (CUNT&RUN)' [14] — allows ChIP-seq from as few as 1,000 cells, depending on the abundance of the transcription factor of interest. Further optimization of these methods for hepatocyte nuclei will be useful in obtaining cell type-specific cistromes in repopulating hepatocytes.

FUTURE DIRECTIONS

The downstream effectors of *Slc7a11* in regenerating hepatocytes

Slc7a11 overexpression promotes liver regeneration after acute injury, however, the effects of xCT activation in chronic injury has not been studied. Upregulation of *Slc7a11* is observed in human gastrointestinal tumors [15], breast cancer cells [16], and hepatocellular carcinoma [17] to increase glutathione (GSH) synthesis for the defense of reactive oxygen species (ROS) and promote cell growth [15,16]. It is plausible that xCT activation in the setting of chronic liver injury plays a similar role in reducing oxidative stress to confer an advantage for hepatocyte survival or replication.

While *Slc7a11* is not an oncogene, the safety of long-term xCT activation should be rigorously examined, especially in the inflammatory microenvironment often observed in chronic liver injury that could ultimately lead to tumorigenesis [18]. On the other hand, transient xCT induction could be considered as a treatment for acute and chronic liver injury. In APAP-induced liver failure, N-acetylcysteine is often used to restore intracellular GSH levels and prevent hepatic necrosis [19]. The efficacy of short-term upregulation of xCT via viral delivery of *Slc7a11* or drug treatment can be assessed in the settings of liver injury to determine the extent of prevention of ROS-mediated cell death and promotion of hepatocyte survival.

To identify the mechanisms of *Slc7a11* activation to enhance liver regeneration following acute injury, coexpression of *Fah* and *Slc7a11* cDNA in conjunction with the GFP-L10a fusion protein in the $Fah^{-/-}$ mouse would allow for specific isolation and expression profiling of repopulating hepatocytes with *Slc7a11* induction. TRAP-seq of these cells could determine the effects of *Slc7a11* overexpression on gene expression. Similarly, implementation of the clustered regularly interspaced short palindromic repeats (CRISPR) system to mutate *Slc7a11* with the expression of FAH and GFP-L10a could establish downstream targets necessary to promote liver regeneration that are dependent on *Slc7a11* activation. In particular, I hypothesize that genes involved in GSH metabolism, including *Gsta* and *Gstm* isoforms, as well as redox-sensitive transcription factors, such as NRF2 and AP1, will be activated following the upregulation of *Slc7a11* and inhibited after

Slc7a11 mutation to support the induction of redox pathways [20]. Gain- and loss-of-function experiments of the top effectors of *Slc7a11* activation could be carried out to further assess their functional significance during liver regeneration.

Regulation of oxidative response during liver regeneration

Expression profiling of regenerating hepatocytes identified massive induction of multiple redox pathway genes. Genes involved in the oxidation/reduction network have been implicated in liver injury and regeneration [21–23], and depletion of GSH availability or inhibition of GSH synthesis delays regeneration and exacerbates toxic hepatic injury [24,25]. What remains to be shown is the spatiotemporal regulation of redox balance in replicating hepatocytes during liver regeneration.

Recently, a method was established to determine the redox status of zebrafish cells *in situ* [26]. The effects of a biliary toxin were measured and determined to show that the toxin induces a more oxidized state in extrahepatic biliary cells [26]. The assay utilizes the redox-sensitive GFP biosensor, termed roGFP, that contains an engineered dithiol/disulfide switch sensitive to cytosolic redox states [27]. Different redox levels alter the state of cysteine amino acid residues, resulting in a shift in emission at two excitation wavelengths (405 and 488 nm). The coupling of roGFP to glutaredoxin (GRX1), an endogenous enzyme that catalyzes the GSH/GSSG equilibrium, allows for the specific determination of the cytoplasmic GSH redox potential by roGFP [27]. A high 405/488 signal indicates an oxidized sensor and conversely, a low signal reflects a reduced state.

The GRX1-roGFP biosensor could be adapted to the *Fah*$^{-/-}$ model to assess the intracellular redox potential of repopulating hepatocytes. Mapping of the spatial and temporal redox status in repopulating hepatocytes will enable the elucidation of the oxidative stress response during the regenerative process. Furthermore, the expression of GRX1-roGFP could be coupled with overexpression and inhibition of *Slc7a11* to determine the effects of varying xCT levels on the redox environment of repopulating hepatocytes.

Regulation of HNF4α occupancy during liver regeneration

HNF4α is a crucial factor that maintains mature hepatocytes in a differentiated state [28] by suppressing cell cycle gene expression and inhibiting hepatocyte proliferation [29,30]. Increased hepatocyte BrdU incorporation and Ki67 staining were observed in mice with conditional *Hnf4a* deletion, demonstrating the requirement of HNF4α to inhibit quiescent hepatocytes from reentering the cell cycle.

In the current study, I observed a loss of HNF4α binding to liver enhancers during repopulation, but have not investigated the mechanisms that led to its decrease in occupancy. Several possibilities include a loss of liver enhancer accessibility that results in HNF4α eviction [31], downregulation of *Hnf4a* expression [20,32] or protein abundance [33], and decreased HNF4α nuclear localization [34] that prevents its binding to liver enhancers. In fact, TRAP-seq identified a 50% decrease of Hnf4a transcripts in 4-week repopulating hepatocytes [20]. Whether other mechanisms contribute to the alteration of HNF4α occupancy is currently not known.

Elucidating the functional significance of altered HNF4α binding in the regenerating liver could also inform the utility of inhibiting HNF4α as a strategy to promote repopulation. It is plausible that HNF4α occupancy is required to maintain a euchromatic conformation at enhancers regulating liver functions [35], and a loss of binding could cause nucleosomes to become less accessible during liver regeneration. Targeted HNF4α deletion in repopulating hepatocytes in conjunction with the expression of GFP-L10a and SUN1-GFP proteins would enable the understanding of the direct effects of modified HNF4α occupancy on gene expression and chromatin accessibility.

The functional significance of CTCF in repopulating hepatocytes

CTCF plays numerous roles in genome regulation as an activator [36] or repressor [37] to modulate transcriptional activities, as an insulator to prevent enhancer-promoter interactions [38], as an organizer of chromatin structures to form topologically-associated domains [39], and as a modulator of long-range chromatin interactions to mediate looping [40], to name a few.

Understanding the functional importance of CTCF during liver repopulation will shed light on its utility as a therapeutic target and enable identification of additional regulators of the regenerative process. Incorporation of targeted degradation of CTCF mediated by the auxin-inducible degron system [41] with the *Fah*$^{-/-}$ mouse and cell type-specific isolation technologies would provide a model to study the effects of CTCF deficiency in repopulating hepatocytes. Genomic strategies to analyze changes in chromatin conformation [42,43] after the induction of CTCF degredation including chromosome conformation capture (3C) [44], chromosome conformation capture-on-chip (4C) [45], circular chromosome conformation capture (4C) [46], chromosome conformation capture carbon copy (5C) [47], Hi-C [48], and chromatin interaction analysis by paired-end tag sequencing (ChIA-PET) [49] could provide insight to the functional role of CTCF in nuclear organization and genome topology during liver regeneration.

The ability of CTCF to interact with distinct proteins in a context-dependent manner enables its diverse functions for transcriptional regulation [50,51]. Transcriptional cofactors are recruited by CTCF to specific loci for transcriptional activation and repression include Y-box DNA/RNA-binding factor (YB1) that enhances *Myc* repression [52], YY1 for X chromosome inactivation [53], class II transactivator (CIITA) to induce expression of major histocompatibility complex class II (MHC-II) genes [54], and general transcription factor II-I (TFII-I) to promote metabolic gene transcription [55].

Chromatin proteins also cooperate with CTCF to mediate insulation, looping, and transcription. The cohesin complex coordinates transcriptional insulation [56,57], H2A and H2A.Z induce localization to the nucleolus for insulation [58], and Suz12 recruits the polycomb repressive complex 2 to suppress the maternal *Igf2* promoter [59]. Other proteins demonstrated to interact with CTCF include Poly(ADP-ribose) polymerase 1 (PARP1) for post-translational modification of CTCF to modulate chromatin insulation properties [60], the nucleolar protein nucleophosmin to localize β globulin insulator sites to the nuclear periphery for insulation [58], and RNA polymerase II that induces pausing to regulate alternative exon usage [61].

In the current study, I identified increased CTCF occupancy at promoters with elevated accessibility during liver regeneration. Stratification of changes in transcript levels revealed several

likely protein partners that cooperate with CTCF to differentially-mediate gene activation or repression. The transcriptional activator ZBTB3 is colocalized with CTCF at upregulated genes involved in cell growth and proliferation, whereas the transcriptional repressor YY1 co-occupies CTCF-bound downregulated promoters related to cell death regulation in repopulating hepatocytes. Assays to coimmunoprecipitate CTCF and ZBTB3 or YY1 should be performed to evaluate the direct or indirect interactions between CTCF and its cofactors. Experiments that implement genome-wide methods to examine ZBTB3 and YY1 binding sites could also be utilized to identify additional loci of colocalization. Finally, studies to manipulate levels of ZBTB3 and YY1 in repopulating hepatocytes could inform the functional significance of these transcription factors in liver regeneration.

CONCLUSIONS

With the development of cell type-specific technologies to profile transcriptomic and epigenomic changes that occur specifically in the repopulating hepatocytes, I identified *Slc7a11* as a potential therapeutic target to promote liver regeneration after acute injury. Future work to assess the utility of *Slc7a11* in the setting of chronic liver injury, the safety of viral-mediated or drug-induced transient or long-term xCT activation, and the mechanism of *Slc7a11* to support hepatocyte replication will allow a more extensive understanding of the regulation of the oxidative/reduction network during liver repopulation.

Furthermore, my work provides insights on the combinatorial modulation of increased promoter accessibility and decreased liver-enriched enhancer accessibility underlying liver repopulation. These chromatin changes enable the activation of cell growth pathways and repression of liver metabolic functions. The mechanism of decreased HNF4α occupancy in liver-enriched enhancers and its effects on the liver metabolic gene program will enable the evaluation of whether HNF4α inhibition could be used as a strategy to induce hepatocyte replication during liver repopulation. The effects of CTCF on chromatin modification, the regulation of differential CTCF occupancy, and the mediation of transcriptional activity with additional CTCF cofactors are intriguing questions that may reveal the importance of nuclear organization and genome topology to fine-tune gene expression during the regenerative process.

REFERENCES

1. Liu J, Krautzberger AM, Sui SH, Hofmann OM, Chen Y, Baetscher M, et al. Cell-specific translational profiling in acute kidney injury. J Clin Invest. 2014;124: 1242–1254.
2. Mo A, Mukamel EA, Davis FP, Luo C, Henry GL, Picard S, et al. Epigenomic Signatures of Neuronal Diversity in the Mammalian Brain. Neuron. 2015;86: 1369–1384.
3. Good AL, Haemmerle MW, Oguh AU, Doliba NM, Stoffers DA. Metabolic stress activates an ERK/hnRNPK/DDX3X pathway in pancreatic β cells. Mol Metab. 2019; doi:10.1016/j.molmet.2019.05.009
4. Heiman M, Kulicke R, Fenster RJ, Greengard P, Heintz N. Cell type-specific mRNA purification by translating ribosome affinity purification (TRAP). Nat Protoc. 2014;9: 1282–1291.
5. Buenrostro JD, Giresi PG, Zaba LC, Chang HY, Greenleaf WJ. Transposition of native chromatin for fast and sensitive epigenomic profiling of open chromatin, DNA-binding proteins and nucleosome position. Nat Methods. 2013;10: 1213–1218.
6. Madrigal P. On Accounting for Sequence-Specific Bias in Genome-Wide Chromatin Accessibility Experiments: Recent Advances and Contradictions. Front Bioeng Biotechnol. 2015;3: 144.
7. Karabacak Calviello A, Hirsekorn A, Wurmus R, Yusuf D, Ohler U. Reproducible inference of transcription factor footprints in ATAC-seq and DNase-seq datasets using protocol-specific bias modeling. Genome Biol. 2019;20: 42.
8. Li Z, Schulz MH, Look T, Begemann M, Zenke M, Costa IG. Identification of transcription factor binding sites using ATAC-seq. Genome Biol. 2019;20: 45.
9. Becker JS, McCarthy RL, Sidoli S, Donahue G, Kaeding KE, He Z, et al. Genomic and Proteomic Resolution of Heterochromatin and Its Restriction of Alternate Fate Genes. Mol Cell. 2017;68: 1023–1037.e15.
10. kundajelab. kundajelab/atac_dnase_pipelines. In: GitHub [Internet]. [cited 26 Aug 2019]. Available: https://github.com/kundajelab/atac_dnase_pipelines
11. Kidder BL, Hu G, Zhao K. ChIP-Seq: technical considerations for obtaining high-quality data. Nat Immunol. 2011;12: 918–922.
12. Kasinathan S, Orsi GA, Zentner GE, Ahmad K, Henikoff S. High-resolution mapping of transcription factor binding sites on native chromatin. Nat Methods. 2014;11: 203–209.
13. Brind'Amour J, Liu S, Hudson M, Chen C, Karimi MM, Lorincz MC. An ultra-low-input native ChIP-seq protocol for genome-wide profiling of rare cell populations. Nat Commun. 2015;6: 6033.
14. Skene PJ, Henikoff S. An efficient targeted nuclease strategy for high-resolution mapping of DNA binding sites. Elife. 2017;6. doi:10.7554/eLife.21856
15. Ishimoto T, Nagano O, Yae T, Tamada M, Motohara T, Oshima H, et al. CD44 variant regulates redox status in cancer cells by stabilizing the xCT subunit of system xc(-) and thereby promotes tumor growth. Cancer Cell. 2011;19: 387–400.
16. Timmerman LA, Holton T, Yuneva M, Louie RJ, Padró M, Daemen A, et al. Glutamine sensitivity analysis identifies the xCT antiporter as a common triple-negative breast tumor therapeutic target. Cancer Cell. 2013;24: 450–465.
17. Kinoshita H, Okabe H, Beppu T, Chikamoto A, Hayashi H, Imai K, et al. Cystine/glutamic acid transporter is a novel marker for predicting poor survival in patients with hepatocellular carcinoma. Oncol Rep. 2013;29: 685–689.
18. Hernandez-Gea V, Toffanin S, Friedman SL, Llovet JM. Role of the microenvironment in the pathogenesis and treatment of hepatocellular carcinoma. Gastroenterology. 2013;144: 512–527.
19. Mitchell JR, Jollow DJ, Potter WZ, Gillette JR, Brodie BB. Acetaminophen-induced hepatic necrosis. IV. Protective role of glutathione. J Pharmacol Exp Ther. 1973;187: 211–217.
20. Wang AW, Wangensteen KJ, Wang YJ, Zahm AM, Moss NG, Erez N, et al. TRAP-seq identifies cystine/glutamate antiporter as a driver of recovery from liver injury. J Clin Invest. 2018;128: 2297–2309.

21. Marhenke S, Lamlé J, Buitrago-Molina LE, Cañón JMF, Geffers R, Finegold M, et al. Activation of nuclear factor E2-related factor 2 in hereditary tyrosinemia type 1 and its role in survival and tumor development. Hepatology. 2008;48: 487–496.
22. Diesen DL, Kuo PC. Nitric oxide and redox regulation in the liver: part II. Redox biology in pathologic hepatocytes and implications for intervention. J Surg Res. 2011;167: 96–112.
23. Hu M, Zou Y, Nambiar SM, Lee J, Yang Y, Dai G. Keap1 modulates the redox cycle and hepatocyte cell cycle in regenerating liver. Cell Cycle. 2014;13: 2349–2358.
24. Riehle KJ, Haque J, McMahan RS, Kavanagh TJ, Fausto N, Campbell JS. Sustained Glutathione Deficiency Interferes with the Liver Response to TNF-α and Liver Regeneration after Partial Hepatectomy in Mice. J Liver Disease Transplant. 2013;1. Available: https://www.ncbi.nlm.nih.gov/pubmed/24611135
25. Pajaud J, Ribault C, Ben Mosbah I, Rauch C, Henderson C, Bellaud P, et al. Glutathione transferases P1/P2 regulate the timing of signaling pathway activations and cell cycle progression during mouse liver regeneration. Cell Death Dis. 2015;6: e1598.
26. Zhao X, Lorent K, Wilkins BJ, Marchione DM, Gillespie K, Waisbourd-Zinman O, et al. Glutathione antioxidant pathway activity and reserve determine toxicity and specificity of the biliary toxin biliatresone in zebrafish. Hepatology. 2016;64: 894–907.
27. Albrecht SC, Barata AG, Grosshans J, Teleman AA, Dick TP. In vivo mapping of hydrogen peroxide and oxidized glutathione reveals chemical and regional specificity of redox homeostasis. Cell Metab. 2011;14: 819–829.
28. Späth GF, Weiss MC. Hepatocyte nuclear factor 4 expression overcomes repression of the hepatic phenotype in dedifferentiated hepatoma cells. Mol Cell Biol. 1997;17: 1913–1922.
29. Bonzo JA, Ferry CH, Matsubara T, Kim J-H, Gonzalez FJ. Suppression of hepatocyte proliferation by hepatocyte nuclear factor 4α in adult mice. J Biol Chem. 2012;287: 7345–7356.
30. Walesky C, Gunewardena S, Terwilliger EF, Edwards G, Borude P, Apte U. Hepatocyte-specific deletion of hepatocyte nuclear factor-4α in adult mice results in increased hepatocyte proliferation. Am J Physiol Gastrointest Liver Physiol. 2013;304: G26–37.
31. Bai L, Morozov AV. Gene regulation by nucleosome positioning. Trends Genet. 2010;26: 476–483.
32. Wang AW, Wang YJ, Zahm AM, Morgan AR, Wangensteen KJ, Kaestner KH. The dynamic chromatin architecture of the regenerating liver [Internet]. doi:10.1101/664862
33. Simó R, Barbosa-Desongles A, Hernandez C, Selva DM. IL1β down-regulation of sex hormone-binding globulin production by decreasing HNF-4α via MEK-1/2 and JNK MAPK pathways. Mol Endocrinol. 2012;26: 1917–1927.
34. Vető B, Bojcsuk D, Bacquet C, Kiss J, Sipeki S, Martin L, et al. The transcriptional activity of hepatocyte nuclear factor 4 alpha is inhibited via phosphorylation by ERK1/2. PLoS One. 2017;12: e0172020.
35. Iwafuchi-Doi M, Donahue G, Kakumanu A, Watts JA, Mahony S, Pugh BF, et al. The Pioneer Transcription Factor FoxA Maintains an Accessible Nucleosome Configuration at Enhancers for Tissue-Specific Gene Activation. Mol Cell. 2016;62: 79–91.
36. Klenova EM, Nicolas RH, Paterson HF, Carne AF, Heath CM, Goodwin GH, et al. CTCF, a conserved nuclear factor required for optimal transcriptional activity of the chicken c-myc gene, is an 11-Zn-finger protein differentially expressed in multiple forms. Mol Cell Biol. 1993;13: 7612–7624.
37. Lobanenkov VV, Nicolas RH, Adler VV, Paterson H, Klenova EM, Polotskaja AV, et al. A novel sequence-specific DNA binding protein which interacts with three regularly spaced direct repeats of the CCCTC-motif in the 5'-flanking sequence of the chicken c-myc gene. Oncogene. 1990;5: 1743–1753.
38. Bell AC, West AG, Felsenfeld G. The protein CTCF is required for the enhancer blocking activity of vertebrate insulators. Cell. 1999;98: 387–396.
39. Dixon JR, Selvaraj S, Yue F, Kim A, Li Y, Shen Y, et al. Topological domains in mammalian genomes identified by analysis of chromatin interactions. Nature. 2012;485: 376–380.

40. Splinter E, Heath H, Kooren J, Palstra R-J, Klous P, Grosveld F, et al. CTCF mediates long-range chromatin looping and local histone modification in the beta-globin locus. Genes Dev. 2006;20: 2349–2354.
41. Nora EP, Goloborodko A, Valton A-L, Gibcus JH, Uebersohn A, Abdennur N, et al. Targeted Degradation of CTCF Decouples Local Insulation of Chromosome Domains from Genomic Compartmentalization. Cell. 2017;169: 930–944.e22.
42. de Wit E, de Laat W. A decade of 3C technologies: insights into nuclear organization. Genes Dev. 2012;26: 11–24.
43. Denker A, de Laat W. The second decade of 3C technologies: detailed insights into nuclear organization. Genes Dev. 2016;30: 1357–1382.
44. Dekker J, Rippe K, Dekker M, Kleckner N. Capturing chromosome conformation. Science. 2002;295: 1306–1311.
45. Simonis M, Klous P, Splinter E, Moshkin Y, Willemsen R, de Wit E, et al. Nuclear organization of active and inactive chromatin domains uncovered by chromosome conformation capture-on-chip (4C). Nat Genet. 2006;38: 1348–1354.
46. Zhao Z, Tavoosidana G, Sjölinder M, Göndör A, Mariano P, Wang S, et al. Circular chromosome conformation capture (4C) uncovers extensive networks of epigenetically regulated intra- and interchromosomal interactions. Nat Genet. 2006;38: 1341–1347.
47. Dostie J, Richmond TA, Arnaout RA, Selzer RR, Lee WL, Honan TA, et al. Chromosome Conformation Capture Carbon Copy (5C): a massively parallel solution for mapping interactions between genomic elements. Genome Res. 2006;16: 1299–1309.
48. Lieberman-Aiden E, van Berkum NL, Williams L, Imakaev M, Ragoczy T, Telling A, et al. Comprehensive mapping of long-range interactions reveals folding principles of the human genome. Science. 2009;326: 289–293.
49. Fullwood MJ, Liu MH, Pan YF, Liu J, Xu H, Mohamed YB, et al. An oestrogen-receptor-alpha-bound human chromatin interactome. Nature. 2009;462: 58–64.
50. Phillips JE, Corces VG. CTCF: master weaver of the genome. Cell. 2009;137: 1194–1211.
51. Zlatanova J, Caiafa P. CTCF and its protein partners: divide and rule? J Cell Sci. 2009;122: 1275–1284.
52. Chernukhin IV, Shamsuddin S, Robinson AF, Carne AF, Paul A, El-Kady AI, et al. Physical and functional interaction between two pluripotent proteins, the Y-box DNA/RNA-binding factor, YB-1, and the multivalent zinc finger factor, CTCF. J Biol Chem. 2000;275: 29915–29921.
53. Donohoe ME, Zhang L-F, Xu N, Shi Y, Lee JT. Identification of a Ctcf cofactor, Yy1, for the X chromosome binary switch. Mol Cell. 2007;25: 43–56.
54. Majumder P, Gomez JA, Chadwick BP, Boss JM. The insulator factor CTCF controls MHC class II gene expression and is required for the formation of long-distance chromatin interactions. J Exp Med. 2008;205: 785–798.
55. Peña-Hernández R, Marques M, Hilmi K, Zhao T, Saad A, Alaoui-Jamali MA, et al. Genome-wide targeting of the epigenetic regulatory protein CTCF to gene promoters by the transcription factor TFII-I. Proc Natl Acad Sci U S A. 2015;112: E677–86.
56. Stedman W, Kang H, Lin S, Kissil JL, Bartolomei MS, Lieberman PM. Cohesins localize with CTCF at the KSHV latency control region and at cellular c-myc and H19/Igf2 insulators. EMBO J. 2008;27: 654–666.
57. Wendt KS, Yoshida K, Itoh T, Bando M, Koch B, Schirghuber E, et al. Cohesin mediates transcriptional insulation by CCCTC-binding factor. Nature. 2008;451: 796–801.
58. Yusufzai TM, Tagami H, Nakatani Y, Felsenfeld G. CTCF tethers an insulator to subnuclear sites, suggesting shared insulator mechanisms across species. Mol Cell. 2004;13: 291–298.
59. Li T, Hu J-F, Qiu X, Ling J, Chen H, Wang S, et al. CTCF regulates allelic expression of Igf2 by orchestrating a promoter-polycomb repressive complex 2 intrachromosomal loop. Mol Cell Biol. 2008;28: 6473–6482.
60. Yu W, Ginjala V, Pant V, Chernukhin I, Whitehead J, Docquier F, et al. Poly(ADP-ribosyl)ation regulates CTCF-dependent chromatin insulation. Nat Genet. 2004;36: 1105–1110.

61. Shukla S, Kavak E, Gregory M, Imashimizu M, Shutinoski B, Kashlev M, et al. CTCF-promoted RNA polymerase II pausing links DNA methylation to splicing. Nature. 2011;479: 74–79.